NASA Contractor Report 165679

AN ASYMPTOTIC UNSTEADY LIFTING-LINE THEORY WITH ENERGETICS AND OPTIMUM MOTION OF THRUST-PRODUCING LIFTING SURFACES

Ali Reza Ahmadi

MASSACHUSETTS INSTITUTE OF TECHNOLOGY
Department of Aeronautics and Astronautics
Cambridge, Massachusetts 02139

Grant NGR 22-009-818
April 1981

National Aeronautics and
Space Administration

Langley Research Center
Hampton, Virginia 23665

AN ASYMPTOTIC UNSTEADY LIFTING-LINE THEORY WITH ENERGETICS AND OPTIMUM MOTION OF THRUST-PRODUCING LIFTING SURFACES

by

Ali Reza Ahmadi

ABSTRACT

A low-frequency unsteady lifting-line theory has been developed for a harmonically-oscillating wing of large aspect ratio. The wing is assumed to be chordwise rigid but completely flexible in the span direction. The theory is developed by use of the method of matched asymptotic expansions which reduces the problem from a singular integral equation to quadrature. The wing displacements are prescribed and the pressure field, airloads and unsteady induced downwash are obtained in closed form. The influence of reduced frequency, aspect ratio, planform shape and mode of oscillation on wing aerodynamics is demonstrated through numerical examples. Compared with lifting-surface theory, computation time is reduced significantly. The theory identifies and resolves the errors in the unsteady lifting-line theory of James (1975) and raises questions about the complete validity of that of Van Holten (1975).

Using the present theory, the energetic quantities associated with the propulsive performance of a finite wing oscillating in combined pitch and heave, namely the power required to maintain the wing oscillations, the thrust, the energy loss rate due to vortex shedding in the wake and the leading-edge suction force have been obtained in closed form. Numerical examples are presented for an elliptic wing. The region of validity of the present unsteady lifting-line theory is found to be considerably larger than anticipated, containing the values of reduced frequency and aspect ratio which are of greatest interest in most applications.

The optimum solution of Wu (1971b) for a rigid airfoil has been recast in terms of the normal modes of the energy-loss-rate matrix to shed light on the structure of the solution. It is found that one of the modes, termed the invisible mode, plays a central role in the solution and is responsible for the nonuniqueness of the solution. Using the results of the present unsteady lifting-line theory, the optimum motion of a finite rigid wing has also been analyzed rigorously. It is found that the solution is unique (no invisible mode). Numerical results for the optimum motion of an elliptic wing are presented.

Finally, an alternate approach has been presented for the calculation of the energetic quantities in two and three dimensions, namely the use of the integral form of the conservation laws. This approach has the advantages of being quite general, physically enlightening and avoiding the direct calculation of the leading-edge suction force. However, the

distribution of bound circulation and pressure on the wing are required.

Suggestions for future work on the basis of the present investigation are also given.

ACKNOWLEDGEMENTS

The author wishes to express his sincere gratitude to his thesis supervisor, Professor Sheila Widnall, for her patience, understanding and competent supervision in the course of this investigation.

Special thanks are also due to Professors Marten Landahl, Wesley Harris and Rene Miller for their suggestions, comments and encouragement; to Mr. Paul Missel for typing the manuscript; to M.I.T. Student Information Processing Board for their assistance in the use of the MULTICS EMACS word processing system; to fellow graduate students for their interest and discussions; and to my roommates and many other friends near and far for their friendship and support.

Finally, I would like to express my deep gratitude to my family for their moral and financial support.

The work reported in this thesis was in part funded by NASA Langley Research Center, Low-Speed Aerodynamics Branch, Subsonic-Transonic Aerodynamics Division, under Grant NGR 22-009-818, monitored by Mr. Danny Hoad.

THIS PAGE INTENSIONALLY LEFT BLANK

TABLE OF CONTENTS

LIST OF SYMBOLS

A	aspect ratio
b	semi span or span
b_n	coefficients of chordwise Fourier cosine series for downwash at the wing
b_L	position of pitch axis in Lighthill's description
B	$(\equiv F - (F^2 + G^2))$
c	semi chord or chord
c_o	root semi chord
C_ℓ , C_L	sectional and total lift coefficients
C_m , C_M	sectional and total moment coefficients
C_p	pressure coefficient
C_E , $C_{\mathcal{E}}$	energy loss rate coefficients in two and three dimensions
C_P , $C_{\mathcal{P}}$	sectional and total input power coefficients
C_T , $C_{\mathcal{T}}$	sectional and total thrust coefficients
$C_{T,o}$, $C_{\mathcal{T},o}$	prescribed thrust in two and three dimensions
$\overline{C}_{T,o}$, $\overline{C}_{\mathcal{T},o}$	proportional loading parameter in two and three dimensions
C_{T_P}, $C_{\mathcal{T}_P}$	sectional and total coefficients of thrust from normal force at the wing
C_{T_s}, $C_{\mathcal{T}_s}$	sectional and total leading-edge suction coefficients
$\mathbb{C}$	Theodorsen's function $(\equiv F + j\,G)$
D	$(\equiv F^2 + G^2)$
$E, \mathcal{E}$	energy loss rate in two and three dimensions
f^i	complex inner acceleration potential $(\equiv \psi^i + i\,\sigma^i)$
F, G	real and imaginary parts of Theodorsen's function
F_1 , F_2 , F_3	weighting functions for the Sears eigensolution

$\vec{F}_B$	force exerted by the fluid on wing
g^i	complex velocity in the inner region ($\equiv u^i - i\, w^i$)
h	transverse displacement of wing or wake
h_o	heave amplitude
h_L	heave amplitude in Lighthill's description
$H_n^{(2)}$	Hankel function of the second kind of order n
i	spatial complex unit
$\vec{i}, \vec{j}, \vec{k}$	unit vectors in x, y, z or X, Y, Z directions
I_n	modified Bessel function of the first kind of order n
$\mathcal{I}_i, \mathcal{I}_j$	imaginary part with respect to i and j
j	temporal complex unit
J_n	Bessel function of the first kind of order n
k	reduced frequency based on semi chord
k_o	reduced frequency based on root semi chord
K_n	modified Bessel function of the second kind of order n
$\underline{K}$	matrix of quadratic form for C_{T_S}
KE	kinetic energy
$\overline{\mathcal{K}}$	modified kernel function of Reissner
l, L	sectional and total lift
l_o	quasi-steady section lift
L	abscissa of downstream end of wake
L_n	modified Struve function of order n
m, M	sectional and total moment about y-axis
$\vec{n}$	unit normal vector pointing away from control volume
p	perturbation pressure
p_∞	free stream pressure
P, $\mathcal{P}$	sectional and total input power

q	second moment of section lift about y-axis
$\vec{q}$	perturbation velocity vector
$\vec{Q}$	total velocity vector
r,θ	polar coordinates
$\mathcal{R}_i$, $\mathcal{R}_j$	real part with respect to i and j
S	far boundary
$S(k)$	Sears function
S_a	wing planform area
S_w	wake surfaces
t	time
T, $\mathcal{T}$	sectional and total thrust
T_p, $\mathcal{T}_p$	sectional and total thrust from normal force at the wing
T_s, $\mathcal{T}_s$	sectional and total leading-edge suction force
u, v, w	x, y, z or X, Y, Z components of $\vec{q}$
U	free stream velocity
V	control volume
W_o	prescribed downwash at the wing
$\tilde{W}_g$	complex amplitude of unsteady induced downwash
W_I	unsteady induced downwash
w_θ	perturbation velocity component in θ-direction of (r, θ)
x, y, z	cartesian coordinates fixed to mean position of the wing
X, Y, Z	cartesian coordinates fixed in the fluid
$\vec{X}$	$(\equiv (x, y, z))$
x_ℓ	abscissa of leading edge
x_t	abscissa of trailing edge
Y_n	Bessel function of the second kind of order n
Z_ϕ	amplitude ratio of heave with respect to pitch

α	complex pitch amplitude
α_p	phase advance of pitch with respect to heave
α_L	pitch amplitude in Lighthill's description
β	leading-edge sweep angle
γ	bound vorticity or the Euler constant (.57721...)
γ_1	$(\equiv e^{\gamma})$
$\gamma_1, \gamma_2, \gamma_3$	weighting functions for the normal modes of $\underline{E}$
Γ	bound circulation
δ	streamwise vorticity of wing or wake
ϵ	small parameter denoting the order of magnitude of perturbations
ζ	spatial complex variable $(\equiv x + i z)$
η	hydrodynamic efficiency
θ	chordwise angular variable
θ'	spanwise angular variable
θ_L	Lighthill's proportional feathering parameter
λ	$(\equiv [(\hat{\zeta} - c)/(\hat{\zeta} + c)]^{1/2})$; wavelength of periodic wake
μ	$(\equiv (\bar{\omega} \mid y - \eta \mid))$
μ_0	reduced frequency based on semi span $(\equiv \bar{\omega} b)$
ν	reduced frequency based on the magnified semi chord
ξ_c	nondimensional heave amplitude
ξ_1, ξ_2	real and imaginary parts of pitch amplitude α
Π	kernel function of unsteady lifting-line theory
ρ	fluid density
σ	wing surfaces
σ^i	conjugate harmonic function of ψ^i
τ	period of simple harmonic oscillation

ϕ	perturbation velocity potential
$\underline{\phi_1}$, $\underline{\phi_2}$, $\underline{\phi_3}$	normal modes of $\underline{E}$ (normalized)
χ	distance measured along the leading edge
ψ	acceleration potential
ω	radian frequency of simple harmonic oscillation
$\bar{\omega}$	($\equiv \omega/U$)
Ω, $\mathfrak{Q}$	two- and three-dimensional reduced circulation
$(\ )_a$	airfoil or wing
$(\ )_w$	wake
$(\ )_u$, $(\ )_\ell$	upper and lower surfaces of wing or wake
$(\ )_t$, $(\ )_x$	partial derivative with respect to t and x
$(\ )'$	derivative with respect to the indicated argument
$(\ )^i$, $(\ )^o$	inner and outer problems
$(\ )_H$, $(\ )_p$	heave and pitch oscillations
$\vec{(\ )}$	vector quantity
$\bar{(\ )}$	time average
$(\ )^*$	nondimensional quantity
$(\ )^{\circledast}$	complex conjugate with respect to j
$\underline{(\ )}$	matrix quantity
$(\ )^T$	transpose of matrix
$\hat{(\ )}$	magnified inner variables
$\tilde{(\ )}$	complex amplitude of harmonic functions
$(\ )_{2D}$	two-dimensional or strip-theory quantity

CHAPTER I

INTRODUCTION

Important unsteady and three-dimensional effects occur for a wide range of problems of practical interest involving oscillating finite wings. Many of these cannot be calculated by the use of strip-theory and quasi-steady aerodynamics. The high cost of numerical implementation of current unsteady lifting-surface theory, on the one hand, and the success of Prandtl's lifting-line theory, on the other, have prompted several investigators in the past few years to seek to extend the lifting-line concept to unsteady flows. Another advantage of the lifting-line theories is that the results can be obtained in closed form which would be suited for optimization studies. Unfortunately, existing unsteady lifting-line theories are mostly incomplete and/or incorrect, with almost no numerical results available. The present work includes the development and applications of an unsteady lifting-line theory for a harmonically-oscillating straight wing of large aspect ratio which is completely flexible in the span direction. Extensive numerical results are presented.

One area of application which has received some attention in recent years is the study of the propulsive performance and optimum shapes and motions of oscillating rigid or flexible wings. Optimum refers to those displacements of the wing which minimize the average energy loss rate in the wake due to vortex shedding (1) subject to the condition of fixed

---

(1) This quantity is alternately referred to as the wake energy since, as we

average thrust. This would be helpful in understanding certain modes of animal propulsion in nature, such as flapping flight of birds and undulations of lunate tails of some fish which are typically associated with high hydrodynamic efficiency. Studies in this area to date have been mostly in two dimensions where the theory is well developed and the closed-form results have been used to determine the optimum motion of a rigid and a flexible airfoil. In three dimensions, the studies have been based on numerical and approximate unsteady lifting-surface theories, where the numerical results have precluded a rigorous determination of the optimum. In the current study, using the present unsteady lifting-line theory, the energetic quantities, namely the power required to maintain the wing oscillations, the thrust, the energy loss rate in the wake and the leading-edge suction force are determined in closed form for a finite wing oscillating in combined pitch and heave. Then, using the latter results, the optimum motion is determined rigorously. The present work also includes an alternate method of determining the energetics of flapping flight, namely the use of the integral form of the conservation laws. This approach, however, is found not to be well suited for optimization studies.

The studies presented in this work are based on linearized arerodynamic theory and as such are restricted to small-amplitude transverse oscillations of the wing. The free stream velocity is assumed to be small enough to consider the fluid as incompressible, and yet large enough so that the Reynold's number based on a characteristic length of the wing is large. The viscous effects are then confined to a thin boundary layer at the wing and a thin trailing wake. The energetic quantities are

---

will see in Chapter VI, it is related to the kinetic energy content of the far wake.

$O(\epsilon^2)$ where $\epsilon > 0$ is a small parameter denoting the order of magnitude of the perturbations. The energetic quantities are, hence, alternately referred to as the quadratic quantities. Since the quantities of interest are primarily due to the inertial forces, they can be determined from potential flow theory. The analyses are restricted to the purely unsteady component of the wing motion.

Due to the diversity of the topics under consideration, a survey of the literature and further introductory remarks are presented in the introduction section of the following chapters.

CHAPTER II

UNSTEADY LIFTING-LINE THEORY AS A SINGULAR PERTURBATION PROBLEM

2.1 Introduction

Prandtl's lifting-line theory (Prandtl (1918)) was the first successful attempt to solve the linearized problem of the uniform motion of a wing of large aspect ratio. After six decades, Prandtl's theory is still in use in preliminary design and analysis. Since the advent of high-speed computers, however, detailed design and analysis has been increasingly carried out using steady and unsteady numerical lifting-surface theories (see, e.g., Landahl and Stark (1968)). These generally involve the numerical solution of a singular integral equation and typically require large amounts of computer time especially for unsteady flows.

In the area of unsteady wing theory, in the meantime, a large number of approximate and ad hoc theories have been developed. These may be termed irrational approximate theories since the order of magnitude of the errors introduced by the approximations is not known. There also exist a few rather specialized exact solutions (see, e.g., Schade and Krienes (1947)) which are, nevertheless, valuable in understanding certain aspects of finite wing problems such as the flow field near the wing tips.

Quite a different approach began with the important discovery of Friedrichs (1953) that the motion of a high-aspect-ratio wing can be formulated as a singular perturbation problem. Using the method of matched asymptotic expansions (MAE), Van Dyke (1963) developed an asymptotic lifting-line theory which reduced the problem from an integral equation to

quadrature and reproduced Prandtl's result to the order of its validity. Such theories can be carried out to higher orders systematically, as was demonstrated by Van Dyke, although this is often unnecessary. Theories of this type may be termed rational approximations, since the order of magnitude of the errors is known.

During the last few years, a few investigators have developed asymptotic theories for high-aspect-ratio wings in unsteady motion. These have been termed unsteady lifting-line theories (1). These theories are still in their infancy, as can be seen from an examination of the few published works, one of which is incorrect and for the others some questions remain about their validity and utility. Also, since there is an almost total lack of numerical examples and correlations with lifting-surface and experimental results in these works, the assessment of their value is more difficult.

James (1975) has published a work on an unsteady lifting-line theory for a straight flexible wing in unsteady motion. His treatment of the problem uses a semi-intuitive MAE approach. His unsteady induced downwash is found to be in error (as well as being infinite) which renders his three-dimensional unsteady results incorrect. He also suggests that his theory is valid for all reduced frequencies, whereas the formulation clearly assumes low reduced frequencies. Further, he does not treat and

---

(1)
In the classical sense, this is a misnomer since in unsteady flow, as was first pointed out by Reissner (1944), the lowest-order induced downwash is not a constant across the chord, except in the steady flow limit. Hence, one can no longer speak of a loaded line. However, in analogy with steady flow, we will use the term unsteady lifting-line theory for the asymptotic solution, where the outer solution involves a loaded line and the inner solution is an oscillating airfoil with an induced downwash that is not constant across the chord.

resolve the inherent nonuniqueness of the solution in the acceleration potential formulation of the problem.

Cheng (1975) has proposed an unsteady lifting-line theory for a wing with curved and/or swept planform in harmonic oscillation. His formulation is in terms of the velocity potential which he determines to leading order in inverse aspect ratio. The work does not include calculation of the aerodynamic loading, the unsteady induced downwash and some of the important details, nor is the work presented in a form ideal for such calculations. To this author's knowledge, Cheng was the first to identify the various frequency domains for the influence of unsteadiness on the induced downwash. These domains are described below.

Van Holten (1974, 1975, 1976, 1977) has developed lifting-line theories for a rigid rectangular wing in uniform motion, with and without yaw and transverse harmonic oscillation, and also as a helicopter rotor blade in forward flight. It is implicit in his analysis that the unsteady induced downwash is a constant across the chord. As already mentioned, this is not the case in unsteady flow, except in the steady flow limit. He also regards his theory as valid for all reduced frequencies; this is unlikely since it uses a constant induced downwash at each chord. His analysis leads to an integral equation which must be solved numerically. Van Holten was the first to point out the correct physical interpretation of the induced downwash in steady and unsteady flows. The same interpretation comes out of the present work.

The problem of a harmonically oscillating three dimensional wing involves three characteristic length scales, namely the chord c, the span b and the wavelength of the periodic wake $\lambda = 2\pi U/\omega$ as shown in Figure 2.1. As far as the influence of unsteadiness on the three-dimensional effects

are concerned, Cheng (1975) has identified five ranges of λ for a high-aspect-ratio wing ($c \ll b$):

I.	$c \ll b \ll \lambda$	very low frequency
II.	$c \ll b = O(\lambda)$	low frequency
III.	$c \ll \lambda \ll b$	intermediate frequency
IV.	$c = O(\lambda) \ll b$	high frequency
V.	$\lambda \ll c \ll b$	very high frequency

Domain I corresponds to very low frequencies where quasi-steady aerodynamic theory is adequate. Domain V, on the other hand, corresponds to very high frequencies where the self-averaging effect of the high-frequency periodic wake renders the problem locally two-dimensional. In domain II, the the reduced frequency based on the span $\omega b/U = O(1)$, whereas in domain IV the reduced frequency based on the chord $\omega c/U = O(1)$. The analysis of the problem in domains II and IV involves two distinct regions in space corresponding to length scales c and b, whereas the analysis of domain III involves three regions in space corresponding to c, b and λ.

Cheng further points out that an important result of the condition $\lambda \ll b$ is that the three-dimensional effects produced by the far wake vanish with λ/b and become much smaller than the local three-dimentional effects. The above frequency domains are depicted qualitatively in a reduced frequency aspect ratio diagram in Figure 2.2.

Chapters II - V are devoted to the development and applications of an unsteady lifting-line theory valid in domains I and II. It seems, from the numerical results, that the theory may be valid in parts of domains III - V as well. The wing model used is shown in Figure 2.3a where the chord is $O(A^{-1})$ and the span is O(1). A similar asymptotic theory can be developed

for domains IV and V using a wing model with chord of O(1) and span of O(A). Such a theory may also be valid in parts of domains I - III, in which case the two theories together might form a unified unsteady lifting-line theory for the entire frequency spectrum. Otherwise, a third theory would be needed for domain III to bridge the gap between the low- and high-frequency theories. The latter will probably be the most difficult of the three. However, since most applications of interest fall in domains I and II, this region will be our focus.

The present theory is formulated in terms of the acceleration potential ψ. The advantages of this formulation are that ψ is continuous across the wake and the pressure on the wing is obtained directly from ψ. However, the solution is not unique since multiples of eigensolutions with $\partial\psi/\partial z = 0$ at the wing may be added. Uniqueness is achieved by determining the downwash by integration of ψ from far upstream to some point on the wing.

An asymptotic expansion is carried out to leading order in inverse aspect ratio. All of the results of the present theory are obtained in closed form and are thus suited for optimization studies. Numerical results for the present theory compare favorably with other theories including unsteady lifting-surface theories. Compared with the latter, the required computation time is reduced significantly.

2.2 Problem Formulation

Consider a thin almost planar wing of large aspect ratio, executing small-amplitude harmonic oscillations normal to the wing planform, in a uniform stream of inviscid incompressible fluid. The wing has a straight mid-chord line positioned normal to the free stream.

The wing planform is described by

$$X = \pm c(y)/A \qquad |y| \leq b \qquad z = 0 \tag{2.1}$$

in a coordinate system (x,y,z) fixed to the mean position of the wing as shown in Figure 2.3a. The free stream velocity U is directed along the positive x-axis. Here, A is the wing aspect ratio defined as

$$A = (2b)^2 / S_a \tag{2.2}$$

where b is the semi span length and S_a is the wing planform area. c(y)/A is the semi chord. Both b and c(y) are assumed to be $O(A^0)$.

The transverse displacements of the wing (mid-camber surface) are described by

$$z = h(x,y,t) = \left[h_0(y)/A + \alpha(y)\, x \right] e^{j\omega t} \qquad |x| \leq c(y)/A \qquad |y| \leq b \tag{2.3}$$

or, equivalently, by

$$z = h(x,y,t) = \left\{ \tfrac{1}{2} (c_0/A)\, \xi_0(y) + \left[\xi_1(y) + j\, \xi_2(y) \right] x \right\} e^{j\omega t} \qquad |x| \leq c(y)/A \qquad |y| \leq b \tag{2.4}$$

where ξ_c, ξ_1 and ξ_2 are nondimensional quantities; c_0/A is the root semi chord; j is the temporal complex unit; ω is the radian frequency of oscillation; and t is time. The above relations define a wing which is flexible in the span direction, capable of executing arbitrary torsional and bending oscillations. The wing sections, however, are rigid airfoils performing heaving motion of amplitude

$$h_o(y)/A = \frac{1}{2}\,(c_o/A)\,\xi_o(y) \qquad (2.5)$$

and pitching motion, about the mid chord, of amplitude

$$|\alpha(y)| = |\xi_1(y) + j\,\xi_2(y)| \qquad (2.6)$$

with phase angle

$$\tan^{-1}\left[\xi_2(y)/\xi_1(y)\right] \qquad (2.7)$$

leading the heaving motion. The heaving motion is taken as positive in the positive z-direction and the pitching motion is taken as positive in the direction of negative rotation about the y-axis as shown in Figure 2.3b.

We require that the arbitrary functions $h_o(y)$ and $\alpha(y)$ (or, equivalently, $\xi_o(y)$, $\xi_1(y)$ and $\xi_2(y)$) be such that the wing displacements satisfy the conditions of linearized theory, namely

$$\partial h/\partial x\ ,\ \partial h/\partial y\ ,\ U^{-1}\partial h/\partial t \ll 1 \qquad (2.8)$$

Implicit in the above restrictions on the choice of h(x,y,t) and c(y) is the fundamental assumption of lifting-line theory that the spanwise flow perturbations are small compared with those in planes normal to the span.

In this work, we use the forms (2.3) and (2.4) interchangeably, with the latter being especially convenient in numerical calculations. The wing shapes and motions described by (2.1), (2.3) and (2.4) embraces a broad class of interesting problems involving unsteady motion of spanwise-flexible wings.

The above problem can be formulated in terms of the acceleration potential Ψ defined as

$$\Psi(\vec{x},t) = \left[p_\infty - p(\vec{x},t)\right]/\rho \qquad (2.9)$$

where $\vec{X} = (x,y,z)$, p is pressure, ρ is fluid density and p_∞ is the free stream pressure. It follows from the linearized Euler equation and the continuity equation that ψ is governed by the Laplace equation

$$\nabla_3^2 \psi(\vec{x},t) = 0 \tag{2.10}$$

where the subscript $(\,)_3$ indicates a three-dimensional Laplacian. The linearized boundary condition at the wing specifies the downwash.

$$w(\vec{x},t) = \left(\frac{\partial}{\partial t} + U\frac{\partial}{\partial x}\right) h(x,y,t) = W_o(x,y,t)$$

$$|x| \le c(y)/A \qquad |y| \le b \qquad z = 0\pm \tag{2.11a}$$

For h(x,y,t) in (2.3), this becomes

$$W_o(x,y,t) = \left[j\omega h_o(y)/A + U\alpha(y) + j\omega\alpha(y)\,x\right] e^{j\omega t}$$

$$|x| \le c(y)/A \qquad |y| \le b \qquad z = 0\pm \tag{2.11b}$$

Substituting (2.11a) in the z-component of the linearized Euler equation, we can express the tangency condition in terms of ψ.

$$\frac{\partial}{\partial z}\psi(\vec{x},t) = \left(\frac{\partial}{\partial t} + U\frac{\partial}{\partial x}\right) W_o(x,y,t)$$

$$= \left(\frac{\partial}{\partial t} + U\frac{\partial}{\partial x}\right)^2 h(x,y,t)$$

$$|x| \le c(y)/A \qquad |y| \le b \qquad z = 0\pm \tag{2.12}$$

Along the trailing edge, the Kutta condition requires that the pressure remain bounded.

$$|\psi(\vec{x},t)| < \infty \qquad x = c(y)/A \qquad |y| \le b \qquad z = 0 \tag{2.13}$$

Since ψ is an odd function of z, it follows that

$$\psi(\vec{x},t) = 0 \qquad |x| > c(y)/A \qquad z = 0 \tag{2.14}$$

Further, we require the pressure disturbances to vanish at infinity.

$$\psi(\vec{x},t) \to 0 \qquad \sqrt{x^2+y^2+z^2} \to \infty \tag{2.15}$$

The solution of the linearized boundary value problem (1) defined by (2.10) - (2.15) can be expressed in terms of a distribution of three-dimensional pressure doublets over the projection of the wing planform on the xy-plane.

$$\tilde{\psi}(\vec{x}) = \frac{-1}{4\pi\rho} \int_{-b}^{b} d\eta \int_{-c(y)/A}^{c(y)/A} d\xi \; \Delta\tilde{p}(\xi,\eta) \frac{\partial}{\partial z} \frac{1}{R} \tag{2.16}$$

where

$$R = \left[(x-\xi)^2 + (y-\eta)^2 + z^2 \right]^{1/2} \tag{2.17}$$

and $\Delta p = p_\ell - p_u$ is the local pressure jump across the wing, with $(\,)_u$ and $(\,)_\ell$ denoting the upper and lower wing surfaces respectively. This can be readily seen from (2.16) by taking the limit as $z \to 0\pm$ with x and y fixed.

$$\rho\left[\tilde{\psi}(x,y,0+) - \tilde{\psi}(x,y,0-)\right] = \Delta\tilde{p}(x,y) \tag{2.18}$$

In the following sections, using the MAE method, we find the solution for ψ, for given wing shapes and motions, which is uniformly valid

---

(1) We are justified by linearity to write all dependent variables as

$$g(\vec{x},t) = \tilde{g}(\vec{x})\, e^{j\omega t}$$

throughout the flow field. The value of ψ at the wing yields the wing pressure distribution (see (2.18)) which can be integrated to obtain various aerodynamic quantities of interest.

Formally, as aspect ratio tends to infinity, we consider two simplified asymptotic limits of the problem: the outer limit and the inner limit. The outer limit corresponds to holding the span fixed and letting the chord tend to zero, where the wing collapses to a loaded line. The inner limit corresponds to holding the chord fixed and letting the span tend to infinity, where the two-dimensional unsteady airfoil solution is emphasized. The outer and inner limits are both incomplete representations of the full problem, each lacking some essential features of the problem: the basic unsteady airfoil solution in the outer limit and the three-dimensional effects in the inner limit. Matching the two expansions resolves this incompleteness. As mentioned earlier, however, this solution is not unique since multiples of eigensolutions with $\partial\psi/\partial z = 0$ at the wing may be present. Uniqueness is achieved by determining the downwash by integration of ψ from far upstream to some point on the wing.

2.3 Outer Solution for the Acceleration Potential

Here, we seek an expansion for ψ valid in the outer region (distances from the wing of the order of wing span, viz. $O(A^0)$) where the wing shrinks to a loaded line as $A \to \infty$. Formally, this is obtained from (2.16) by expanding the kernel function R^{-1} in a Taylor Series for small ξ and integrating across the chord. Using

$$R^{-1} = R^{-1} - \xi \frac{\partial}{\partial x}(R^{-1}) + \frac{1}{2}\xi^2 \frac{\partial^2}{\partial x^2}(R^{-1}) + O(\xi^3)$$

$$R^2 > \xi^2 \qquad \xi^2 \ll 1 \qquad (2.19)$$

where

$$R = \left[r^2 + Y_0^2 \right]^{1/2}$$

$$r^2 = x^2 + z^2 \qquad Y_0 = Y - \eta \tag{2.20}$$

we obtain the three-term outer expansion

$$\tilde{\psi}^0(\vec{x}) \sim \frac{-1}{4\pi\rho} \left\{ \frac{\partial}{\partial z} \int_{-b}^{b} \frac{\tilde{\ell}(Y)}{R}\, d\eta \right.$$

$$+ \frac{\partial^2}{\partial x \partial z} \int_{-b}^{b} \frac{\tilde{m}(Y)}{R}\, d\eta + \frac{1}{2} \frac{\partial^3}{\partial x^2 \partial z} \int_{-b}^{b} \frac{\tilde{q}(Y)}{R}\, d\eta$$

$$\left. + \text{HOT} \right\} \tag{2.21}$$

where $(\,)^0$ indicates the outer region, HOT denotes higher order terms and

$$\tilde{\ell}(Y) = \int_{-C(Y)/A}^{C(Y)/A} \Delta\tilde{p}(\xi, Y)\, d\xi \sim O(A^{-1}) \qquad \uparrow + \tag{2.22}$$

$$\tilde{m}(Y) = -\int_{-C(Y)/A}^{C(Y)/A} \xi\, \Delta\tilde{p}(\xi, Y)\, d\xi \sim O(A^{-2}) \qquad \circlearrowleft + \tag{2.23}$$

$$\tilde{q}(Y) = \int_{-C(Y)/A}^{C(Y)/A} \xi^2\, \Delta\tilde{p}(\xi, Y)\, d\xi \sim O(A^{-3}) \qquad \circlearrowright + \tag{2.24}$$

This outer expansion is in agreement with that of James (1975) who gives the first two terms of (2.21).

The outer expansion, thus, consists of spanwise distributions of

three-dimensional multipoles along the loaded line. The first terms is a distribution of dipoles of strength equal to section lift. The second term is a distribution of quadrupoles of strength equal to section moment about the mid chord (positive nose up). The higher order terms consist of distributions of higher order multipoles of strength equal to higher moments of section lift about the mid chord. Hence, retaining more terms renders the outer expansion an increasingly accurate representation of the full problem. The sign and order of magnitude of the strength of the first three terms are indicated in (2.22) - (2.24).

Inner Expansion of Outer Expansion

Later, for the purpose of matching, we will need an inner expansion of this outer expansion, i.e., an approximation for (2.21) as $r \to 0$ (or as $A \to \infty$ with $\hat{r} \equiv Ar = O(A^0)$). To this end, first we carry out the indicated differentiations to obtain

$$\tilde{\psi}^0(\vec{x}) \sim \frac{-1}{4\pi\rho} \left\{ \int_{-b}^{b} \tilde{l}(\eta) \frac{-z}{[r^2 + y_0^2]^{3/2}} \, d\eta \right.$$

$$+ \int_{-b}^{b} \tilde{m}(\eta) \frac{3xz}{[r^2 + y_0^2]^{5/2}} \, d\eta$$

$$+ \int_{-b}^{b} \tilde{q}(\eta) \frac{3z[z^2 - 4x^2 + y_0^2]}{2[r^2 + y_0^2]^{7/2}} \, d\eta$$

$$\left. + \text{HOT} \right\} \qquad (2.25)$$

Due to the increasingly singular nature of the kernel functions of (2.25), straight forward expansions are not adequate and will give rise to

divergent integrals. This can be avoided by first integrating under the integral with respect to y and placing $\partial/\partial y$ in front of the integral; an idea familiar from slender-body theory for related integrals (see Heaslet and Lomax (1953)). Repeated applications of this idea to (2.25) leads to

$$\tilde{\psi}^{o}(\vec{x}) \sim \frac{-1}{4\pi\rho}\left\{\frac{-z}{2r^2}\frac{\partial^3}{\partial y^3}\int_{-b}^{b}\tilde{\ell}(\eta)\left[y_o\sqrt{r^2+y_o^2}\right.\right.$$

$$\left.+ r^2 \log\left(y_o+\sqrt{r^2+y_o^2}\right)\right]d\eta$$

$$+\frac{xz}{r^4}\frac{\partial^3}{\partial y^3}\int_{-b}^{b}\tilde{m}(\eta)\, y_o\sqrt{r^2+y_o^2}\; d\eta$$

$$+\frac{3}{2}z\frac{\partial^4}{\partial y^4}\int_{-b}^{b}\tilde{q}(\eta)\left\{\frac{r^2+4(z^2-4x^2)}{45r^6}\left[r^2+y_o^2\right]^{3/2}\right.$$

$$\left.\left.+\frac{r^2-z^2+4x^2}{15r^4}\sqrt{r^2+y_o^2}\right\}d\eta + HOT\right\} \qquad (2.26)$$

We can now expand the integrals. First, we break up each integral into three parts.

$$I = \int_{-b}^{b} = \int_{-b}^{y-\epsilon} + \int_{y-\epsilon}^{y+\epsilon} + \int_{y+\epsilon}^{b} \qquad (2.27)$$

$$= I_1 + I_\epsilon + I_2$$

where $\epsilon > 0$ is a small neighborhood of $y = \eta$. In I_1 and I_2, we expand the kernels for $r \to 0$ with ϵ fixed, noting that $y_o > 0$ for the former and $y_o < 0$ for the latter. In I_ϵ, we expand the integrand for $\epsilon \to 0$ with r fixed. In each case we find

$$I_\epsilon \sim O(\epsilon) \tag{2.28}$$

which vanishes as $\epsilon \to 0$. Next, we combine I_1 and I_2 for each of the integrals in (2.26), let $\epsilon \to 0$, take the indicated derivatives and introduce the magnified (inner) variables

$$\begin{aligned} \hat{x} &= Ax = \hat{r}\cos\theta \\ \hat{z} &= Az = \hat{r}\sin\theta \\ \hat{r} &= Ar = A\sqrt{x^2+y^2} \end{aligned} \tag{2.29}$$

to obtain the inner expansion of the three-term outer expansion.

$$\tilde{\psi}^{oi}(\vec{x}) \sim \frac{1}{2\pi\rho}\Bigg\{ A\,\tilde{\ell}(y)\,\frac{\sin\theta}{\hat{r}} + \frac{1}{4A}\,\hat{r}\sin\theta\cdot$$

$$\cdot\Big[\frac{\partial^3}{\partial y^3}\int_{-b}^{b}\tilde{\ell}(\eta)\log|y-\eta|\,\mathrm{sgn}(y-\eta)\,d\eta$$

$$+\Big(1+2\log\frac{2A}{\hat{r}}\Big)\,\tilde{\ell}''(y)\Big] + O(A^{-3}\tilde{\ell})\Bigg\} \quad \text{dipole}$$

$$-A^2\,\tilde{m}(y)\,\frac{\sin 2\theta}{\hat{r}^2}$$

$$-\frac{1}{4}\,\tilde{m}''(y)\sin 2\theta + O(A^{-2}\tilde{m}) \quad \text{quadrupole}$$

$$+A^3\,\tilde{q}(y)\,\frac{\sin 3\theta}{\hat{r}^3}$$

$$\left.\begin{aligned} &-\frac{1}{8} A \tilde{q}''(y) \frac{\sin\theta - \sin 3\theta}{\hat{r}} \\ &+ O(A^{-1}\tilde{q}) \end{aligned}\right\} \text{octapole}$$

$$+ \text{HOT} \Big\} \quad A \to \infty \quad \hat{r} \sim O(A^0) \quad |y| \leq b \qquad (2.30)$$

where $(\,)'$ denotes derivative with respect to the indicated argument.

Here, the terms denoted by "dipole" are the inner expansion of the first term of the outer expansion, (2.21). As $r \to 0$, the spanwise distribution of three-dimensional dipoles reduces to a two-dimensional dipole plus additional terms of higher order which represent the three-dimensional correction. A similar explanation applies to the terms denoted by "quadrupole" and "octapole".

Van Holten (1975), using the method of separation of variables, has solved the outer problem for a rigid rectangular wing in steady flow and obtained the dipole and the quadropole expansions, as in (2.30), but the corresponding result for the oscillating rigid wing is not given. The two expansions are in overall agreement, though detailed correlation of the corresponding coefficients is not feasible. James (1975) has also obtained the first term of the dipole and the quadrupole expansions as well as the order of magnitude of the higher order terms. Except for a missing factor of A, his result is in agreement with (2.30) (apparently a misprint).

2.4 Inner Solution and Eigensolutions for the Acceleration Potential

The inner region is that part of the flow field where distances from the wing are of the order of the chord, i.e., $O(A^{-1})$. As $A \to \infty$, the chord

and, hence, the inner region become vanishingly small. In order to study the details of the flow near the wing, we magnify the variables in the cross-sectional plane of the wing so that the two-dimensional (airfoil) character of the flow is emphasized. Thus,

$$\begin{aligned} \hat{x} &= Ax \\ \hat{y} &= y \\ \hat{z} &= Az \end{aligned} \tag{2.31}$$

The characteristic length scale in the inner region is the magnified semi chord c(y).

In the boundary value problem at hand, time enters in through the boundary condition at the wing. In the Laplace equation and the remaining boundary conditions, it appears only as a parameter. In terms of the inner variables, the wing boundary condition becomes

$$W_o^i = \left(\frac{1}{A}\frac{\partial}{\partial t} + U\frac{\partial}{\partial \hat{x}}\right)\hat{h} = W_o \tag{2.32}$$

$$|\hat{x}| \leq c(y) \qquad |y| \leq b \qquad \hat{z} = 0\pm$$

where $\hat{h} = Ah$ and $(\,)^i$ denotes the inner region. In (2.32), we may think of At as a stretched time

$$\hat{t} = At \tag{2.33}$$

This is strictly for mathematical convenience and does not change the solution.

In the inner region, we further assume that the acceleration potential may be expanded in an asymptotic series in inverse aspect ratio of the form

$$\psi^i(\hat{\vec{x}},\hat{t}) \sim \psi_0^i(\hat{\vec{x}},\hat{t}) + A^{-1}\log A\ \psi_1^i(\hat{\vec{x}},\hat{t})$$
$$+ A^{-1}\psi_2^i(\hat{\vec{x}},\hat{t}) + A^{-2}\log A\ \psi_3^i(\hat{\vec{x}},\hat{t}) \qquad (2.34)$$
$$+ A^{-2}\psi_4^i(\hat{\vec{x}},\hat{t}) + \cdots \qquad A\to\infty$$

where $\hat{\vec{x}} = (\hat{x},y,\hat{z})$. Since in inviscid flows physical quantities are independent of scale (see,e.g., Ashley and Landahl (1965), pp. 5-7), the first term of the expansion is $O(A^0)$. James (1975) assumed an expansion whose leading term is $O(A^{-1})$ which is incorrect. This is, however, balanced by the missing factor of A in his ψ^{oi} and hence the structure of his solution is not affected. We have included logarithmic terms in (2.34) because of the anticipated matching to ψ^{oi}, (2.30), which contains a logarithmic term. Another source of logarithmic terms in the inner solution is the low-reduced-frequency expansion of Theodorsen's function discussed later in this section. Matching will show, however, that the $O(A^{-1}\log A)$ term in (2.34) is not needed.

Introducing (2.31) - (2.34) into the full problem, (2.10) - (2.15), we obtain a series of simplified problems for the ψ_n^i. The lowest order inner solution ψ_o^i satisfies the following boundary value problem.

$$\hat{\nabla}_2^2\psi_0^i(\hat{\vec{x}},\hat{t}) = \left(\frac{\partial^2}{\partial\hat{x}^2} + \frac{\partial^2}{\partial\hat{z}^2}\right)\psi_0^i = 0$$

$$\frac{\partial}{\partial\hat{z}}\psi_0^i(\hat{\vec{x}},\hat{t}) = \left(\frac{\partial}{\partial\hat{t}} + U\frac{\partial}{\partial\hat{x}}\right)W_0^i(\hat{x},Y,\hat{t})$$

$$|\hat{x}| \le c(Y) \qquad |Y| \le b \qquad \hat{z} = 0\pm \qquad (2.35)$$

$$\psi_0^i(\hat{\vec{x}},\hat{t}) = 0 \qquad |\hat{x}| > c(Y) \qquad \hat{z} = 0$$

$$|\psi_o^i(\hat{\vec{x}},\hat{t})| < \infty \qquad \hat{x} = c(y) \quad |y| \le b \quad \hat{z} = 0$$

$$\psi_o^i(\hat{\vec{x}},\hat{t}) \to ? \qquad \hat{r} \to \infty$$

where the subscript $(\ )_2$ indicates a two-dimensional Laplacian. The main simplification here is in the reduction of the three-dimensional Laplace equation to a two-dimensional one. We have assigned all of the boundary condition at the wing W_o^i to ψ_o^i. It can be shown that this does not affect the complete inner solution ψ^i. The reason for this choice is that it makes the lowest order inner solution ψ_o^i the exact two-dimensional unsteady airfoil solution ψ_{2D}^i which is the dominant feature of the inner solution.

The loss of the boundary condition at infinity is due to the stretching of the variables and implies the presence of certain eigensolutions in the solution. Hence, ψ_o^i consists of multiples of these eigensolutions, ψ_{2D}^i and multiples of eigensolutions with $\partial\psi^i/\partial\hat{z} = 0$ at the wing. The eigensolutions will be determined later in this section.

The boundary value problem governing ψ_1^i, ψ_2^i and ψ_3^i is:

$$\hat{\nabla}_2^2 \psi(\hat{\vec{x}},\hat{t}) = 0$$

$$\frac{\partial\psi(\hat{\vec{x}},\hat{t})}{\partial\hat{z}} = 0 \qquad |\hat{x}| \le c(y) \quad |y| \le b \quad \hat{z} = 0\pm$$

$$\psi(\hat{\vec{x}},\hat{t}) = 0 \qquad |\hat{x}| > c(y) \quad \hat{z} = 0 \qquad (2.36)$$

$$|\psi(\hat{\vec{x}},\hat{t})| < \infty \qquad \hat{x} = c(y) \quad |y| \le b \quad \hat{z} = 0$$

$$\psi(\hat{\vec{x}},\hat{t}) \to ? \qquad \hat{r} \to \infty$$

The solution of this homogenous boundary value problem consists of eigensolutions alone.

ψ_4^i is the solution of the boundary value problem:

$$\hat{\nabla}_2^2 \psi_4^i(\hat{\vec{x}}, \hat{t}) = -\frac{\partial^2}{\partial y^2} \psi_o^i(\hat{\vec{x}}, \hat{t})$$

$$\frac{\partial \psi_4^i(\hat{\vec{x}}, \hat{t})}{\partial \hat{z}} = 0 \qquad |\hat{x}| \leq c(y) \quad |y| \leq b \quad \hat{z} = 0 \pm$$

$$\psi_4^i(\hat{\vec{x}}, \hat{t}) = 0 \qquad |\hat{x}| > c(y) \quad \hat{z} = 0 \qquad (2.37)$$

$$|\psi_4^i(\hat{\vec{x}}, \hat{t})| < \infty \qquad \hat{x} = c(y) \quad |y| \leq b \quad \hat{z} = 0$$

$$\psi_4^i(\hat{\vec{x}}, \hat{t}) \rightarrow ? \qquad \hat{r} \rightarrow \infty$$

The solution of (2.37) consists of a homogeneous solution, a particular solution and eigensolutions of the Laplace equation. ψ_4^i enters into the solution to determine higher order three-dimensional effects.

Wu's Unsteady Airfoil Theory

To determine the solution of (2.35), we note that with the additional boundary condition

$$\psi_o^i(\hat{\vec{x}}, \hat{t}) \rightarrow 0 \qquad \hat{r} \rightarrow \infty$$

ψ_o^i is the solution of a classical two-dimensional boundary value problem. Wu (1971a) has obtained the general solution of this problem which is valid throughout the flow field. For steady-state harmonic oscillations and in

terms of the inner variables, his solution, for arbitrary shapes and motions of the wing sections, is given by

$$f^{i}(\hat{\zeta},y,\hat{t}) = \frac{1}{\pi i}\left[\frac{\hat{\zeta}-c}{\hat{\zeta}+c}\right]^{1/2}\int_{-c}^{c}\left[\frac{c+\hat{\xi}}{c-\hat{\xi}}\right]^{1/2}\frac{\varphi(\hat{\xi},y,\hat{t})}{\hat{\xi}-\hat{\zeta}}\,d\hat{\xi} \qquad (2.38)$$

$$\varphi(\hat{x},y,\hat{t}) = U A_0(y,\hat{t}) + \varphi_1(\hat{x},y,\hat{t}) \qquad (2.38a)$$

$$\varphi_1(\hat{x},y,\hat{t}) = -\left(\frac{\partial}{\partial\hat{t}} + U\frac{\partial}{\partial\hat{x}}\right)\int_{-c}^{\hat{x}} W_0^{i}(\hat{\xi},y,\hat{t})\,d\hat{\xi} \qquad |\hat{x}| \le c(y) \qquad (2.38b)$$

$$U A_0(y,\hat{t}) = \frac{U}{2}\,a_0(y,\hat{t}) - \frac{1}{\pi}\int_{-c}^{c}\frac{d\hat{\xi}}{\sqrt{c^2-\hat{\xi}^2}}\,\varphi_1(\hat{\xi},y,\hat{t}) \qquad (2.38c)$$

$$a_0(y,\hat{t}) = b_1(y,\hat{t}) - \left[b_0(y,\hat{t}) + b_1(y,\hat{t})\right]\mathbb{C}(k) \qquad (2.38d)$$

$$W_0^{i}(\hat{x},y,\hat{t}) = \left(\frac{\partial}{\partial\hat{t}} + U\frac{\partial}{\partial\hat{x}}\right)\hat{h}(\hat{x},y,\hat{t}) = \frac{1}{2}\,b_0(y,\hat{t}) + \sum_{n=1}^{\infty} b_n(y,\hat{t})\cos n\theta \qquad (2.38e)$$

$$b_n(y,\hat{t}) = \frac{2}{\pi}\int_{0}^{\pi} W_0^{i}(\hat{x},y,\hat{t})\cos n\theta\,d\theta \qquad n = 0,1,2,\cdots \qquad (2.38f)$$

Here, $f^{i}(\hat{\zeta},y,\hat{t})$ is the complex acceleration potential with respect to the inner variables defined as

$$f^i(\hat{\zeta}, y, \hat{t}) = \psi^i(\hat{\bar{x}}, \hat{t}) + i\,\sigma^i(\hat{\bar{x}}, \hat{t}) \qquad (2.39)$$

where σ^i is the conjugate harmonic function of ψ^i and i is the spatial complex unit (note, $ij \neq -1$). Further,

$$\hat{\zeta} = \hat{x} + i\,\hat{z}$$
$$\hat{x} = c(y)\cos\theta \qquad (2.40)$$

and k is the reduced frequency based on the local semi chord, namely

$$k(y) = \frac{\omega}{U}\,\frac{c(y)}{A} \sim O(A^{-1}) \qquad (2.41)$$

In (2.38d), $\mathbb{C}(k)$ is Theodorsen's function defined as

$$\mathbb{C}(k) = F(k) + j\,G(k) = \frac{H_1^{(2)}(k)}{H_1^{(2)}(k) + j\,H_0^{(2)}(k)} \qquad (2.42)$$

where $H_n^{(2)}$ is the Hankel function of the second kind of order n defined as

$$H_n^{(2)}(z) = J_n(z) - j\,Y_n(z) \qquad (2.43)$$

J_n and Y_n are Bessel functions of the first and second kind of order n respectively. It follows from (2.42) and (2.43) that

$$F(k) = \frac{J_1(J_1 + Y_0) + Y_1(Y_1 - J_0)}{(J_1 + Y_0)^2 + (Y_1 - J_0)^2}$$
$$G(k) = \frac{-(Y_1 Y_0 + J_1 J_0)}{(J_1 + Y_0)^2 + (Y_1 - J_0)^2} \qquad (2.44)$$

where the argument of all Bessel functions is k. $\mathbb{C}(k)$ is plotted as a complex vector in Figure 2.4.

Wu's solution yields the acceleration potential throughout the flow field as is needed for the present MAE analysis. Wu's solution is also unique having been formulated directly in terms of the downwash at the wing w_c^i instead of the vertical acceleration $\partial\psi_o^i/\partial\hat{z}$.

Calculation of the pressure field from (2.38) for most wing displacements of interest requires evaluation of integrals of the form

$$Q_n(\hat{\xi},y) = \int_{-c}^{c} \left[\frac{c+\hat{\xi}}{c-\hat{\xi}}\right]^{1/2} \frac{\hat{\xi}^n}{\hat{\xi}-\hat{\xi}}\, d\hat{\xi} \qquad (2.45)$$

$$n = 0,1,2,\ldots$$

The first five members of this family are evaluated and listed in part 1 of Appendix A.

Using Wu's method, the exact two-dimensional unsteady airfoil solution ψ_{2D}^i is determined. For later use, we list here the acceleration potential in complex form.

$$\tilde{f}_{2D}^i(\hat{\xi},y) = -i\left\{B_1(y)\left[-\hat{\xi}^2 + \left(\hat{\xi}^2 + c\hat{\xi} + \frac{c^2}{2}\right)\lambda\right] + B_2(y)\left[-\hat{\xi} + \sqrt{\hat{\xi}^2 - c^2}\right] + B_3(y)\left[\lambda - 1\right]\right\} \qquad (2.46a)$$

where

$$\tilde{\psi}_{2D}^i(\hat{\vec{x}}) = \mathcal{R}_i\left[\tilde{f}_{2D}^i(\hat{\xi},y)\right] \qquad (2.46b)$$

$\mathcal{R}_i$ denotes the real part of a complex quantity with respect to i and

$$\lambda = \left[\frac{\hat{\xi}-c}{\hat{\xi}+c}\right]^{1/2} \qquad (2.47)$$

$$B_1(y) = \frac{1}{2c^2}\, U^2 k^2 \alpha \tag{2.48}$$

$$B_2(y) = \frac{1}{c} U^2 \left[k_0 k \left(\frac{h_0}{c_0}\right) - 2jk\alpha \right] \tag{2.49}$$

$$B_3(y) = U^2 \left\{ -\frac{1}{4}(k^2 - 2jk)\alpha \right.$$

$$\left. - \left[jk_0 \left(\frac{h_0}{c_0}\right) + \left(1 + \frac{j}{2} k\right)\alpha \right] \mathbb{C}(k) \right\} \tag{2.50}$$

where

$$k_0 = \frac{\omega}{U} \frac{c_0}{A} \tag{2.51}$$

is the reduced frequency based on the the root semi chord c_0/A. The lowest order inner solution is then given by

$$\tilde{\psi}_0^i(\hat{\vec{X}}) = \tilde{\psi}_{2D}^i(\hat{\vec{X}}) + \text{ eigensolutions} \tag{2.52}$$

Eigensolutions of the Acceleration Potential

Next, we determine the eigensolutions of the inner solution. These satisfy the homogeneous problem defined in (2.36). We consider two cases. First, we assume $\psi(\hat{\vec{X}},\hat{t}) \to 0$ as $\hat{r} \to \infty$. The solution of this problem can be obtained using Wu's method. However, first we must express the boundary condition at the wing $\partial\psi/\partial\hat{z} = 0$ in terms of downwash. This can be done by inverting the z-component of the linearized Euler equation

$$\frac{\partial}{\partial\hat{z}} \psi(\hat{\vec{X}},\hat{t}) = \left(\frac{\partial}{\partial\hat{t}} + U\frac{\partial}{\partial\hat{x}}\right) w^i(\hat{\vec{X}},\hat{t}) \tag{2.53}$$

written for convenience in terms of the inner variables. The downwash at

the wing is given by

$$\tilde{W}_o^i(\hat{x},y,0\pm) = \frac{1}{U} \lim_{\hat{z}\to 0\pm} \int_{-\infty}^{\hat{x}} \frac{\partial}{\partial \hat{z}} \tilde{\psi}(\hat{\xi},y,\hat{z})\, e^{j\bar{\omega}(\hat{\xi}-\hat{x})A^{-1}}\, d\hat{\xi}$$

$$|\hat{x}| \le c(y) \qquad |y| \le b \qquad (2.54)$$

where $\bar{\omega} = \omega/U$. Using $\partial\psi/\partial\hat{z} = 0$ on the wing, this becomes

$$W_o^i(\hat{x},y,0\pm,\hat{t}) = \tilde{W}_g(y)\, e^{-j\bar{\omega}\hat{x}A^{-1}}\, e^{j\omega\hat{t}A^{-1}}$$

$$|\hat{x}| \le c(y) \qquad |y| \le b \qquad (2.55)$$

where

$$\tilde{W}_g(y) = \frac{1}{U} \lim_{\hat{z}\to 0\pm} \int_{-\infty}^{-c(y)} \frac{\partial \tilde{\psi}(\hat{\xi},y,\hat{z})}{\partial \hat{z}}\, e^{j\bar{\omega}\hat{\xi}A^{-1}}\, d\hat{\xi} \qquad (2.56)$$

Physically, the above result indicates that, in the presence of a harmonically oscillating wing, a fluid particle traveling from far upstream attains a sinusoidal downwash velocity of varying amplitude (a convecting gust). Since for the present eigensolution $\partial\psi/\partial\hat{z} = 0$ at the wing, the complex amplitude of the sinusoidal gust $\tilde{W}_g(y)$ is constant across the chord, although it varies with y. Therefore, one eigensolution is essentially the solution to the Sears problem: the interaction of a convecting sinusoidal gust of constant amplitude with an airfoil.

Using (2.55), we can rewrite the boundary condition at the wing in terms of downwash as

$$\frac{\partial \Psi}{\partial \hat{z}}(\hat{\vec{x}},\hat{t}) = \left(\frac{\partial}{\partial \hat{t}} + U\frac{\partial}{\partial \hat{x}}\right)\left[-\tilde{W}_g(y)\, e^{-j\bar{\omega}\hat{x}A^{-1}}\, e^{j\omega\hat{t}A^{-1}}\right] = 0$$

$$|\hat{x}| \le c(y) \quad |y| \le b \quad \hat{z} = 0\pm \qquad (2.57)$$

Using Wu's method, the solution of (2.36) with $\Psi \to 0$ as $\hat{r} \to \infty$ is determined. For later use, we present here the acceleration potential in complex form.

$$\tilde{f}^{i}_{Sears}(\hat{y},y) = -i\,U\,\tilde{W}_g(y)\,S(k)\,[\lambda - 1] \qquad (2.58a)$$

where

$$\tilde{\Psi}^{i}_{Sears}(\hat{\vec{x}}) = \mathcal{R}_i\left[\tilde{f}^{i}_{Sears}(\hat{y},y)\right] \qquad (2.58b)$$

λ is defined in (2.47) and S(k) is the Sears function defined as

$$S(k) = j\,J_1(k) + [J_0(k) - j\,J_1(k)]\,C(k) \qquad (2.59)$$

S(k) is shown as a complex vector in Figure 2.5. (2.58a) is a generalization of Sear's original result (Sears (1941)) in that it gives the pressure throughout the flow field.

In passing, we note that a similar analysis yields the eigensolution for the steady case as a flat plate at an angle of attack. This result can also be obtained from (2.58a) in the limit of steady flow ($\omega \to 0$).

In addition to Ψ^{i}_{Sears}, there are an infinite number of eigensolutions which satisfy (2.36) but do not vanish at infinity. They can be found by inspection as

$$\tilde{\Psi}^{i}_{1}(\hat{\vec{x}}) = \tilde{\Psi}^{i}_{2D,\,heave}(\hat{\vec{x}}) + (\omega/A)^2\,\hat{z} \qquad (2.60)$$

$$\tilde{\Psi}^{i}_{2}(\hat{\vec{x}}) = \tilde{\Psi}^{i}_{2D,\,pitch}(\hat{\vec{x}}) + (\omega/A)^2\,\hat{x}\hat{z} - 2j\,\frac{\omega U}{A}\,\hat{z} \qquad (2.61)$$

.
.
.

The first member of this family, (2.60), consists of the pressure field of an airfoil in heaving motion of unit amplitude and the pressure field necessary to cancel out the resulting vertical acceleration at the airfoil so that $\partial\Psi/\partial\hat{z}=0$. The second eigensolution, (2.61), consists of the pressure field of an airfoil in pitching motion of unit arplitude and the pressure field necessary to cancel out the resulting vertical acceleration at the airfoil. The other eigensolutions involve oscillating airfoils with chordwise bending. In each eigensolution, while the airfoil term vanishes at infinity, the remaining terms do not. As we will see, in the present theory to obtain the leading three-dimensional corrections, only Ψ^{c}_{Seavs} is required. The other eigensolutions enter in at higher orders.

Expansion of Inner Solution for Small Reduced Frequency

In the present model, since the wing chord $c(y)/A \sim O(A^{-1})$ (see Figures 2.3a and 2.3b), the reduced frequency based on the chord $k(y) = (\omega/U)c(y)/A$ is also $O(A^{-1})$. Hence, $k \to 0$ as $A \to \infty$. Therefore, we must expand all elements of the inner solution for small k. These contain Theodorsen's function which we expand first.

$$\mathcal{C}(k) \sim 1 + jk \log(\gamma_1 k/2) - \frac{\pi}{2} k + O(k^2 \log^2 k) \qquad (2.62)$$

$$\mathcal{C}(k) \sim 1 - \nu\left[\frac{\pi}{2} - j \log(\gamma_1 \nu/2)\right] A^{-1} - j\nu A^{-1} \log A + O(A^{-2} \log^2 A) \qquad (2.63)$$

where $\log \gamma_1 = \gamma = .57721\ldots$ is the Euler constant and $\nu(y) = \omega c(y)/U$ is the reduced frequency based on the magnified semi chord c(y). The

expansion in (2.63) displays the aspect ratio dependencies explicitly.

The expansion of Ψ^i_{2D} for small k is obtained from (2.46b) using (2.63).

$$\tilde{\Psi}^i_{2D}(\hat{\bar{x}}) \sim \tilde{\Psi}^i_{2D,1}(\hat{\bar{x}}) + A^{-1}\log A\ \tilde{\Psi}^i_{2D,2}(\hat{\bar{x}}) + A^{-1}\tilde{\Psi}^i_{2D,3}(\hat{\bar{x}}) + O(A^{-2}\log^2 A) \qquad (2.64)$$

where

$$\tilde{\Psi}^i_{2D,1}(\hat{\bar{x}}) = -U^2\alpha\ \mathcal{J}_i[\lambda] \qquad (2.64a)$$

$$\tilde{\Psi}^i_{2D,2}(\hat{\bar{x}}) = j\nu U^2\alpha\ \mathcal{J}_i[\lambda] \qquad (2.64b)$$

$$\tilde{\Psi}^i_{2D,3}(\hat{\bar{x}}) = -j\nu U^2\left\{\left\{\left[\log(\gamma_1\nu/2) + j\frac{\pi}{2}\right]\alpha + \frac{h_o}{c}\right\}\cdot \mathcal{J}_i[\lambda] + \frac{2\alpha}{c}\mathcal{J}_i\left[-\hat{s} + \sqrt{\hat{s}^2 - c^2}\right]\right\} \qquad (2.64c)$$

are all $O(A^0)$ quantities. We note that the $A^{-1}\log A$ term in (2.64) originates in the expansion of Theodorsen's function as mentioned earlier. $\mathcal{J}_i$ denotes the imaginary part of a complex quantity with respect to i.

We will see shortly that there is no need to expand Ψ^i_{Sears} for small k. The expansions for the other eigensolutions are readily obtained from the above expansion for Ψ^i_{2D}. Setting $\alpha = 0$ and $h_o = 1$ in (2.64) - (2.64c), we obtain the expansion for $\Psi^i_{2D,\,heave}$ which leads to

$$\tilde{\Psi}^i_1(\hat{\bar{x}}) \sim (\omega/A)^2\hat{z} - A^{-1}j\omega U\ \mathcal{J}_i[\lambda] + O(A^{-2}\log^2 A) \qquad (2.65)$$

Similarly, setting $\alpha = 1$ and $h_o = 0$ in (2.64) - (2.64c), we obtain the expasion for $\Psi^i_{2D,\,pitch}$ and, hence,

$$\tilde{\Psi}_2^i(\hat{\vec{x}}) \sim \left(\frac{\omega}{A}\right)^2 \hat{x}\hat{z} - 2j\,\frac{\omega U}{A}\,\hat{z} - U^2\,\mathcal{G}_i[\lambda]$$
$$+ A^{-1}\log A\; j\nu U^2\,\mathcal{G}_i[\lambda]$$
$$- A^{-1} j\nu U^2 \left\{\left[\log(\gamma_1\nu/2) + j\frac{\pi}{2}\right]\mathcal{G}_i[\lambda]\right.$$
$$\left. + \frac{2}{c}\,\mathcal{G}_i\left[-\hat{y} + \sqrt{\hat{y}^2 - c^2}\,\right]\right\} + O(A^{-2}\log^2 A) \qquad (2.66)$$

Similar expansions can be obtained for the remaining eigensolutions.

The inner expansion, thus, becomes

$$\tilde{\Psi}^i(\hat{\vec{x}}) \sim \tilde{\Psi}^i_{0,1}(\hat{\vec{x}}) + A^{-1}\log A\;\tilde{\Psi}^i_{0,2}(\hat{\vec{x}})$$
$$+ A^{-1}\,\tilde{\Psi}^i_{0,3}(\hat{\vec{x}}) + O(A^{-2}\log^2 A) \qquad (2.67)$$

Each element of this expansion contains all possible eigensolutions, i.e.,

$$\tilde{\Psi}^i_{0,n}(\hat{\vec{x}}) = \tilde{\Psi}^i_{2D,n}(\hat{\vec{x}}) + F_n(y)\,\tilde{\Psi}^i_{Sears}(\hat{\vec{x}})$$
$$+ f_n(y)\,\tilde{\Psi}^i_1(\hat{\vec{x}}) + g_n(y)\,\tilde{\Psi}^i_2(\hat{\vec{x}}) + \cdots \qquad (2.68)$$
$$n = 1, 2, 3, \cdots$$

where the as-yet-unknown functions F_n, f_n, g_n, ... are the respective weighting functions for the eigensolutions present in $\Psi^i_{0,n}$. These will be determined by matching the acceleration potential in the field and the downwash at the wing. Without loss of generality, we assume that F_n, f_n, g_n,... are $O(A^0)$. Also,

$$\tilde{\Psi}^i_{Sears}(\hat{\vec{x}}) = \mathcal{G}_i[\lambda] \qquad (2.69)$$

where we have absorbed the terms multiplying $\mathcal{G}_i[\lambda]$ in Ψ^i_{Sears}, (2.58b), into the unknown function $F_n(y)$. Hence, there is no need to expand Ψ^i_{Sears}

for small k since ψ^{i}_{Sears} is independent of k.

Outer Expansion of Inner Expansion

In the next section, for the purpose of matching, we will need the outer expansion of the inner expansion, i.e., an expansion for (2.67) as $\hat{r}\to\infty$ or, equivalently, an expansion for $A\to\infty$ with $r = \hat{r}/A = O(A^{0})$. This can be done using the following expansions (written in terms of the outer variables).

$$\mathcal{G}_i[\lambda] \sim \left(\frac{c}{A}\right)\frac{\sin\theta}{r} - \frac{1}{2}\left(\frac{c}{A}\right)^2\frac{\sin 2\theta}{r^2} + \frac{1}{2}\left(\frac{c}{A}\right)^3\frac{\sin 3\theta}{r^3} + O(A^{-4}) \tag{2.70}$$

$$\frac{1}{c}\mathcal{G}_i\left[-\hat{s} + \sqrt{\hat{s}^2 - c^2}\right] \sim \frac{1}{2}\left(\frac{c}{A}\right)\frac{\sin\theta}{r} + O(A^{-3}) \tag{2.71}$$

Using (2.70) and (2.71), the outer expansion of (2.64a) - (2.64c) is found to be

$$\tilde{\psi}^{io}_{2D,1}(\hat{\vec{x}}) \sim \frac{1}{2\pi\rho}\left\{\left[-2\pi\rho U^2\left(\frac{c}{A}\right)\alpha\right]\frac{\sin\theta}{r} + \left[\pi\rho U^2\left(\frac{c}{A}\right)^2\alpha\right]\frac{\sin 2\theta}{r^2} + \left[-\pi\rho U^2\left(\frac{c}{A}\right)^3\alpha\right]\frac{\sin 3\theta}{r^3} + O(A^{-4})\right\} \tag{2.72}$$

$$\tilde{\psi}^{io}_{2D,2}(\hat{\vec{x}}) \sim \frac{1}{2\pi\rho}\left\{\left[2\pi\rho U^2 j\nu\left(\frac{c}{A}\right)\alpha\right]\frac{\sin\theta}{r} + \left[-\pi\rho U^2 j\nu\left(\frac{c}{A}\right)^2\alpha\right]\frac{\sin 2\theta}{r^2} + O(A^{-3})\right\} \tag{2.73}$$

$$\tilde{\psi}^{io}_{2D,3}(\hat{\vec{x}}) \sim \frac{1}{2\pi\rho}\left\{-2\pi\rho U^2 j\nu\left\{\left[\log(\gamma_1\nu/2) + j\frac{\pi}{2} + 1\right]\alpha + \frac{h_o}{c}\right\}\cdot\left(\frac{c}{A}\right)\frac{\sin\theta}{r} +\right.$$

$$+\pi\rho U^2 j\nu \left\{ \left[\log(\gamma_1 \nu/2) + j\frac{\pi}{2} \right] \alpha + \frac{h_0}{c} \right\} \left(\frac{c}{A}\right)^2 \frac{\sin 2\theta}{r^2} + O(A^{-3}) \Big\} \tag{2.74}$$

The outer expansion of ψ^i_{Sears} is given by (2.70). The outer expansion of the other eigensolutions are obtained from (2.65) and (2.66) using (2.70) and (2.71). Thus,

$$\tilde{\Psi}_1^{io}(\hat{\vec{x}}) \sim \frac{\omega^2}{A} r \sin\theta + \frac{1}{2\pi\rho}\left[-2\pi\rho U^2 j\nu \frac{1}{A^2} \frac{\sin\theta}{r} + O(A^{-3}) \right] \tag{2.75}$$

$$\tilde{\Psi}_2^{io}(\hat{\vec{x}}) \sim \frac{1}{2}\omega^2 r^2 \sin 2\theta - 2j\omega U r \sin\theta + \frac{1}{2\pi\rho}\left[-2\pi\rho U^2 \left(\frac{c}{A}\right) \frac{\sin\theta}{r} + O(A^{-2}) \right] \tag{2.76}$$

This completes the inner expansion and its outer expansion. The result of James (1975) for ψ^{io} is basically correct, except it lacks the eigensolutions, it has not been expanded for $k \to 0$ and has an extra factor of A^{-1}. Van Holten (1975) does not give an expression for ψ^{io}. In the next section, the inner and outer solutions for the acceleration potential are matched.

2.5 Matching

As mentioned earlier, the inner and outer solutions are incomplete representations of the full problem, each lacking some essential features. The inner solution is incomplete since it lacks the boundary condition at infinity which gives rise to eigensolutions, the amount of which are still unknown. The outer solution is also incomplete in that it lacks the

boundary conditions at the wing. As a result, the load distribution in the outer solution is unknown (Δp or the strength of the multipoles, i.e., l, m, q, ...).

The solution is completed (except for determining the amount of some of the eigensolutions) by matching the inner and outer solutions for the acceleration potential. The amount of the remaining eigensolutions is determined when the downwash at the wing is matched. Here, we employ the asymptotic matching principle of Van Dyke (1975). For the sake of brevity, we employ the notation:

$m\mathrm{I}$: m-term inner expansion

$n\phi$: n-term outer expansion

The asymptotic matching principle then reads

$$m\mathrm{I}\,(n\phi) = n\phi\,(m\mathrm{I}) \tag{2.77}$$

We now summarize a step-by-step application of the matching principle to the present problem. The matching order is depicted schematically in Figure 2.6. We will use the outer expansion (2.21); the inner expansion of the outer expansion (2.30); the inner expansion (2.67) and (2.68); and the outer expansion of the inner expansion (2.70) - (2.76). The inner and outer expansions must be matched with respect to the same spatial variables.

<u>Matching, m = n = 1</u>

1ϕ:

$$\tilde{\psi}^{o}(\vec{X}) \sim \frac{-1}{4\pi\rho}\frac{\partial}{\partial z}\int_{-b}^{b}\frac{\tilde{\ell}(\eta)}{R}\,d\eta \tag{2.78}$$

where $R = \sqrt{x^2 + (y-\eta)^2 + z^2}$.

1I(1ϕ):

$$\tilde{\psi}^{oi}(\vec{x}) \sim \frac{1}{2\pi\rho} A \tilde{\ell}(y) \frac{\sin\theta}{\hat{r}} \qquad (2.79)$$

where $\hat{r} = Ar = A\sqrt{x^2 + z^2}$.

1I:

$$\tilde{\psi}^{i}(\hat{\vec{x}}) \sim \tilde{\psi}^{i}_{o,1}(\hat{\vec{x}}) = \tilde{\psi}^{i}_{2D,1}(\hat{\vec{x}}) + F_1(y)\,\tilde{\psi}^{i}_{Sears}(\hat{\vec{x}})$$

$$+ f_1(y)\,\tilde{\Psi}^{i}_{1}(\hat{\vec{x}}) + g_1(y)\,\tilde{\Psi}^{i}_{2}(\hat{\vec{x}}) + \cdots \qquad (2.80)$$

1ϕ(1I):

$$\tilde{\psi}^{io}(\hat{\vec{x}}) \sim \frac{1}{2\pi\rho}\left[-2\pi\rho U^2\alpha + 2\pi\rho F_1(y)\right]\left(\frac{\varsigma}{A}\right) \frac{\sin\theta}{r}$$

$$+ f_1(y)\,\tilde{\Psi}^{io}_{1}(\hat{\vec{x}}) + g_1(y)\,\tilde{\Psi}^{io}_{2}(\hat{\vec{x}}) + \cdots \qquad (2.81)$$

where Ψ^{io}_1 and Ψ^{io}_2 are given in (2.75) and (2.76). Matching (2.79) and (2.81), we obtain

$$\tilde{\ell}(y) = -2\pi\rho U^2\left(\frac{\varsigma}{A}\right)\alpha + 2\pi\rho\left(\frac{\varsigma}{A}\right)F_1(y) \qquad (2.82)$$

$$f_1(y) = g_1(y) = \cdots = 0 \qquad (2.83)$$

Thus, to leading order, the solution contains no eigensolutions, except possibly ψ^{i}_{Sears}. Section lift consists of the two-dimensional quasi-steady value plus a possible contribution from ψ^{i}_{Sears}.

<u>Matching, m = 1, n = 2</u>

2ϕ:

$$\tilde{\psi}^{o}(\vec{x}) \sim \frac{-1}{4\pi\rho}\left\{\frac{\partial}{\partial z}\int_{-b}^{b}\frac{\tilde{\ell}(\eta)}{R}\,d\eta + \right.$$

$$+\frac{\partial^2}{\partial x \partial z}\int_{-b}^{b}\frac{\tilde{m}(\eta)}{R}\,d\eta\Bigg\} \qquad (2.84)$$

1I(2ϕ):

$$\tilde{\psi}^{oi}(\vec{x}) \sim \frac{1}{2\pi\rho}\left\{A\,\tilde{\ell}(y)\,\frac{\sin\theta}{\hat{r}} - A^2\,\tilde{m}(y)\,\frac{\sin 2\theta}{\hat{r}^2}\right\} \qquad (2.85)$$

1I:

$$\tilde{\psi}^{i}(\hat{\vec{x}}) \sim \tilde{\psi}^{i}_{2D,1}(\hat{\vec{x}}) + F_1(y)\,\tilde{\psi}^{i}_{Sears}(\hat{\vec{x}}) \qquad (2.86)$$

2ϕ(1I):

$$\tilde{\psi}^{io}(\hat{\vec{x}}) \sim \frac{1}{2\pi\rho}\left\{\left[-2\pi\rho U^2\alpha + 2\pi\rho\,F_1(y)\right]\left(\frac{c}{A}\right)\frac{\sin\theta}{r}\right.$$

$$\left.+\left[\pi\rho U^2\alpha - \pi\rho\,F_1(y)\right]\left(\frac{c}{A}\right)^2\frac{\sin 2\theta}{r^2}\right\} \qquad (2.87)$$

Matching (2.85) and (2.87), we obtain

$$\tilde{\ell}(y) = -2\pi\rho U^2\left(\frac{c}{A}\right)\alpha + 2\pi\rho\left(\frac{c}{A}\right)F_1(y) \qquad (2.88)$$

$$\tilde{m}(y) = -\pi\rho U^2\left(\frac{c}{A}\right)^2\alpha + \pi\rho\left(\frac{c}{A}\right)^2 F_1(y) \qquad (2.89)$$

At this stage, section lift and moment have their two-dimensional quasi-steady value plus possible contributions from ψ^{i}_{Sears}.

<u>Matching, m = n = 2</u>

2ϕ:

$$\tilde{\psi}^{o}(\vec{x}) \sim \frac{-1}{4\pi\rho}\left\{\frac{\partial}{\partial z}\int_{-b}^{b}\frac{\tilde{\ell}(\eta)}{R}\,d\eta\right.$$

$$\left.+\frac{\partial^2}{\partial x\partial z}\int_{-b}^{b}\frac{\tilde{m}(\eta)}{R}\,d\eta\right\} \qquad (2.90)$$

2I(2ϕ):

$$\tilde{\psi}^{oi}(\vec{x}) \sim \frac{1}{2\pi\rho}\left\{ A\,\tilde{\ell}(\gamma)\,\frac{\sin\theta}{\hat{r}} - A^2\,\tilde{m}(\gamma)\,\frac{\sin 2\theta}{\hat{r}^2}\right\} \qquad (2.91)$$

2I:

$$\tilde{\psi}^{i}(\hat{\vec{x}}) \sim \tilde{\psi}^{i}_{2D,1}(\hat{\vec{x}}) + F_1(\gamma)\,\tilde{\psi}^{i}_{Sears}(\hat{\vec{x}}) + A^{-1}\log A\;\tilde{\psi}^{i}_{0,2}(\hat{\vec{x}}) + A^{-1}\,\tilde{\psi}^{i}_{0,3}(\hat{\vec{x}}) \qquad (2.92)$$

2ϕ(2I):

$$\tilde{\psi}^{io}(\hat{\vec{x}}) \sim \frac{1}{2\pi\rho}\left\{\left[-2\pi\rho U^2\alpha + 2\pi\rho F_1(\gamma)\right]\left(\frac{c}{A}\right)\frac{\sin\theta}{r} + \left[\pi\rho U^2\alpha - \pi\rho F_1(\gamma)\right]\left(\frac{c}{A}\right)^2\frac{\sin 2\theta}{r^2}\right\}$$

$$+A^{-1}\log A\,\frac{1}{2\pi\rho}\left\{\left[2\pi\rho U^2 j\nu\alpha + 2\pi\rho F_2(\gamma)\right]\left(\frac{c}{A}\right)\frac{\sin\theta}{r} + 2\pi\rho f_2(\gamma)\,\tilde{\Psi}^{io}_1(\hat{\vec{x}}) + 2\pi\rho g_2(\gamma)\,\tilde{\Psi}^{io}_2(\hat{\vec{x}}) + \cdots\right\}$$

$$+A^{-1}\frac{1}{2\pi\rho}\left\{-2\pi\rho U^2 j\nu\left\{\left[\log(\gamma_1\nu/2) + j\frac{\pi}{2} + 1\right]\alpha + \frac{h_o}{A}\right\}\left(\frac{c}{A}\right)\frac{\sin\theta}{r} + 2\pi\rho F_3(\gamma)\left(\frac{c}{A}\right)\frac{\sin\theta}{r} + 2\pi\rho f_3(\gamma)\,\tilde{\Psi}^{io}_1(\hat{\vec{x}}) + 2\pi\rho g_3(\gamma)\,\tilde{\Psi}^{io}_2(\hat{\vec{x}}) + \cdots\right\} \qquad (2.93)$$

Matching (2.91) and (2.93), we obtain

$$\tilde{\ell}(y) = -2\pi\rho U^2 \left(\frac{c}{A}\right)\alpha + 2\pi\rho\left(\frac{c}{A}\right) F_1(y)$$

$$+ A^{-1}\log A\left[2\pi\rho U^2 j\nu\left(\frac{c}{A}\right)\alpha + 2\pi\rho\left(\frac{c}{A}\right) F_2(y)\right]$$

$$+ A^{-1}\left\{-2\pi\rho U^2 j\nu\left\{\left[\log(\gamma_1\nu/2) + j\frac{\pi}{2} + 1\right]\alpha\right.\right.$$

$$\left.\left. + \frac{h_o}{c}\right\}\left(\frac{c}{A}\right) + 2\pi\rho\left(\frac{c}{A}\right) F_3(y)\right\} \qquad (2.94)$$

$$\tilde{m}(y) = -\pi\rho U^2\left(\frac{c}{A}\right)^2\alpha + \pi\rho\left(\frac{c}{A}\right)^2 F_1(y) \qquad (2.95)$$

$$f_2(y) = g_2(y) = \cdots = 0 \qquad (2.96)$$

$$f_3(y) = g_3(y) = \cdots = 0 \qquad (2.97)$$

Thus, we find that to $O(A^{-2})$ only the sears eigensolution ψ^c_{Sears} is present in the solution. Furthermore, while section moment remains the same as in the previous level of matching (see (2.89)), section lift is further refined with two-dimensional unsteady information plus a possible contribution from ψ^c_{Sears}. We will see in the next section that the latter represents the three-dimensional unsteady correction.

Matching, m = 2, n = 3

3ϕ:

$$\tilde{\psi}^o(\vec{x}) \sim \frac{-1}{4\pi\rho}\left\{\frac{\partial}{\partial z}\int_{-b}^{b}\frac{\tilde{\ell}(\eta)}{R}\,d\eta + \frac{\partial^2}{\partial x\partial z}\int_{-b}^{b}\frac{\tilde{m}(\eta)}{R}\,d\eta\right.$$

$$\left. + \frac{1}{2}\frac{\partial^3}{\partial x^2\partial z}\int_{-b}^{b}\frac{\tilde{q}(\eta)}{R}\,d\eta\right\} \qquad (2.98)$$

2I(3ϕ):

$$\tilde{\psi}^{oi}(\vec{x}) \sim \frac{1}{2\pi\rho}\left\{ A\,\tilde{\ell}(y)\,\frac{\sin\theta}{\hat{r}} - A^2\,\tilde{m}(y)\,\frac{\sin 2\theta}{\hat{r}^2} + A^3\,\tilde{q}(y)\,\frac{\sin 3\theta}{\hat{r}^3}\right\} \qquad (2.99)$$

2I:

$$\tilde{\psi}^{i}(\hat{\vec{x}}) \sim \tilde{\psi}^{i}_{2D,1}(\hat{\vec{x}}) + F_1(y)\,\tilde{\psi}^{i}_{Sears}(\hat{\vec{x}}) + A^{-1}\log A\left[\tilde{\psi}^{i}_{2D,2}(\hat{\vec{x}}) + F_2(y)\,\tilde{\psi}^{i}_{Sears}(\hat{\vec{x}})\right] + A^{-1}\left[\tilde{\psi}^{i}_{2D,3}(\hat{\vec{x}}) + F_3(y)\,\tilde{\psi}^{i}_{Sears}(\hat{\vec{x}})\right] \qquad (2.100)$$

3ϕ(2I):

$$\begin{aligned}\tilde{\psi}^{io}(\hat{\vec{x}}) \sim \frac{1}{2\pi\rho}\Bigg\{&\left[-2\pi\rho U^2\alpha + 2\pi\rho F_1(y)\right]\left(\frac{c}{A}\right)\frac{\sin\theta}{r} + \left[\pi\rho U^2\alpha - \pi\rho F_1(y)\right]\left(\frac{c}{A}\right)^2\frac{\sin 2\theta}{r^2} \\ &+\left[-\pi\rho U^2\alpha + \pi\rho F_1(y)\right]\left(\frac{c}{A}\right)^3\frac{\sin 3\theta}{r^3}\Bigg\} \\ +A^{-1}\log A\,\frac{1}{2\pi\rho}\Bigg\{&\left[2\pi\rho U^2 j\nu\alpha + 2\pi\rho F_2(y)\right]\left(\frac{c}{A}\right)\frac{\sin\theta}{r} \\ &-\left[\pi\rho U^2 j\nu\alpha + \pi\rho F_2(y)\right]\left(\frac{c}{A}\right)^2\frac{\sin 2\theta}{r^2}\Bigg\} \\ +A^{-1}\,\frac{1}{2\pi\rho}\Bigg\{&-2\pi\rho U^2 j\nu\left\{\left[\log(\gamma_1\nu/2) + j\frac{\pi}{2} + 1\right]\alpha + \frac{h_o}{c}\right\}\left(\frac{c}{A}\right)\frac{\sin\theta}{r} \\ &+\pi\rho U^2 j\nu\left\{\left[\log(\gamma_1\nu/2) + j\frac{\pi}{2}\right]\alpha + \frac{h_o}{c}\right\}\left(\frac{c}{A}\right)^2\frac{\sin 2\theta}{r^2} +\end{aligned}$$

$$+ 2\pi\rho F_3(y)\left(\frac{c}{A}\right)\frac{\sin\theta}{r} - \pi\rho F_3(y)\left(\frac{c}{A}\right)^2\frac{\sin 2\theta}{r^2}\Bigg\} \tag{2.101}$$

Matching (2.99) and (2.101), we find that section lift is given by (2.94) and

$$\begin{aligned}\tilde{m}(y) = {} & -\pi\rho U^2\left(\frac{c}{A}\right)^2\alpha + \pi\rho\left(\frac{c}{A}\right)^2 F_1(y) \\ & + A^{-1}\log A\left[\pi\rho U^2 j\nu\left(\frac{c}{A}\right)^2\alpha + \pi\rho\left(\frac{c}{A}\right)^2 F_2(y)\right] \\ & + A^{-1}\Bigg\{-\pi\rho U^2 j\nu\Bigg\{\left[\log(\gamma_1\nu/2) + j\frac{\pi}{2}\right]\alpha + \frac{h_0}{c}\Bigg\}\cdot \\ & \cdot\left(\frac{c}{A}\right)^2 + \pi\rho\left(\frac{c}{A}\right)^2 F_3(y)\Bigg\}\end{aligned} \tag{2.102}$$

$$\tilde{q}(y) = -\pi\rho U^2\left(\frac{c}{A}\right)^3\alpha + \pi\rho\left(\frac{c}{A}\right)^3 F_1(y) \tag{2.103}$$

In this level of matching, we find that, while section lift remains the same as in the previous level, section moment is further refined with two-dimensional unsteady information plus a possible contribution from ψ^i_{Seavs}. We will see, in the next section, that the latter represent the three-dimensional unsteady correction. At this level, we also note the appearance of the second moment of section lift, namely q(y), which has its two-dimensional quasi-steady value, namely $-\pi\rho U^3 (c/A)^3 \alpha$.

The next level of matching (m = n = 3) involves ψ^i_4 which is the solution of the Poisson equation in (2.37). The outer expansion of ψ^i_4 has the behavior $r \log r \sin\theta$, $r \sin\theta$ and $\sin 2\theta$ which will match with higher-order terms of ψ^{oi}, (2.30). Further, at this level, for the first

time, the eigensolution Ψ_1^i, which also has the behavior r sin θ in the outer region, may enter into the solution. However, for reasons we already mentioned, we will not carry out the analysis to higher orders. We will see in the next section that the present analysis through (m = 3, n = 2) level contains the leading three-dimensional correction.

We can now construct a composite solution, namely one which is uniformly valid (to $O(A^{-2})$) throughout the flow field. Such a solution is given by

$$\begin{aligned}\psi^c &= \psi^i + \psi^o - \psi^{io} \\ &= \psi^i + \psi^o - \psi^{oi}\end{aligned} \tag{2.104}$$

where $\psi^{io} = \psi^{oi}$ is the common solution. To $O(A^{-2})$, ψ^i is given by (2.100) which, using (2.64) - (2.64c), may be written as

$$\tilde{\psi}^i(\hat{\vec{x}}) = \tilde{\psi}^i_{2D}(\hat{\vec{x}}) + \left[F_1(y) + \bar{A}^{-1}\log A\, F_2(y) + \bar{A}^{-1}F_3(y)\right]\tilde{\psi}^i_{Sears}(\hat{\vec{x}}) \tag{2.105}$$

without altering its accuracy. We will see in the next section that using (2.105) instead of (2.100) will facilitate downwash calculation greatly. To $O(A^{-2})$,

$$\tilde{\psi}^o(\vec{x}) = \frac{-1}{4\pi\rho}\frac{\partial}{\partial z}\int_{-b}^{b}\frac{\tilde{\ell}_o(\eta)}{\sqrt{x^2+(y-\eta)^2+z^2}}\,d\eta \tag{2.106}$$

$$\begin{aligned}\tilde{\psi}^{io}(\hat{\vec{x}}) &= \tilde{\psi}^{oi}(\vec{x}) \\ &= \frac{1}{2\pi\rho}\tilde{\ell}_o(y)\frac{\sin\theta}{r} = \frac{1}{2\pi\rho}\tilde{\ell}_o(y)\frac{z}{x^2+z^2}\end{aligned} \tag{2.107}$$

where

$$\tilde{\ell}_o(y) = -2\pi \rho U^2 \left(\frac{c}{A}\right) \alpha \qquad (2.108)$$

is the two-dimensional quasi-steady section lift. Here, ψ^o consists of a spanwise distribution of three-dimensional dipoles of strength $\tilde{\ell}_o(y)$ and ψ^{io} is a two-dimensional dipole of strength $\tilde{\ell}_o(y)$. ψ^{io} is chosen in such a way that it is equal to ψ^o in the inner region to $O(\bar{A}^{-2})$ and it is equal to ψ^i in the outer region to $O(\bar{A}^{-2})$.

Clearly, the problem is not complete yet since the solution as it stands is nonunique due to the presence of multiples of ψ^i_{Sears} as indicated by the as-yet-unknown weighting functions $F_1(y)$, $F_2(y)$ and $F_3(y)$. In the next section, we will determine F_1, F_2 and F_3 and, thus, complete the solution to $O(\bar{A}^{-2})$.

2.6 Integration of Composite Pressure Field to Achieve Uniqueness

To achieve uniqueness for the solution, we determine the downwash by integrating the composite pressure field ψ^c from far upstream to some point on the wing.

The linearized Euler equation in the z-direction is given by

$$\left(\frac{\partial}{\partial t} + U\frac{\partial}{\partial x}\right) w(\vec{x},t) = \frac{\partial}{\partial z}\psi^c(\vec{x},t) \qquad (2.109)$$

Inverting this, we obtain the downwash.

$$\tilde{w}(\vec{x}) = U^{-1}\int_{-\infty}^{x} \frac{\partial}{\partial z}\tilde{\psi}^c(\xi,y,z)\, e^{j\bar{\omega}(\xi-x)}\, d\xi \qquad (2.110)$$

where the linearized path of integration is the straight line, parallel to

the x-axis, from far upstream to the point in question. For points on the wing, the path is defined as

$$\xi = -\infty \rightarrow x \qquad |x| \leq c(y)/A$$
$$y = \text{fixed} \qquad |y| \leq b \qquad (2.111)$$
$$z = 0\pm$$

which passes over (or under) the leading edge where one might expect difficulty due to the singular behavior of pressure and downwash there. An examination of $\partial\psi^c/\partial z$ near the leading edge reveals that

$$\frac{\partial\psi^c}{\partial z} \sim \frac{\partial\psi^i}{\partial\hat{z}} \sim \mathcal{R}_i\left[(\hat{\zeta}+c)^{-3/2}\right] \qquad \hat{\zeta} \rightarrow -c(y) \qquad (2.112)$$

which is not integrable.

Calculation of Downwash at the Wing Due to ψ^i

First, We calculate the downwash due to ψ^i, say w^i, which is obtained from (2.110), after replacing ψ^c by ψ^i and introducing the inner variables. The difficulty at the leading edge can be resolved by considering the general case of $\hat{z} \neq 0$. After expressing the integral in terms of complex variables, an integration by parts can be performed. This reduces the order of the leading-edge singularity to -1/2 which is integrable. Then, we can take $\lim \hat{z} \rightarrow 0\pm$. Since the downwash field is an even function of $\hat{z}$, it suffices to consider $\lim \hat{z} \rightarrow 0+$ only.

Introducing the complex variable $\hat{\zeta} = \hat{x} + i\hat{z}$ and the complex acceleration potential for ψ^i, namely $f^i(\hat{\zeta}, y, \hat{t})$, (2.39), into (2.110), we obtain, for $\hat{z} \neq 0$,

$$\tilde{W}^i(\hat{\vec{X}}) = -U^{-1}\mathcal{J}_i\left\{\int_{-\infty+i\hat{z}}^{\hat{\zeta}} \frac{\partial}{\partial\hat{\zeta}_1}\tilde{f}^i(\hat{\zeta}_1,Y)\, e^{j\bar{\omega}(\hat{\zeta}_1-\hat{\zeta})A^{-1}}\, d\hat{\zeta}_1\right\} \tag{2.114}$$

where $\hat{\zeta}_1 = \hat{\xi}_1 + i\,\hat{z}$. Integrating by parts and noting that $\tilde{f}^i(-\infty + i\,\hat{z}, y) = 0$ (because both f^i_{2D} and f^i_{Sears} (see below) vanish as $\hat{r}\to\infty$), we obtain

$$\tilde{W}^i(\hat{\vec{X}}) = -U^{-1}\mathcal{J}_i\left[\tilde{f}^i(\hat{\zeta},Y)\right] \tag{2.115}$$

$$+\frac{j\bar{\omega}}{UA}\mathcal{J}_i\left\{\int_{-\infty+i\hat{z}}^{\hat{\zeta}} \tilde{f}^i(\hat{\zeta}_1,Y)\, e^{j\bar{\omega}(\hat{\zeta}_1-\hat{\zeta})A^{-1}}\, d\hat{\zeta}_1\right\}$$

where f^i has a square-root singularity at the leading edge which is integrable. Hence, we can take $\lim \hat{z}\to 0+$, resulting in

$$\tilde{W}^i(x,Y,0+) = -U^{-1}\mathcal{J}_i\left[\tilde{f}^i(x+i0+,Y)\right] \tag{2.116}$$

$$+\frac{j\bar{\omega}}{UA}\int_{-\infty}^{\hat{x}}\mathcal{J}_i\left[\tilde{f}^i(\hat{\xi}+i0+,Y)\right]e^{j\bar{\omega}(\hat{\xi}-\hat{x})A^{-1}}\, d\hat{\xi}$$

$$|\hat{x}| \le c(y) \qquad |Y| \le b$$

The above procedure is depicted schematically in Figure 2.7.

To $O(A^{-2})$, f^i consists of f^i_{2D} and $\mathfrak{f}^i_{Sears}$ where $\mathfrak{f}^i_{Sears}$ is the complex form of ψ^i_{Sears}. $\mathfrak{f}^i_{Sears}$ is obtained from (2.58a) after removing the factor $UW(y)S(k)$ which is absorbed into the function $F_\eta(y)$. As expected, substituting f^i_{2D}, (2.46a), in (2.116) yields the prescribed downwash at the wing, i.e.,

$$\tilde{W}^{i}_{2D}(\hat{x},y,0+) = W^{i}_{o}(\hat{x},y) \qquad |\hat{x}| \leq c(y) \qquad |y| \leq b \tag{2.117}$$

In arriving at this result we have made use of some of the analytic properties of the functions $[(\hat{\zeta}-c)/(\hat{\zeta}+c)]^{1/2}$ and $[\hat{\zeta}^2-c^2]^{1/2}$ which are listed in Table 2.1 below. Each of the functions has a branch cut from $\hat{\zeta} = -c$ to $\hat{\zeta} = c$ defined by

$$\begin{aligned} 0 &\leq \arg(\hat{\zeta}+c) < 2\pi \\ 0 &\leq \arg(\hat{\zeta}-c) < 2\pi \end{aligned} \tag{2.118}$$

Further, we have made use of the integrals developed in part 2 of Appendix A.

	$\left[\frac{\hat{\zeta}-c}{\hat{\zeta}+c}\right]^{1/2}$	$\sqrt{\hat{\zeta}^2-c^2}$
$\lvert\hat{x}\rvert \leq c \quad \hat{z}=0+$	$i\left[\frac{c-\hat{x}}{c+\hat{x}}\right]^{1/2}$	$i\sqrt{c^2-\hat{x}^2}$
$\lvert\hat{x}\rvert \leq c \quad \hat{z}=0-$	$-i\left[\frac{c-\hat{x}}{c+\hat{x}}\right]^{1/2}$	$-i\sqrt{c^2-\hat{x}^2}$
$\hat{x} < -c \quad \hat{z}=0$	$\left[\frac{\hat{x}-c}{\hat{x}+c}\right]^{1/2}$	$-\sqrt{\hat{x}^2-c^2}$
$\hat{x} > c \quad \hat{z}=0$	$\left[\frac{\hat{x}-c}{\hat{x}+c}\right]^{1/2}$	$\sqrt{\hat{x}^2-c^2}$

Table 2.1. Some of the analytic properties of $[(\hat{\zeta}-c)/(\hat{\zeta}+c)]^{1/2}$ and $[\hat{\zeta}^2-c^2]^{1/2}$.

The downwash at the wing due to f^i_{Sears}, say W^i_{Sears}, is obtained from (2.58a) and (2.116), using some of the above mentioned integrals and Table 2.1.

$$\tilde{W}^i_{Sears}(\hat{x}, y, 0+) = \frac{j\pi}{2U} k\, e^{-j\bar{\omega}\hat{x}A^{-1}} \left[H_1^{(2)}(k) + j H_0^{(2)}(k)\right] \tag{2.119}$$

Clearly, the downwash at the wing due to f^i_{Sears} is that in (2.57).

Putting the above results for W^i in (2.110), for points on the wing, and setting the computed downwash equal to the prescribed value W^i_0, we obtain the following equation for F_1, F_2 and F_3.

$$\cancel{\tilde{W}^i_0(\hat{x}, y)} = \cancel{\tilde{W}^i_0(\hat{x}, y)}$$

$$+ \frac{j\pi}{2U} k\, e^{-j\bar{\omega}x} \left[F_1(y) + A^{-1}\log A\, F_2(y) + A^{-1} F_3(y)\right]\left[H_1^{(2)}(k) + jH_0^{(2)}(k)\right]$$

$$+ \lim_{z\to 0+} \left[\tilde{W}^o(x,y,z) - \tilde{W}^{oi}(x,y,z)\right] e^{-j\bar{\omega}x} \tag{2.120}$$

$$|x| \leq c(y)/A \qquad |y| \leq b$$

where

$$e^{-j\bar{\omega}x}\tilde{W}^o(x,y,z) = \frac{1}{U}\int_{-\infty}^{x} \frac{\partial}{\partial z}\tilde{\Psi}^o(\xi,y,z)\, e^{j\bar{\omega}(\xi-x)}\, d\xi \tag{2.121}$$

$$e^{-j\bar{\omega}x}\tilde{W}^{oi}(x,y,z) = \frac{1}{U}\int_{-\infty}^{x} \frac{\partial}{\partial z}\tilde{\Psi}^{oi}(\xi,y,z)\, e^{j\bar{\omega}(\xi-x)}\, d\xi \tag{2.122}$$

are the downwash velocities due to the outer and common solutions respectively. They are grouped together, in (2.120), because, as we will see below, while each of them is singular as $z \to 0$, their difference is finite. Further, in (2.120), we note that the downwash due to ψ^i_{zD} identically cancels out with the prescribed value at the wing. This demonstrates the advantage of assigning all of the wing boundary condition W_o^i to the lowest order inner solution ψ^i_o which makes $\psi^i_o = \psi^i_{zD}$ (see (2.35)) and of replacing the two-term expansion of ψ^i_{zD} in ψ^i by ψ^i_{zD} (see(2.105)).

We now consider the balance of the two remaining terms in (2.120). After cancelling out the common sinusoidal dependence on x, we conclude that, since the first term is independent of x, the second term must be independent of x too. Hence, we need to evaluate the second term for one value of x only. It is convenient to choose x = 0. $\tilde{W}^o(0,y,z)$ is then the downwash due to ψ^o near the loaded line which consists of a spanwise distribution of three-dimensional dipoles of strength $\tilde{l}_o(y)$ (see (2.106)). Similarly, $\tilde{W}^{oi}(0,y,z)$ is the downwash due to ψ^{oi} near the two-dimensional dipole of strength $\tilde{l}_o(y)$. Clearly, both downwash velocities are singular for x = 0 and z = 0. Hence, we seek an expansion for each, for x = 0 and small positive z. In each case, lim $x \to 0$ must be carried out before lim $z \to 0$, otherwise infinite downwash velocities will be encountered. Physically, this can be seen by considering the downwash, as a concentrated vortex, say at the origin, is approached along the z- or alternately the x-axes.

In order to be consistent, first we expand the Hankel functions in (2.120) for $A \to \infty$ (or $k \to 0$). Using the definition of Hankel function of

the second kind (see (2.43)) and the asymptotic expansions for Bessel functions of the first and second kind of order zero and one for small arguments, it can be shown that

$$\left\{-j\frac{\pi}{2}k\left[H_1^{(2)}(k)+j\,H_0^{(2)}(k)\right]\right\}^{-1}\sim 1+O(A^{-1}\log A) \qquad (2.123)$$

Using this result, (2.120) becomes

$$F_1(Y)+A^{-1}\log A\,F_2(Y)+A^{-1}F_3(Y)\sim U\lim_{z\to 0+}$$

$$\left[\tilde{W}^{o}(0,Y,z)-\tilde{W}^{oi}(0,Y,z)\right]\left[1+O(A^{-1}\log A)\right] \qquad (2.124)$$

To determine F_1, F_2 and F_3, it only remains to determine $\lim_{z\to 0+}[\tilde{W}^{o}(0,y,z) - \tilde{W}^{oi}(0,y,z)]$.

Calculation of $W^{o}(0,y,z,t)$ as $z\to 0+$

Substituting ψ^{o}, (2.106), in (2.121) with x = 0 and interchanging the order of integration, we obtain

$$\tilde{W}^{o}(0,Y,z)=\frac{1}{4\pi\rho U}\int_{-b}^{b}d\eta\,\tilde{\ell}_o(\eta)\left\{-\frac{\partial^2}{\partial z^2}\int_{-\infty}^{0}\frac{e^{j\bar{\omega}\lambda}}{\sqrt{\lambda^2+Y_o^2+z^2}}\,d\lambda\right\} \qquad (2.125)$$

We recognize the expression in the braces as the three-dimensional, nonplanar ($z \neq 0$) unsteady kernel function of lifting-surface theory in incompressible flow for $x_o = 0$. The general form of the kernel function is

$$K_{3D}(X_o,Y_o,z)=-e^{-j\bar{\omega}X_o}\frac{\partial^2}{\partial z^2}\int_{-\infty}^{X_o}\frac{e^{j\bar{\omega}\lambda}}{\sqrt{\lambda^2+Y_o^2+z^2}}\,d\lambda \qquad (2.126)$$

with the corresponding integral equation of unsteady lifting-surface theory given by

$$\tilde{w}_o(x,y,0\pm) = \frac{1}{4\pi\rho U} \iint_{S_a} \Delta\tilde{p}(\xi,\eta) \lim_{z\to 0\pm} K_{3D}(x_o, y_o, z)\, d\xi\, d\eta \tag{2.127}$$

where

$$x_o = x - \xi$$
$$y_o = y - \eta \tag{2.128}$$

To evaluate the kernel function of (2.125), we start with the general form in (2.126). K_{3D} can be evaluated in terms of special functions. For example, see Widnall (1964) for $z \neq 0$ and Watkins, Runyan and Woolston (1955) for $z = 0$. The latter contains many useful integrals and relations for the evaluation of the kernel function. The full nonplanar K_{3D} is given by

$$-e^{j\bar{\omega}x_o} K_{3D}(x_o, y_o, z) = \frac{-\bar{\omega}}{r_1}\left\{K_1(\bar{\omega}r_1) + j\frac{\pi}{2}\left[I_1(\bar{\omega}r_1) - L_1(\bar{\omega}r_1)\right] - j\right\} + \frac{\bar{\omega}^2 z^2}{r_1^2}\left\{K_2(\bar{\omega}r_1) - j\frac{\pi}{2}\left[I_2(\bar{\omega}r_1) - L_2(\bar{\omega}r_1)\right] + j\frac{\bar{\omega}r_1}{3} - \frac{j}{\bar{\omega}r_1}\right\} + \frac{y_o^2}{r_1^3}\left\{\frac{j\bar{\omega}}{r_1}\int_0^{x_o} \frac{\lambda e^{j\bar{\omega}\lambda}}{\sqrt{\lambda^2 + r_1^2}}\, d\lambda - \frac{x_o e^{j\bar{\omega}x_o}}{r_1\sqrt{r_1^2 + x_o^2}}\right\} + \frac{z^2}{r_1^2}\left\{-\frac{\bar{\omega}^2}{r_1^2}\int_0^{x_o} \frac{\lambda^2 e^{j\bar{\omega}\lambda}}{\sqrt{\lambda^2 + r_1^2}}\, d\lambda - \frac{j\bar{\omega}x_o^2 e^{j\bar{\omega}x_o}}{r_1^2\sqrt{r_1^2 + x_o^2}} + \frac{(2r_1^2 + x_o^2)x_o e^{j\bar{\omega}x_o}}{r_1^2(x_o^2 + r_1^2)^{3/2}}\right\} \tag{2.129}$$

where I_n, K_n and L_n are modified Bessel functions of the first and second

kind of order n and modified Struve function of order n respectively and

$$r_1 = \sqrt{y_o^2 + z^2} \tag{2.130}$$

For $x_o = 0$, (2.129) reduces to

$$K_{3D}(0, y_o, z) = \frac{\bar{\omega}}{r_1}\left\{K_1(\bar{\omega} r_1) + j\frac{\pi}{2}\left[I_1(\bar{\omega} r_1) - L_1(\bar{\omega} r_1)\right] - j\right\}$$
$$- \frac{\bar{\omega}^2 z^2}{r_1^2}\left\{K_2(\bar{\omega} r_1) - j\frac{\pi}{2}\left[I_2(\bar{\omega} r_1) - L_2(\bar{\omega} r_1)\right] + j\frac{\bar{\omega} r_1}{3} - \frac{j}{\bar{\omega} r_1}\right\} \tag{2.131}$$

In order to understand the nature of the singularities involved in (2.125), we note that, from the vortex viewpoint, the outer solution consists of a loaded line which is a harmonically oscillating concentrated vortex with the accompanying wake of shed and trailing vorticity. As in the steady flow case, we expect the contribution of the trailing vorticity to the downwash at the loaded line ($x = 0$, $z \to 0+$) to be finite. This contribution can be expressed as an integral with a second order singularity in the span direction (or after an integration by parts, a Cauchy singularity). The contribution of the straight loaded line is clearly zero. The contribution of the shed vorticity is logarithmically infinite; an idea familiar from lifting surface theory, namely that the downwash at the edge of a vortex sheet, containing vorticity parallel to the edge and of finite strength, contains a logarithmic singularity.

Formally, we substitute (2.131) into (2.125) and, by inspection, group the terms in the kernel so as to identify the above mentioned logarithmic term and the classical second order singularity of wing theory. Let,

$$\tilde{W}^{\circ}(0, y, z) = \tilde{W}_1^{\circ}(0, y, z) + \tilde{W}_2^{\circ}(0, y, z)$$
$$+ \tilde{W}_3^{\circ}(0, y, z) + \tilde{W}_4^{\circ}(0, y, z) \tag{2.132}$$

where

$$\tilde{W}_1^o(0,Y,Z) = \frac{1}{4\pi\rho U}\int_{-b}^{b} d\eta\ \tilde{\ell}_o(\eta)\left[-j\frac{\bar{\omega}}{r_1} + j\frac{\bar{\omega}z^2}{r_1^3}\right] \qquad (2.133)$$

$$\tilde{W}_2^o(0,Y,Z) = \frac{1}{4\pi\rho U}\int_{-b}^{b} d\eta\ \tilde{\ell}_o(\eta)\left[\frac{\bar{\omega}}{r_1}K_1(\bar{\omega}r_1) - \frac{\bar{\omega}^2z^2}{r_1^2}K_2(\bar{\omega}r_1)\right] \qquad (2.134)$$

$$\tilde{W}_3^o(0,Y,Z) = \frac{1}{4\pi\rho U}\int_{-b}^{b} d\eta\ \tilde{\ell}_o(\eta)\, j\frac{\pi}{2}\left\{\frac{\bar{\omega}}{r_1}\left[I_1(\bar{\omega}r_1) - L_1(\bar{\omega}r_1)\right] + \frac{\bar{\omega}^2z^2}{r_1^2}\left[I_2(\bar{\omega}r_1) - L_2(\bar{\omega}r_1)\right]\right\} \qquad (2.135)$$

$$\tilde{W}_4^o(0,Y,Z) = \frac{1}{4\pi\rho U}\int_{-b}^{b} d\eta\ \tilde{\ell}_o(\eta)\left[-\frac{1}{3}j\frac{\bar{\omega}^3z^2}{r_1}\right] \qquad (2.136)$$

$\tilde{W}_1^o$, (2.133), contains the logarithmic term which can be isolated using the following procedure familiar from slender-body theory (see, e.g., Ashley and Landahl (1965), pp. 102-103). We note that the logarithmic term arises from the term $(-j\bar{\omega}/r_1)$ in the kernel of the integral in (2.133).

$$\tilde{W}_1^o(0,Y,Z) = \frac{-j\bar{\omega}}{4\pi\rho U}\int_{-b}^{b}\frac{\tilde{\ell}_o(\eta)\,Y_o^2}{\left[Y_o^2+Z^2\right]^{3/2}}\,d\eta$$

$$= \frac{-j\bar{\omega}}{4\pi\rho U}\left\{\tilde{\ell}_o(Y)\int_{-b}^{b}\frac{Y_o^2}{\left[Y_o^2+Z^2\right]^{3/2}}\,d\eta + \int_{-b}^{b}\left[\tilde{\ell}_o(\eta)-\tilde{\ell}_o(Y)\right]\frac{Y_o^2}{\left[Y_o^2+Z^2\right]^{3/2}}\,d\eta\right\} \qquad (2.137)$$

It can be shown that the last term here can be approximated as

$$\int_{-b}^{b} \left[\tilde{\ell}_o(\eta) - \tilde{\ell}_o(y)\right] \frac{y_o^2}{\left[y_o^2 + z^2\right]^{3/2}} d\eta$$

$$= \int_{-b}^{b} \frac{\tilde{\ell}_o(\eta) - \tilde{\ell}_o(y)}{|y-\eta|} d\eta + O(z^2 \log z) \qquad (2.138)$$

where the last integral has a removable singularity at $y = \eta$. The first term on the right hand side of (2.137) can be integrated and expanded for small z, to obtain

$$\int_{-b}^{b} \frac{y_o^2}{\left[y_o^2 + z^2\right]^{3/2}} d\eta = -2 - z \log (z/b)$$

$$+ \log 4\left[1-(y/b)^2\right] + O(z^2 \log z) \qquad (2.139)$$

Combining the above results, we obtain an expansion for $\tilde{W}_1^o$ for small z.

$$\tilde{W}_1^o(0,y,z) = \frac{-j\bar{\omega}}{4\pi\rho U} \tilde{\ell}_o(y)\left\{-2 - z \log (z/b) + \log 4\left[1-(y/b)^2\right]\right\}$$

$$- \frac{j\bar{\omega}}{4\pi\rho U} \int_{-b}^{b} \frac{\tilde{\ell}_o(\eta) - \tilde{\ell}_o(y)}{|y-\eta|} d\eta + O(z^2 \log z) \qquad (2.140)$$

$\tilde{W}_2^o$, (2.134), contains the classical second order span singularity of wing theory. First we break down the integral into three parts.

$$\int_{-b}^{b} = \int_{-b}^{y-\epsilon} + \int_{y-\epsilon}^{y+\epsilon} + \int_{y+\epsilon}^{b} \qquad (2.141)$$

where $\epsilon > 0$ denotes a small neighborhood of the singularity at $y = \eta$. In the integral containing the singularity, we introduce the expansions

$$K_1(z) \sim z^{-1} + O(z \log z) \quad z \to 0 \qquad (2.142)$$

$$K_2(z) \sim 2z^{-2} + O(z^2 \log z) \quad z \to 0 \tag{2.143}$$

$$\tilde{\ell}_0(\eta) \sim \tilde{\ell}_0(y) + (\eta - y)\tilde{\ell}_0'(y) + \frac{1}{2}(\eta - y)^2 \tilde{\ell}_0''(y) + \cdots \tag{2.144}$$

and the change of variables

$$\zeta = \eta - y$$

Then, we integrate term by term and take lim $z \to 0+$, to obtain

$$-\frac{2}{\epsilon}\tilde{\ell}_0(y) + O(\epsilon) \tag{2.145}$$

Clearly, the first term here is the contribution of the first term in (2.144). The second term of (2.144) makes no contribution and the contribution of the higher-order terms is $O(\epsilon)$ which vanishes as $\epsilon \to 0$.

As $z \to 0+$ and $\epsilon \to 0$, we recognize (2.145) together with the remaining two nonsingular integrals in (2.141) as the definition of the principle value of an integral with a second order singularity given, e. g., by Mangler (1951), namely

$$\oint_a^b \frac{F(\eta)}{(y-\eta)^2}\,d\eta = \lim_{\epsilon \to 0}\left[\int_a^{y-\epsilon} \frac{F(\eta)}{(y-\eta)^2}\,d\eta + \int_{y+\epsilon}^b \frac{F(\eta)}{(y-\eta)^2}\,d\eta - (2/\epsilon)\,F(y)\right] \tag{2.146}$$

In (2.134), since the contribution of the part of the kernel containing K_2 to the integral is $O(z^2)$, as $z \to 0+$, it vanishes everywhere except near the singularity, where it together with the rest of the kernel gives rise to (2.145). Therefore, we may drop the part of the kernel containing K_2 and put an x on the integral sign to signify the principle

value defined in (2.146). $\tilde{W}_2^o$, then, becomes

$$\tilde{W}_2^o(0,y,z) = \frac{1}{4\pi\rho U} \oint_{-b}^{b} \frac{\tilde{\ell}_o(\eta)}{(y-\eta)^2} \mu K_1(\mu)\, d\eta + O(z^2) \tag{2.147}$$

where

$$\mu = \bar{\omega}\,|y-\eta| \tag{2.148}$$

and we have written the integrand so as to display the $(y-\eta)^{-2}$ singularity explicitly.

Next, we consider $\tilde{W}_3^o$, defined in (2.135). First, we break down the integral into three parts as in (2.141). In the integral containing $\eta = y$, we expand the integrand using the following asymptotic expansions for small arguments

$$I_1(z) - L_1(z) \sim \frac{1}{2} z + O(z^2) \tag{2.149}$$

$$I_2(z) - L_2(z) \sim \frac{1}{8} z^2 + O(z^3) \tag{2.150}$$

to obtain the approximation

$$\int_{y-\epsilon}^{y+\epsilon} d\eta\, \tilde{\ell}_o(\eta)\, j\frac{\pi}{4}\bar{\omega}^2 + O(z^2) \tag{2.151}$$

It is seen that the contribution of the part of the kernel containing $I_2 - L_2$ to the integral is $O(z^2)$ everywhere and thus vanishes as $z \to 0+$. On the other hand, the contribution of the rest of the kernel is $O(1)$ and, hence, they are retained. $\tilde{W}_3^o$ then becomes

$$\tilde{W}_3^{\circ}(0,Y,z) = \frac{1}{4\pi\rho U}\int_{-b}^{b}\frac{\tilde{\ell}_0(\eta)}{(Y-\eta)^2}\, j\frac{\pi}{2}\,\mu\left[I_1(\mu)-L_1(\mu)\right]d\eta + O(z^2) \tag{2.152}$$

This integral is nonsingular. Here, we have written it in a form to be combined with $\tilde{W}_2^{\circ}$, (2.147), later.

$\tilde{W}_4^{\circ}$, defined in (2.136), is given by

$$\tilde{W}_4^{\circ}(0,Y,z) = \frac{1}{4\pi\rho U}\left(-\frac{1}{3}\,j\,\bar{\omega}^3 z^2\right)\int_{-b}^{b}\frac{\tilde{\ell}_0(\eta)}{\sqrt{Y_0^2+z^2}}\,d\eta \tag{2.153}$$

This integral appears in slender body theory where it is shown to be $O(\log z)$ as $z\to 0$ (see,e.g., Ashley and Landahl (1965), pp. 102-103). Hence,

$$\tilde{W}_4^{\circ}(0,Y,z) \sim O(z^2\log z) \tag{2.154}$$

Combining the above results, we obtain the following expansion for $\tilde{W}^{\circ}(0,y,z)$ as $z\to 0+$.

$$\tilde{W}^{\circ}(0,Y,z) \sim \frac{1}{4\pi\rho U}\,\text{⨍}_{-b}^{b}\frac{\tilde{\ell}_0(\eta)}{(Y-\eta)^2}\,\Pi(\bar{\omega}|Y-\eta|)\,d\eta$$

$$-\frac{j\bar{\omega}}{4\pi\rho U}\int_{-b}^{b}\frac{\tilde{\ell}_0(\eta)-\tilde{\ell}_0(Y)}{|Y-\eta|}\,d\eta$$

$$-\frac{j\bar{\omega}}{4\pi\rho U}\,\tilde{\ell}_0(Y)\left\{-2-2\log(z/b)+\log 4\left[1-(Y/b)^2\right]\right\}.$$

$$+O(z^2\log z) \qquad |Y|\le b \tag{2.155a}$$

where

$$\Pi(\mu) = \mu\left\{K_1(\mu)+j\frac{\pi}{2}\left[I_1(\mu)-L_1(\mu)\right]\right\} \tag{2.155b}$$

The unsteady induced downwash of James (1975) is closely related to $\tilde{w}^o$. In the present notation, it is given by

$$\tilde{w}_I(o,y,o+) \sim \frac{1}{4\pi\rho U} \oint_{-b}^{b} \frac{\tilde{\ell}(\eta)}{(y-\eta)^2} \Pi'(\bar{\omega}|y-\eta|)\, d\eta \qquad (2.156)$$

where

$$\Pi'(\mu) = \Pi(\mu) - j\mu \qquad (2.157)$$

Thus, Π' is just the first term of the three-dimensional unsteady kernel function K_{3D} for $x_o = 0$ (see (2.131)). James does not show that the integral in (2.156) is a principle value integral as indicated. In fact, it is not. This integral contains a nonremovable logarithmic singularity discussed in the above (arising from $(-j\mu)$ term in Π') and is, hence, infinite.

Calculation of $w^{oi}(o,y,z,t)$ as $z \to 0+$

Substituting ψ^{oi}, (2.107), in (2.122), with $x = 0$, and interchanging the order of integration, we obtain

$$\tilde{w}^{oi}(o,y,z) = \frac{1}{2\pi\rho U} \tilde{\ell}_o(y) \left\{ \frac{\partial}{\partial z} \int_{-\infty}^{0} \frac{z}{\lambda^2 + z^2} e^{j\bar{\omega}\lambda}\, d\lambda \right\} \qquad (2.158)$$

We recognize the expression in the braces as the two-dimensional, nonplanar ($z \neq 0$) unsteady kernel function of airfoil theory in incompressible flow with $x_o = 0$. The general form of the kernel function is

$$K_{2D}(x_o, z) = e^{-j\bar{\omega}x_o} \frac{\partial}{\partial z} \int_{-\infty}^{x_o} \frac{z}{\lambda^2 + z^2} e^{j\bar{\omega}\lambda}\, d\lambda \qquad (2.159)$$

with the corresponding integral equation of unsteady airfoil theory given by

$$\tilde{W}_o(x,0\pm) = \frac{1}{2\pi\rho U}\int_{LE}^{TE} \Delta\tilde{p}(\xi)\lim_{z\to 0\pm} K_{2D}(x_o,z)\,d\xi \qquad (2.160)$$

To evaluate the kernel function of (2.158), we start with the general form of the kernel in (2.159). Using partial fractions, K_{2D} may be written as

$$K_{2D}(x_o,z) = \frac{j}{2} e^{-j\bar{\omega}x_o}\frac{\partial}{\partial z}\left[\int_{-\infty}^{x_o}\frac{e^{j\bar{\omega}\lambda}}{\lambda+jz}\,d\lambda - \int_{-\infty}^{x_o}\frac{e^{j\bar{\omega}\lambda}}{\lambda-jz}\,d\lambda\right] \qquad (2.161)$$

In the first integral, we make the substitution

$$s = \bar{\omega}(\lambda + jz) \qquad (2.162)$$

and, in the second,

$$s = \bar{\omega}(\lambda - jz) \qquad (2.163)$$

to obtain

$$K_{2D}(x_o,z) = \frac{j}{2} e^{-j\bar{\omega}x_o}\frac{\partial}{\partial z}\left[e^{\bar{\omega}z}\int_{-\infty+j\bar{\omega}z}^{\bar{\omega}(x_o+jz)} s^{-1}e^{js}\,ds - e^{-\bar{\omega}z}\int_{-\infty-j\bar{\omega}z}^{\bar{\omega}(x_o-jz)} s^{-1}e^{js}\,ds\right] \qquad (2.164)$$

To evaluate these integrals, we make a further substitution

$$t = js \qquad (2.165)$$

resulting in

$$K_{2D}(x_o, z) = \frac{j}{z} e^{-j\bar{\omega} x_o} \frac{\partial}{\partial z} \left[e^{\bar{\omega} z} \int_{-\bar{\omega}(z+j\infty)}^{\bar{\omega}(-z+jx_o)} t^{-1} e^{t}\, dt \right.$$
$$\left. - e^{-\bar{\omega} z} \int_{\bar{\omega}(z-j\infty)}^{\bar{\omega}(z+jx_o)} t^{-1} e^{t}\, dt \right] \qquad (2.166)$$

We evaluate these integrals by contour integration. For reasons mentioned earlier, we consider $z > 0$. x_o is arbitrary.

The contours for the evaluation of the first integral in (2.166), say I_1, for $x_o > 0$, $x_o = 0$ and $x_o < 0$, are shown in Figure 2.8. In each case, the integrals along C_1, C_2 and C_3, in the indicated directions, are denoted by I_1, I_2 and I_3 respectively. C_3 consists of a circular arc of radius R centered at the origin. According to the residue theorem

$$I_1 - I_2 + I_3 = 0 \qquad (2.167)$$

It can be shown that, as $R \to \infty$, I_3 vanishes, resulting in

$$I_1 = I_2 = Ei(\eta_1) \qquad (2.168)$$

where

$$\eta_1 = \bar{\omega}(-z + j x_o) \qquad (2.169)$$

and Ei is the complex exponential integral defined as

$$Ei(\zeta) = \int_{-\infty}^{\zeta} t^{-1} e^{t}\, dt \qquad (2.170)$$

with a branch cut along the positive real axis.

The contours for the evaluation of the second integral in (2.166), say J_1, for $x_o > 0$, $x_o = 0$ and $x_o < 0$ are shown in Figure 2.9. The integrals along C_1, C_2, C_3 and C_4, in the indicated directions, are denoted by J_1, J_2, J_3 and J_4 respectively. C_3 and C_4 are circular arcs of radius R and ρ correspondingly. Again, J_3 vanishes as $R \to \infty$. In the following, we apply the residue theorem to each of the contours.

i) $x_o > 0$

$$J_1 - J_2 + J_3 = 2\pi j \; Res\,(t=0) \tag{2.171}$$

The residue of the simple pole at the origin is unity. Hence,

$$\begin{aligned} J_1 &= 2\pi j + J_2 \\ &= 2\pi j + Ei(\vartheta_2) \end{aligned} \tag{2.172}$$

where

$$\vartheta_2 = \bar{\omega}(z + j x_o) \tag{2.173}$$

ii) $x_o = 0$

$$J_1 - J_2 + J_3 - J_4 = 2\pi j \; Res\,(t=0) \tag{2.174}$$

J_4 is one half the residue of the simple pole at the origin, as $\rho \to 0$. Hence,

$$\begin{aligned} J_1 &= \pi j + J_2 \\ &= \pi j + Ei(\vartheta_2) \end{aligned} \tag{2.175}$$

iii) $x_o < 0$

$$J_1 - J_2 + J_3 = 0$$

Hence,

$$J_1 = J_2 = Ei(\vartheta_2) \tag{2.176}$$

The three cases in the above can be combined to obtain, for all x_0,

$$J_1 = Ei(\vartheta_2) + \pi j \left[1 + \frac{x_0}{|x_0|} \right] \tag{2.177}$$

where the generalized function in the brackets is defined as

$$\frac{x_0}{|x_0|} = \begin{cases} 1 & x_0 > 0 \\ 0 & x_0 = 0 \\ -1 & x_0 < 0 \end{cases} \tag{2.178}$$

Substituting I_1, (2.168), and J_1, (2.177), in (2.166) and carrying out the indicated differentiation, we obtain

$$K_{2D}(x_0, z) = \frac{-x_0}{x_0^2 + z^2} + \frac{j\bar{\omega}}{2} \left\{ e^{-\vartheta_1} Ei(\vartheta_1) + e^{-\vartheta_2} \left[Ei(\vartheta_2) + \pi j \left(1 + \frac{x_0}{|x_0|} \right) \right] \right\} \tag{2.179}$$

This is the two-dimensional, nonplanar unsteady kernel function of airfoil theory. The first term of (2.179) is the steady two-dimensional kernel function.

To find the limiting form of the kernel function indicated in (2.158), we use the following expansions.

$$Ei(\vartheta_R \pm j0) = Ei(-\vartheta_R) \mp \pi j + 2 \sum_{n=0}^{\infty} \frac{\vartheta_R^{(2n+1)}}{(2n+1)!\,(2n+1)} \qquad \vartheta_R > 0 \tag{2.180}$$

$$Ei(-\zeta_R) = \gamma + \log \zeta_R + \sum_{n=1}^{\infty} (-\zeta_R)^n/(n!\,n) \qquad \zeta_R > 0 \tag{2.181}$$

where ζ_R is the real part of the complex argument ζ. The first expansion is found in Erdélyi (1953) and the second in Gröbner and Hofreiter (1961).

It is seen from (2.180) that $Ei(q_2)$, whose argument has a positive real part ($z > 0$), is discontinuous for $x_o = 0$. However, in (2.179), $Ei(q_2)$ and the generalized function $\pi j(1 + x_c/|x_o|)$, which is also discontinuous for $x_o = 0$, together form a continuous function, which is what we expect on physical grounds. The limiting form of K_{2D} as $x_o \to 0$ (actually, $x_o \to 0\pm$) is obtained from (2.179) and (2.180) as

$$K_{2D}(0,z) = \frac{j\bar{\omega}}{2}\left\{ e^{\bar{\omega}z}\, Ei(-\bar{\omega}z) + e^{-\bar{\omega}z}\left[Ei(-\bar{\omega}z) + \pi j + 2\sum_{n=0}^{\infty} \frac{(\bar{\omega}z)^{(2n+1)}}{(2n+1)!\,(2n+1)} \right] \right\} \tag{2.182}$$

As $z \to 0+$, using (2.181), we obtain

$$K_{2D}(0,z) \sim j\bar{\omega}\left[\gamma + j\frac{\pi}{2} + \log(\bar{\omega}z) \right] + O(z) \tag{2.183}$$

In order to check the above two-dimensional analysis, this result was also obtained from a vortex model.

Substituting (2.183) into (2.158), we obtain the following expansion for $\tilde{W}^{oi}(0,y,z)$ as $z \to 0+$.

$$\tilde{W}^{oi}(0,y,z) \sim \frac{1}{2\pi\rho U}\, j\bar{\omega}\, \tilde{f}_o(y)\left[\gamma + j\frac{\pi}{2} + \log(\bar{\omega}z) \right] + O(z) \tag{2.184}$$

Physically, this represents the self-induced downwash just above (or below) a harmonically-oscillating two-dimensional pressure doublet, or a

harmonically-oscillating two-dimensional vortex with the accompanying wake of shed vorticity. From the latter viewpoint, it is evident that $\tilde{W}^{oi}(0,y,z)$ is entirely due to the unsteady wake and, hence, vanishes in the limit of steady flow, as seen from (2.184). The logarithmic term in z in $\tilde{W}^{oi}(0,y,z)$ is due to the previously mentioned phenomena of approaching the edge of the shed vortex sheet. As expected, this singularity is identically equal to that in $\tilde{W}^{o}(0,y,z)$.

It follows from (2.155a) and (2.184) that, as $z \to 0+$, $[\tilde{W}^{o}(0,y,z) - \tilde{W}^{oi}(0,y,z)]$ is a finite quantity given by

$$\lim_{z\to 0+} \left[\tilde{W}^{o}(0,y,z) - \tilde{W}^{oi}(0,y,z) \right]$$

$$= \frac{1}{4\pi\rho U} \left\{ \oint_{-b}^{b} \frac{\tilde{l}_o(\eta)}{(y-\eta)^2} \Pi(\bar{\omega}|y-\eta|)\, d\eta \right.$$

$$- j\bar{\omega} \int_{-b}^{b} \frac{\tilde{l}_o(\eta) - \tilde{l}_o(y)}{|y-\eta|}\, d\eta \qquad (2.185)$$

$$+ 2j\bar{\omega}\, \tilde{l}_o(y) \left\{ 1 - \gamma - j\frac{\pi}{2} - \log \mu_o \right.$$

$$\left. \left. - \frac{1}{2} \log 4\left[1 - (y/b)^2 \right] \right\} \right\} \sim O(A^{-1})$$

where

$$\mu_o = \bar{\omega} b \qquad (2.186)$$

is the reduced frequency based on the semi span length b and $\Pi(\bar{\omega}|y-\eta|)$ is given by (2.155b). The order of magnitude of (2.185) follows directly from the fact that $\tilde{l}_o(y) \sim O(A^{-1})$.

Now, we return to (2.124) and, using the above results, determine F_1, F_2 and F_3. Examining the order of magnitude of the terms in (2.124) and

recalling that the unknown weighting functions are $O(A^0)$ (by construction), we conclude that

$$F_1(Y) = 0 \tag{2.187}$$

$$F_2(Y) = 0 \tag{2.188}$$

$$F_3(Y) = UA \lim_{Z \to 0+} \left[\tilde{W}^0(0,Y,Z) - \tilde{W}^{0c}(0,Y,Z) \right] \tag{2.189}$$

We have thus determined the amount of the eigensolutions present in the solution and, hence, completed the MAE analysis of the unsteady lifting-line theory to $O(A^{-2})$.

In summary, we note that, to $O(A^{-2})$, the pressure field is given by (2.104) - (2.107) and section lift and moment are given by (2.94) and (2.102) respectively, with F_1, F_2 and F_3 given by (2.187) - (2.189).

Further, we now list the results of the matching in symbolic form and indicate the order of magnitude and the type of each term.

<u>m = n = 1</u>

$$\tilde{\ell}(Y) \sim \underline{O(A^{-1})} \tag{2.190}$$

<u>m = 1, n = 2</u>

$$\tilde{\ell}(Y) \sim \underline{O(A^{-1})}$$
$$\tilde{m}(Y) \sim \underline{O(A^{-2})} \tag{2.191}$$

<u>m = n = 2</u>

$$\tilde{\ell}(Y) \sim \underline{O(A^{-1})},\ \underline{\underline{O(A^{-2}\log A)}},\ \underline{\underline{O(A^{-2})}},\ \underline{\underline{\underline{O(A^{-2})}}}$$
$$\tilde{m}(Y) \sim \underline{O(A^{-2})} \tag{2.192}$$

m = 2, n = 3

$$\tilde{\ell}(Y) \sim \underline{O(A^{-1})},\ \underline{\underline{O(A^{-2}\log A)}},\ \underline{\underline{O(A^{-2})}},\ \underline{\underline{\underline{O(A^{-2})}}}$$

$$\tilde{m}(Y) \sim \underline{O(A^{-2})},\ \underline{\underline{O(A^{-3}\log A)}},\ \underline{\underline{O(A^{-3})}},\ \underline{\underline{\underline{O(A^{-3})}}}$$

$$\tilde{q}(Y) \sim \underline{O(A^{-3})} \qquad (2.193)$$

where

( ): denotes two-dimensional quasi-steady information,

( ): denotes two-dimensional unsteady information and

( ): denotes three-dimensional unsteady information.

It is thus seen that, in the MAE analysis of the problem, section lift, moment,... as well as the pressure field first take on their two-dimensional quasi-steady values. As the analysis is carried out to higher orders, they are increasingly refined with two- and three-dimensional unsteady information.

CHAPTER III

CALCULATION OF AIRLOADS USING UNSTEADY LIFTING-LINE THEORY

3.1 Introduction

In this chapter, we extend, improve and apply the unsteady lifting-line theory of Chapter II to a number of oscillating wing problems. First, we identify an unsteady induced downwash, analogous to that in steady lifting-line theory. The importance of the induced downwash lies in the fact that, in the present theory, it represents all of the three-dimensional unsteady effects. Then, an improvement to the asymptotic results is presented which increases the accuracy and extends the range of validity of the theory.

As mentioned earlier, presently there are almost no reliable numerical results available for unsteady lifting-line theories. Here, for comparison we present the unsteady induced downwash of Reissner's approximate unsteady lifting-surface theory (Reissner (1947)) which, although is based on an ad hoc analysis, has good experimental confirmation. Computational schemes for the calculation of the unsteady induced downwash for both theories are presented in related appendices. Numerical examples show good agreement between the two theories for a range of values of k_0.

In order to assess the utility of the present theory, we then use it to calculate sectional and total lift and moment coefficients for a family of wing planforms in pitch and heave. The calculations are carried out for a range of reduced frequencies and for several aspect ratios. Whenever possible, the results are correlated with numerical lifting-surface

theories and Reissner's theory. The overall agreement is found to be good.

3.2 Unsteady Induced Downwash

In order to determine the unsteady induced downwash of the present unsteady lifting-line theory, we return to (2.120) which states that the computed downwash from integration of the composite pressure field is equal to the prescribed downwash at the wing. The functions F_1, F_2 and F_3 are given in (2.187) - (2.189). The first term on the right hand side of (2.120) is the downwash at the wing due to the two-dimensional solution ψ^{i}_{2D} which is exactly equal to the prescribed downwash and, hence, cancels out with the left hand side (the prescribed value).

The third term on the right hand side of (2.120) is the downwash at the wing due to the outer solution minus the common solution. The second term is the downwash at the wing due to ψ^{i}_{Sears}. Physically, ψ^{i}_{Sears} represents the modification of the two-dimensional part of the inner solution which arises in response to the three-dimensional effects and cancels them out as seen in this equation. Therefore, the last term on the right hand side is just the unsteady induced downwash.

According to the discussion following (2.120), the balance of the last two terms on the right hand side of this equation leads us to the conclusion that the last term, apart from the common sinusoidal dependence on x, is independent of x. Hence, in the last term, x can be set equal to any constant value on the wing (i.e., $|x| \leq c/A$). For convenience, again we choose $x = 0$. This means that the upper limit of the integrals in (2.121) and (2.122) are set equal to zero.

The induced downwash is then given by

$$W_I(x,y,t) = \tilde{W}_g(y)\, e^{-j\bar{\omega}x}\, e^{j\omega t} \qquad |x| \le c(y)/A \qquad |y| \le b$$

where (3.1)

$$\tilde{W}_g(y) = \lim_{z\to 0+}\left[\tilde{W}^{o}(0,y,z) - \tilde{W}^{oi}(0,y,z)\right] \sim O(A^{-1}) \qquad (3.2)$$

is the complex amplitude of the induced downwash given by (2.185). In (3.1), since $x \sim O(A^{-1})$, to be consistent, we must expand the exponential factor in x for large aspect ratio. This can be done, after normalizing x with the root semi chord c_o/A, to obtain

$$e^{-j\bar{\omega}x} \sim 1 + O(A^{-1}) \qquad (3.3)$$

It follows from (3.1) - (3.3) that, to leading order, for the present low-frequency theory the unsteady induced downwash, like its steady counterpart, is a constant across the chord and of $O(A^{-1})$. W_I is given by

$$W_I(x,y,t) = \tilde{W}_g(y)\, e^{j\omega t} \qquad |x| \le c(y)/A \qquad |y| \le b \qquad (3.4)$$

Physical Interpretation of Unsteady Induced Downwash

It follows from the above discussion and those following (2.122), (2.131) and (2.184) that the unsteady induced downwash for a straight wing, placed in a uniform stream normal to the span, has the following physical interpretation.

Again, we adopt the vortex viewpoint for its physical perspicuity. According to (3.4) and (3.2), to leading order, the unsteady induced downwash at a spanwise station Q consists of the downwash due to vortex

system (I) minus that due to vortex system (II), as shown in Figure 3.1. Vortex system (I) is the outer solution consisting of a harmonically oscillating loaded line (vortex) of strength $\tilde{\Gamma}(y)$ with its accompanying wake of shed and trailing vorticity (or, equivalently, a spanwise distribution of three-dimensional pressure doublets of strength $\tilde{l}_o(y)$). Vortex system (II) is the common solution which is a harmonically oscillating two-dimensional vortex of strength $\tilde{\Gamma}(y)$ (or, equivalently, a two-dimensional pressure doublet of strength $\tilde{l}_o(y)$). As we saw in Section 2.6, the downwash at Q due to both vortex systems is singular but their difference, which is the unsteady induced downwash, is finite.

This also resolves the main error in the unsteady lifting-line theory of James (1975). As pointed out in Section 2.6, his induced downwash is essentially $\tilde{w}^o(0,y,0+)$ and likewise contains a logarithmic singularity in z. In the present theory, the induced downwash is determined a posteriori, being inferred from the solution. James, on the other hand, intuitively writes down an expression for the induced downwash based on the outer solution alone and uses it as the means for connecting the inner and outer solutions.

The physical interpretation of steady induced downwash is quite similar to the unsteady case in the above, except that the shed vorticity is absent from both vortex systems (I) and (II), as shown in Figure 3.2. As pointed out in Section 2.6, $\tilde{w}^{oi}(0,y,0+)$ is entirely due to the unsteady effects. Hence, in the steady case $\tilde{w}^{oi}(0,y,0+) = 0$ and the induced downwash is entirely due to the trailing vorticity of system (I) which is a finite quantity. The above physical interpretation of (steady and unsteady) induced downwash was first given by Van Holten (1976).

In passing, we note that, both in steady and unsteady flows, spanwise

sweep and/or curvature of the wing planform give rise to important additional contributions to the induced downwash. For a brief discussion of these for incompressible flow, see Cheng (1975).

We now express the results of the unsteady lifting-line theory directly in terms of the induced downwash. Substituting (3.4) and (3.2) into (2.189), we obtain

$$F_3(y) = U^2 A \left[\tilde{W}_I(y) / U \right] \tag{3.5}$$

where $\tilde{W}_I(y)/U$ may be thought of as the unsteady induced angle of attack which varies harmonically with time. Using (3.5) and (2.69), the results of the unsteady lifting-line theory, to $O(A^{-2})$, are given by

$$\tilde{\psi}^i(\hat{\vec{x}}) = \tilde{\psi}^i_{2D}(\hat{\vec{x}}) + U^2 \left[\tilde{W}_I(y)/U \right] \mathcal{J}_i[\lambda] \tag{3.6}$$

$$\tilde{\ell}(y) = -2\pi\rho U^2 \left(\frac{c}{A}\right)\alpha + A^{-1} \log A \left[2\pi\rho U^2 j\nu \left(\frac{c}{A}\right)\alpha \right]$$

$$+ A^{-1} \left\{ -2\pi\rho U^2 j\nu \left\{ \left[\log(\gamma_1 \nu/2) + j\frac{\pi}{2} + 1 \right]\alpha + \frac{h_0}{c} \right\} \left(\frac{c}{A}\right) \right.$$

$$\left. + 2\pi\rho U^2 A \left(\frac{c}{A}\right) \left[\tilde{W}_I(y)/U \right] \right\} \tag{3.7}$$

$$\tilde{m}(y) = -\pi\rho U^2 \left(\frac{c}{A}\right)^2 \alpha + A^{-1} \log A \left[\pi\rho U^2 j\nu \left(\frac{c}{A}\right)^2 \alpha \right]$$

$$+ A^{-1} \left\{ -\pi\rho U^2 j\nu \left\{ \left[\log(\gamma_1 \nu/2) + j\frac{\pi}{2} \right]\alpha + \frac{h_0}{c} \right\} \left(\frac{c}{A}\right)^2 \right.$$

$$\left. + \pi\rho U^2 A \left(\frac{c}{A}\right)^2 \left[\tilde{W}_I(y)/U \right] \right\} \tag{3.8}$$

where $\log \gamma_1 = \gamma = .57721\ldots$ is the Euler constant. The outer solution ψ^0 and the common solution ψ^{0i} are given by (2.106) and (2.107) respectively.

An Improvement

The present asymptotic analysis involves a number of exact solutions and functions which have been expanded for large aspect ratio or, alternately, small reduced frequency k. In each case, only the first few terms of the expansions have been retained in accordance with the ordering of the asymptotic analysis. As an example, we cite the expansion of the exact two-dimensional unsteady airfoil solution ψ'_{2D} in (2.64).

We expect that replacing such expansions by the exact functional forms will improve the accuracy and extend the range of validity (in k) of the results. This can be seen in the following way. Consider a function $f(\epsilon)$ which is well behaved for all ϵ. In an asymptotic expansion of f for small ϵ, as ϵ is increased i) the accuracy of the expansion deteriorates and ii) beyond a certain value of ϵ the expansion often diverges. Hence, whenever the exact functional form $f(\epsilon)$ is available, replacing the expansion by f should improve the results. In the present analysis, however, since the overall theory is derived asymptotically for large aspect ratio (or small k), as we will see, the three-dimensional results ultimately diverge with increasing k. This is due to the divergence of the unsteady induced downwash at higher k.

In this way, we make maximum use of the available exact solutions. The errors introduced by the substitutions, in each case, are of the order of the errors of the original asymptotic expressions. Therefore, asymptotically speaking, the accuracy of the results is not influenced.

To improve the unsteady induced downwash, we restore the sinusoidal dependence on x (see (3.1), (3.3) and (3.4)). We also replace $\tilde{l}_o(y)$, which is the strip-theory quasi-steady section lift, with its exact unsteady counterpart $\tilde{l}_{2D}(y)$. $\tilde{l}_{2D}(y)$ is given by

$$\tilde{\ell}_{2D}(y) = \int_{-c(y)/A}^{c(y)/A} \Delta\tilde{p}_{2D}(\xi, y)\, d\xi \qquad (3.9)$$

where

$$\Delta\tilde{p}_{2D}(x,y) = \rho\left[\tilde{\Psi}^{i}_{2D}(x,y,0+) - \tilde{\Psi}^{i}_{2D}(x,y,0-)\right] \qquad (3.10)$$

which can be obtained from (2.46a) and (2.46b) using Table 2.1 (p. 57). $\tilde{l}_{2D}(y)$ is found to be

$$\tilde{\ell}_{2D}(y) = -\pi\rho U^2 \left(\frac{c}{A}\right)\left\{ jk\alpha - k_0 k \left(\frac{h_0}{c_0}\right) + \left[(2+jk)\alpha + 2jk_0\left(\frac{h_0}{c_0}\right)\right] C(k) \right\} \qquad (3.11)$$

The improved unsteady induced downwash then becomes

$$W_I(x,y,t) = \tilde{W}_g(y)\, e^{-j\bar{\omega}x}\, e^{j\omega t} \qquad |x| \le c/A \quad |y| \le b \qquad (3.12a)$$

where

$$\tilde{W}_g(y) = \frac{1}{4\pi\rho U}\left\{ \int_{-b}^{b} \frac{\tilde{\ell}_{2D}(\eta)}{(y-\eta)^2}\, \Pi(\bar{\omega}|y-\eta|)\, d\eta - j\bar{\omega}\int_{-b}^{b} \frac{\tilde{\ell}_{2D}(\eta) - \tilde{\ell}_{2D}(y)}{|y-\eta|}\, d\eta + 2j\bar{\omega}\,\tilde{\ell}_{2D}(y)\left\{ 1 - \gamma - j\frac{\pi}{2} - \log\mu_0 - \frac{1}{2}\log 4\left[1-(y/b)^2\right]\right\}\right\} \qquad |y| \le b \qquad (3.12b)$$

$\Pi(\bar{\omega}|y-\eta|)$ is given by (2.155b). The real and imaginary parts of Π are

shown in Figure 3.3.

It is seen from (3.12a) and (3.12b) that, in the present problem, the three-dimensional effects are manifested in the form of a convecting sinusoidal gust at each section of the wing. The complex amplitude of the gust $\tilde{W}_g(y)$ is a constant across the chord but varies across the span in a manner determined by the wing displacements and planform. We may thus refer to W_I as the induced gust.

Since the problem is linearized, we conclude that the three-dimensional correction to the basic two-dimensional inner solution is the pressure field due to the interaction of the induced sinusoidal gust with the wing. This is the full Sears eigensolution Ψ^i_{Sears} given by (2.58b). Hence, the improved inner solution, to $O(A^{-2})$, is given by

$$\tilde{\Psi}^i(\hat{\bar{X}}) = \tilde{\Psi}^i_{2D}(\hat{\bar{X}}) + \tilde{\Psi}^i_{Sears}(\hat{\bar{X}}) \tag{3.13}$$

Consequently, the improved three-dimensional section lift and moment, say $\tilde{l}(y)$ and $\tilde{m}(y)$, consist of the exact two-dimensional unsteady quantities, $\tilde{l}_{2D}(y)$ and $\tilde{m}_{2D}(y)$, and the lift and moment due to Ψ^i_{Sears}, which we denote by $\tilde{l}_{Sears}(y)$ and $\tilde{m}_{Sears}(y)$. Hence,

$$\tilde{\ell}(Y) = \tilde{\ell}_{2D}(Y) + \tilde{\ell}_{Sears}(Y) \tag{3.14}$$

$$\tilde{m}(Y) = \tilde{m}_{2D}(Y) + \tilde{m}_{Sears}(Y) \tag{3.15}$$

$\tilde{l}_{2D}(y)$ was evaluated in the above and is given by (3.11). In a similar way, we determine $\tilde{m}_{2D}(y)$ which is measured about the mid chord line (positive nose up). Hence,

$$\tilde{m}_{2D}(Y) = -\int_{-C(Y)/A}^{C(Y)/A} \xi\, \Delta\tilde{p}_{2D}(\xi, Y)\, d\xi \tag{3.16}$$

$$\tilde{m}_{2D}(y) = \frac{\pi}{2}\rho U^2 \left(\frac{c}{A}\right)^2 \left\{ \left(jk - \frac{1}{4}k^2\right)\alpha - \left[(2+jk)\alpha + 2jk_o\left(\frac{h_o}{c_o}\right)\right] C(k) \right\} \qquad (3.17)$$

Likewise, section lift and moment due to Ψ^i_{Sears} are determined using (2.58b) and Table 2.1 (p. 57). They are found to be

$$\tilde{\ell}_{Sears}(y) = 2\pi\rho U^2 \left(\frac{c}{A}\right)\left[\tilde{W}_g(y)/U\right] S(k) \qquad (3.18)$$

$$\tilde{m}_{Sears}(y) = \pi\rho U^2 \left(\frac{c}{A}\right)^2 \left[\tilde{W}_g(y)/U\right] S(k) \qquad (3.19)$$

where S(k) is the Sears function defined in (2.59).

The improved form of Ψ^o and Ψ^{oi} are obtained respectively from (2.106) and (2.107) after replacing $\tilde{l}_o(y)$ by $\tilde{l}_{2D}(y)$. The results are

$$\tilde{\Psi}^o(\vec{x}) = \frac{-1}{4\pi\rho}\frac{\partial}{\partial z}\int_{-b}^{b} \frac{\tilde{\ell}_{2D}(\eta)}{\sqrt{x^2+(y-\eta)^2+z^2}}\, d\eta \qquad (3.20)$$

$$\tilde{\Psi}^{oi}(\vec{x}) = \frac{1}{2\pi\rho}\,\tilde{\ell}_{2D}(y)\,\frac{z}{x^2+z^2} \qquad (3.21)$$

As a check, it can be shown that if the above improved results are expanded for large aspect ratio, keeping the appropriate number of terms in each case, the original asymptotic results are recovered. All of the necessary expansions have already been given except the one for the Sears function S(k) which can be obtained from (2.59), (2.62) and the asymptotic expansions for Bessel functions of the first and second kind of order zero and one for small arguments. The results are

$$S(k) \sim 1 - \frac{\pi}{2}k + jk\log(\gamma_1 k/2) + O(k^2\log k) \qquad (3.22)$$

$$S(k) \sim 1 + \left[j\nu \log(\gamma_1 \nu/2) - \frac{\pi}{2}\nu \right] A^{-1}$$

$$- j\nu A^{-1} \log A + O(A^{-2} \log A) \qquad (3.23)$$

In the remainder of this work, we will always use the above improved version of the unsteady lifting-line theory.

It can be shown that, in the steady limit ($\omega \to 0$), the results of the unsteady lifting-line theory reduce to the classical steady results (see, e.g., Van Dyke (1963)).

Reissner's Unsteady Induced Downwash

It is desirable to compare the three-dimensional corrections from the present theory with those of other line and surface theories. As mentioned previously, there are presently no reliable unsteady lifting-line calculations available. Further, there exists no exact analytical solution for the general oscillating lifting-surface problem. From among the many approximate unsteady lifting-surface theories, for comparison here we choose Reissner's theory (Reissner (1947)) for which satisfactory experimental confirmation exists. The theory is best suited for straight wings of moderate to high aspect ratio. Like the present unsteady lifting-line theory, Reissner's theory contains the unsteady airfoil theory and steady lifting-line theory as special cases. One advantage of Reissner's theory is that one can readily determine the induced downwash from his simplified integral equation.

In the present notation and for the wing in Figures 2.3a and 2.3b, Reissner's simplified integral equation of unsteady lifting-surface theory is given by

$$\tilde{W}_o(x,y,0\pm) = \frac{-1}{2\pi} \oint_{-C/A}^{C/A} \frac{\tilde{\gamma}(\xi,y)}{x-\xi}\, d\xi + \frac{1}{2} j k_o \tilde{\Omega}(y) \int_{C/A}^{\infty} \frac{e^{-j\bar{\omega}\xi}}{x-\xi}\, d\xi - \frac{1}{4\pi} e^{-j\bar{\omega}x} \left(\frac{c_o}{A}\right) \oint_{-b}^{b} \frac{d\tilde{\Omega}}{d\eta} \frac{\bar{K}(\bar{\omega}|y-\eta|)}{y-\eta}\, d\eta$$

$$|x| \leq C/A \qquad |y| \leq b \tag{3.24}$$

where $\tilde{\gamma}$ is the bound vorticity and $\tilde{\Omega}$ is the three-dimensional reduced circulation which is related to the circulation $\tilde{\Gamma}(y)$ through

$$\tilde{\Gamma}(y) = \left(\frac{c_o}{A}\right) \tilde{\Omega}(y)\, e^{-j\bar{\omega}\, c(y)/A} \tag{3.25}$$

Here, we have introduced the modified kernel function $\bar{K}$ so as to explicitly display the Cauchy singularity of the last integral. $\bar{K}$ is nonsingular and defined as

$$\bar{K}(q) = 1 - j\, q\, F(q) \tag{3.26}$$

where

$$F(q) = \frac{1}{q} \oint_{0}^{\infty} e^{-j\lambda} \left[1 - \frac{\sqrt{\lambda^2 + q^2} - |q|}{\lambda} \right] d\lambda \tag{3.27}$$

The integral here is known as the Cicala function which is an odd function of its argument. Using the tabulated values of this function in Reissner (1947), the values of $\bar{K}$ have been computed. They are listed in Table 3.1 (p. 339) and plotted in Figure 3.4. $\bar{K}(q)$ is an even function of its

argument.

The unsteady induced downwash can be identified from (3.24) by noting that the first and the second terms on the right hand side are respectively the downwash due to the bound vorticity and the shed vorticity, both of which are treated as two dimensional with strength equal to that at station y. These two terms correspond to the downwash due to the inner solution (namely $\tilde{W}_o^i + \tilde{W}_{Sears}^i$ in the present theory to $O(A^{-2})$). Therefore, the last term in (3.24) is the unsteady induced downwash. Hence

$$W_I(x,y,t) = \tilde{W}_g(y)\, e^{-j\bar{\omega}x}\, e^{j\omega t} \qquad |x| \leq c/A \quad |y| \leq b \qquad (3.28a)$$

where

$$\tilde{W}_g(y) = \frac{-1}{4\pi}\left(\frac{c_o}{A}\right) \int_{-b}^{b} \frac{d\tilde{\Lambda}}{d\eta}\, \frac{\bar{K}(\bar{\omega}|y-\eta|)}{y-\eta}\, d\eta \qquad |y| \leq b \qquad (3.28b)$$

It is noteworthy that Reissner's W_I, like that from the present theory, consists of a convecting sinusoidal gust whose complex amplitude $\tilde{W}_g(y)$ is a constant across the chord, but varies along the span in a manner determined by the wing displacements and planform. Since $\tilde{\Lambda}$ is normalized with respect to the root semi chord c_o/A (see(3.25)), it is $O(A^o)$. Therefore, as in the present theory, $\tilde{W}_g$ and W_I for Reissner's theory are both $O(A^{-1})$. In the next section, numerical examples for W_I for both theories are presented.

In Reissner's theory, the three-dimensional reduced circulation $\tilde{\Lambda}$ is obtained from an integro-differential equation of the lifting-line type by numerical methods. For wings of large aspect ratio, however, in the spirit of perturbation theory, we may replace $\tilde{\Lambda}$ with its strip-theory

counterpart, say $\tilde{\Omega}$, given below. Since $W_I \sim O(A^{-1})$, any three-dimensional refinement of $\tilde{\Omega}$ will give rise to higher-order corrections to W_I which may be neglected for the present purposes. The strip-theory value of the reduced circulation, for the wing under consideration, is given by

$$\tilde{\Omega}(y) = \frac{4 \int_{-c/A}^{c/A} \left[\frac{c/A+\xi}{c/A-\xi}\right]^{1/2} \tilde{W}_o(\xi, y)\, d\xi}{\pi j k_o \left(\frac{c}{A}\right) \left[H_1^{(2)}(k) + j H_o^{(2)}(k)\right]} \qquad (3.29)$$

Stirctly speaking, we should replace $\tilde{\Omega}$ with its quasi-steady strip-theory value which can be obtained from (3.29) by expanding for large aspect ratio (hence, also for small k). The use of the exact unsteady value herein is an improvement over the latter, analogous to the improved version of the unsteady lifting-line theory. In the remainder of this work, we always use $\tilde{\Omega}(y)$ in conjunction with Reissner's unsteady induced downwash.

It can be shown, that, in the limit of steady flow, (3.24) reduces to the integral equation of steady lifting-line theory, and (3.28a) and (3.28b) reduce to steady induced downwash.

3.3 Numerical Evaluation of Unsteady Induced Downwash

In this section, we focus attention on the numerical evaluation of the unsteady induced downwash of the present unsteady lifting-line theory and Reissner's theory. Sample calculations for both theories are also presented and compared. First, we review some ideas on the applicability of lifting-line theory to various wing planform shapes (with straight span). For a fuller discussion of the steady case see Van Dyke (1963). The latter contains errors which have been corrected in Van Dyke (1975).

The fundamental assumption that physical quantities vary slowly in the

span direction is violated near blunt wing tips where the flow does not become two-dimensional no matter how large the aspect ratio. This gives rise to local regions of nonuniformity near the tips, the size of which are larger for blunter tips. The nonuniformities show up as singularities, at the tips, in the spanwise distribution of various physical quantities, such as section lift and moment. The nonuniformities can be corrected by constructing additional asymptotic expansions valid in the immediate vicinity of the tips and matching them to the inner solution.

For steady lifting-line theory, to $O(A^{-3})$, Van Dyke (1963) has found that, for elliptic and more slender planforms, the spanwise distribution of lift and moment contain, at worst, integrable singularities at the tips and, hence, convergent total results are obtained. Further, he has found that the extent of the region of nonuniformity at the tips for these planforms is quite small. For the elliptic wing it is $O(A^{-2})$ and for the lenticular wing (parabolic leading and trailing edges) it is exponentially small. Since the loads vanish at the tips, the resulting errors in the total integrated quantities, for wings of large aspect ratio, is expected to be quite small. For planforms with blunter tips, such as the rectangular one, the resulting tip singularities are not integrable and, hence, total quantities cannot be obtained.

In the present theory, to $O(A^{-2})$, all of the results are obtained in closed form. However, the presence of a complicated integral in the expression for the unsteady induced downwash (see (3.12b)) precludes analytical determination of the behavior of the solution near the tips in the general unsteady case. Extensive numerical calculations for the present theory (presented in the following sections) indicate that, for elliptic and more slender planforms, for the unsteady motions considered,

there are no nonintegrable singularities in the spanwise distribution of various linear and quadratic quantities.

In order to evaluate the unsteady induced downwash, we first nondimensionalize all physical quantities using

$$x^* = x / (c_o/A) \tag{3.30}$$

$$y^* = y / b \tag{3.31}$$

$$t^* = Ut / (c_o/A) \tag{3.32}$$

$$W_I^* = W_I / U \tag{3.33}$$

$$\tilde{W}_g^* = \tilde{W}_g / U \tag{3.34}$$

$$\tilde{\Omega}^* = \Omega / U \tag{3.35}$$

$$\tilde{C}_{\ell_{2D}} = \tilde{\ell}_{2D} / \left[\tfrac{1}{2} \rho U^2 \left(2 \tfrac{c_o}{A}\right) \right] \tag{3.36}$$

where ( )* denotes nondimensional quantities. The nondimensional form of the unsteady induced downwash of the present theory, (3.12a) and (3.12b), is given by

$$W_I^*(x^*, y^*, t^*) = \tilde{W}_g^*(y^*)\, e^{jk_o(t^* - x^*)} \qquad \begin{matrix} |x^*| \leq c(y)/c_o \\ |y^*| \leq 1 \end{matrix} \tag{3.37a}$$

where

$$\tilde{W}_g^*(y^*) = \frac{1}{4\pi} \left\{ \frac{(c_o/A)}{b} \fint_{-1}^{1} \frac{\tilde{C}_{\ell_{2D}}(\eta^*)}{(y^* - \eta^*)^2} \Pi(\mu_o |y^* - \eta^*|)\, d\eta^* \right.$$

$$-jk_o \int_{-1}^{1} \frac{\tilde{C}_{\ell 2D}(\eta^*) - \tilde{C}_{\ell 2D}(y^*)}{|y^* - \eta^*|} \, d\eta^*$$

$$+ 2jk_o \, \tilde{C}_{\ell 2D}(y^*) \left\{ 1 - \gamma - j\frac{\pi}{2} - \log \mu_o \right.$$

$$\left. - \frac{1}{2} \log 4 (1 - y^{*2}) \right\} \qquad |y^*| \leq 1 \qquad (3.37b)$$

Similarly, in nondimensional form, the unsteady induced downwash of Reissner's theory, (3.28a) and (3.28b) (with $\tilde{\Delta}$ replaced by $\tilde{\Omega}$), is given by

$$W_I^*(x^*, y^*, t^*) = W_g^*(y^*) \, e^{jk_o(t^* - x^*)}$$

$$|x^*| \leq c(y)/c_o \qquad |y^*| \leq 1 \qquad (3.28a)$$

where

$$\tilde{W}_g^*(y^*) = \frac{-1}{4\pi} \frac{(c_o/A)}{b} \oint_{-1}^{1} \frac{d\tilde{\Omega}^*}{d\eta^*} \frac{\bar{K}(\mu_o |y^* - \eta^*|)}{y^* - \eta^*} \, d\eta^*$$

$$|y^*| \leq 1 \qquad (3.38b)$$

Numerical schemes for the evaluation of the unsteady induced downwash of the present theory and Reissner's theory are presented in Appendices B and C respectively.

Comparison of Unsteady Induced Downwash of Unsteady Lifting-Line Theory and Reissner's Theory

Since both theories predict an induced downwash of the form

$$W_I^*(x^*, y^*, t^*) = \tilde{w}_g^*(y^*)\, e^{jk_o(t^* - x^*)} \qquad (3.39)$$

it suffices to compare $\tilde{w}_g^*$ from the two theories. Before presenting the numerical examples, we point out a general result of unsteady finite wing theory, namely that as the aspect ratio and/or the reduced frequency are increased, the induction effects diminish in intensity and the three-dimensional results approach the strip-theory values. In other words, we expect $|\tilde{w}_g^*|$ to tend to zero as the aspect ratio and/or the reduced frequency are increased.

Using the numerical schemes discussed in Appendices B and C, $\tilde{w}_g^*$ from the present unsteady lifting-line theory (ULLT) and Reissner's theory are calulated for a rigid, flat plate elliptic wing in harmonic oscillation. The wing planform is given by

$$\chi = c(y)/A = \frac{4}{\pi A}\sqrt{1-(y/b)^2} \qquad |y| \leq b$$

In the numerical calculations, without loss of generality, we always take $b = 1$. Two modes of oscillation are considered: pitch and heave. Since, in the present work, the positive direction of pitching and heaving motions are defined contrary to the usual notation (see Figure 2.3b), all linear quantities presented herein will have an extra overall minus sign. As a characteristic reduced frequency for the wing, here and throughout, we use the reduced frequency based on the root semi chord, namely $k_o = (\omega/U)(c_o/A)$.

The first mode considered is pitching about the mid chord where the wing motion is defined by (2.4) with $\xi_o = 0$ and $\xi_1 =$ constant. We may also choose $\xi_2 = 0$ as a reference phase. Hence,

$$h(x,y,t) = \xi_1 x\, e^{j\omega t} \qquad |x| \leq c(y)/A \qquad |y| \leq b \qquad (3.40)$$

Here, we define a normalized $\tilde{W}_g^*$ as

$$\tilde{W}_{g_p}^* = \tilde{W}_g^* / \xi_1 \qquad (3.41)$$

The amplitude and phase of $\tilde{W}_{g_p}^*$ at the center section ($y^* = 0$) of an elliptic wing of aspect ratio A = 10 in pitch are shown in Figure 3.5 as a function of k_o. Shown are the results for the original aysmptotic version of the present unsteady lifting-line theory, its improved version and Reissner's theory. It is interesting to note that the results of Reissner's theory agree more closely with those of the improved version of the present theory than the original asymptotic one, and that over a larger range of k_o. This is as one might expect. In the remainder of this work, we always use the improved version of the present theory.

In the limit of steady flow, the pitching wing tends to a wing at an angle of attack ξ_1 and all three results approach that of steady lifting-line theory, namely

$$|\tilde{W}_{g_p}^*| = 2/A$$
$$\text{phase of } \tilde{W}_{g_p}^* = 0 \qquad (3.42)$$

It is seen from the above figure that for Reissner's theory, $|\tilde{W}_{g_p}^*|$ tends to zero as k_o is increased, as expected. On the other hand, as pointed out earlier, we expect the results of the present asymptotic theory ultimately to diverge, as k_o is increased. This is clearly seen in the above figure where, as k_o is increased, first the phase and then the amplitude of $\tilde{W}_{g_p}^*$ diverge. The high-frequency behavior of the results of the two theories is directly related to the behavior of their kernel functions,

Π and $\bar{K}$, for large values of their arguments, as seen in Figures 3.3 and 3.4. It is noted that as their arguments increase, $\bar{K}$ tends to zero, but Π grows without bounds.

The amplitude and phase of $\tilde{w}^*_{g_p}$ at the center section of an elliptic wing of A = 5 in pitch are shown in Figure 3.6. Compared with the results of A = 10 in the above, here the agreement between the two theories is not as precise but it occurs over a much larger range of k_o. The closer agreement between the two theories at higher A is due to the fact that both theories are more accurate at higher A. On the other hand, since $k_o \sim O(A^{-1})$, the lifting-line theory is valid for a smaller range of k_o for larger aspect ratios and a larger range of k_o for moderate aspect ratios.

The other mode of wing oscillation considered is heave where the wing displacements are given by (2.4) with $\xi_1 = \xi_2 = 0$ and ξ_o = constant, i.e.,

$$h(x,y,t) = \frac{1}{2}(c_o/A)\,\xi_o\, e^{j\omega t} \qquad (3.43)$$

$$|x| \le c(y)/A \qquad |y| \le b$$

Here, we define a normalized $\tilde{w}^*_g$ as

$$\tilde{w}^*_{g_H} = \tilde{w}^*_g / (\tfrac{1}{2} j k_o \xi_o) \qquad (3.44)$$

where the quantity in the denominator is essentially the angle due to the heaving motion, namely

$$\alpha_H = -U^{-1}\,\partial h/\partial t = -\tfrac{1}{2} j k_o \xi_o \qquad (3.45)$$

The main advantage of using $\tilde{w}^*_{g_H}$ over $\tilde{w}^*_g$ is that, whereas $\tilde{w}^*_g$ tends to zero as $k_o \to 0$, $\tilde{w}^*_{g_H}$ remains O(1), so that the behavior of the unsteady induced downwash for small k_o can be studied more readily.

The amplitude and phase of $\tilde{W}^*_{g_H}$ at the center section of an elliptic wing in heave are shown in Figure 3.7 for A = 10 and in Figure 3.8 for A = 5. As far as the agreement between the two theories is concerned, here we see the same trend that we saw in the above for the pitching wing. In the limit of steady flow, the result of both theories approach that of quasi-steady lifting-line theory for a heaving wing, namely

$$|\tilde{W}^*_{g_H}| \to 2/A$$
$$\text{phase of } \tilde{W}^*_{g_H} \to 0 \qquad (3.46)$$

which is the same as that for the pitching wing (see (3.42)). This is because, as $k_o \to 0$, both the pitching and heaving wings tend to a wing at an angle of attack (ξ_1 for the former and α_H for the latter), so that

$$\tilde{W}^*_{g_P} = \tilde{W}^*_{g_H} \qquad \omega \to 0 \qquad (3.47)$$

In the next section, spanwise distribution of section lift from the present theory and Reissner's theory are presented and compared with the strip-theory results. They clearly indicate the spanwise distribution of $\tilde{W}^*_g$ for both theories. It is seen that at other spanwise stations, as at $y^* = 0$ in the above, the present theory predicts a somewhat stronger induced downwash than Reissner's theory, especially near the wing tips.

It must be noted, however, that, in the neighborhood of the tips, the three-dimensional unsteady flow field is complex and has not yet been studied in detail. Garrick (1957) has pointed out that the primary weakness of Reissner's theory is in treating the wing tips. Also, the results of the present theory, near the tips, are to be viewed merely as a rough approximation. Further remarks on the tip flow field are made in the

next section.

Based on the above numerical examples and correlations, Figure 3.9 roughly depicts the region in a k_o - A diagram where we expect the present theory to be valid. With increasing k_o, the dashed and solid lines roughly depict the values of k_o beyond which respectively the phase and amplitude of the unsteady induced downwash gradually start to diverge. We tentatively conclude that the theory is valid to the left of the dashed line for moderate to high aspect ratios. On the basis of may more calculations and correlations, this picture will be further refined in Section 4.3.

In Figures 3.5 - 3.8, we note that, as k_o increases from zero, initially $|\tilde{W}_g^*|$ drops off rapidly ($k_o \tilde{<} .2$), followed by a much slower variation at higher k_o. The reason for the rapid initial decline of $|\tilde{W}_g^*|$ is the change in the nature of the wake. While in steady flow the wake consists of trailing vortices, each having constant strength, in unsteady flow, the trailing vortices have periodically varying strength along their length. Also, the strength of the shed vorticity varies periodically. The self-cancelling effect of this periodic unsteady wake causes the reduction in $|\tilde{W}_g^*|$.

Therefore, even for small values of k_o, the amplitude of $\tilde{W}_g^*$ is considerably smaller than the corresponding steady value. This means that for small k_o, quasi-steady theories underestimate the unsteady effects or, alternately, overestimate the three-dimensional corrections. This indicates the importance of fully-unsteady aerodynamic theories, such as the present one, as opposed to quasi-steady ones, even for relatively small reduced frequencies.

3.4 Calculation of Airloads for Oscillating Wings

In this section, to assess the utility of the present theory, we use it to calculate the spanwise distribution of the unsteady induced downwash and section lift and moment coeffieients, as well as the total lift and moment coefficients for an oscillating wing. The calculations are carried out over a range of values of k_o and A and for several planform shapes and modes of oscillation. In each case, k_o and A are chosen within the region of validity of the theory as shown in Figure 3.9.

The planforms considered are defined by (after Van Dyke (1963))

$$X = c(y)/A = k_n \left[1 - (y/b)^2 \right]^{n/2} / A \qquad |y| \leq b \tag{3.48}$$

It follows from the definition of aspect ratio, (2.2), that

$$k_n = b^2 \left\{ \int_0^b \left[1 - (y/b)^2 \right]^{n/2} dy \right\}^{-1} \tag{3.49}$$

so that

n	k	planform
0	b	rectangular
1	$(4/\pi)b$	elliptic
2	$(3/2)b$	lenticular
3	$(16/3\pi)b$	cusp-tipped

These planforms are shown in Figure 3.10 for A = 6. Most of the calculations presented herein are for the elliptic planform which is of fundamental interest to us. To study the influence of planform shape, the lenticular and cusp-tipped planforms are also considered. For reasons already cited, we will not consider the rectangular planform. The planform

area for wings belonging to the above family is $4b^2/A$.

In all numerical examples, the strip-theory results (ST) are also shown to indicate the extent of the three-dimensional corrections and because, as mentioned earlier, we expect the three-dimensional results to approach their strip-theory counterparts as A and/or k_o are increased. Whenever possible the results are correlated with Reissner's theory and numerical lifting-surface theories.

In the numerical calculations, without loss of generality, we always take b = 1. Also, since the planforms considered are spanwise symmetric, all spanwise calculations are carried out for half of the span at eleven stations, with the station closest to the tip located at $y^*= .999$. In terms of the spanwise angular variable $\theta = \cos y^*$ (see Appendix B), the station closest to the tip is 3° from the tip and the rest are equally spaced at 8.7° along the semi span. Numerical values for the steady limit are obtained for $k_o= 10^{-4}$ because, for $k_o = 0$, some of the Bessel functions involved are singular. Much smaller values of k_o could be used for the steady limit without any numerical difficulty but 10^{-4} was found to be adequate. The accuracy of the numerical results is three decimal places or better.

Two modes of oscillation are considered: pitch and heave. For a wing in pitch, whose displacements are given by (3.40), we define sectional and total lift and moment coefficients as

$$\tilde{C}_{\ell_p}(y^*) = \tilde{\ell}(y) \Big/ \left[\tfrac{1}{2}\rho U^2 \left(2\tfrac{c_o}{A}\right) \xi_1\right] \qquad (3.50)$$

$$\tilde{C}_{m_p}(y^*) = \tilde{m}(y) \Big/ \left[\tfrac{1}{2}\rho U^2 \left(2\tfrac{c_o}{A}\right)^2 \xi_1\right] \qquad (3.51)$$

$$\tilde{C}_{L_P} = \left[\tfrac{1}{2}\rho U^2 S_a \xi_1\right]^{-1} \int_{-b}^{b} \tilde{\ell}(y)\, dy \qquad (3.52)$$

$$\tilde{C}_{M_P} = \left[\tfrac{1}{2}\rho U^2 S_a \left(2\tfrac{c_0}{A}\right) \xi_1\right]^{-1} \int_{-b}^{b} \tilde{m}(y)\, dy \qquad (3.53)$$

Similarly, for a wing in heave, whose displacements are given by (3.43), we define

$$\tilde{C}_{\ell_H}(y^*) = \tilde{\ell}(y) \Big/ \left[\tfrac{1}{2}\rho U^2 \left(2\tfrac{c_0}{A}\right) \xi_0\right] \qquad (3.54)$$

$$\tilde{C}_{m_H}(y^*) = \tilde{m}(y) \Big/ \left[\tfrac{1}{2}\rho U^2 \left(2\tfrac{c_0}{A}\right)^2 \xi_0\right] \qquad (3.55)$$

$$\tilde{C}_{L_H} = \left[\tfrac{1}{2}\rho U^2 S_a \xi_0\right]^{-1} \int_{-b}^{b} \tilde{\ell}(y)\, dy \qquad (3.56)$$

$$\tilde{C}_{M_H} = \left[\tfrac{1}{2}\rho U^2 S_a \left(2\tfrac{c_0}{A}\right) \xi_0\right]^{-1} \int_{-b}^{b} \tilde{m}(y)\, dy \qquad (3.57)$$

Moments are measured about the mid-chord line (y-axis) and taken as positive in the nose-up direction.

Before presenting the numerical results, a few remarks are in order concerning the flow field near the wing tips. As pointed out earlier, predictions of lifting-line theory near blunt tips are to be taken only as a rough approximation.

Starting with the exact solution of Kinner (1937) for a circular wing in steady flow, Jordan (1971a, 1971b) has carried out a detailed study of

the flow field near a circular (or parabolic) wing tip. He finds that, contrary to the classical assumption of (essentially) elliptic span loading, the actual loading contains a logarithmic term near the tip. As a consequence, the induced downwash contains a logarithmic singularity which gives rise to an infinite upwash at the tip. Also, in relation to an oscillating rectangular wing tip, Landahl (1968) has found a similar logarithmic term in the span loading. It might be possible to derive similar results for an oscillating circular (or parabolic) wing tip, using the exact solution of Schade and Krienes (1947) for an oscillating circular wing. Presumably, similar logarithmic terms in the span loading and downwash would be uncovered.

Effect of k_o on Wing Aerodynamics

Consider an elliptic wing of A = 6 in pitching motion. Spanwise distribution of phase and amplitude of $\tilde{w}^*_{g_p}$ are shown in Figure 3.11 for several values of k_o. In the steady limit, the classical result is reproduced, namely unifrom induced downwash across the span, of amplitude 2/A and zero phase. As expected, with increasing k_o, the amplitude of induced downwash diminishes everywhere along the span except in a small neighborhood of the tip where it becomes more intense (possibly infinite at the tip). The latter is due to the increase in the strength of the local wake vorticity (at the blunt tip) which grows stronger with increasing k_o.

Figures 3.12 and 3.13 depict spanwise distribution of lift and moment coefficients for k_o = 0, 0.1, 0.2 and 0.3. The real and imaginary parts of each coefficient are denoted by R and I respectively. We note that, in the steady limit, the results of steady lifting-line theory are recovered. Also, it is seen that, with increasing k_o, three-dimensional section lift

and moment coefficients approach their strip-theory counterparts, as expected.

Figures 3.14 - 3.16 depict spanwise distribution of the unsteady induced downwash and lift and moment coefficients for an elliptic wing of $A = 6$ in heave for $k_o = 0.1$, 0.2 and 0.3. For $k_o = 0$ both lift and moment are zero. With increasing k_o, the heave-induced angle of incidence increases resulting in the growth of the lift and moment amplitudes. Also, the three-dimensional results approach their two-dimensional counterparts as in the above. In passing, we note that a better way of presenting the heave data is to normalize lift and moment coefficients with $(1/2)jk_o\xi_o$, as we did for the induced downwash in Section 3.3, rather than with ξ_o. Here, we have adopted the latter for ease of comparison with Reissner's results below. Examples of the former are given later in this section in connection with total lift and moment coefficients for the wing.

Effect of Aspect Ratio on Wing Aerodynamics

Consider an elliptic wing oscillating in pitch at $k_o = .2$. Spanwise distribution of phase and amplitude of $\tilde{w}^*_{3_p}$ are shown in Figure 3.17 for several values of aspect ratio. In each case, the steady results (i.e., amplitude of 2/A and phase of zero) are also shown for comparison. It is seen that, with increasing A and fixed k_o, the amplitude of the unsteady induced downwash is reduced everywhere, rendering the problem increasingly two-dimensional locally.

Spanwise distribution of lift and moment coefficients for the same wing are shown in Figures 3.18 and 3.19 for $k_o = .2$ and $A = 4$, 6 and 8. It is seen that, with increasing A and fixed k_o, three-dimensional lift and moment coefficients approach their strip-theory values, as suggested in the

above.

Effect of Planform Shape on Wing Aerodynamics

To study the influence of planform shape on the aerodynamics of the wing, we consider three planforms: cusp-tipped, lenticular and elliptic, defined in (3.48), (3.49) and the accompanying tabulation.

The cusp-tipped planform is the ideal one for theories of lifting-line type, because the chord distribution tends to zero infinitely slowly at the tips, thus, avoiding any nonuniformity. For the lenticular wing, the chord varies linearly near the tips which gives rise to a logarithmic singularity at the tips (at least in steady flow). The chord for the elliptic planform, on the other hand, varies infinitely rapidly near the tips. Fortunately, however, as we have seen in the above numerical examples, the elliptic planform does not give rise to any nonintegrable singularities at the tips (at least for the examples considered), as in the steady case.

Spanwise distribution of steady induced downwash for the above planforms is shown in Figure 3.20. They are in complete agreement with the classical steady results. Spanwise distribution of the real and imaginary parts of $\tilde{W}^{*}_{g_p}$ for the same wings, oscillating in pitch ($k_o = .2$), are shown in Figure 3.21. It is seen that, for the cusp-tipped wing, the amplitude of the unsteady induced downwash is finite everywhere along the span, as in the steady case. For the lenticular wing, it seems to have a weakly singular behavior at the tips. For the elliptic wing, the induced downwash is fairly constant across the span except near the tips where it grows somewhat more intense but appears to remain finite (it might have a weak singularity there). Determination of the exact nature of the latter would require analytic work on the integral expression for the unsteady induced

downwash in the neighborhood of the tips, which, as was pointed out earlier, would be quite tedious.

Spanwise distribution of lift coefficient for the three planforms is shown in Figure 3.22 for steady flow and in Figure 3.23 for pitching motion ($k_o = .2$). Influence of the planform shape on spanwise load distribution is clearly seen in steady and unsteady flows, especially near the tips where lift varies as the chord (see (B.5)). It is also seen that, in each case, the unsteady effects significantly reduce the amplitude of induced downwash except near the tips.

Spanwise distribution of moment coefficient for the three planforms is shown in Figure 3.24 for the steady case and in Figure 3.25 for pitching motion ($k_o = .2$). The above comments about the lift distribution apply to the moment distributions as well. All of the steady results here and in the above are in full agreement with those of steady lifting-line theory.

Comparison with Reissner's Theory

Reissner and Stevens (1947) have carried out extensive numerical calculations for Reissner's theory for rectangular and elliptic wings in various types of oscillatory motion. Here, we compare their lift distribution for an elliptic wing in pitch and heave with those of the present theory. Unfortunately, their calculations are only for $A = 3$ which is rather low for the present theory, but we find the agreement to be surprisingly good for the given conditoins.

Spanwise distribution of lift coefficient for an elliptic wing in heave is shown in Figure 3.26 for $A = 3$ and $k_o = .212$, .424 and .847. It is seen that the results of the two theories are in reasonably good agreement over most of the span except in a relatively small region near

the tips where the results of the present theory change sign before vanishing at the tips. This is due to the stronger induced dwonwash predicted by the lifting-line theory under the conditions of relatively large k_o and small A, as pointed out earlier.

Spanwise distribution of lift coefficient for an elliptic wing in pitch is shown in Figure 3.27 for A = 3 and k_o = .212, .424 and .847. As far as the comparison of the results of the two theories is concerned, the above remarks for the heaving wing apply here as well. In the light of the discussion at the end of Section 3.3 (comparison of the unsteady induced downwash from the two theories), we expect the agreement between the two theories to be considerably better at higher aspect ratios.

Figure 3.28 depicts spanwise distribution of lift coefficient for an elliptic wing in steady flow from the two theories. The reason for the poor agreement lies in the fact that, in the steady limit, whereas the present theory approaches the form

$$C_{\ell_p}(y^*) = 2\pi\left(1-\frac{2}{A}\right)\sqrt{1-y^{*2}} + O(A^{-2}) \qquad (3.58)$$

of steady lifting-line theory (which is the direct result of the MAE analysis), Reissner's theroy approaches Prandtl's recast from of the above, namely

$$C_{\ell_p}(y^*) = \frac{2\pi\sqrt{1-y^{*2}}}{1+2/A} + O(A^{-2}) \qquad (3.59)$$

Asymptotically, the two forms are completely equivalent, to $O(A^{-2})$, with their difference being a measure of the error band of steady lifting-line theory. The latter quickly diminishes at higher aspect ratios as seen in Figure N.3 of Van Dyke (1975), where it is also seen that the results of

numerical lifting-surface theory lie between the above predictions. The above comparisons also indicate that, for fixed A, the error band of the unsteady lifting-line theory, which is equal to that of steady lifting-line theory for $\omega = 0$, diminishes with increasing k_0. Further comparisons of the results of the two theories are presented below.

In summary, we find the overall agreement between the two theories to be reasonably good, considering the low A, and expect it to be much better for moderate to large A. The present asymptotic theory, thus, provides formal justification for Reissner's ad hoc theory.

Total Lift and Moment Coefficients for Oscillating Wings

To study the influence of k_0, aspect ratio and mode of oscillation on total lift and moment coefficients for oscillating wings, we consider an elliptic wing in pitch and heave.

Spanwise integration of section lift and moment coefficients are carried out using Legendre-Gauss quadrature ((B.11) and (B.12)), after a spanwise cosine substitution to handle numerical difficulties arising from blunt wing tips (see Appendix B). It was determined, through numerical experiments, that the sixteen-point Legendre-Gauss quadrature scheme is adequate to obtain accuracy of three decimal places or better. Taking advantage of the spanwise symmetry of lift and moment distributions, the spanwise integrals were carried out for half of the span and the results doubled.

The total lift and moment coefficients for an elliptic wing in pitch are shown as complex vector diagrams in Figures 3.29 - 3.31 for A = 3, 6 and 16. In each case the corresponding strip-theory results (ST) and the values of steady lift coefficient from numerical lifting-surface theory

(SLST) are shown for comparison. The latter are taken from Figure N.3 of Van Dyke (1975). Here again, it is seen that in general, with increasing A and/or k_o, the results of the present theory approach the corresponding strip-theory values, as expected.

The calculations for A = 3, which is rather low for the present theory, were carried out for the sake of comparison with those of Reissner's theory which are also shown in Figure 3.29. The agreement between the two theories is reasonably good (considering the low aspect ratio) except at very low k_o. The latter is associated with the fact that, in the steady limit (as already discussed in relation to spanwise lift distribution), the present theory approaches the form

$$C_{L_p} = -2\pi \left(1 - \frac{2}{A}\right) + O(A^{-2}) \qquad (3.60)$$

of steady lifting-line theory, whereas Reissner's theory approaches Prandtl's recast form of the above, namely

$$C_{L_p} = \frac{-2\pi}{1 + 2/A} + O(A^{-2}) \qquad (3.61)$$

In the figures, numerical results from the latter form are shown for comparison and denoted by SLLT2 (second form of steady lifting-line theory). The difference between the two forms is a measure of the error band of steady lifting-line theory, which diminishes rapidly with increasing aspect ratio, as seen in the above figures (for $\omega = 0$). We note that the rapid turn in the lift curve of unsteady lifting-line theory for A = 3 and low k_o (Figure 3.29) is reduced to a small kink for A = 6 (Figure 3.30) and completely dissappears for large A, as seen in Figure 3.31 for A = 16. It is also seen that the value of k_o at which the rapid turn occurs decreases with increasing A ($k_o \approx .2$ for A = 3, $k_o \approx .06$ for A = 6

and $k_o \approx 0$ for A = 16). This seems to be due to the change in the relative size of various terms in W_I at different A, since only the first term in (3.37b) depends on A explicitly. Further, for A = 16 and $k \gtrsim .5$, the lift and moment curves gradually start to diverge from the corresponding strip-theory results, as seen in Figure 3.31. This is due to the divergence of the present theory at higher k_o.

Total lift and moment coefficients for an elliptic wing in heave are shown as complex vector diagrams in Figures 3.32 - 3.34 for A = 3, 6 and 16. The A = 3 case is again considered only for comparison with Reissner's results which are also shown in Figure 3.32. The agreement between the two theories, for the given conditions, is fairly good, especially at higher k_o.

As mentioned earlier, it is more enlightening to normalize the lift and moment coefficients for a heaving wing with $(1/2)jk_o\xi_o$. Here, we present the rest of the heave data in this form. Since we have already normalized these coefficients with ξ_o, it only remains to divide by $(1/2)jk_o$. Hence,

$$\tilde{C}_{L_H}/(\tfrac{1}{2}jk_o) = \left[\tfrac{1}{2}\rho U^2 S_a (\tfrac{1}{2}jk_o\xi_o)\right]^{-1}\int_{-b}^{b}\tilde{\ell}(y)dy \qquad (3.62)$$

$$\tilde{C}_{M_H}/(\tfrac{1}{2}jk_o) = \left[\tfrac{1}{2}\rho U^2 S_a (2\tfrac{c_o}{A})(\tfrac{1}{2}jk_o\xi_o)\right]^{-1}\int_{-b}^{b}\tilde{m}(y)dy \qquad (3.63)$$

The rest of the heave data is depicted in Figures 3.33 and 3.34.

The rapid turn of the lift curve for low k_o and moderate A, observed in the above for the pitching wing, is also seen here in the heave data when normalized with respect to $(1/2)jk_o\xi_o$. For A = 6, the lift curve

displays an unexpected loop for low k_o as seen in Figure 3.33. This behavior disappears completely for large A, as seen in Figure 3.34 for A = 16. We also note that the related moment curves (pitch and heave) display a rapid turn (under the same conditions) which decreases in size and finally disappears with increasing A. This seems to be another manifestation of the same effect.

This behavior of the results of the present theory may be due to the presence of the term $k_o \log \mu_o$ in the expression for the unsteady induced downwash (see (3.37a) and (3.37b)). This term has an infinite slope at $\omega = 0$ and the behavior in question might be the recovery of the results from this strong initial change. This behavior, however, is not fully understood and calls for further investigation.

In relation to the heave data, we also note that, for A = 16 and $k \gtrsim .5$, the lift and moment curves gradually diverge from the corresponding strip-theory results (see Figure 3.34). This is due to the divergence of the present theory at higher k_o. We also note that, with increasing k_o and/or A, the results of the present theory generally approach the strip-theory values, as expected.

CHAPTER IV

ENERGETICS OF THREE-DIMENSIONAL FLAPPING FLIGHT USING UNSTEADY LIFTING-LINE THEORY

4.1 Intruduction

Until recently, most theoretical studies of the propulsive performance of three-dimensional wings were based on unsteady strip-theory calculations or quasi-steady lifting-line theory (see, e.g., Archer, Sapuppo and Betteridge (1979)), neither of which is completely adequate.

Bennett (1970) accounted for three dimensionality and unsteadiness in an approximate way by extending the unsteady lifting-surface theory of Reissner (1947) to calculate thrust and hydrodynamic efficiency. His theory, like that of Reissner, is an irrational approximation. Later, Chopra (1974), using superposition (Fourier series) of sinusoidal lifting ribbons of infinite span, calculated the performance of a rigid rectangular wing in combined pitch and heave. His approach is limited to the rectangular planform.

Recently, a few investigators have employed numerical unsteady lifting-surface theory to study this problem. Chopra and Kambe (1977) employed the kernel function method for a family of rigid wings most of which are swept back. Lan (1979) has used the "quasi-vortex-lattice" method for rigid wings of rectangular and arrow planform including a tandem wing configuration. Agreement between the two works is not as good as expected and warrants further work on the lifting-surface approach to this problem.

Lighthill (1970) suggested the use of unsteady lifting-line theory for

the study of performance of high-aspect-ratio lunate tails (or flapping wings). In this chapter, we employ the present unsteady lifting-line theory to study the energetics of three-dimensional flapping flight. The present approach has several advantages: i) All of the results are obtained in closed form and, hence, are suited for optimization studies. ii) In comparison with unsteady lifting-surface theory, considerably less computation time is required. iii) In the present acceleration potential formulation of the problem, the suction force is obtained exactly (linearized). This is in contrast with other methods (numerical) in steady and unsteady flows where the suction force is obtained approximately (see, e.g., Wagner (1969) and Lan (1979)).

Working within the framework of linearized theory, we use the present unsteady lifting-line theory to calculate both spanwise distribution and total integrated value of the following quantities: power required to maintain the wing oscillations; leading-edge suction force; thrust; and energy loss rate due to vortex shedding. It is not meaningful to speak of sectional energy loss rate since this quantity is defined only for the entire wing. The analysis in this chapter is for a rigid wing but can be modified to accomodate a spanwise-flexible wing. The total integrated quantities are needed for the optimization studies in Chapter V. Numerical examples for the above quantities are presented and correlated with lifting-surface results, where such data is available. The overall agreement is found to be good.

On the basis of the numerical examples in Chapters III and the present chapter, the range of validity of the present unsteady lifting-line theory is then discussed in more detail. It is found that the theory is valid over a larger range of reduced frequency and aspect ratio that originally

anticipated. This is, in part, due to the improvement scheme discussed in Section 3.2.

4.2 Energetics of Three-Dimensional Flapping Flight

Focusing attention on the unsteady part of the wing motion, we consider a rigid thin wing of relatively large aspect ratio in combined pitch and heave:

$$h(x,y,t) = \left[h_o/A + \alpha x \right] e^{j\omega t}$$

$$= \left[\frac{1}{2} (c_o/A)\, \xi_o + (\xi_1 + j\, \xi_2)\, x \right] e^{j\omega t} \qquad (4.1)$$

$$|x| \leq c(y)/A \qquad |y| \leq b$$

as shown in Figures 2.3a and 2.3b. As we will see below, all of the energetic quantities turn out to be quadratic forms in (ξ_o, ξ_1, ξ_2). We start with the basic definition of the quantities in question and derive closed-form expressions for them. Since, for harmonic motion, the time average of these quantities is of interest, we only calculate their time averages.

The time average, denoted by $\overline{(\ )}$, is defined as

$$\overline{T} = \frac{1}{\tau} \int_{t_o}^{t_o+\tau} T(t)\, dt \qquad (4.2)$$

where t_o is an arbitrary constant. For harmonic motion, τ is usually chosen as the period of oscillation. It can be shown that the following rules hold for the time average of products of complex harmonic quantities.

If

$$A = \mathcal{R}_j \left[\tilde{A}\, e^{j\omega t} \right] \qquad B = \mathcal{R}_j \left[\tilde{B}\, e^{j\omega t} \right] \tag{4.3}$$

then,

$$\overline{AB} = \frac{1}{2} \mathcal{R}_j \left[\tilde{A}\, \tilde{B}^{\circledast} \right] = \frac{1}{2} \mathcal{R}_j \left[\tilde{B}\, \tilde{A}^{\circledast} \right] \tag{4.4}$$

$$\overline{\frac{\partial}{\partial t}(AB)} = 0 \tag{4.5}$$

where $\mathcal{R}_j$ and $(\,)^{\circledast}$ respectively denote the real part and the complex conjugate of a complex quantity with respect to j.

Power Required to Maintain Wing Oscillations

The average sectional power required to maintain the wing oscillations is given by

$$\overline{P}(Y) = -\int_{-C(Y)/A}^{C(Y)/A} \overline{\Delta p(x,Y,t)\, \frac{\partial h}{\partial t}(x,Y,t)}\, dx \tag{4.6}$$

Substituting for h from (4.1) and using the averaging rule in (4.4), we obtain

$$\overline{P}(Y) = \frac{1}{2} \mathcal{R}_j \left\{ j\omega \frac{h_a}{A}\, \tilde{\ell}(Y) - j\omega \alpha^{\circledast}\, \tilde{m}(Y) \right\} \tag{4.7}$$

This represents the rate of work of unsteady lift (done at the rate of heaving velocity) and the rate of work of unsteady moment (done at the rate of angular pitching velocity).

Introducing the nondimensional coefficients

$$C_p(y^*) = \bar{P}(y) / \left[\frac{\pi}{4} \rho U^3 \left(\frac{c_0}{A} \right) \right] \tag{4.8}$$

$$\tilde{C}_\ell(y^*) = \tilde{\ell}(y) / \left[\frac{1}{2} \rho U^2 \left(2 \frac{c_0}{A} \right) \right] \tag{4.9}$$

$$\tilde{C}_m(y^*) = \tilde{m}(y) / \left[\frac{1}{2} \rho U^2 \left(2 \frac{c_0}{A} \right)^2 \right] \tag{4.10}$$

in (4.7), we obtain

$$C_p(y^*) = \frac{k_0}{\pi} \mathcal{J}_j \left[-\xi_0 \tilde{C}_\ell(y^*) + 4(\xi_1 - j\,\xi_2) \tilde{C}_m(y^*) \right] \tag{4.11}$$

where $\mathcal{J}_j$ denotes the imaginary part of a complex quantity with respect to j and $\tilde{C}_\ell(y^*)$ and $\tilde{C}_m(y^*)$ are obtained from the unsteady lifting-line theory (see (3.14) and (3.15)).

We now introduce the following notation for the linear quantities.

$$B = (B_0' + j\,B_0'')\,\xi_0 + (B_1' + j\,B_1'')\,\xi_1 + (B_2' + j\,B_2'')\,\xi_2 \tag{4.12}$$

where B denotes $\tilde{W}_g^*(y^*)$, $\tilde{C}_\ell(y^*)$, $\tilde{C}_m(y^*)$, $\tilde{C}_L$ or $\tilde{C}_M$ and the coefficients B_n' and B_n'' are real with respect to j. It follows from the second form of (4.1) that the following symmetry relations hold.

$$B_1' = B_2'' \qquad B_1'' = -B_2' \tag{4.13}$$

Expressing $\tilde{C}_\ell(y^*)$ and $\tilde{C}_m(y^*)$ in (4.11) in the notation of (4.12) and using the above symmetry relations, we obtain $C_p(y^*)$ as a quadratic form in (ξ_0, ξ_1, ξ_2).

$$C_p(y^*) = \frac{k_0}{\pi} \left\{ -C_{\ell_0}''(y^*)\,\xi_0^2 + 4\,C_{m_1}''(y^*)\,(\xi_1^2 + \xi_2^2) \right.$$

$$+\frac{1}{2}\left[4C''_{m_o}(y^*) - C''_{\ell_1}(y^*)\right] 2\xi_0\xi_1$$

$$-\frac{1}{2}\left[4C'_{m_o}(y^*) + C'_{\ell_1}(y^*)\right] 2\xi_0\xi_2 \qquad (4.14)$$

The general form of a quadratic form in three variables is

$$F = Q_{11}\xi_0^2 + 2Q_{12}\xi_0\xi_1 + 2Q_{13}\xi_0\xi_2 + Q_{22}\xi_1^2 + 2Q_{23}\xi_1\xi_2 + Q_{33}\xi_2^2 \qquad (4.15)$$

or, in matrix notation,

$$F = \underline{\xi}^T \underline{Q}\, \underline{\xi} \qquad (4.16)$$

where $(\underline{\ })$ denotes a matrix, $(\underline{\ })^T$ denotes the transpose of a matrix and

$$\underline{\xi} = \begin{Bmatrix} \xi_0 \\ \xi_1 \\ \xi_2 \end{Bmatrix} \qquad (4.17)$$

$$\underline{Q} = \begin{bmatrix} Q_{11} & Q_{12} & Q_{13} \\ Q_{12} & Q_{22} & Q_{23} \\ Q_{13} & Q_{23} & Q_{33} \end{bmatrix} \qquad (4.18)$$

$\underline{Q}$ is the matrix of the quadratic form which is symmetric by construction (for a discussion of quadratic forms see, e.g., Hildebrand (1965)). A more general form of quadratic forms involves a non-symmetric $\underline{Q}$.

We saw in the above that for the matrix of the quadratic form for $C_p(y^*)$

$$Q_{22} = Q_{33} \qquad Q_{23} = 0 \qquad (4.19)$$

which follow directly from the symmetry relations (4.13). As we will see below, in a similar way, the matrix of the quadratic form for all of the quantities in question (sectional and total) has the properties in (4.19). It is noteworthy that, for the same reason, all of the quadratic forms for the two-dimensional motion of a rigid airfoil in pitch and heave also have these properties (see Wu (1971b)).

The average total power required to maintain the wing oscillations is given by

$$\overline{\mathcal{P}} = \int_{-b}^{b} \overline{P}(y)\, dy \tag{4.20}$$

or, in nondimensional form,

$$\begin{aligned} C_{\mathcal{P}} &= \overline{\mathcal{P}} \Big/ \left[\tfrac{\pi}{4}\rho U^3 \left(\tfrac{1}{2} S_a\right)\right] \\ &= \tfrac{1}{2}\left(\frac{c_o}{b}\right) \int_{-1}^{1} C_p(y^*)\, dy^* \end{aligned} \tag{4.21}$$

Leading-Edge Suction Force

Thrust consists of the suction force at the leading edge and a contribution from the normal force at the wing. First, we evaluate the suction force. In two dimensions, the steady suction force is derived rigorously (see, e.g., Robinson and Laurmann (1956), p. 126). It is known that the suction force arises from the singular pressure at the leading edge and is proportional to the square of the strength of the leading-edge square-root singularity in velocity. The suction force can be evaluated

using Blasius' theorem or the momentum theorem. Wu (1961, 1971a) has calculated the unsteady suction force in two dimensions using the acceleration potential. He shows that, in the neighborhood of the leading edge of an oscillating airfoil, the velocity potential and its time derivative remain bounded and, hence, do not contribute to the suction force. The problem of determining the unsteady suction force thus reduces to that in steady flow, with time appearing only as a parameter.

In three dimensions, we employ the present unsteady lifting-line theory, according to which, at each wing section, the three-dimensional effects are manifested as a convecting sinusoidal gust (the unsteady induced downwash). The interaction of this gust with wing sections modifies the local two-dimensional pressure field by an amount of the Sears solution $\tilde{\Psi}^{i}_{Sears}$ determined by the complex amplitude of the unsteady induced downwash. The Sears solution modifies the strength of the leading-edge singularity and thus modifies the suction force. Since the latter is a quadratic quantity, we can not simply combine the contribution from the two effects. We must return to the three-dimensional pressure field in the inner region where the complex acceleration potential is given by

$$\tilde{f}^{i}(\hat{\xi},Y) = \tilde{f}^{i}_{2D}(\hat{\xi},Y) + \tilde{f}^{i}_{Sears}(\hat{\xi},Y) \qquad (4.22)$$

Here, $\tilde{f}^{i}_{2D}$ and $\tilde{f}^{i}_{Sears}$ are given by (2.46a) and (2.58a) respectively. Wu (1961) has shown that, in two dimensions, near the leading edge the complex velocity

$$\tilde{g}^{i}(\hat{\xi},Y) = \tilde{u}^{i}(\hat{\vec{X}}) - i\,\tilde{w}^{i}(\hat{\vec{X}}) \qquad (4.23)$$

behaves like $\tilde{f}^{i}$. Since both $\tilde{f}^{i}_{2D}$ and $\tilde{f}^{i}_{Sears}$ are (locally) two dimensional,

we may use this result. Expanding $\tilde{f}^{i}_{2D}$ and $\tilde{f}^{i}_{Sears}$ near the leading edge, we obtain

$$\tilde{g}^{i}(\hat{\xi},y) \sim \frac{1}{\sqrt{2}}\left[\tilde{a}_0(y) + 2\,S(k)\,\tilde{W}_g(y)\right]\left[\frac{c(y)}{\hat{\xi}+c(y)}\right]^{1/2} + O(1) \qquad \hat{\xi} \to -c(y) \qquad (4.24)$$

where S(k) is the Sears function defined in (2.59), $\tilde{a}_0(y)$ is given by (2.38d) and $\tilde{W}_g(y)$ is given by (3.12b).

The suction force is then obtained by applying Blasius' theorem to a small circle surrounding the leading edge. The result is

$$T_s(y,t) = -\frac{\pi}{8}\rho\,\frac{c(y)}{A}\left\{\mathcal{R}_j\left[a_0(y,\hat{t}) + 2\,S(k)\,\tilde{W}_g(y)\,e^{j\omega t}\right]\right\}^2 \qquad (4.25)$$

T_s is the suction force per unit length of the leading edge, directed along the outward normal to the leading edge, as shown in Figure 4.1, and taken to be positive in that direction. Numerically, T_s is also equal to the streamwise component of the suction force per unit span.

Averaging T_s over time and keeping only the leading three-dimensional correction, we obtain

$$\bar{T}_s(y) = \frac{\pi}{4}\rho\,\frac{c}{A}\,\mathcal{R}_j\left[|\tilde{a}_0(y)|^2 + 4\,S^{\circledast}(k)\,\tilde{a}_0(y)\,\tilde{W}_g^{\circledast}(y)\right] \qquad (4.26)$$

where it is seen that the suction force is proportional to the local chord length. The neglected higher-order term is proportional to $|S(k)\tilde{W}_g(y)|^2$.

The nondimensional form of (4.26) is given by

$$C_{T_s}(y^*) = \left(\frac{c}{c_0}\right)\mathcal{R}_j\left[|\tilde{a}_0^*(y^*)|^2 + 4\,S^{\circledast}(k)\,\tilde{a}_0^*(y^*)\,\tilde{W}_g^{*\circledast}(y^*)\right] \qquad (4.27)$$

where

$$C_{T_s}(y^*) = \bar{T}_s(y)\Big/\left[\frac{\pi}{4}\rho U^2\left(\frac{c_0}{A}\right)\right] \qquad (4.28)$$

$$\tilde{a}_o^*(y^*) = \tilde{a}_o(y)/U \tag{4.29}$$

It follows from (2.38d) - (2.38f) and (4.1) that

$$\tilde{a}_o^*(y^*) = \tilde{b}_1^*(y^*) - \left[\tilde{b}_o^*(y^*) + \tilde{b}_1^*(y^*)\right] C(k) \tag{4.30}$$

where

$$\tilde{b}_o^*(y^*) = \tilde{b}_o(y)/U = j k_o \xi_o + 2(\xi_1 + j\xi_2) \tag{4.31}$$

$$\tilde{b}_1^*(y^*) = \tilde{b}_1(y)/U = j k (\xi_1 + j\xi_2) \tag{4.32}$$

The quadratic form of $C_{T_s}(y^*)$ is obtained from (4.27) after substituting for $\tilde{a}_o^*$ from the above and introducing the notation of (4.12) for $\tilde{w}_g^*$ together with the symmetry relations (4.13). The result is

$$\begin{aligned} C_{T_s}(y^*) = \left(\frac{c}{c_o}\right)\Big\{ & \left[k_o^2 D(k) + 4(a_1 c_1 + b_1 d_1)\right] \xi_o^2 \\ & + \left[k^2 + (4+k^2) D(k) - 2k^2 F(k) - 4k G(k)\right. \\ & \left. + 4(a_2 c_2 + b_2 d_2)\right] (\xi_1^2 + \xi_2^2) \\ & + \left[-k_o k B(k) + 2(a_1 c_2 + a_2 c_1 + b_1 d_2 + b_2 d_1)\right] 2\xi_o \xi_1 \\ & + \left[2k_o D(k) - k_o k G(k) + 2(a_1 c_3 + a_3 c_1\right. \\ & \left. + b_1 d_3 + b_3 d_1)\right] 2\xi_o \xi_2 \Big\} \end{aligned} \tag{4.33}$$

where F and G are the real and imaginary parts of Theodorsen's function

$\mathbb{C}(k)$ (see (2.42) and (2.44)) and

$$D(k) = F^2(k) + G^2(k)$$
$$B(k) = F(k) - D(k) \tag{4.34}$$

Further,

$$\begin{aligned}
a_1(y^*) &= k_0 G(k) \\
a_2(y^*) &= k\, G(k) - 2 F(k) \\
a_3(y^*) &= 2 G(k) + k\,[F(k) - 1] \\
b_1(y^*) &= -k_0 F(k) \\
b_2(y^*) &= -2 G(k) - k\,[F(k) - 1] \\
b_3(y^*) &= k\, G(k) - 2 F(k) \\
c_1(y^*) &= S_R(k)\, W_0'(y^*) - S_I(k)\, W_0''(y^*) \\
c_2(y^*) &= S_R(k)\, W_1'(y^*) - S_I(k)\, W_1''(y^*) \\
c_3(y^*) &= S_R(k)\, W_2'(y^*) - S_I(k)\, W_2''(y^*) \\
d_1(y^*) &= S_R(k)\, W_0''(y^*) + S_I(k)\, W_0'(y^*) \\
d_2(y^*) &= S_R(k)\, W_1''(y^*) + S_I(k)\, W_1'(y^*) \\
d_3(y^*) &= S_R(k)\, W_2''(y^*) + S_I(k)\, W_2'(y^*)
\end{aligned} \tag{4.35}$$

where S_R and S_I are the real and imaginary parts of the Sears function S(k) and W_n^i and W_n^n are the coefficients of $\tilde{W}_g^*$, namely

$$\begin{aligned}
\tilde{W}_g^*(y^*) = &\left[W_0'(y^*) + j\, W_0''(y^*)\right] \xi_0 \\
&+ \left[W_1'(y^*) + j\, W_1''(y^*)\right] \xi_1 \\
&+ \left[W_2'(y^*) + j\, W_2''(y^*)\right] \xi_2
\end{aligned} \tag{4.36}$$

In the absence of three-dimensional corrections ($\tilde{W}_g^* = 0$), the above expression for $C_{T_s}(y^*)$ reduces to the two-dimensional result of Wu (1971b).

The average total leading-edge suction force for the wing, in the streamwise direction, is given by

$$\overline{\mathcal{T}}_s = \int_{tip}^{tip} \overline{T}_s(y) \cos\beta \, d\chi \tag{4.37}$$

where χ is the distance along the leading edge and β is the local leading-edge sweep angle as shown in Figure 4.1. Since $\cos\beta \, d\chi = dy$, (4.37) may be written as

$$\overline{\mathcal{T}}_s = \int_{-b}^{b} \overline{T}_s(y) \, dy \tag{4.38}$$

where it is seen that the average suction force per unit span in the streamwise direction is just $\overline{T}_s(y)$ as pointed out earlier. The nondimensional form of (4.38) is given by

$$\begin{aligned} C_{\mathcal{T}_s} &= \overline{\mathcal{T}}_s \Big/ \left[\frac{\pi}{4} \rho U^2 \left(\frac{1}{2} S_a \right) \right] \\ &= \frac{1}{2} \left(\frac{c_o}{b} \right) \int_{-1}^{1} C_{T_s}(y^*) \, dy^* \end{aligned} \tag{4.39}$$

Thrust from the Normal Force

In addition to the leading-edge suction force, the streamwise component of the unsteady normal force at the wing also contributes to the

thrust. The time average of this contribution, denoted by $\overline{T}_p$, is given by

$$\overline{T}_p(y) = \int_{-c(y)/A}^{c(y)/A} \Delta p(x,y,t)\, \frac{\partial h}{\partial x}(x,y,t)\, dx \qquad (4.40)$$

Substituting for h from (4.1), we obtain

$$\overline{T}_p(y) = \frac{1}{2}\, \mathcal{R}_j \left[\alpha^{\circledast}\, \tilde{\ell}(y) \right] \qquad (4.41)$$

or, in nondimensional form,

$$\begin{aligned} C_{T_p}(y^*) &= \overline{T}_p(y) \Big/ \left[\frac{\pi}{4} \rho U^2 \left(\frac{c_o}{A} \right) \right] \\ &= \frac{2}{\pi}\, \mathcal{R}_j \left[\alpha^*\, \tilde{C}_\ell(y^*) \right] \end{aligned} \qquad (4.42)$$

Introducing the notation of (4.12) for $\tilde{C}_\ell(y^*)$ together with the symmetry relations (4.13), we obtain the quadratic form for $C_{T_p}(y^*)$.

$$\begin{aligned} C_{T_p}(y^*) = \frac{2}{\pi} \Big\{ & C'_{\ell_1}(y^*) \left(\xi_1^2 + \xi_2^2 \right) \\ & + \left[\frac{1}{2}\, C'_{\ell_0}(y^*) \right] 2\, \xi_0 \xi_1 \\ & + \left[\frac{1}{2}\, C''_{\ell_0}(y^*) \right] 2\, \xi_0 \xi_2 \Big\} \end{aligned} \qquad (4.43)$$

The average total thrust from the normal force for the wing is given by

$$\overline{\mathcal{T}}_p = \int_{-b}^{b} \overline{T}_p(y)\, dy \qquad (4.44)$$

or, in nondimensional form,

$$C_{\mathcal{T}_P} = \bar{\mathcal{T}}_P \Big/ \left[\frac{\pi}{4}\rho U^2 \left(\frac{1}{2} S_a\right)\right]$$
$$= \frac{1}{2}\left(\frac{c_o}{b}\right)\int_{-1}^{1} C_{T_P}(y^*)\, dy^* \qquad (4.45)$$

Thrust

The average section thrust is the sum of the averages of the leading-edge suction force and the thrust from the normal force, i.e.,

$$\bar{T}(y) = \bar{T}_s(y) + \bar{T}_p(y) \qquad (4.46)$$

or, in nondimensional form,

$$C_T(y^*) = \bar{T}(y) \Big/ \left[\frac{\pi}{4}\rho U^2 \left(\frac{c_o}{A}\right)\right]$$
$$= C_{T_S}(y^*) + C_{T_P}(y^*) \qquad (4.47)$$

where $C_{T_S}(y^*)$ and $C_{T_P}(y^*)$ are given by (4.33) and (4.43) respectively.

The average total thrust for the wing is given by

$$\bar{\mathcal{T}} = \int_{-b}^{b} \bar{T}(y)\, dy \qquad (4.48)$$

or, in nondimensional form,

$$C_{\mathcal{T}} = \bar{\mathcal{T}} \Big/ \left[\frac{\pi}{4}\rho U^2 \left(\frac{1}{2} S_a\right)\right]$$

$$= \frac{1}{2}\left(\frac{c_o}{b}\right)\int_{-1}^{1} C_T(y^*)\, dy^* \qquad (4.49)$$

It can be shown that, in the limit of steady flow, the above results for average sectional and total thrust reduce to one half of the sectional and total induced drag respectively. For example, for an elliptic wing, we find

$$C_T(y^*)/\xi_1^2 = \frac{-8}{A}\sqrt{1-y^{*2}} \qquad (4.50)$$

$$C_J/\xi_1^2 = -8/A \qquad (4.51)$$

which are one half of the known steady results. The extra factor of one half is due to the time averaging (see (4.4)) which is not meaningful in steady flow and, hence, must be discarded.

Energy Loss Rate

As pointed out earlier, energy loss rate is not defined for individual wing sections. The average total energy loss rate for the wing, denoted by $\overline{\mathcal{E}}$, is obtained from the principle of conservation of mechanical energy (derived rigorously in Chapter VI in two and three dimensions):

$$\overline{\mathcal{E}} = \overline{\mathcal{P}} - U\,\overline{\mathcal{J}} \qquad (4.52)$$

or, in nondimensional form,

$$C_{\mathcal{E}} = \overline{\mathcal{E}}\Big/\left[\frac{\pi}{4}\rho U^3\left(\frac{1}{2}S_a\right)\right] = C_{\mathcal{P}} - C_{\mathcal{J}} \qquad (4.53)$$

The hydrodynamic efficiency of the motion is defined as

$$\eta = C_T / C_P = 1 - C_E / C_P \qquad (4.54)$$

This completes the derivation of the average sectional and total values of the energetic quantities for a rigid wing in combined pitch and heave. It is noteworthy, that, within the framework of the present linearized theory, the results are exact and contain three-dimensional corrections of order W_I. Only in the evaluation of the suction force we encountered a correction term of order W_I^2 (in addition to one of order W_I) which we discarded as higher order. The implication of the latter near the wing tips, where the amplitude of W_I can become large, is discussed later in this section.

Here, we have considered the purely unsteady motion of the wing with no steady lift. In some applications, the latter is present and essential. For example, in birdflight where steady lift is required to overcome the body weight. The presence of steady lift in the problem gives rise to additional steady components for the linear quantities (induced downwash, pressure, lift, moment etc.) which must be combined with their respective unsteady components before calculating the energetic quantities, as in this section. The average value of the quantities of interest, however, turn out to be simply the sum of the steady and unsteady components, since the cross product terms, being proportional to $e^{j\omega t}$, average to zero. For example, the average thrust is reduced by an amount equal to the induced drag.

In this section we have considered the unsteady motion of a rigid wing. In some applications, such as in the unsteady undulations of lunate

tails, which are rather rigid structures, this model is quite adequate. But in other applications, such as in birdflight a model is needed which permits arbitrary variation of the amplitude of pitch and heave and the associated phase difference across the span, namely a spanwise-flexible wing model. The present unsteady lifting-line theory provides us with just such a model (see (2.3) and (2.4)) through the choice of $h_o(y)$ and $\alpha(y)$ or, alternately, $\xi_o(y)$, $\xi_1(y)$ and $\xi_2(y)$.

For numerical calculations, it is best to choose a number of suitable spanwise modes (1) for each of ξ_o, ξ_1 and ξ_2, as we have done for the chordwise motion of the wing. The associated numerical schemes can be developed from those presented in Appendix B for the rigid wing, after straightforward modifications. This also determines the size of the matrices of the quadratic forms for the energetic quantities. For example, if we choose three modes for each of ξ_o, ξ_1 and ξ_2, the size of the resulting matrices will be 9x9 (in contrast to 3x3 for the rigid wing).

Numerical Examples

To study the influence of the three-dimensional corrections on the spanwise distribution of the energetic quantities, we consider a rigid elliptic wing in pitch and heave. Since the wing is spanwise symmetric, the calculations are done for half of the span, at eight stations with the station closest to the tip located at $y^* = .9999$. The stations are the abscissas of the sixteen-point Legendre-Gauss quadrature (for the full span) for the normalized spanwise angular variable $(2/\pi \cos^{-1} y^* - 1)$.

---

(1) The actual number depends on the particular modes chosen and the desired accuracy.

Calculations are carried out for $k_0 = 0$, 0.1 and 0.3. To indicate the extent of the three-dimensional corrections, in each case, the corresponding strip-theory result (ST) is also shown.

The spanwise distribution of the average power required to maintain the wing oscillations for an elliptic wing (A = 8) in heave and pitch are shown respectively in Figures 4.2 and 4.3. The numerical results are obtained from (4.14). It is seen that the three-dimensional theory predicts less power than the strip theory. This is due to the fact that the three-dimensional effects normally reduce the amplitude of unsteady lift and moment, as was seen in Section 3.4. We also note that it takes more power to oscillate a wing at higher k_0, as expected.

Before presenting the numerical results for the leading-edge suction force, it is instructive to consider the suction force for a two-dimensional airfoil. This is obtained from (4.33) with the unsteady induced downwash set equal to zero ($\tilde{W}^*_g = 0$). Figure 4.4 depicts the average suction force for a two-dimensional airfoil in heave and pitch as a function of the reduced frequency k. It is seen that, with increasing k, for the heaving airfoil, the average suction force increases monotonically, whereas for the pitching airfoil, it first decreases to about one half of its steady value and grows nomotonically thereafter. The unexpected behavior of the latter is due to the influence of unsteady effects on the flow around the leading edge. In the limit of steady flow, the average suction force for the pitching airfoil approaches one half of its steady value of 8 (the reason for the extra factor of 1/2 was given earlier).

The spanwise distribution of the suction force for an elliptic wing (A = 8) in heave and pitch is calculated from (4.33) and shown respectively in Figures 4.5 and 4.6. It is seen from the figures that the

three-dimensional effects reduce the suction force. This is because the induced downwash normally opposes the flow around the leading-edge, thereby reducing the strength of the leading-edge square-root singularity and, hence, also the suction force. The variation of the suction force with k_o for both wings is consistent with the basic two-dimensional results in Figure 4.4.

We also note that for both wings, for $k_o = 0.3$ in a small neighborhood of the tip, the suction force becomes negative. But we know, on physical grounds, that the suction force must be positive or zero everywhere along the span. The explanation for this lies in the higher-order correction term of order $|W_I|^2$ in the expression for $C_{T_s}(y^*)$ which we discarded. This term is always positive. The correction term of order W_I which was retained, on the other hand, can become negative. As we saw in Section 3.4, near the tips and at higher k_o, the amplitude of W_I can become large. Under these condtions (and in the absence of the $|W_I|^2$ term), the W_I term can become large and negative and overtake the two-dimensional term which is always positive, thereby producing an overall negative result. Retaining the $|W_I|^2$ term will always prevent this occurrence, but the related steady result will be inconsistent with that of steady lifting-line theory which contains only the W_I term. As pointed out in Section 3.4, the lifting-line results near blunt tips are to be considered only as a rough approximation, since the actual flow field does not become two-dimensional no matter how large the aspect ratio. Since the region of negative suction force constitutes only a small neighborhood of the tips (of the order of 1% of the semi span, in the above examples) and since the suction force is tending to zero at the tips, we expect the effect of this on the total thrust to be negligible.

The spanwise distribution of thrust for an elliptic wing (A = 8) in heave is also shown in Figure 4.5 and was discussed in the above in relation to the suction force. This is because, for a heaving wing, the normal force at the wing is always in the z-direction and hence all of the thrust is supplied by the suction force. The spanwise distribution of thrust for an elliptic wing (A = 8) in pitch is shown in Figure 4.7 for k_o = 0, 0.1 and 0.3. For these values of k_o, the pitching wing produces drag (see the corresponding two-dimensional results in Figure 6.7). It is seen that, in the steady limit, we obtain one half of the sectional induced drag for an elliptic wing at incidence, as pointed out earlier. In Figure 4.7, the reason the magnitude of the three-dimensional results is larger than the corresponding strip-theory values is the additional drag associated with the trailing vorticity which is absent in the strip theory.

All of the spanwise distributions presented in this section display the property that, with increasing k_o, the three-dimensional results approach their strip-theory values, as expected.

Next, we consider the overall propulsive performance of an oscillating rigid wing and ask what level of thrust $C_{\mathcal{T}}$ the wing is capable of producing and at what hydrodynamic efficiency η. It should be noted that the calculation of η, (4.54), requires the calculation of two of the three quantities $C_{\mathcal{T}}$, $C_{\mathcal{P}}$ and $C_{\mathcal{E}}$, with the third determined from conservation of energy, (4.53).

In order to correlate the present numerical results with the limited numerical lifting-surface results available, we temporarily adopt Lighthill's description for the wing displacements (see Lighthill (1970)), namely

$$h(x,y,t) = \left[h_L - j\alpha_L (x - b_L)\right] e^{j\omega t} \qquad |x| \leq c(y)/A \quad |y| \leq b \tag{4.55}$$

where h_L and α_L are real quantities with respect to j, signifying the amplitude of heave and pitch respectively. The phase difference between the two modes of oscillation is 90° and the position of the axis of pitch is given by $x = b_L$, $z = 0$. This description of the wing motion is completely equivalent to that employed in the present work (see (2.3) and (2.4)). The explicit relationships between the two are given in the next chapter.

The total value of the energetic quantities for the wing are obtained by integrating the spanwise distribution of these quantities using Legendre-Gauss quadrature together with a spanwise cosine substitution to handle numerical difficulties arising at blunt wing tips (as in Appendix B). Through numerical experiments, a sixteen-point Legendre-Gauss quadrature scheme was found to be adequate to obtain three decimal places of accuracy. Taking advantage of the spanwise symmetry, all of the necessary integrals are carried out for half of the span and the results doubled. Further, all of the required spanwise integrals are evaluated simultaneously so as to save computation time. The integrands involve the unsteady induced downwash and various special functions, with most of the savings coming from fewer calculations of the former.

Figure 4.8 depicts the strip-theory results for C_J and η for an elliptic wing in combined pitch and heave, with the axis of pitch located at 3/4 of the center-section chord, for several values of Lighthill's feathering parameter

$$\theta_L = U\alpha_L / (\omega h_L) \qquad (4.56)$$

θ_L is a measure of the deviation of the wing slope from the tangent to the path traversed in space by the pitch axis. $\theta_L = 1$ represents perfect geometric feathering and $\theta_L = 0$ represents pure heaving motion. The results closely resemble the corresponding two-dimensional ones of Lighthill (1970) with η tending to 100% as $k_o \to 0$ for all values of θ_L, as expected. It should be noted that, as $k_o \to 0$, all configurations with $\theta_L \neq 0$ tend to pure heaving motion as can be seen from the following form of (4.56).

$$\theta_L = \alpha_L / [k_o h_L / (c_o/A)] \qquad (4.57)$$

In the absence of numerical lifting-surface results for oscillating elliptic wings, here we correlate the results of the present theory for an elliptic wing with those of Chopra and Kambe (1977) for a rectangular wing. See Figure 4.9. Both wings are of $A = 8$, oscillating in combined pitch and heave, with the axis of pitch located at 3/4 chord (at the center section for the elliptic wing).

Based on experience from steady flow, one might expect the elliptic wing to have better propulsive performance than the rectangular wing. Also, the calculations of Bennett (1970) for a linearly flapping wing indicate that the elliptic wing has better performance (C_T and η) than the other planforms considered including the rectangular one. While this may not be true for all modes of oscillation, it indicates that one might expect, at least in some cases, better performance from the elliptic wing. In Figure 4.9, we find the elliptic wing to have comparable and in most

cases higher $C_{\mathcal{J}}$ and η than the rectangular wing, except for low k_o where η for the elliptic wing drops unexpectedly. As $k_o \to 0$, we expect η to continue to increase because, as pointed out eariler, for all θ_L, the wing motion tends to pure heave (see the corresponding two-dimensional results in Figure 6.7). This behavior seems to be directly related to the unexpected behavior of the $\tilde{C}_L$ curve for low k_o and moderate A discussed in Section 3.4 (see, e.g., Figures 3.30 and 3.33). Figure 4.10, which depicts $C_{\mathcal{J}}$ and η for an elliptic wing of A = 16, also gives support to this argument, in that, for A = 16 the drop in η at low k_o has all but disappeared, in the same way that the corresponding behavior of the $\tilde{C}_L$ curve also disappears for A = 16 (see Figures 3.31 and 3.34). We also note that, with increasing k_o and/or A (within the range of validity of the unsteady lifting-line theory), the present three-dimensional results approach their strip-theory counterparts, as expected.

We end this section with a comparison of the recently published numerical lifting-surface results of Lan (1979) with those of Chopra and Kambe (1977). Figure 4.11 depicts $C_{\mathcal{J}}$ and η from the two theories for a rectangular wing in combined pitch and heave, with axis of pitch located at 3/4 chord. The values of η from the two theories agree quite well. However, the values of $C_{\mathcal{J}}$ predicted by Lan's theory are generally smaller than those of Chopra and Kambe. The same trend is observed in the comparison of $C_{\mathcal{J}}$ from Lan's theory and that of Bennett (1970) for a linearly flapping rectangular wing (see Lan (1976)), where the values of $C_{\mathcal{J}}$ predicted by Lan's theory are considerably smaller than those of Bennett. In the absence of an exact analytic theory with which to compare (for the rectangular wing), we conclude that there is need for further work on numerical lifting-surface theories for the purpose of calculating the

propulsive performance of oscillating wings.

4.3 Region of Validity of Unsteady Lifting-Line Theory

A tentative discussion of the region of validity of the present unsteady lifting-line theory (in a k_e - A diagram) was presented in Section 3.3 and shown in Figure 3.9. On the basis of the calculations and correlations presented in Chapter III and the present chapter, we now continue that discussion, seeking to refine that picture (1). First, a few remarks are in order concerning the order of magnitude of the errors.

Since the present theory is an asymptotic one for large aspect ratio, the accuracy of the results improves with increasing A and vice versa. The order of magnitude of the errors in the present theory is $O(A^{-2})$. This represents an error of the order of 11% for A = 3, 4% for A = 5 and 1% for A = 10, as shown in Figure 4.12. Also shown in this figure is a curve corresponding to errors of $O(A^{-1})$ which may be thought of as the errors involved in using the strip theory alone (for a high-aspect-ratio wing) or the order of magnitude of the corrections to the latter by the present lifting-line theory. A third curve represents errors of $O(A^{-3})$, namely those associated with the next higher-order lifting-line theory. It is seen that the first-order theory represents significant corrections to the strip-theory results, with small residual errors of only a few per cent for $A \gtrsim 5$. Further, on the basis of the order of magnitude of the errors, there seems to be little gained by developing a higher-order lifting-line theory (considering that we have neglected viscous and nonlinear effects).

---

(1) Ideally, at least some of the present calculations should be carried out on a reliable unsteady numerical lifting-surface program for comparison.

However, such a theory may be advantageous in refining some of the details of the present theory, thereby also improving the region of validity and the accuracy of the theory.

Figure 4.13 depicts the region in a k_o- A diagram where the present theory is most accurate and useful. In the light of the above discussion, we have marked off the area for $A \tilde{<} 5$ as the region where aspect ratio is too small for the theory to give good accuracy.

Another implication of the assumption of large A, in the present theory, is that the reduced frequence based on the wing semi chord c(y)/A is small. As pointed out earlier, this means that the theory is restricted to lower values of k_o. This is roughly indicated in Figure 4.13 by the broken and solid lines (taken from Figure 3.9) to the right of which, respectively, the phase and amplitude of induced downwash gradually start to diverge, with the latter causing larger errors in the results. In fact, the results are found to be valid well to the right of the broken line, as shown in Figure 4.13 by the crosshatched area.

As mentioned earlier, in the steady limit, the present theory reduces to the classical steady lifting-line theory. We also saw, in Sections 3.4 and 4.2, that, for small k_o and moderate A, some of the total aerodynamic coefficients for the wing display certain unexpected behavior (see Figures 3.30, 3.33 and 4.9). As pointed out in Section 3.4, this might be due to the term containing $k_o \log \mu_o$ in the induced downwash, (see (3.37a) and (3.37b). This behavior, however, is not fully understood and calls for further investigation. Further numerical lifting-surface results will be helpful here. This behavior may turn out to be an inherent weakness of the present theory, in which case, it might be necessary to carry out the analysis to one order higher in inverse aspect ratio to resolve it.

For the present purposes, we identify the region in question (small k_o and moderate A) in the k_o - A diagram, Figure 4.13, as one where the error band of the present theory is wider than that at higher k_o, though perhaps smaller than that for steady lifting-line theory, as suggested earlier.

The unshaded area in Figure 4.13 roughly depicts the region where the present theory is most accurate and useful, with the accuracy improving with increasing A. This region encompasses a larger range of values of k_o and A than originally anticipated and contains values of k_o and A which are of greatest interest in applications.

CHAPTER V

OPTIMUM MOTION OF THRUST-PRODUCING LIFTING SURFACES

5.1 Introduction

The optimum shape problems considered here involve the determination of those transverse displacements of a lifting surface which produce a prescribed level of thrust at minimum energy cost in maintaining the oscillations. The primary motivation for these studies is to gain a clearer understanding of the high efficiencies observed in certain modes of animal propulsion in nature, such as bird flight and fish swimming. The general theory may also be useful in other applications, such as in aeroelasticity and optimum energy extraction from fluid streams.

Undoubtedly, the highly refined aerodynamic shapes and motions of the animal as a whole and the thrust-producing lifting surfaces in particular play a key role in achieving high efficiencies. In the current study, we are concerned with wing motions of birds with high-aspect-ratio wings and small to moderate flapping amplitude, such as gulls and albatross in cruising flight. In the aquatic realm, we are concerned with similar motions of high-aspect ratio lunate tails, typical of many fast-moving fish, such as sharks and the cetacean mammals. Such wing and tail motions are typically associated with relatively high Reynolds numbers, of the order of 10^5 and higher (based on a characteristic chord length). Under these conditions, viscous effects are confined to a thin boundary layer at the surface and a thin trailing vortex wake. Outside the boundary layer and the wake, the flow may be treated as potential. The inertial forces,

which are much larger than the viscous forces, are primarily responsible for the propulsive forces. The viscous forces are responsible for skin friction and creation of circulation around the wing (Kutta condition) and only in the latter role do they affect the propulsive forces. Thus, the aerodynamic quantities of interest can be obtained from a potential flow model based on linearized unsteady wing theory.

In two dimensions, the only rigorous analysis of the optimum shape problem is due to Wu (1971b) (1) who considered a rigid and a flexible airfoil. His study is based on the aerodynamic theory of Wu (1971a) and includes a detailed analysis of the optimum motion of a rigid airfoil in small-amplitude combined pitch and heave and a discussion of the general case of a flexible airfoil. He finds that (in two dimensions) the optimum solution is not unique.

In three dimensions, there has been no rigorous study of the optimum shape problem. This is in part due to a lack of an adequate three-dimensional unsteady aerodynamic theory with closed-form results. Here, it is desirable to determine the optimum shapes and motions of rigid, semi-rigid and flexible lifting surfaces.

In this chapter, Wu's solution for the optimum motion of a rigid airfoil is recast in terms of the normal modes of the matrix of the quadratic form for energy loss rate. This sheds some light on the structure of the optimum solution. Then, using the results of the present unsteady lifting-line theory in Chapter IV, the optimum motion of a three-dimensional rigid wing is determined. Numerical results for the

---

(1) In a parallel study, Wu (1972) has determined the optimum mode of energy extraction from gravity waves by means of an oscillating rigid airfoil.

optimum are presented for an elliptic wing over a range of reduced frequencies and for several aspect ratios.

5.2 Optimum Motion of a Rigid Airfoil

The general problem of determining the optimum shapes and motions of an oscillating lifting surface may be stated as follows: from within a prescribed class of shape functions h(x,y,t), find the optimum one which minimizes the mean energy loss rate subject to the condition of fixed mean thrust.

In this section, we focus attention on the optimum motion of a rigid airfoil oscillating in combined pitch and heave:

$$h(x,t) = \left[\frac{1}{2} c \xi_0 + (\xi_1 + j\xi_2) x\right] e^{j\omega t} \qquad |x| \leq c \qquad (5.1)$$

This is the same as (2.4) with c(y)/A replaced by c. The energetic quantities for this case can be obtained from the three-dimentional results of Section 4.2, after replacing c(y)/A by c and setting the induced downwash $W_I = 0$. In two dimensions, we denote the average value of the energy loss rate, the power required, the thrust and the suction force, respectively, by $\bar{E}$, $\bar{P}$, $\bar{T}$ and $\bar{T}_s$, and define the non-dimensional coefficients

$$C_E = \bar{E} / \left[\frac{\pi}{4} \rho U^3 c\right] \qquad (5.2)$$

$$C_P = \bar{P} / \left[\frac{\pi}{4} \rho U^3 c\right] \qquad (5.3)$$

$$C_T = \bar{T} / \left[\frac{\pi}{4} \rho U^2 c\right] \qquad (5.4)$$

$$C_{T_s} = \overline{T}_s / \left[\frac{\pi}{4} \rho U^2 c \right] \tag{5.5}$$

In matrix notation, the corresponding quadratic forms are given by

$$C_E = \underline{\xi}^T \underline{E} \underline{\xi} \tag{5.6}$$

$$C_P = \underline{\xi}^T \underline{P} \underline{\xi} \tag{5.7}$$

$$C_T = \underline{\xi}^T \underline{T} \underline{\xi} \tag{5.8}$$

$$C_{T_s} = \underline{\xi}^T \underline{K} \underline{\xi} \tag{5.9}$$

where $\underline{\xi}^T = \{\xi_0, \xi_1, \xi_2\}$ and from Section 4.2

$$\underline{E} = B(k) \begin{bmatrix} k^2 & k^2 & 2k \\ k^2 & 4+k^2 & 0 \\ 2k & 0 & 4+k^2 \end{bmatrix} \tag{5.10}$$

$$\underline{P} = k \begin{bmatrix} kF & k/2+G & F-kG \\ k/2+G & k(1-F)-2G & 0 \\ F-kG & 0 & k(1-F)-2G \end{bmatrix} \tag{5.11}$$

$$\underline{T} = \underline{P} - \underline{E} \tag{5.12}$$

$$\underline{K} = \begin{bmatrix} k^2 D & -k^2 B & 2kD - k^2 G \\ -k^2 B & k^2 + (4+k^2)D - 2k^2 F - 4kG & 0 \\ 2kD - k^2 G & 0 & k^2 + (4+k^2)D - 2k^2 F - 4kG \end{bmatrix} \tag{5.13}$$

where D(k) and B(k) are defined in (4.34) and F and G are the real and imaginary parts of Theodorsen's function (see (2.42) and (2.44). k is the

reduced frequency $k = \omega c/U$. The above results are in full agreement with those of Wu (1971b).

The optimum problem under consideration is to minimize the quadratic form C_E subject to the constraint

$$C_T = C_{T,0} > 0 \qquad (5.14)$$

This variational problem is equivalent to minimizing a new function $C'_E = C_E - \lambda C_P$ subject to the same constraint, λ being a Lagrange multiplier. Wu (1971b) has pointed out that application of variational methods to this problem fails to yield the optimum because the quadratic form C_E is singular (1) , since of the three eigenvalues of $\underline{E}$:

$$\mu_1 = 0 \qquad \mu_2 = B(k)\,(4+k^2) \qquad \mu_3 = B(k)\,(4+2k^2)$$

one is identically zero. He points out that the quadratic form C_E must first be reduced to a nonsingular one of a lower order which is then tractable by the usual variational methods.

Here, we first indicate the general method of reducing the singular quadratic form C_E. This also points out the advantage of Wu's approach to the problem. Wu's solution is then presented and recast in terms of the eigenvectors (normal modes) of $\underline{E}$ to shed light on the structure of the optimum solution.

The reduction of the singular quadratic form C_E is formally accomplished through the orthogonal transformation

$$\underline{\xi} = \underline{S}\,\underline{\zeta} \qquad (5.15)$$

---

(1)
C_P is indefinite in two and three dimensions.

where $\underline{\xi}^T = \{\xi_0, \xi_1, \xi_2\}$ and $\underline{S}$ is the orthonormal modal matrix of $\underline{E}$. The successive columns of $\underline{S}$ consist of the normal modes of $\underline{E}$ (in normalized form). Putting (5.15) in (5.6), we obtain

$$C_E = \underline{\xi}^T \underline{E}' \underline{\xi} \qquad (5.16)$$
$$= B(k) \left[(4+k^2)\, \xi_1^2 + (4+2k^2)\, \xi_2^2 \right]$$

where

$$\underline{E}' = \underline{S}^T \underline{E}\, \underline{S} \qquad (5.17)$$

is a diagonal matrix consisting of the respective eigenvalues of $\underline{E}$. The singular quadratic form C_E is thus reduced to the canonical form involving two variables. After writing C_P in terms of the new variables, we proceed with the usual variational approach. This, however, leads to an 8th degree algebraic equation in λ. For given k, the roots can be determined numerically. The optimum solution is the one corresponding to the highest η. In this way, various aspects of the optimum solution can be determined numerically, but it requires a considerable amount of work. This demonstrates the advantage of Wu's (1971b) method which leads to a quadratic equation in λ which can be solved analytically, with the subsequent study of the optimum problem requiring much less work.

Before considering Wu's solution, we first discuss the normal modes of $\underline{E}$, in terms of which, the solution will be recast. These are given by

$$\underline{\phi_1} = \left[(4+k^2)(4+2k^2)\right]^{-1/2} \begin{Bmatrix} (4+k^2)(4+2k^2) \\ -k^2 \\ -2k \end{Bmatrix} \text{ for } \mu_1 \qquad (5.18)$$

$$\underline{\phi_2} = (4+k^2)^{-1/2} \begin{Bmatrix} 0 \\ 2 \\ -k \end{Bmatrix} \quad \text{for } \mu_2 \qquad (5.19)$$

$$\underline{\phi}_3 = (4+2k^2)^{-1/2} \begin{Bmatrix} k \\ k \\ 2 \end{Bmatrix} \quad \text{for } \mu_3 \qquad (5.20)$$

The first and third modes consist of combined pitch and heave whereas the second mode represents pure pitching motion. The first mode has some very interesting properties and plays a central role in the present optimum solution. Hence, we discuss its properties in some detail.

It can be shown, from (5.6) - (5.9), that for $\underline{\xi} = \underline{\phi}_1$

$$\bar{E} = \bar{P} = \bar{T} = 0 \qquad \text{or} \qquad C_E = C_P = C_T = 0 \qquad (5.21)$$

$\underline{\phi}_1$ is, in fact, the same as the special set of values $\{\xi_0, \hat{\xi}_1, \hat{\xi}_2\}$ of Wu (1971b), who points out that these are a direct result of the condition

$$\tilde{b}_0 + \tilde{b}_1 = 0 \qquad (5.22)$$

where b_n are the coefficient of the chordwise Fourier cosine series representation of the downwash at the airfoil W_0 (as in (2.38e) and (2.38f)). Condition (5.22) also corresponds to zero circulation around the airfoil. This can be seen from (2.38e), (3.25) and (3.29) (after repalcing c/A by c), namely that

$$\tilde{\Gamma} \sim \tilde{\Omega} \sim (\tilde{b}_0 + \tilde{b}_1) \qquad (5.23)$$

and, hence, no vorticity is shed from the airfoil. In passing, we note that (5.22) and (5.23) are also valid for a flexible airfoil.

In the light of the above considerations, we will refer to $\underline{\phi}_1$ as the invisible mode. It must be noted that, due to the unsteadiness of the

airfoil motion, the leading-edge suction force is nonzero and, hence, the thrust from the normal force is also nonzero ($\bar{T}_p = -\bar{T}_s \neq 0$). Further, the unsteady lift and moment are nonzero due to the added mass effects.

Wu (1971a, 1971b) has shown that $C_E \sim |\tilde{b}_0 + \tilde{b}_1|^2$ and $C_P \sim (\tilde{b}_0 + \tilde{b}_1)$. It follows that the hydrodynamic efficiency of the invisible mode is 100%. This is analogous to the Froude efficiency of a propeller which tends to 100% as the disc loading vanishes. Since the invisible mode violates the condition of fixed positive thrust, (5.14), by itself it does not constitute the optimum.

The invisible mode is perfect unsteady feathering. It can be shown that, as $k \to 0$, the invisible mode tends to perfect geometric feathering (or quasi-steady feathering) where the airfoil pitching motion is such that the airfoil stays tangent to the path traversed in space by the heaving motion of the pitch axis.

The amplitude ratio and the phase advance of pitch relative to heave, defined respectively as

$$Z_p = \left[(\xi_1 / \xi_0)^2 + (\xi_2 / \xi_0)^2 \right]^{1/2} \qquad (5.24)$$

$$\alpha_p = \tan^{-1} (\xi_2 / \xi_1) \qquad (5.25)$$

are shown for the three normal modes of $\underline{E}$ in Figures 5.1 and 5.2. For obvious reasons, Z_p is not defined for the second mode. The quasi-steady feathering results are also shown for reference. It is seen that, as suggested in the above, the invisible mode tends to quasi-steady feathering as $k \to 0$.

Wu's (1971b) solution for the optimum problem at hand is presented in Figures 5.3 - 5.7. Shown are η, Z_p, α_p and C_{T_s}/C_T versus k and $\bar{C}_{T,0}$

versus k_c (defined below). The numerical results are obtained from a computer program which employs Wu's method. Wu's analysis shows that ξ_o is a free parameter in the problem and, hence, the solution is not unique. $\overline{C}_{T,0} = C_{T,0}/\xi_o^2$, the proportional loading parameter, is also a free parameter. In Figures 5.3 - 5.5, the lines designated $k = k_c$ and $k = k_m$ denote respectively the value of k below which no optimum exists and the value of k for which the fraction of thrust coming from the leading-edge suction force is a minimum as determined from Figure 5.6, where it is seen that outside a small range of k surrounding $k = k_m$, the contribution of the suction force becomes so large as to be difficult to realize in practice without leading-edge stall. We will refer to the optimum motion for $k = k_m$ as the superoptimum. Wu has pointed out that, in practice, it is preferable to operate at values of k slightly larger than k_m where Z_p and α_p vary relatively slowly and η is somewhat higher. The superoptimum line in Figure 5.3 indicates the advantage of operating at low $\overline{C}_{T,0}$ corresponding to large heave amplitude. Small values of $\overline{C}_{T,0}$ render the optimum valid to lower k and make η larger at the same k. Figure 5.4 indicates that the optimum normally involves a small amount of pitch relative to heave, of the order of 10%. Figure 5.7 depicts k_c as a function of $\overline{C}_{T,0}$. For given $\overline{C}_{T,0}$, the optimum exists for $k \geq k_c$. For further details of the present optimum problem see Wu (1971b).

In Figures 5.3 - 5.5, η, Z_p and α_p for the invisible mode are also shown, superimposed on Wu's solution. It is seen that, with decreasing $\overline{C}_{T,0}$ and/or increasing k, the optimum solutions approach the invisible mode which forms an upper envelope for the family. This leads us to believe that the invisible mode must play a central role in the optimum solution.

In order to understand the structure of the optimum and the role of

the invisible mode in it, we recast the solution in terms of the normal modes of $\underline{E}$ (one of which is the invisible mode). Thus, denoting the known optimum solution by $\underline{\xi}^*$, we set

$$\underline{\xi}^* = \sum_{i=1}^{3} \gamma_i \, \underline{\phi}_i \tag{5.26}$$

where the weighting functions γ_i indicate the amount of each of the modes in $\underline{\xi}^*$ and $\underline{\phi}_i$ are given by (5.18) - (5.20). To determine γ_i, we premultiply both sides of (5.26) by $\underline{\phi}_j^T$ and use the orthogonality property $\underline{\phi}_j^T \, \underline{\phi}_i = \delta_{ij}$, to obtain

$$\gamma_j = \underline{\phi}_j^T \, \underline{\xi}^* \qquad j = 1, 2, 3 \tag{5.27}$$

The three equations in (5.27) determine only two of the three functions γ_1, γ_2 and γ_3 because, as mentioned earlier, ξ_0 is arbitrary. Thus, we find

$$\gamma_2/\gamma_1 = \frac{\phi_{21} + \phi_{22}(\xi_1^*/\xi_0) + \phi_{23}(\xi_2^*/\xi_0)}{\phi_{11} + \phi_{12}(\xi_1^*/\xi_0) + \phi_{13}(\xi_2^*/\xi_0)} \tag{5.28}$$

$$\gamma_3/\gamma_1 = \frac{\phi_{31} + \phi_{32}(\xi_1^*/\xi_0) + \phi_{33}(\xi_2^*/\xi_0)}{\phi_{11} + \phi_{12}(\xi_1^*/\xi_0) + \phi_{13}(\xi_2^*/\xi_0)} \tag{5.29}$$

and rewrite (5.26) as

$$\underline{\xi}^* = \gamma_1 \left[\underline{\phi}_1 + (\gamma_2/\gamma_1) \, \underline{\phi}_2 + (\gamma_3/\gamma_1) \, \underline{\phi}_3 \right] \tag{5.30}$$

where we have chosen the amount of the invisible mode γ_1 to be the free parameter rather than ξ_0. Accordingly, we replace Wu's proportional loading parameter $\bar{C}_{T,0}$ with a modified loading parameter $\tilde{C}_{T,0} = C_{T,0}/\gamma_1^2$ which

is related to the former through

$$\tilde{C}_{T,0} = \bar{C}_{T,0} \left[\phi_{11} + (\gamma_2/\gamma_1)\,\phi_{21} + (\gamma_3/\gamma_1)\,\phi_{31} \right]^2 \qquad (5.31)$$

The numerical results for the recast optimum are obtained from the numerical values of $\bar{s}_1^*/\bar{s}_0$ and $\bar{s}_2^*/\bar{s}_0$, which are obtained from the above mentioned computer program for calculating Wu's solution. The amount of the second and third modes, relative to the invisible mode, present in the solution, are shown in Figures 5.8 and 5.9. It is seen that in general, with decreasing $\bar{C}_{T,0}$ and/or increasing k, both γ_2/γ_1 and γ_3/γ_1 diminish, and the invisible mode increasingly dominates the solution. Figure 5.10 depicts $\tilde{C}_{T,0}$ as a function of k and $\bar{C}_{T,0}$. We note that, for small values of k and $\bar{C}_{T,0}$, $\tilde{C}_{T,0} \approx \bar{C}_{T,0}$. This is due to the fact that, under these conditions, the solution is dominated by the invisible mode which tends to pure heave as $k \to 0$ (see (5.18)).

The results for the recast optimum are summarized in Figure 5.11 - 5.13 for $\bar{C}_{T,0} = 10^{-4}$, 5×10^{-3} and 10^{-1}. The figures depict η as a function of γ_2/γ_1, and γ_3/γ_1 with k and $\tilde{C}_{T,0}$ as parameters. It is seen that in general the optimum consists primarily of the invisible mode with a small amount of the third mode (of the order of 10%) and even a smaller amount of the second mode (of the order of 1%). The invisible mode is responsible for the high η achieved by the optimum, whereas the other modes are necessary to attain the prescribed level of thrust. We also note that the superoptimum achieves higher η at lower values of $\bar{C}_{T,0}$, as was pointed out earlier. From the recast form of the optimum, it becomes clear that the reason for the nonuniqueness of the present solution is the invisible mode, an arbitrary amount of which (γ_1) is present in the solution.

Strictly speaking, the recast results should be presented with $\tilde{C}_{T,0}$ as

a parameter rather than $\bar{C}_{T,0}$, as in the above. However, since there is a one-to-one correspondence between ξ_0 and γ_1 (as seen from (5.27) with j = 1) and, hence, also between $\bar{C}_{T,0}$ and $\tilde{C}_{T,0}$ (as seen in Figure 5.10), the above presentation is adequate.

Wu (1971b) has also considered the general optimum shape problem for a two-dimensional flexible airfoil (infinite degrees of freedom). He finds that C_E is singular (1), as one would expect, and that the nonsingular form of C_E is again of order two. He finds that the optimum shape h(x,t) can be determined only to a certain degree but not to the extent of finding a unique h(x,t). This lack of complete determinateness of the optimum shape problem, he points out, is an intrinsic feature of the problem.

5.3 Optimum Motion of a Rigid Wing

In this section we employ the present unsteady lifting-line theory (Chapters II - IV), to study the optimum motion (2) of a high-aspect-ratio rigid wing in combined pitch and heave:

$$h(x,y,t) = \left[\frac{1}{2}(c_0/A)\,\xi_0 + (\xi_1 + j\,\xi_2)\,x\right] e^{j\omega t}$$

$$|x| \leq c(y)/A \qquad |y| \leq b \qquad (5.32)$$

(see Figures 2.3a and 2.3b). The use of lifting-line theory restricts the

---

(1)
For a flexible airfoil, the condition (5.22) corresponds to an infinite family of invisible modes.

(2)
Here, we could alternately use the results of Chapter VI which are valid for all wing shapes and motions and all reduced frequencies. However, the subsequent analysis and computation of the optimum motion would be considerably more tedious.

analysis to wings of large aspect ratio, with slender planform (see Section 3.3) and relatively low reduced frequencies (based on semi chord).

The needed energetic quantities have been calculated in Section 4.2. In matrix notation, they are given by

$$C_{\mathcal{E}} = \underline{\xi}^T \underline{\mathcal{E}}\, \underline{\xi} \tag{5.33}$$

$$C_{\mathcal{P}} = \underline{\xi}^T \underline{\mathcal{P}}\, \underline{\xi} \tag{5.34}$$

$$C_{\mathcal{T}} = \underline{\xi}^T \underline{\mathcal{T}}\, \underline{\xi} \tag{5.35}$$

$$C_{\mathcal{T}_s} = \underline{\xi}^T \underline{\mathcal{K}}\, \underline{\xi} \tag{5.36}$$

where $\underline{\mathcal{E}}$, $\underline{\mathcal{P}}$, $\underline{\mathcal{T}}$ and $\underline{\mathcal{K}}$ are the respective matrices of the quadratic forms. They are symmetric by construction and have the properties in (4.19).

Here, as in two dimensions, the quadratic form $C_{\mathcal{P}}$ is indefinite and it is crucial first to identify the type of the quadratic form $C_{\mathcal{E}}$. To this end we temporarily adopt the strip-theory viewpoint and investigate the possibility of distributing two-dimensional invisible modes across the span. It follows from (5.22), (5.32), (2.38e) and (2.38f) that the invisible mode at station y is given by

$$\begin{aligned} \xi_1 / \xi_0 &= -k_0 k / (4 + k^2) \\ \xi_2 / \xi_0 &= -2 k_0 / (4 + k^2) \end{aligned} \tag{5.37}$$

Here, the right hand sides are functions of y because $k = k(y)$, but the left hand sides are fixed since the wing is rigid. Therefore, (5.37) can be enforced at one or more spanwise stations

(depending on the planform) but not at all stations (for reasons already mentioned, we exclude the rectangular planform). Wherever (5.37) is violated, spanwise vorticity is shed and the circulation is nonzero and varies with y which gives rise to trailing vorticity. Including the three-dimensional effects modifies this picture slightly, but, since the corrections are of higher order, the basic picture remains the same. Physically, this means that there exists no nontrivial unsteady motion of a rigid wing which does not produce a wake of vorticity. In other words, there exists no invisible mode for the rigid wing of finite span and $C_{\mathcal{E}}$ is positive definite.

The optimum problem at hand may be stated as: minimize the quadratic form $C_{\mathcal{E}}$ subject to

$$C_{\mathcal{J}} = C_{\mathcal{J},0} > 0 \qquad (5.38)$$

As in two dimensions, this is equivalent to minimizing a new function $C'_{\mathcal{E}} = C_{\mathcal{E}} - \lambda C_{\mathcal{P}}$ subject to the same condition, λ being a Lagrange multiplier. Denoting the elements of $\underline{\mathcal{E}}$ and $\underline{\mathcal{P}}$ by E_{ij} and P_{ij} respectively, we have

$$C_{\mathcal{E}} = E_{11}\,\xi_0^2 + E_{22}\,(\xi_1^2 + \xi_2^2) + 2E_{12}\,\xi_0\xi_1 + 2E_{13}\,\xi_0\xi_2 \qquad (5.39)$$

$$C_{\mathcal{P}} = P_{11}\,\xi_0^2 + P_{22}\,(\xi_1^2 + \xi_2^2) + 2P_{12}\,\xi_0\xi_1 + 2P_{13}\,\xi_0\xi_2 \qquad (5.40)$$

Since $C_{\mathcal{E}}$ is positive definite, the optimum is obtained using the usual variational methods. Thus, we set

$$\frac{\partial}{\partial \xi_i}\,(C_{\mathcal{E}} - \lambda C_{\mathcal{P}}) = 0 \qquad i = 0,1,2 \qquad (5.41)$$

$$C_{\mathcal{J}} = C_{\mathcal{P}} - C_{\mathcal{E}} = C_{\mathcal{J},0} > 0 \qquad (5.42)$$

λ is the solution of the cubic secular equation

$$|\underline{\mathcal{E}} - \lambda \underline{\mathcal{P}}| = 0$$

or

$$(E_{zz} - \lambda P_{zz}) \left[(E_{11} - \lambda P_{11})(E_{zz} - \lambda P_{zz}) - (E_{1z} - \lambda P_{1z})^2 - (E_{13} - \lambda P_{13})^2 \right] = 0 \qquad (5.43)$$

The root $\lambda_3 = E_{zz}/P_{zz}$ corresponds to pure pitching motion which clearly is not the optimum. The remaining roots, λ_1 and λ_2, are the solutions of the quadratic equation

$$a\lambda^2 + b\lambda + c = 0 \qquad (5.44)$$

where

$$a = P_{11} P_{zz} - P_{1z}^2 - P_{13}^2$$

$$b = 2E_{1z} P_{1z} + 2 E_{13} P_{13} - E_{11} P_{zz} - E_{zz} P_{11} \qquad (5.45)$$

$$c = E_{11} E_{zz} - E_{1z}^2 - E_{13}^2$$

λ_1 and λ_2 would be real, as required for physically meaningful solutions, if $b^2 - 4ac \geq 0$.

Substituting λ in (5.41), we obtain

$$\xi_1 / \xi_0 = - (E_{1z} - \lambda P_{1z}) / (E_{zz} - \lambda P_{zz}) \qquad (5.46)$$

$$\xi_2/\xi_0 = -(E_{13}-\lambda P_{13})/(E_{22}-\lambda P_{22}) \qquad (5.47)$$

The hydrodynamic efficiency is given by

$$\eta = 1 - \frac{E_{11}+E_{22}[(\xi_1/\xi_0)^2+(\xi_2/\xi_0)^2]+2E_{12}(\xi_1/\xi_0)+2E_{13}(\xi_2/\xi_0)}{P_{11}+P_{22}[(\xi_1/\xi_0)^2+(\xi_2/\xi_0)^2]+2P_{12}(\xi_1/\xi_0)+2P_{13}(\xi_2/\xi_0)} \qquad (5.48)$$

The λ corresponding to the larger η $(0 \leqslant \eta \leqslant 1)$ is the optimum. ξ_0 is then obtained from condition (5.42).

$$\xi_0^2 = C_{\mathcal{T},0}\left\{(P_{11}-E_{11})+(P_{22}-E_{22})[(\xi_1/\xi_0)^2+(\xi_2/\xi_0)^2]\right.$$
$$\left.+2(P_{12}-E_{12})(\xi_1/\xi_0)+2(P_{13}-E_{13})(\xi_2/\xi_0)\right\}^{-1} \qquad (5.49)$$

In analogy with the two-dimensional optimum, we may rewrite this as an expression for the proportional loading parameter $\bar{C}_{\mathcal{T},0} = C_{\mathcal{T},0}/\xi_0^2$. It is seen that, in contrast with the two-dimensional case, the present optimum solution is unique. This is a direct result of $C_{\underline{\xi}}$ being positive definite.

The amplitude ratio and the phase advance of pitch relative to heave are obtained from (5.24) and (5.25). The fraction of thrust coming from the leading-edge suction force is given by

$$C_{\mathcal{T}_s}/C_{\mathcal{T}} = (\bar{C}_{\mathcal{T},0})^{-1}\left\{K_{11}+K_{22}[(\xi_1/\xi_0)^2+(\xi_2/\xi_0)^2]\right.$$
$$\left.+2K_{12}(\xi_1/\xi_0)+2K_{13}(\xi_2/\xi_0)\right\} \qquad (5.50)$$

where K_{ij} denotes elements of $\underline{\mathcal{K}}$ (see (5.36)).

In understanding the present optimum, it is helpful to express the

solution in terms of both the present description of wing displacements, (5.32), and Lighthill's alternate description, (4.55) (Lighthill (1970)). As mentioned earlier, Lighthill's description is completely equivalent to the present one. In fact, it can be shown that in the present notation

$$h_L/(C_0/A) = -\frac{1}{2}\,\xi_0 \sin\alpha_p \qquad (5.51)$$

$$\alpha_L = \sqrt{\xi_1^2 + \xi_2^2} = \xi_0 Z_p \qquad (5.52)$$

$$b_L/(C_0/A) = -\frac{1}{2}\cos\alpha_p / Z_p \qquad (5.53)$$

Further, Lighthill's proportional feathering parameter, (4.56), becomes

$$\theta_L = -2 Z_p \csc\alpha_p / k_0 \qquad (5.54)$$

Numerical results for the optimum are obtained from a program that employs the present unsteady lifting-line theory and the above analysis. Figures 5.14 - 5.18 depict the optimum motion for an elliptic wing in terms of the present notation and also that of Lighthill. Calculations are carried out for $0 \leqslant k_0 \leqslant 1$ and $A = 8$ and 16. Strip-theory calculations are also shown for comparison. For each A, the results are cut off at the value of k_0 corresponding to the range of validity of the lifting-line theory at the given A (see Figure 4.13). It is seen that, with increasing A, the three-dimensional results approach the corresponding strip-theory values as expected. The strip theory optimum was, alternately, obtained using Wu's aerodynamic theory (Wu (1971a)). Numerical results for an elliptic wing show complete agreement. This serves as a check for the present analysis. Figure 5.14 shows that the highest η is achieved by the strip-theory case. This is due to the absence of the unsteady induced

downwash which normally increases C_{ξ}, decreases $C_{\wp}$ and, hence, reduces $\eta = 1 - C_{\xi}/C_{\wp}$ (as explained in Section 4.2).

Also shown in Figure 5.14 is the optimum motion in terms of Lighthill's notation. We note that the optimum position of the pitch axis is at about 73%-root chord and remains fairly constant with increasing k_o. In relation to θ_L, first we recall that $\theta_L = 0$ and $\theta_L = 1$ represent pure heave and perfect geometric feathering respectively. To understand the behavior of θ_L for the optimum, we consider the two-dimensional quasi-steady case where for positive (average) thrust $0 < \theta_L < 1$; for zero thrust $\theta_L = 1$; and for negative thrust $\theta_L > 1$. These ideas can be seen in Figure 5.19, recalling that, in quasi-steady flow, thrust is just the horizontal component of lift. In three-dimensions, the induced downwash normally reduces the effective incidence of wing sections, thereby reducing the thrust. In order to restore the thrust, we increase the effective incidence of the wing by lowering θ_L further below unity. This, on the one hand, represents a greater angular deviation of the wing from geometric feathering in the direction of positive thrust ($0 < \theta_L < 1$), and, on the other, is a reduction in pitch amplitude (measured from the horizontal). We see the same trend in Figure 5.14 where θ_L for cases of finite A are farther below unity than the strip theory values. Presumably, the same trend holds at higher k_o (as seen in Figure 5.14) where the problem is more complex due to the unsteady effects.

Figures 5.15 - 5.17 depict the optimum motion in terms of the present notation. With decreasing aspect ratio, Figure 5.15 indicates a slight reduction in the amplitude of pitch relative to heave; Figure 5.16 shows a slight increas in phase advance of pitch relative to heave; and Figure 5.17 shows an increase in the proportional loading parameter. As mentioned

earlier, since $C_{T,0}$ is prescribed (see (5.38)), Figure 5.17 is to be interpreted as giving ξ_0 (nondimensional heave amplitude) which decreases with decreasing A and/or increasing k_0. It is, thus, seen that, with decreasing A, both pitch and heave amplitudes are reduced. Further, the behavior of θ_L in Figure 5.14 and Z_p in Figure 5.15 indicate that the amplitude of pitch is reduced more than that of heave (nondimensional).

From the above considerations, the three-dimensional optimum can be described as follows. Compared with the strip-theory case, the wing of finite aspect ratio oscillates with smaller heave amplitude. This is because, for fixed k_0, the larger the heave amplitude, the stronger the trailing and shed vorticity and, hence, the stronger the unsteady induced downwash which tends to reduce η as explained in the above. With smaller heave amplitude, we ask how the wing maintains the prescribed level of thrust. The answer lies in the pitch amplitude which, measured from the position of perfect geometric feathering ($\theta_L = 1$), is increased in the direction of increasing thrust ($\theta_L < 1$).

Figure 5.18 depicts the fraction of thrust coming from the leading-edge suction force. The ratio decreases with decreasing A, as expected, since the unsteady induced downwash then grows stronger and this reduces the suction force (as pointed out in Section 4.2). We note that, in contrast with the two-dimensional optimum, here there is no superoptimum ($k_0 = 0$ is a trivial solution). Figure 5.18 indicates the range of k_0 where C_{T_s}/C_T is acceptably small. For example, for $(C_{T_s}/C_T) < 40\%$, $k_0 \tilde{<} 0.2$ which is a somewhat small range. Chopra and Kambe (1977), using a numerical unsteady lifting-surface theory, have found that, for fixed thrust, leading-edge sweepback reduces C_{T_s}/C_T for sweep angles up to about 30°, beyond which efficiency drops markedly. Leading-edge sweepback, thus,

increases the range of k_o where $C_{\mathcal{J}_s}/C_{\mathcal{J}}$ is acceptably small.

In summary, we notice the following differences between the two- and three-dimensional optimum solutions (rigid airfoil and rigid wing). The three-dimensional optimum solution is unique while the two-dimensional one is nonunique. The numerical examples considered indicate no k_c and k_m for the three-dimensional optimum. Hence, contrary to the two-dimensional case, in three-dimensions there is no superoptimum and the solution seems to exist for all reduced frequencies. The above differences also make Wu's strip-theory application of the two-dimensional optimum to a three-dimensional rigid wing questionable (Wu (1971b)).

We end this section with a few comments on the optimum shape problem for flexible wings. In particular, we consider the semi-rigid wing defined by

$$h(x,y,t) = \left\{ \frac{1}{2}(c_o/A)\,\xi_o(y) + \left[\xi_1(y) + j\,\xi_2(y)\right] x \right\} e^{j\omega t}$$

$$|x| \leq c(y)/A \qquad |y| \leq b \qquad (5.55)$$

(see Figures 2.3a and 2.3b). As pointed out in Section 4.2, here it is best to assume a number of suitably chosen spanwise modes for each of $\xi_o(y)$, $\xi_1(y)$ and $\xi_2(y)$. The present unsteady lifting-line theory can then be used to calculate the energetic quantities needed for optimization (as in Section 4.2). Here, $C_{\mathcal{P}}$ is indefinite. To determine the type of the quadratic form $C_{\mathcal{E}}$, again, we temporarily adopt the strip-theory viewpoint and investigate the possibility of distributing two-dimensional invisible modes across the span. It follows from (5.22), (5.55), (2.38e) and (2.38f) that the invisible mode at station y is given by

$$\xi_1(y)/\xi_o(y) = -k_o\,k/(4+k^2)$$

$$\xi_2(y)/\xi_0(y) = -2k_0/(4+k^2) \qquad (5.56)$$

Since for the semi-rigid wing, $\xi_0(y)$, $\xi_1(y)$ and $\xi_2(y)$ are arbitrary functions of y, (5.56) can be maintained at every spanwise station y. This means that sectional thrust and power required as well as the circulation are identically zero across the span. Hence, no spanwise or streamwise vorticity is shed from the wing. Physically, this means that, for the semi-rigid wing, there exists a nontrivial unsteady motion (defined by (5.56)) for which $C_\xi = C_\wp = C_\jmath = \Gamma(y,t) = 0$, i.e., there exists an invisible mode, and C_ξ is positive semi definite. The spanwise distribution of heave amplitude $\xi_0(y)$ remaines arbitrary.

Since C_ξ is positive semi definite, the subsequent optimization requires that the singular quadratic form C_ξ first be reduced to a nonsingular one of a lower order which can be handled by the usual variational methods (see Wu (1971b)).

It is also seen from the above discussion that there exists an invisible mode for a flexible wing (chordwise and spanwise) and, hence, C_ξ is positive semi definite. Here, there is need for a lifting-line or surface theory with closed-form results capable of handling a completely flexible wing.

CHAPTER VI

ENERGETICS OF FLAPPING FLIGHT USING INTEGRAL FORM OF CONSERVATION LAWS

6.1 Introduction

An alternate approach for calculating the energetic quantities for an oscillating lifting-surface in two or three dimensions is to employ the integral form of the conservation laws. Here, we calculate the thrust using the momentum theorem. Then, we employ the principle of conservation of mechanical energy to calculate the energy loss rate (wake energy) and the thrust.

This approach requires the distribution of bound vorticity and pressure on the lifting surface. In two dimensions, we employ the unsteady airfoil theory of Schwarz (1940) and thus obtain the energetic quantities in closed form. The results for an airfoil in combined pitch and heave are found to be in complete agreement with the known results. For more complex shapes and motions of the airfoil, however, the method involves tedious integrals. In three dimensions, in the absence of an exact analytic wing theory, the final results must be obtained by use of numerical unsteady lifting-surface theory or an approximate wing theory, such as that of Reissner (1947).

The proposed method has several advantages. i) It is quite general, being valid for arbitrary wing planform, aspect ratio, reduced frequency and mode of oscillation (small amplitudes). ii) It is physically enlightening, in that it relates the thrust and the energy loss rate to the properties of the far wake. iii) It avoids the direct calculation of the

leading-edge suction force.

A survey of the literature on the energetics of three-dimensional flapping flight is presented in Section 4.1. A survey of the literature on the two-dimensional case is presented below.

The first calculation of the energetic quantities for an oscillating airfoil is due to von Kármán and Burgers (1935) who considered the simplest case of an airfoil in heave. They calculated the thrust in two ways: i) using the balance of energy and ii) by direct calculation of the force. Garrick (1936) carried out a similar analysis for an airfoil in combined pitch and heave with an oscillating aileron. Later, Wu (1961), using the acceleration potential and the unsteady airfoil theory of Küssner and Schwarz (1940), calculated the energetic quantities for an airfoil with chordwise bending (traveling waves with arbitrary amplitude envelope). His Fourier series method is quite laborious. Siekmann (1962, 1963) used a vortex model and the Söhngen inversion formula to calculate the energetic quantities for an airfoil with chordwise bending (traveling waves with quadratically-varying amplitude envelope). Another calculation for an airfoil in combined pitch and heave is due to Lighthill (1970) who employed the acceleration potential.

The most general and extensive study of this type is due to Wu (1971a). His work includes a general unsteady airfoil theory for a flexible airfoil in variable forward-speed motion. He calculates the unsteady lift, moment and the energetic quantities. Results for the special case of steady-state harmonic oscillation are also given.

The above works are in full agreement with each other. They are all based on linearized aerodynamic theories and, hence, are restricted to small-amplitude oscillations. Chopra (1976) has carried out an analysis of

an airfoil in large-amplitude heave combined with small-amplitude pitch with respect to the local flight path. The theory is based on a vortex model and a rigid wake and is applicable to regular or irregular heaving motion. His numerical results clearly indicate the influence of heave amplitude on thrust and hydrodynamic efficiency.

6.2 Calculation of Thrust Using Momentum Theorem in Two Dimensions

Consider a thin, two-dimensional flexible airfoil in small-amplitude transverse oscillation in a uniform stream of inviscid incompressible fluid. Thrust can be calculated by applying the momentum theory to the fluid contained within a fixed control volume V which is bounded on the inside by the airfoil surface σ and the wake surface S_w and on the outside by a far boundary S consisting of S_1, S_2, S_3 and S_4 as shown in Figure 6.1. The coordinate system (x,z) is placed at the mean position of the airfoil, c is the airfoil semi chord and L is the abscissa of the downstream end of the wake. Whenever the wake extends beyond S_3, L is taken as the abscissa of S_3. The free stream velocity U is in the direction of the positive x-axis. The control volume V is stationary in the (x,z) frame.

With body forces neglected, the momentum theorem states that

$$\vec{F}_B(t) = -\int_S p\vec{n}\,dS - \int_{S+S_w+\sigma} \rho\vec{Q}\,(\vec{Q}\cdot\vec{n})\,dS - \int_V \frac{\partial}{\partial t}(\rho\vec{Q})\,dV \qquad (6.1)$$

where $\vec{F}_B$ is the force exerted by the fluid on the airfoil, $\vec{Q}$ is the velocity vector and $\vec{n}$ is the unit normal vector at the boundaries pointing away from V.

Since we assume that the airfoil thickness does not vary with time,

the effects of thickness and steady camber and angle of attack can be treated separately by steady airfoil theory. These effects do not contribute to thrust in two dimensions. Hence, in the following, σ refers to the flexible mid-camber line of the airfoil. Since thrust is a quadratic quantity, all quadratic terms will be retained in the analysis. Physically, this means that the actual airfoil and wake geometry must be considered, except where such considerations contribute only higher-order terms.

It is convenient to introduce into (6.1) the perturbation velocity

$$\vec{q} = \vec{Q} - U\vec{i} = u\vec{i} + w\vec{k} \tag{6.2}$$

where u and w are the perturbation velocity components in the x and z directions respectively. $\vec{i}$ and $\vec{k}$ are the corresponding unit vectors. (6.1) can be simplified somewhat through the use of the continuity equation

$$\int_{S+S_w+\sigma} (\vec{Q}\cdot\vec{n})\, dS = 0 \tag{6.3}$$

Introducing (6.2) and (6.3) into (6.1) and considering that S is a closed surface, we obtain

$$\vec{F}_B(t) = -\int_S (p-p_\infty)\vec{n}\, dS - \rho\int_{S+S_w+\sigma} \vec{q}\,(\vec{Q}\cdot\vec{n})\, dS - \rho\int_V \frac{\partial}{\partial t}\vec{q}\, dV \tag{6.4}$$

Thrust is the x-component of $\vec{F}_B$, i.e.,

$$T(t) = -\int_{S_1}(p-p_\infty)\, dS + \int_{S_3}(p-p_\infty)\, dS + \rho\int_{S+S_w+\sigma} u(\vec{Q}\cdot\vec{n})\, dS +$$

$$+ \rho \int_V \frac{\partial}{\partial t} \vec{q} \, dV \qquad (6.5)$$

In the first two integrals we use the Bernoulli equation:

$$p - p_\infty = -\rho \left[\phi_t + U u + \frac{1}{2} (u^2 + w^2) \right] \qquad (6.6)$$

where $( )_t$ denotes the partial derivative with respect to time and ϕ is the perturbation velocity potential ($\vec{q} = \nabla \phi$). The volume integral in (6.5) can be converted to a surface integral by use of the gradient theorem:

$$\int_{V'} \nabla \psi \, dV = \int_{S'} \psi \vec{n} \, dS \qquad (6.7)$$

where S' is the surface(s) bounding the volume V' and ψ has continuous partial derivatives in V' and on S'. Hence, the volume integral becomes

$$\int_V \frac{\partial u}{\partial t} \, dV = \vec{i} \cdot \int_V \nabla(\phi_t) \, dV$$

$$= -\int_{S_1} \phi_t \, dS + \int_{S_3} \phi_t \, dS \qquad (6.8)$$

$$+ \int_{S_w + \sigma} \frac{\partial}{\partial t} (\Delta\phi) \, \vec{i} \cdot \vec{n}_u \, dS + \int_{(LE)} \phi_t \, \vec{i} \cdot \vec{n} \, dS$$

where $\Delta\phi = \phi_u - \phi_l$ is the jump in the velocity potential across the airfoil or the wake. The last integral on the right hand side of (6.8) is around the leading edge. As pointed out in Section 4.2, near the leading edge of an oscillating airfoil ϕ and ϕ_t remain bounded. Hence, the integral around the leading edge which is over a vanishingly small region

is identically zero. A similar integral around the trailing edge of the wake is also zero.

The integral over $\sigma + S_w$ in (6.8) is to be carried out only on the upper side of these surfaces. Figure 6.2 depicts a segment of the airfoil or wake vortex sheet. χ is the distance along the sheet and h(x,t) is the lateral displacement of the sheet from the x-axis. It follows from the definition of the velocity potential that

$$\begin{aligned} \Delta\phi &= \int_{LE}^{\chi} \gamma(\chi_1, t)\, d\chi_1 \\ &= \int_{-c}^{x} \gamma(\xi, t)\, d\xi + O(\epsilon^2) \end{aligned} \tag{6.9}$$

where γ is the vorticity per unit length. The approximate form is to be carried out along the linearized vortex sheet which lies on the x-axis. The unit normal vector at the sheet is given by

$$\begin{aligned} \vec{n}_u &= h_x \vec{i} - \vec{k} + O(\epsilon^2) \\ \vec{n}_\ell &= -\vec{n}_u \end{aligned} \tag{6.10}$$

where $(\ )_x$ denotes the partial derivative with respect to x.

Substituting (6.9) and (6.10) into the third integral on the right hand side of (6.8) and integrating by parts, we obtain

$$\begin{aligned} \int_{S_w+\sigma} \frac{\partial}{\partial t}(\Delta\phi)\, \vec{i}\cdot\vec{n}_u\, dS &= h_w(L,t)\, \frac{\partial}{\partial t}\Gamma(L,t) \\ &\quad - \int_{-c}^{L} \frac{\partial}{\partial t}\left[\gamma(x,t)\right] h(x,t)\, dx \end{aligned} \tag{6.11}$$

where $(\ )_w$ denotes the wake and

$$\Gamma(L,t) = \int_{-C}^{L} \gamma(\xi,t)\, d\xi \tag{6.12}$$

The volume integral in (6.5) then becomes

$$\int_V \frac{\partial u}{\partial t}\, dV = -\int_{S_1} \phi_t\, dS + \int_{S_3} \phi_t\, dS + h_w(L,t)\frac{\partial}{\partial t}\Gamma(L,t) - \int_{-C}^{L} \frac{\partial}{\partial t}\left[\gamma(x,t)\right] h(x,t)\, dx \tag{6.13}$$

Next, we consider the momentum flux integral over $S + S_w + \sigma$ in (6.5). In terms of the perturbation velocities, (6.2), the part of the integral which is over S becomes

$$\int_S u(\vec{Q}\cdot\vec{n})\, dS = -\int_{S_1} (Uu+u^2)\, dS - \int_{S_2} uw\, dS + \int_{S_3} (Uu+u^2)\, dS + \int_{S_4} uw\, dS \tag{6.14}$$

It follows from (6.2), (6.10) and the downwash at σ and S_w, namely

$$\left[\frac{\partial}{\partial t} + (U+u)\frac{\partial}{\partial x}\right] h(x,t) = w(x,t) \qquad z = h(x,t) \tag{6.15}$$

that, on these surfaces,

$$(\vec{Q}\cdot\vec{n})_u = -(\vec{Q}\cdot\vec{n})_\ell = -\frac{\partial h}{\partial t} + O(\epsilon^2) \tag{6.16}$$

Using this result, the momentum flux integral over σ and S_w becomes

$$\int_{S_w+\sigma} u\,(\vec{Q}\cdot\vec{n})\,dS = -\int_{S_w+\sigma} \Delta u\,\frac{\partial h}{\partial t}\,dS + \int_{(LE)} u(\vec{Q}\cdot\vec{n})\,dS \qquad (6.17)$$

where $\Delta u = u_u - u_\ell$. The integral around the leading edge, being over a vanishingly small region, is identically zero since, at the leading edge, $(\vec{Q}\cdot\vec{n})$ is finite and u has a square-root singularity which is integrable. A similar integral around the trailing edge of the wake is likewise zero. It can be shown, using the intrinsic coordinate system (s,n) (see Figure 6.2), that

$$\Delta u = \gamma + O(\epsilon^3) \qquad (6.18)$$

Hence,

$$\int_{S_w+\sigma} u(\vec{Q}\cdot\vec{n})\,dS = -\int_{-c}^{L} \gamma(x,t)\,\frac{\partial}{\partial t}\,h(x,t)\,dx \qquad (6.19)$$

Substituting (6.6), (6.13), (6.14) and (6.19) into (6.5), we obtain

$$T(t) = \frac{\rho}{2}\int_{S_1}(w^2-u^2)\,dS - \frac{\rho}{2}\int_{S_3}(w^2-u^2)\,dS$$

$$-\rho\int_{S_2} uw\,dS + \rho\int_{S_4} uw\,dS \qquad (6.20)$$

$$+\rho\,h_w(L,t)\,\frac{\partial}{\partial t}\,\Gamma(L,t) - \rho\int_{-c}^{L}\frac{\partial}{\partial t}\left[\gamma(x,t)\,h(x,t)\right]dx$$

Next, we move the far boundary S to infinity. It is shown in Appendix D that, in this limit, the integrals over S_1, S_2 and S_4 in (6.20) vanish. Hence,

$$T(t) = -\frac{1}{2}\rho \int_{S_3} (w^2 - u^2)\, dS \qquad (6.21)$$

$$+ \rho h_w(L,t) \frac{\partial}{\partial t}\Gamma(L,t) - \rho \int_{-c}^{L} \frac{\partial}{\partial t}\left[\gamma(x,t)\, h(x,t)\right] dx$$

This result is quite general, being valid for any small-amplitude transverse motion of the airfoil and vanishes for steady flow in accordane with d'Alembert's paradox.

In the remainder of this section, we consider the case of steady-state harmonic oscillation, where, in analogy with steady flow, we refer to S_3 as the Trefftz plane. L is then the abscissa of that plane ($L \to \infty$). Here, we use the unsteady airfoil theory of Schwarz (1940) (1) to calculate the thrust from (6.21).

The amplitude of the airfoil circulation and wake vorticity are respectively given by

$$\tilde{\Gamma} = c\, e^{-jk}\, \tilde{\Omega} \qquad (6.22)$$

$$\tilde{\gamma}_w(x) = -jk\, \tilde{\Omega}\, e^{-j\bar{\omega}x} \qquad (6.23)$$

where $k = \omega c/U$ is the reduced frequence and $\tilde{\Omega}$ is the reduced circulation. From Schwarz

$$\tilde{\Omega}(k) = \frac{4 \int_{-c}^{c} \left[\frac{c+\xi}{c-\xi}\right]^{1/2} \tilde{W}_o(\xi)\, d\xi}{\pi j c k \left[H_1^{(2)}(k) + j H_o^{(2)}(k)\right]} \qquad (6.24)$$

---

(1) Schwarz's theory is presented in Bisplinghoff, Ashley and Halfmann (1955).

where $\tilde{W}_o$ is the prescribed linearized downwash at the airfoil:

$$W_o(x,t) = \left(\frac{\partial}{\partial t} + U\frac{\partial}{\partial x}\right)\tilde{h}_a(x)\, e^{j\omega t} \qquad (6.25)$$

$$|x| \le c \qquad z = 0\pm$$

$(\ )_a$ denotes the airfoil.

It follows from (6.12), (6.22) and (6.23) that

$$\tilde{\Gamma}(L) = c\,\tilde{\Omega}\, e^{-j\bar{\omega}L} \qquad (6.26)$$

and

$$\frac{\partial}{\partial t}\Gamma(L,t) = -U\,\gamma_w(L,t) \qquad (6.27)$$

Substituting this result into (6.21), we obtain

$$T(t) = -\frac{\rho}{2}\int_{S_3}(w^2 - u^2)\,dS - \rho U\, h_w(L,t)\,\gamma_w(L,t)$$
$$-\rho\int_{-c}^{L}\frac{\partial}{\partial t}\left[\gamma(x,t)\,h(x,t)\right]dx \qquad (6.28)$$

The average thrust is obtained from (6.28) using the averaging rules in (4.4) and (4.5).

$$\bar{T} = -\rho U\,\overline{h_w(L,t)\,\gamma_w(L,t)} - \frac{\rho}{2}\int_{S_3}(\overline{w^2} - \overline{u^2})\,dS \qquad (6.29)$$

It is shown in Appendix E that for the case of steady-state harmonic oscillation

$$\overline{u^2} = \overline{w^2} \qquad (6.30)$$

in the far wake. Hence, the integral term in (6.29) is identically zero and the expression for the average thrust reduces to

$$\overline{T} = -\rho U \overline{h_w(L,t)\,\gamma_w(L,t)} \tag{6.31}$$

In the absence of the mechanism of diffusion, the wake vorticity is convected downstream without change. Hence, $\gamma_w(L,t)$ is obtained from (6.23). The determination of $h_w(L,t)$, on the other hand, requires some work, since the ultimate displacement of an element of the deformable wake is determined by its entire past history, in which it is subjected to a varying field of downwash along its path from the trailing edge to the Trefftz plane. This asymptotic displacement of the wake is determined in the next section.

It is enlightening to examine the phase difference of the displacement and vorticity of the far wake. Let,

$$h_w(L,t) = |h_w|\, e^{j\alpha}\, e^{j\omega t} \tag{6.32}$$

$$\gamma_w(L,t) = |\gamma_w|\, e^{j\beta}\, e^{j\omega t} \tag{6.33}$$

where the amplitude and phase of $h_w(L,t)$ and $\gamma_w(L,t)$ are respectively denoted by $|h_w|$ and $|\gamma_w|$, and α and β. Substituting these in (6.31), we obtain

$$\overline{T} = -\tfrac{1}{2}\rho U\, |h_w|\, |\gamma_w| \cos(\alpha-\beta) \tag{6.34}$$

For the sake of discussion, we assume that $|h_w|$ and $|\gamma_w|$ are fixed and consider the following special cases.

i) If $\alpha - \beta = \pi/2$, $\overline{T} = 0$ (1).

ii) If $\alpha - \beta = \pi$, we have the case of maximum average thrust (for fixed $|h_w|$ and $|\gamma_w|$). This does not necessarily correspond to the optimum motion which is the solution of a constrained variational problem (Chapter V).

iii) If $\alpha - \beta = 0$, we have the case of maximum average drag (for fixed $|h_w|$ and $|\gamma_w|$).

iv) Cases with $0 < (\alpha - \beta) < \pi/2$ correspond to those shapes and motions of the airfoil which, in the average, produce drag, whereas cases with $\pi/2 < (\alpha - \beta) < \pi$ correspond to thrust-producing configurations. Figure 6.3 depicts a thrust- and a drag-type far wake corresponding to cases (ii) and (iii) in the above.

Temporarily, we adopt the viewpoint of an observer fixed in the fluid. From the principle of action and reaction we conclude that (6.31) represents the average flux of momentum associated with the wake vortices crossing the Trefftz plane. In the case of thrust-producing configurations, the wake vorticity is so oriented as to give rise to a net flux of momentum in the downstream direction. Similarly, the drag-producing configurations give rise to a net flux of momentum in the upstream direction. The commonly observed Karman vortex street is a drag-type wake.

---

(1) It can be seen from the results of Appendix E (see (E.1), (E.2) and (E.9)) that the self-induced downwash of a linearized wake with sinusoidally varying strength is out of phase with the vorticity distribution by $\pi/2$. Hence, the self-induced displacement of such a wake is also out of phase with the vorticity by $\pi/2$ and the corresponding contribution to the average thrust is zero.

6.3 Asymptotic Wake Displacement in Two Dimensions

In the preceding section we found that the average thrust of a harmonically-oscillating airfoil is proportional to the time average of the far-wake displacement and vorticity. Since thrust is $O(\epsilon^2)$ and the wake vorticity is $O(\epsilon)$, we need to determine the wake displacement to $O(\epsilon)$. This can be accomplished using a linearized (planar) wake model as shown below.

The wake consists of free vortices which move with the fluid. The linearized downwash at the wake is given by

$$w_w(x,t) = \left(\frac{\partial}{\partial t} + U\frac{\partial}{\partial x}\right) h_w(x,t) \qquad (6.35)$$

$$x \geq c \qquad z = 0\pm$$

or

$$\tilde{w}_w(x) = j\omega \tilde{h}_w(x) + U\frac{d}{dx}\tilde{h}_w(x) \qquad (6.36)$$

$$x \geq c \qquad z = 0\pm$$

To invert this equation, we multiply through by $e^{j\bar{\omega}x}$ and integrate from the trailing edge up to x ($x > c$). The solution which passes through the trailing edge is given by

$$\tilde{h}_w(x) = \tilde{h}(c)\, e^{-j\bar{\omega}(x-c)} + U^{-1}\int_c^x \tilde{w}_w(\xi)\, e^{-j\bar{\omega}(x-\xi)}\, d\xi$$

$$x \geq c \qquad (6.37)$$

The determination of the wake displacement from (6.37) requires the downwash at the plane of the wake which is given by

$$\tilde{w}_w(\xi) = \frac{-1}{2\pi}\int_{-c}^{c} \frac{\tilde{\gamma}_a(x)}{\xi - x}\, dx +$$

$$+\frac{jk}{2\pi}\tilde{\Omega}\oint_{c}^{\infty}\frac{e^{-j\bar{\omega}x}}{\xi-x}\,dx \qquad \xi\geq c \qquad z=0\pm \qquad (6.38)$$

The first term here is the contribution of the airfoil and the second is that of the wake. The vorticity distribution on the airfoil is given by Schwarz (1940) as

$$\tilde{\gamma}_a(x)=\frac{2}{\pi}\left[\frac{c-x}{c+x}\right]^{1/2}\left\{\oint_{-c}^{c}\left[\frac{c+\lambda}{c-\lambda}\right]^{1/2}\frac{\tilde{W}_o(\lambda)}{x-\lambda}\,d\lambda\right.$$

$$\left.+\frac{jk}{2}\tilde{\Omega}\int_{c}^{\infty}\left[\frac{\lambda+c}{\lambda-c}\right]^{1/2}\frac{e^{-j\bar{\omega}\lambda}}{x-\lambda}\,d\lambda\right\} \qquad |x|\leq c \qquad (6.39)$$

Substituting (6.39) into (6.38), interchanging the order of integration in the first two terms and making use of the following integrals from Appendix A

$$\int_{-c}^{c}\left[\frac{c-x}{c-x}\right]^{1/2}\frac{dx}{(x-\lambda)(\xi-x)}=\frac{-\pi}{\lambda-\xi}\left\{\left[\frac{\lambda-c}{\lambda+c}\right]^{1/2}-\left[\frac{\xi-c}{\xi+c}\right]^{1/2}\right\}$$

$$\lambda,\xi\geq c \qquad (6.40)$$

$$\oint_{-c}^{c}\left[\frac{c-x}{c+x}\right]^{1/2}\frac{dx}{(x-\lambda)(\xi-x)}=\frac{\pi}{\lambda-\xi}\left[\frac{\xi-c}{\xi+c}\right]^{1/2} \qquad |\lambda|\leq c \qquad \xi\geq c$$

$$(6.41)$$

we find

$$\tilde{W}_w(\xi)=\frac{-1}{\pi}\left[\frac{\xi-c}{\xi+c}\right]^{1/2}\left\{\int_{-c}^{c}\left[\frac{c+\lambda}{c-\lambda}\right]\frac{\tilde{W}_o(\lambda)}{\lambda-\xi}\,d\lambda \qquad (6.42)\right.$$

$$\left.+\frac{jk}{2}\tilde{\Omega}\oint_{c}^{\infty}\left[\frac{\lambda+c}{\lambda-c}\right]^{1/2}\frac{e^{-j\bar{\omega}\lambda}}{\lambda-\xi}\,d\lambda\right\} \qquad \xi\geq c \qquad z=0\pm$$

where the first term is the quasi-steady contribution and the second term represents all direct and indirect contributions from the wake.

Substituting (6.42) into (6.37), we obtain

$$\tilde{h}_w(x) = e^{-j\bar{\omega}x}\left\{\tilde{h}(c)\,e^{jk}\right. \tag{6.43}$$

$$-\frac{1}{\pi U}\int_c^x d\xi \int_{-c}^{c} d\lambda \left[\frac{\xi-c}{\xi+c}\right]^{1/2}\left[\frac{c+\lambda}{c-\lambda}\right]^{1/2}\frac{\tilde{W}_0(\lambda)\,e^{j\bar{\omega}\xi}}{\lambda-\xi}$$

$$\left.-\frac{jk\tilde{\Omega}}{2\pi U}\int_c^x d\xi \oint_c^{\infty} d\lambda \left[\frac{\xi-c}{\xi+c}\right]^{1/2}\left[\frac{\lambda+c}{\lambda-c}\right]^{1/2}\frac{e^{j\bar{\omega}(\xi-\lambda)}}{\lambda-\xi}\right\} \quad x \geq c$$

Here, the first term is the displacement of a rigid wake which is the sinusoidal trace of the trailing edge. The second term is due to the quasi-steady effects and the third term represents all direct and indirect contributions from the wake.

The asymptotic displacement of the wake is obtained from (6.43) by setting $x = \infty$ in the upper limit of the integrals. In the notation of Section 6.2, this is $\tilde{h}(L)$ where L is the abscissa of the Trefftz plane $(L \to \infty)$.

$$\tilde{h}_w(L) = e^{-j\bar{\omega}x}\left\{\tilde{h}(c)\,e^{jk}\right. \tag{6.44}$$

$$-\frac{1}{\pi U}\int_c^{\infty} d\xi \int_{-c}^{c} d\lambda \left[\frac{\xi-c}{\xi+c}\right]^{1/2}\left[\frac{c+\lambda}{c-\lambda}\right]^{1/2}\frac{\tilde{W}_0(\lambda)\,e^{j\bar{\omega}\xi}}{\lambda-\xi}$$

$$\left.+\frac{jk\tilde{\Omega}}{\pi U}\int_c^{\infty} d\xi \oint_c^{\infty} d\lambda \left[\frac{\xi-c}{\xi+c}\right]^{1/2}\left[\frac{\lambda+c}{\lambda-c}\right]^{1/2}\frac{e^{j\bar{\omega}(\xi-\lambda)}}{\xi-\lambda}\right\}$$

The double integral in the last term is a universal one. It is evaluated

in Appendix A and found to be equal to

$$\frac{\pi^2 c}{4}\left\{J_0^2(k)+Y_0^2(k)-j\int_k^\infty\left[J_1^2(k_1)+Y_1^2(k_1)-J_0^2(k_1)-Y_0^2(k_1)\right]dk_1\right\} \tag{6.45}$$

In passing, we note that, in the limit of steady flow, the asymptotic displacement of the wake contains a logarithmic singularity which arises from the second term of (6.44) and can be expressed as log L or log k.

For future work, it would be of interest to calculate the near-wake displacement for a heaving airfoil from (6.43) and to compare (at least qualitatively) with the experimental results of Bratt (1953) and Ohashi and Ishikawa (1972), and the computational results of Giesing (1968). Some of the integrals in (6.43) may need to be evaluated numerically. Further, it would be of interest to calculate the far-wake displacement of a heaving airfoil from (6.44) and to correlate with the analytical results of Weihs (1972) who studied the behavior of semi-infinite double rows of vortices.

Substituting (6.45), (6.44) and (6.23) into the expression for the average thrust, (6.31), and introducing the nondimensional quantities in (5.4) and

$$\begin{aligned} x^* &= x/c \\ h^* &= h/c \\ w_o^* &= w_o/U \\ \Omega^* &= \Omega/U \end{aligned} \tag{6.46}$$

we obtain the following expression for the thrust coefficient of a

harmonically oscillating airfoil.

$$C_T = \frac{-2}{\pi} k \mathcal{R}_j \left\{ j\tilde{\Omega}^{*}\circledast \tilde{h}^{*}(1)\, e^{jk} \right.$$

$$-\frac{j}{\pi}\tilde{\Omega}^{*}\circledast \int_1^{\infty} d\xi^{*} \int_{-1}^{1} d\lambda^{*} \left[\frac{\xi^{*}-1}{\xi^{*}-1}\right]^{1/2} \left[\frac{1+\lambda^{*}}{1-\lambda^{*}}\right]^{\frac{1}{2}} \frac{\tilde{W}_0^{*}(\lambda^{*})\, e^{jk\xi^{*}}}{\lambda^{*}-\xi^{*}}$$

$$\left. -\frac{\pi}{8} k \left|\tilde{\Omega}^{*}\right|^2 \left[J_0^2(k) + Y_0^2(k)\right] \right\} \qquad (6.47)$$

This form has the advantage that it relates the thrust to the airfoil shapes and motions (see (6.24) and (6.25)). We also note that, in the steady limit, $C_T \to 0$ as expected.

As an example and a check, we consider an airfoil in heaving motion, where

$$h_a(x,t) = h_0\, e^{j\omega t} \qquad |x| \le c \qquad (6.48)$$

$$\tilde{W}_0^{*} = jk\, h_0^{*} \qquad |x^{*}| \le 1 \qquad z^{*} = 0\pm \qquad (6.49)$$

Substituting (6.49) into (6.24) and (6.47) and using the following integrals from Ashley and Landahl (1965)

$$\int_{-1}^{1} \left[\frac{1+\lambda^{*}}{1-\lambda^{*}}\right]^{1/2} \frac{d\lambda^{*}}{\lambda^{*}-\xi^{*}} = \pi \left\{1 - \left[\frac{\xi^{*}+1}{\xi^{*}-1}\right]^{1/2}\right\} \qquad \xi^{*} \ge 1 \qquad (6.50)$$

$$\int_1^{\infty} \left\{\left[\frac{\xi^{*}-1}{\xi^{*}+1}\right]^{1/2} - 1\right\} e^{jk\xi^{*}}\, d\xi^{*} = \left\{ e^{jk}/(jk) \right. \qquad (6.51)$$

$$\left. -\frac{\pi}{2}\left[H_1^{(2)\circledast}(k) + j\, H_0^{(2)\circledast}(k)\right] \right\}$$

we obtain the following known result for the thrust coefficient of a heaving airfoil (see, e.g., Wu (1971b)).

$$C_{T_H} = 4k^2 D(k) h_o^{*2} \tag{6.5.2}$$

where D(k) is defined in (4.34).

Kelly, Rentz and Siekmann (1964) have carried out experiments to measure the thrust of oscillating flexible plates. They found good agreement with existing theories, after adding turbulent skin friction drag to the theoretical results. Figure 6.4 depicts their results for the case of heaving motion. Also shown are the result of Smith and Stone (1961) who neglected the influence of the unsteady wake, resulting in gross overestimation of the thrust. This indicates the importance of the unsteady effects in calculating the thrust.

6.4 Calculation of Wake Energy and Thrust Using Conservation of Energy in Two Dimensions

Consider a thin, two-dimensional flexible airfoil moving at constant velocity U along a rectilinear path in unbounded, inviscid incompressible fluid which is at rest at infinity. The airfoil executes small-amplitude transverse oscillations, thereby producing thrust and a wake of vorticity. Since the fluid is nondissipative and incompressible, it can store energy only in kinetic form. Hence, the work done by the airfoil on the fluid ultimately shows up in the far wake in the form of kinetic energy. In order to determine this relationship quantitatively, we apply the principle of conservation of mechanical energy to the fluid contained in a fixed control volume V bounded on the inside by the airfoil and wake surfaces, σ

and S_w, and on the outside by a far boundary S (consisting of S_1, S_2, S_3 and S_4) which is located infinitely far from the airfoil and the wake, as shown in Figure 6.5. The fluid contained in V is thus free from discontinuities. The coordinate system (X,Z) is at rest with respect to the undisturbed fluid while the coordinate system (x,z), which is parallel to (X,Z), is fixed to the mean position of the airfoil and, hence, moves in the negative X-direction with velocity U. Both coordinate systems are, thus, inertial and obserbers in both frames measure the same forces. The (x,z) observer measures a velocity field $\vec{Q}$ consisting of a free stream $U\vec{i}$ and a perturbation field $\vec{q} = u\vec{i} + w\vec{k}$. The (X,Z) observer, on the other hand, measures $\vec{q}$. The control volume V is stationary with respect to the (X,Z) frame.

Here, as in Section 6.2, we assume that the airfoil thickness does not vary with time and consider the purely unsteady motion of the flexible mid-camber line of the airfoil. With body forces neglected, the balance of energy for the fluid in V is given by

$$\int_V \frac{\partial}{\partial t}\left(\frac{1}{2}\rho|\vec{q}|^2\right) dV = -\int_{S+S_w+\sigma} p\vec{n}\cdot\vec{q}\, dS \qquad (6.53)$$

where we have adopted the viewpoint of the (X,Z) observer because the (x,z) observer measures an infinite amount of energy for the fluid in V. (6.53) states that the rate of change of the total kinetic energy of the fluid in V is equal to the rate of work of the external forces on the same fluid.

Since pressure is continuous across the wake,

$$-\int_{S_w} p\vec{n}\cdot\vec{q}\, dS = 0 \qquad (6.54)$$

Also, it can be shown that, for S infinitely removed from the airfoil and the wake,

$$-\int_S p\,\vec{n}\cdot\vec{q}\;dS = 0 \qquad (6.55)$$

The integral over the airfoil surface can be written as the sum of integrals over the upper and lower surfaces and the leading and trailing edges of the airfoil, namely

$$-\int_\sigma p\,\vec{n}\cdot\vec{q}\;dS = \qquad (6.56)$$

$$= -\left[\int_{\sigma_u} + \int_{\sigma_\ell} + \int_{(LE)} + \int_{(TE)}\right] p\,\vec{n}\cdot\vec{q}\;dS$$

where (LE) and (TE) denote respectively integrations around the leading and trailing edges of the airfoil, both of which are of vanishingly small extent. The latter integral is identically zero due to the Kutta condition. The former is the rate of work of the leading-edge suction force T_s on the fluid, i.e., $-UT_s$.

In (6.56), $\vec{q}$ is the velocity of the airfoil mid-camber line

$$\vec{q} = -U\vec{i} + \frac{\partial}{\partial t} h_a\,\vec{k} \qquad (6.57)$$

and $\vec{n}$ is the unit normal vector at the airfoil, with respect to the (X,Z) frame, which is given by

$$\vec{n}_u = \frac{\partial}{\partial X} h_a\,\vec{i} - \vec{k} + O(\epsilon^2)$$
$$\vec{n}_\ell = -\vec{n}_u \qquad (6.58)$$

Using (6.57) and (6.58), the integrals over the upper and lower surfaces of the airfoil may be combined to obtain

$$-\left[\int_{\sigma_u} + \int_{\sigma_\ell}\right] p\,\vec{n}\cdot\vec{q}\,dS = \tag{6.59}$$

$$= -U T_p - \int_{LE}^{TE} \Delta p \frac{\partial}{\partial X} h_a \, dX$$

where

$$T_p = \int_{LE}^{TE} \Delta p \frac{\partial}{\partial X} h_a \, dX \tag{6.60}$$

is the thrust contribution from the normal force at the airfoil.

Combining the above results and noting that $T = T_s + T_p$, (6.53) becomes

$$\int_V \frac{\partial}{\partial t}\left(\tfrac{1}{2}\rho|\vec{q}|^2\right) dV = -UT - \int_{LE}^{TE} \Delta p \frac{\partial}{\partial t} h_a \, dX \tag{6.61}$$

where it is seen that, in the limit of steady flow, thrust tends to zero, as expected. Averaging (6.61) over the time interval τ, we obtain

$$\frac{1}{\tau}\Delta(KE) = -U\bar{T} - \int_{LE}^{TE} \overline{\Delta p \frac{\partial}{\partial t} h_a} \, dX \tag{6.62}$$

where

$$\frac{1}{\tau}\Delta(KE) = \frac{1}{\tau}\left\{\left[\int_V \tfrac{1}{2}\rho|\vec{q}|^2 dV\right]_{t=t_o+\tau} - \left[\int_V \tfrac{1}{2}\rho|\vec{q}|^2 dV\right]_{t=t_o}\right\} \tag{6.63}$$

is the average rate of the total kinetic energy of the fluid in V during τ. t_o is an arbitrary constant.

(6.62) can be rearranged as

$$-\int_{LE}^{TE} \overline{\Delta p \frac{\partial}{\partial t} h_a}\, dX = U\bar{T} + \frac{1}{\tau}\Delta(KE) \qquad (6.64)$$

which states that the average power required to maintain the airfoil oscillations is equal to the average rate of work of thrust plus the average rate of increase of the kinetic energy of the fluid. The latter is the average energy loss rate since it represents energy imparted to the fluid which cannot be recovered. As we will see later, this quantity can be determined from the properties of the far wake. In terms of the notation of Section 5.2, (6.64) may be written as

$$\bar{P} = U\bar{T} + \bar{E} \quad \text{or} \quad C_P = C_T + C_E \qquad (6.65)$$

which is a statement of conservation of energy for the present problem. Thus, the input power is partly used to produce thrust, and thereby useful work, and partly wasted in generating a wake of vorticity. The hydrodynamic efficiency of the motion is defined as the ratio of the useful power to the input power, i.e.,

$$\eta = C_T / C_P = 1 - C_E / C_P \qquad (6.66)$$

which indicates that, for given input power, one must minimize the energy loss rate in order to maximize the hydrodynamic efficiency.

In the remainder of this section, we consider the case of steady-state harmonic oscillation of radian frequency ω. We choose τ to be the period

$2\pi/\omega$, during which one wavelength $\lambda = 2\pi U/\omega$ of the periodic wake is generated. Here, $\Delta(KE)$ is the kinetic energy content of one wavelength of the far wake. This can be seen by comparing the flow field at times t and $t + \tau$. The flow field near the airfoil is the same in both cases. But the far wake for $t + \tau$ is one wavelength longer than that for t. Hence, $\Delta(KE)$ is the kinetic energy content of a slice of the far wake of length λ as shown in Figure 6.6. From potential flow theroy, the kinetic energy of the fluid in this volume, say V', is given by

$$\Delta(KE) = \int_{V'} \frac{1}{2}\rho|\vec{q}|^2 dV = \frac{1}{2}\rho \int_{S'} \phi \frac{\partial}{\partial n}\phi \, dS \qquad (6.67)$$

where S' is the surface bounding V'. It consists of S_1', S_2', S_3', S_4', S_{w_u} and S_{w_ℓ}. Due to the periodicity of flow properties in the far wake (see Appendix E), the integrals over S_1' and S_3' cancel each other out. As the lateral boundaries S_2' and S_4' are removed to infinity, the integrals over these surfaces vanish since from Appendix E

$$\phi, u, w \sim e^{-\bar{\omega}|z|} \qquad (6.68)$$

The integrals over the upper and lower wake surfaces can be combined using (6.58) to obtain

$$\Delta(KE) = \frac{-1}{2}\rho \int_{X_o}^{X_o+\lambda} \Delta\phi \frac{\partial}{\partial Z}\phi\Big|_{Z=0} dX \qquad (6.69)$$

where X_o is an arbitrary constant and we have neglected terms of $O(\epsilon^3)$. The waviness of the wake, thus, does not appear to this order. It is noteworthy that, while a planar wake is adequate for calculating the wake

energy, the actual wake geometry has to be considered for calculating the thrust using the momentum theorm (Section 6.2). This is because energy is a scalar quantity, whereas momentum is a vector quantity which is sensitive to changes in direction.

(6.69) is essentially the spatial average, with respect to X, over the interval λ (defined in a manner analogous to the time average in (4.2)) of $\Delta\phi$ and $\partial\phi/\partial Z$. Denoting this spatial average by $\overline{(\ )}$, we have

$$\Delta(KE) = -\frac{1}{2}\rho\lambda\ \overline{\Delta\phi\ \partial\phi/\partial Z}\Big|_{Z=0} \qquad (6.70)$$

It is convenient to evaluate $\Delta\phi$ and $\partial\phi/\partial Z$ with respect to the moving frame and then transform the results to the stationary frame. Thus, with respect to the (x,z) frame, using (6.9), (6.22) and (6.23), we find

$$\Delta\phi(x,t) = c\,\tilde{\Omega}\ e^{-j\bar{\omega}x}\ e^{j\omega t} \qquad x \geq c \qquad (6.71)$$

The self-induced downwash at the plane of the wake is given by (E.10) as

$$\frac{\partial\phi}{\partial z}(x,0,t) = -\frac{1}{2}k\,\tilde{\Omega}\ e^{-j\bar{\omega}x}\ e^{j\omega t} \qquad (6.72)$$

The above results are transformed to the stationary frame using the transformation

$$x = X + Ut$$
$$z = Z \qquad (6.73)$$

The results are

$$\Delta\phi(X+Ut) = c\,\tilde{\Omega}\ e^{-j\bar{\omega}X} \qquad (6.74)$$

$$\frac{\partial \phi}{\partial Z}(X+Ut)\Big|_{Z=0} = -\frac{1}{2} k \tilde{\Omega}\, e^{-j\bar{\omega}X} \tag{6.75}$$

It is noteworthy that the (X,Z) observer sees a steady flow field in the far wake.

It follows from (6.74), (6.75), (6.70) and (6.64) that the average energy loss rate is given by

$$\bar{E} = \frac{1}{2}\Delta(KE) = \frac{1}{8}\rho U c k\, |\tilde{\Omega}|^2 \tag{6.76}$$

Since Δp and $\partial h/\partial t$ are physically the same in both frames, the average power required may be expressed in the moving frame as

$$\bar{P} = -\int_{-c}^{c} \overline{\Delta p(x,t)\, \frac{\partial}{\partial t} h_a(x,t)}\, dx \tag{6.77}$$

Introducing the nondimensional quantities in (5.2), (5.3), (6.46) and

$$\begin{aligned} z^* &= z/c \\ t^* &= t/(c/U) \\ \Delta C_p &= \Delta p/(\tfrac{1}{2}\rho U^2) \end{aligned} \tag{6.78}$$

in (6.76) and (6.77), we obtain

$$C_E = \frac{1}{2\pi} k\, |\tilde{\Omega}^*|^2 \tag{6.79}$$

$$C_P = \frac{-2}{\pi} \int_{-1}^{1} \overline{\Delta C_p(x^*,t^*)\, \frac{\partial}{\partial t^*} h_a^*(x^*,t^*)}\, dx^* \tag{6.80}$$

C_T is then found from (6.65).

To calculate C_p, we need the unsteady pressure distribution on the airfoil. Ashley and Landahl (1965) give an efficient method for calculating ΔC_p. Their equation (13 - 54) contains a misprint which has been corrected below. In the present notation ΔC_p is given by

$$\Delta\tilde{C}_p(x^*) = \frac{4}{\pi}\left\{\left[\frac{1-x^*}{1+x^*}\right]^{1/2} \oint_{-1}^{1}\left[\frac{1+\xi^*}{1-\xi^*}\right]^{1/2} \frac{\tilde{W}_o^*(\xi^*)}{x^*-\xi^*}\, d\xi^*\right.$$

$$+\sqrt{1-x^{*2}} \oint_{-1}^{1} \frac{jk\,\tilde{f}(\xi^*)}{(x^*-\xi^*)\sqrt{1-\xi^{*2}}}\, d\xi^* \qquad (6.81)$$

$$\left.+\left[1-\mathbb{C}(k)\right]\left[\frac{1-x^*}{1+x^*}\right]^{1/2} \int_{-1}^{1}\left[\frac{1+\xi^*}{1-\xi^*}\right]^{1/2} \tilde{W}_o^*(\xi^*)\, d\xi^*\right\}$$

where $\tilde{f}$ is the auxiliary function

$$\tilde{f}(x^*) = \int_{-1}^{x^*} \tilde{W}_o^*(\xi_1^*)\, d\xi_1^* \qquad (6.82)$$

We end this section with two numerical examples: an airfoil in heave and pitch. These will also serve as a check of the above analysis. First, we consider an airfoil in heave where

$$\tilde{W}_o^* = jk\,h_o^* \qquad |x^*| \le 1 \qquad z^* = 0\pm \qquad (6.83)$$

The pressure distribution on the airfoil is obtained from (6.81).

$$\Delta\tilde{C}_p(x^*) = -4jk\,h_o^*\left\{\mathbb{C}(k)\left[\frac{1-x^*}{1+x^*}\right]^{1/2} + jk\sqrt{1-x^{*2}}\right\} \qquad (6.84)$$

where we have made use of the following integrals form Van Dyke (1956).

$$\oint_{-1}^{1} \frac{d\xi^*}{\sqrt{1-\xi^{*2}}\ (x^*-\xi^*)} = 0 \qquad (6.85)$$

$$\oint_{-1}^{1} \frac{\xi^* d\xi^*}{\sqrt{1-\xi^{*2}}\ (x^*-\xi^*)} = 0 \qquad (6.86)$$

The input power is then obtained from (6.80).

$$C_{P_H} = 4k^2 F(k)\ h_o^{*2} \qquad (6.87)$$

where $(\ )_H$ denotes the heaving motion. Using the identity

$$B(k) = F - (F^2+G^2) = \frac{2}{\pi k\left[(J_1+Y_0)^2+(Y_1-J_0)^2\right]} \qquad (6.88)$$

from Garrick (1936), the energy loss rate is obtained from (6.79).

$$C_{E_H} = 4k^2 B(k)\ h_o^{*2} \qquad (6.89)$$

The argument of all Bessel functions in (6.88) is k. The thrust is obtained from (6.65).

$$C_{T_H} = 4k^2 D(k)\ h_o^{*2} \qquad (6.90)$$

The hydrodynamic efficiency for the motion is given by

$$\eta_H = D(k) / F(k) \qquad (6.91)$$

For an airfoil in pitching motion about the mid chord

$$h_a(x,t) = \alpha x\ e^{j\omega t} \qquad |x| \le c \qquad (6.92)$$

$$\tilde{W}_o^*(x^*) = jk\alpha x^* + \alpha \qquad |x^*| \le 1 \qquad z^* = 0\pm \qquad (6.93)$$

and

$$\Delta\tilde{C}_p(x^*) = -4\alpha \left\{ \left[\tfrac{1}{2} jk + \left(1 + \tfrac{1}{2} jk\right) C(k) + jk\, x^* \right] \left[\frac{1-x^*}{1+x^*} \right]^{1/2} \right.$$

$$\left. + jk \left(1 + \tfrac{1}{2} jk\, x^*\right) \sqrt{1-x^{*2}} \right\} \qquad (6.94)$$

where we have made use of the integrals in (6.85), (6.86) and the following one also from Van Dyke (1956).

$$\oint_{-1}^{1} \frac{\xi^{*2}\, d\xi^*}{\sqrt{1-\xi^{*2}}\ (x^* - \xi^*)} = -\pi x^* \qquad (6.95)$$

The input power is then obtained from (6.80),

$$C_{P_p} = k \left[k(1-F) - 2G \right] \alpha^2 \qquad (6.96)$$

where $(\ )_p$ denotes pitching motion and we have made use of the following integrals.

$$\int_{-1}^{1} x^* \left[\frac{1-x^*}{1+x^*} \right]^{1/2} dx^* = -\pi/2 \qquad (6.97)$$

$$\int_{-1}^{1} x^{*2} \left[\frac{1-x^*}{1+x^*} \right]^{1/2} dx^* = \pi/2 \qquad (6.98)$$

The energy loss rate and the thrust are obtained from (6.79) and (6.65) respectively.

$$C_{T_P} = 4k^2 \left[(1/k^2 + 1/4)\, D(k) - (1/k^2 + 1/2)\, F(k) \right.$$

$$\left. - (1/2k)\, G(k) + 1/4 \right] \alpha^2 \qquad (6.99)$$

$$C_{E_p} = (4+k^2)\, B(k)\, \alpha^2 \qquad (6.100)$$

The corresponding hydrodynamic efficiency η is obtained from (6.99) and (6.96).

The above results for an airfoil in heave and pitch are in complete agreement with the known results (see, e.g., Wu (1971b)). The thrust and the hydrodynamic efficiency of heave and pitch are plotted in Figure 6.7. It is seen that the heaving motion always produces thrust. Pitching motion, on the other hand, usually produces drag, except for $k \gtrsim 1.781$. The efficiency of the heaving motion approaches 100% as $k \to 0$ and dropps off rapidly with increasing k, approaching 50% as $k \to \infty$. The efficiency of the pitching motion is defined only for $k \gtrsim 1.781$, where it increase monotonically and approaches 50% as $k \to \infty$. In the study of the optimum motion of a rigid airfoil in Section 5.2, we saw that a suitable combination of pitch and heave can achieve remarkably higher efficiencies.

6.5 Extension to Three Dimensions

In this section, we extend the analyses of Sections 6.2 - 6.4 to three dimensions and study the energetics of oscillating flexible finite wings. First, we use the momentum theorem to calculate the thrust. Then, using the principle of conservation of energy, we determine the energy loss rate and the thrust.

Calculation of Thrust Using Momentum Theorem

Consider a thin, almost-planar flexible wing of finite span undergoing small-amplitude transverse oscillations in a uniform stream as shown in

Figure 6.8. Total thrust can be determined from the momentum theorem, (6.1). Here, the far boundary S consists of the right circular cylinder S_2 which is parallel to the main flow and the circular disks S_1 and S_3 of radius R.

We introduce the perturbation velocity $\vec{q}$

$$\vec{q} = \vec{Q} - U\vec{i} = u\vec{i} + v\vec{j} + w\vec{k} \tag{6.101}$$

and the continuity equation into (6.1), take the x-component of the result and use the Bernoulli equation and the gradient theorem, to obtain the total thrust.

$$\begin{aligned} \mathcal{T}(t) = {} & \tfrac{1}{2}\rho \int_{S_1} (v^2 + w^2 - u^2)\, dS \\ & + \rho \int_{S_2} (uv\cos\theta + uw\sin\theta)\, dS \\ & - \tfrac{1}{2}\rho \int_{S_3} (v^2 + w^2 - u^2)\, dS \\ & + \rho \int_{S_w+\sigma} \frac{\partial}{\partial t}(\Delta\phi)\, \vec{i}\cdot\vec{n}_u\, dS \\ & + \rho \int_{S_w+\sigma} \gamma\, (\vec{Q}\cdot\vec{n})_u\, dS \end{aligned} \tag{6.102}$$

v and $\vec{j}$ are the perturbation velocity component and the unit vector in the y-direction respectively and the angle θ is measured from the y-axis in the yz-plane in the positive direction of rotation about the x-axis. See Figure 6.8. In arriving at (6.102), integrals of $\phi_t\, \vec{i}\cdot\vec{n}$ and $u(\vec{Q}\cdot\vec{n})$

around the edges of the wing and wake vortex sheets vanish.

Using (6.16),

$$\vec{n}_u = h_x \vec{i} + h_y \vec{j} - k + O(\epsilon^2)$$

$$\vec{n}_\ell = -\vec{n}_u \tag{6.103}$$

and

$$\Delta\phi(x,y,t) = \int_{X_\ell(y)}^{X} \gamma(\xi,y,t)\, d\xi + O(\epsilon^2) \tag{6.104}$$

(6.102) becomes, after an integration by parts in the next to the last term,

$$\mathcal{T}(t) = \frac{\rho}{2} \int_{S_1} (v^2 + w^2 - u^2)\, dS$$

$$- \frac{\rho}{2} \int_{S_3} (v^2 + w^2 - u^2)\, dS$$

$$+ \rho \int_{S_2} u(v\cos\theta + w\sin\theta)\, dS \tag{6.105}$$

$$+ \rho \int_{-b}^{b} h_w(L(y),y,t)\, \frac{\partial}{\partial t}\Gamma(L(y),y,t)\, dy$$

$$- \rho \int_{-b}^{b} dy \int_{X_\ell(y)}^{L(y)} dx\, \frac{\partial}{\partial t}\left[\gamma(x,y,t)\, h(x,y,t)\right]$$

Here,

$$\Gamma(L(y), y, t) = \int_{x_\ell(y)}^{L(y)} \gamma(\xi, y, t)\, d\xi$$
$$= \Gamma(y,t) + \int_{x_t(y)}^{L(y)} \gamma_w(\xi, y, t)\, d\xi \qquad (6.106)$$

where x_ℓ, x_t and L are respectively the abscissas of the wing leading and trailing edges and the abscissa of the wake trailing edge. $\Gamma(y,t)$ is the bound circulation. Whenever the wake extends beyond S_3, L(y) is to be taken as the abscissa of S_3. It is shown in Appendix F that, as the far boundary S is removed to infinity, the integrals over S_1 and S_2 vanish. The integral over S_3 in general must be retained since, in the long-time limit, the wake usually crosses S_3 and the integral is expected to be nonvanishing. (6.105) then reduces to

$$\mathcal{J}(t) = -\tfrac{1}{2}\rho \int_{S_3} (v^2 + w^2 - u^2)\, dS$$
$$+ \rho \int_{-b}^{b} h_w(L(y), y, t)\, \frac{\partial}{\partial t}\Gamma(L(y), y, t)\, dy \qquad (6.107)$$
$$- \rho \int_{-b}^{b} dy \int_{x_\ell(y)}^{L(y)} dx\, \frac{\partial}{\partial t}\left[\gamma(x, y, t)\, h(x, y, t)\right.$$

This result is quite general, being valid for any small-amplitude motion of a lifting surface including transient motion. Also, it is valid for arbitrary planform (straight or swept back), aspect ratio and reduced frequency. It can be shown that, as the wing semi span b tends to infinity, (6.107) reduces to its two-dimensional counterpart, (6.21). Also, in the limit of steady flow, the classical result for vortex drag is

recovered.

Next, we consider the case of steady-state harmonic oscillations. Here, the wake extends far beyond S_3 ($L \to \infty$). From Reissner (1947)

$$\tilde{\Gamma}(y) = c_o \tilde{\Omega}(y) \; e^{-j\bar{\omega} x_t(y)} \tag{6.108}$$

where c_o is the root semi chord. Reissner has shown that the spanwise component of wake vorticity is given by

$$\tilde{\gamma}_w(x,y) = -j k_o \tilde{\Omega}(y) \; e^{-j\bar{\omega} x} \qquad x \geq x_t(y) \tag{6.109}$$

where k_o is the reduced frequency at the wing center section $k_o = \omega c_o / U$.

Substituting (6.108) and (6.109) into (6.106), we obtain

$$\Gamma(L,y,t) = c_o \tilde{\Omega}(y) \; e^{-j\bar{\omega} L} \; e^{j\omega t} \tag{6.110}$$

and, hence,

$$\frac{\partial}{\partial t} \Gamma(L,y,t) = -U \gamma_w(L,y,t) \tag{6.111}$$

Substituting this into (6.107), we obtain the thrust of a harmonically oscillating wing.

$$\mathcal{T}(t) = -\frac{\rho}{2} \int_{S_3} (v^2 + w^2 - u^2) \, dS$$

$$-\rho U \int_{-b}^{b} h_w(L,y,t) \, \gamma_w(L,y,t) \, dy \tag{6.112}$$

$$-\rho \int_{-b}^{b} dy \int_{x_\ell(y)}^{L} dx \, \frac{\partial}{\partial t} \left[\gamma(x,y,t) \, h(x,y,t) \right]$$

This is the three-dimensional counterpart of (6.28).

The time average of thrust is obtained using the averaging rules in (4.4) and (4.5).

$$\overline{\mathcal{T}} = -\frac{\rho}{2} \int_{S_3} (\overline{v^2} + \overline{w^2} - \overline{u^2})\, dS$$
$$- \rho U \int_{-b}^{b} \overline{h_w(L,y,t)\, \gamma_w(L,y,t)}\, dy \qquad (6.113)$$

where both integrals are over the Trefftz plane. This is the three-dimensional counterpart of (6.29). Evaluation of the first integral in (6.113) requires knowledge of $\overline{u^2}$, $\overline{v^2}$ and $\overline{w^2}$ in the far wake. These are calculated in Appendix G in terms of integrals involving $\tilde{\Omega}$ and $d\tilde{\Omega}/dy$ which, in general, must be evaluated numerically. Evaluation of the second integral in (6.113) requires the spanwise vorticity and the lateral displacement of the far wake. The wake vorticity is given by (6.109).

To determine the asymptotic displacement of the wake, for reasons already cited, it suffices to consider a linearized wake model. The linearized downwash at the wake is given by

$$w_w(x,y,t) = \left(\frac{\partial}{\partial t} + U \frac{\partial}{\partial x}\right) h_w(x,y,t) \qquad (6.114)$$

$$x \geq x_t(y) \qquad |y| \leq b \qquad z = 0\pm$$

As in two dimensions, this can be inverted to obtain the wake displacement.

$$\tilde{h}_w(x,y) = \tilde{h}(x_t(y),y)\, e^{-j\bar{\omega}(x - x_t(y))}$$
$$+ U^{-1} \int_{x_t(y)}^{x} \tilde{w}_w(\xi,y)\, e^{-j\bar{\omega}(x-\xi)}\, d\xi \qquad x \geq x_t(y) \qquad (6.115)$$

The asymptotic displacement of the wake is obtained from this by setting $x = \infty$ in the upper limit of the integral.

Evaluation of (6.115) requires the downwash at the plane of the wake which is induced by the wing and wake vorticity. For (x,y) on the projection of the wake on the xy-plane,

$$\tilde{w}_w(x,y) = \frac{-1}{4\pi} \int_{-b}^{b} d\eta \int_{X_\ell(y)}^{X_t(y)} d\xi \, \frac{(x-\xi)\tilde{\gamma}_a(\xi,\eta) + (y-\eta)\tilde{\delta}_a(\xi,\eta)}{[(x-\xi)^2 + (y-\eta)^2]^{3/2}}$$

$$-\frac{1}{4\pi} \oint_{-b}^{b} d\eta \oint_{X_t(y)}^{\infty} d\xi \, \frac{(x-\xi)\tilde{\gamma}_w(\xi,\eta) + (y-\eta)\tilde{\delta}_w(\xi,\eta)}{[(x-\xi)^2 + (y-\eta)^2]^{3/2}} \qquad (6.116)$$

where $(\ )_a$ denotes the wing and δ is the streamwise component of vorticity which is taken to be positive in the negative direction of rotation about the x-axis.

Reissner (1947) has shown that

$$\tilde{\delta}_w(x,y) = c_o \, d\tilde{\Omega}/dy \; e^{-j\bar{\omega}x} \qquad (6.117)$$

It follows from (6.108) that

$$\tilde{\Omega}(y) = \frac{1}{c_o} e^{j\bar{\omega} X_t(y)} \int_{X_\ell(y)}^{X_t(y)} \tilde{\gamma}_a(\xi,y) \, d\xi \qquad (6.118)$$

δ_a is obtained from the continuity of vorticity on the wing.

$$\tilde{\delta}_a(x,y) = \frac{\partial}{\partial y} \int_{X_\ell(y)}^{x} \tilde{\gamma}_a(\xi,y) \, d\xi \qquad (6.119)$$

Hence, once the bound vorticity γ_a is determined, everything else can be determined (at least numerically). In the absence of an exact theory to

calculate γ_a, we can use numerical unsteady lifting-surface theory or Reissner's approximate theory (Reissner (1947)). The latter gives a closed-form expression for γ_a which contains the results of unsteady airfoil theory and steady lifting-line theory as special cases.

Calculation of Wake Energy and Thrust Using Conservation of Energy

Here, we adopt the viewpoint of the observer fixed in the fluid and consider the same wing moving with velocity U along a rectilinear path in the negative X-direction while executing small-amplitude transverse oscillations, as shown in Figure 6.9. The balance of energy for the fluid in V is given by (6.53) where the cylindrical far boundary S is located infinitely far from the wing and the wake.

As in two dimensions, it can be shown that the right hand side of (6.53) is the rate of work of thrust and unsteady lift, i.e.,

$$\int_V \frac{\partial}{\partial t}\left(\frac{1}{2}\rho|\vec{q}|^2\right) dV = -U\mathcal{T} - \int_\sigma \Delta p \frac{\partial h_a}{\partial t}\, d\sigma \qquad (6.120)$$

Taking the time average of (6.120) over the time interval τ and rearranging, we obtain

$$-\int_\sigma \overline{\Delta p \frac{\partial}{\partial t} h_a}\, d\sigma = U\bar{\mathcal{T}} + \frac{1}{\tau}\Delta(KE) \qquad (6.121)$$

where $\frac{1}{\tau}\Delta(KE)$ is defined in (6.63). (6.121) is a statement of conservation of energy for the present three-dimensional problem. In the notation of Section 4.2, it becomes

$$\bar{\mathcal{P}} = U\bar{\mathcal{T}} + \bar{\mathcal{E}} \quad \text{or} \quad C_{\mathcal{P}} = C_{\mathcal{T}} + C_{\mathcal{E}} \qquad (6.122)$$

The corresponding hydrodynamic efficiency is defined in (4.54).

Next, we consider the case of steady-state harmonic oscillations and choose τ to be the period $2\pi/\omega$. As is two dimensions, $\Delta(KE)$ can be determined from the properties of the far wake, namely

$$\Delta(KE) = -\frac{\rho}{2}\lambda \int_{-b}^{b} \overline{\overline{\Delta\phi \frac{\partial}{\partial z}\phi\Big|_{z=0}}}\, d\eta \qquad (6.123)$$

With respect to the moving frame (x,y,z), $\Delta\phi$ is determined using (6.104), (6.108) and (6.109).

$$\Delta\tilde{\phi}(x,y) = c_o \tilde{\Omega}(y)\, e^{-j\bar{\omega}x} \qquad x \geq x_t(y) \qquad (6.124)$$

Downwash at the plane of the wake is obtained from (G.11) as $z \to 0\pm$.

$$\frac{\partial\tilde{\phi}}{\partial z}(x,y,0) = \frac{-k_o}{2\pi} e^{-j\bar{\omega}x} \oint_{-b}^{b} \tilde{\Omega}'(\eta)\, \mathrm{sgn}(y-\eta)\, K_1(\bar{\omega}|y-\eta|)\, d\eta$$

$$- \frac{k_o^2}{2\pi c_o} e^{-j\bar{\omega}x} \int_{-b}^{b} \tilde{\Omega}(\eta)\, K_o(\bar{\omega}|y-\eta|)\, d\eta \qquad (6.125)$$

In the limit of steady flow, (6.124) and (6.125) reduce to the classical steady results.

The above results for $\Delta\phi$ and $\partial\phi/\partial z$ can be transformed to the (X,Y,Z) frame using the transformation (6.73) with y = Y. The results are

$$\Delta\phi(X+Ut, Y) = c_o \tilde{\Omega}(y)\, e^{-j\bar{\omega}X} \qquad (6.126)$$

$$\frac{\partial\phi}{\partial z}(X+Ut, Y)\Big|_{z=0} = \frac{-k_o}{2\pi} e^{-j\bar{\omega}X} \oint_{-b}^{b} \tilde{\Omega}'(\eta)\, \mathrm{sgn}(y-\eta)\, K_1(\bar{\omega}|y-\eta|)\, d\eta$$

$$- \frac{k_o^2}{2\pi c_o} e^{-j\bar{\omega}X} \int_{-b}^{b} \tilde{\Omega}(\eta)\, K_o(\bar{\omega}|y-\eta|)\, d\eta \qquad (6.127)$$

Using (6.126) and (6.127), the average energy loss rate is obtained.

$$\bar{\mathcal{E}} = \frac{1}{8\pi}\rho U k_0 \mathcal{R}_j \left\{ c_0 \oint_{-b}^{b}\oint_{-b}^{b} \tilde{\mathcal{L}}^{\circledast}(\eta_1)\,\tilde{\mathcal{L}}'(\eta)\,\mathrm{sgn}(\eta_1-\eta)\cdot \right.$$

$$\left. \cdot K_1(\bar{\omega}|\eta_1-\eta|)\,d\eta\,d\eta_1 + k_0 \int_{-b}^{b}\int_{-b}^{b} \tilde{\mathcal{L}}^{\circledast}(\eta_1)\,\tilde{\mathcal{L}}(\eta)\,K_0(\bar{\omega}|\eta_1-\eta|)\,d\eta\,d\eta_1 \right\} \tag{6.128}$$

The average total power required to maintain the wing oscillations is given by

$$\bar{\mathcal{P}} = -\int_{-b}^{b} d\eta \int_{X_\ell(\eta)}^{X_t(\eta)} d\xi\ \overline{\Delta p(\xi,\eta,t)\,\frac{\partial}{\partial t} h_a(\xi,\eta,t)}\,d\xi \tag{6.129}$$

The total thrust is then obtained from (6.122). The present method requires Δp and $\tilde{\mathcal{L}}$ which can be obtained from numerical unsteady lifting-surface theory or Reissner's theory.

In the limit of steady flow, the above results yield one half of the known value of the induced drag, as expected.

CHAPTER VII

SUMMARY AND RECOMMENDATIONS

In summary, a low-frequency unsteady lifting-line theory has been developed, using the MAE method, for a harmonically-oscillating straight wing of large aspect ratio. The wing is assumed to be chordwise rigid but completely flexible in the span direction. The wing displacements are prescribed and the unsteady pressure field, airloads and induced downwash are obtained in closed form. To leading order, the latter consists of a convecting sinusoidal gust whose amplitude is constant across the chord but varies in the span direction. The unsteady induced downwash is $O(A^{-1})$, as in the steady case. The theory is sufficiently general to permit quantitative treatment of a range of interesting problems involving unsteady motions of spanwise-flexible wings in incompressible flow.

Numerical examples clearly show the influence of k_o, A, planform shape and mode of oscillation on the wing aerodynamics. They also indicate that, for elliptic and more slender planforms, the theory yields convergent total results (at least for the examples considered). Comparison with Reissner's theory (Reissner (1947)) and limited numerical lifting-surface results show good overall agreement. The present theory, thus, provides formal justification for Reissner's ad hoc theory. Compared with lifting-surface theory, computation time is reduced significantly.

The present theory also identifies and resolves the errors in the unsteady lifting-line theory of James (1975) who used a semi-intuitive MAE approach. His unsteady induced downwash is found to be in error which renders his results incorrect. He also suggests that his theory is valid

for all reduced frequencies, but his formulation clearly assumes low reduced frequencies. Further, he does not treat and resolve the inherent nonuniqueness of the solution in the acceleration potential formulation of the problem. The present work also raises questions about the complete validity of the unsteady lifting-line theory of Van Holten (1975) who suggests that his theory is valid for all reduced frequencies but finds the unsteady induced downwash to be constant across the chord, a condition which holds only in the steady flow limit. The theory of Cheng (1975) who determined the velocity potential to $O(\bar{A}^{-2})$ does not include calculation of the aerodynamic loading, the unsteady induced downwash and some of the important details.

Using the present theory, the effects of three-dimensionality on the energetic quantities have been determined for a finite wing oscillating in combined pitch and heave. This is the first closed-form analysis of three-dimensional flapping flight. In the present approach, the leading-edge suction force is obtained exactly. Numerical examples for the spanwise distribution of the energetic quantities and the overall propulsive performance of an elliptic wing in combined pitch and heave are presented.

Based on the numerical examples and correlations presented in this work, the region of validity of the present theory has been identified in terms of k_o and A. It is seen that the theory is valid over a considerably larger range of k_o than originally anticipated. The region of validity contains the values of k_o and A which are of greatest interest in most applications. For small k_o and moderate A, the total lift and moment coefficients for an elliptic wing in pitch and heave display an unexpected behavior which is not well understood and calls for further investigation.

Numerical lifting-surface results would be helpful in understanding this behavior. If it is found that this is an inherent weakness of the present theory, carrying out the asymptotic analysis to one order higher in A^{-1} might resolve it. In order to better assess the utility and range of validity of the present theory, there is need for further correlations with lifting-surface theory and also experiments.

The optimum solution of Wu (1971b) for a rigid airfoil has been recast in terms of the normal modes of the quadratic form for the energy loss rate to shed light on the structure of the optimum solution. It is found that one of the normal modes, termed the invisible mode, plays a central role in the solution. The invisible mode is interesting in its own right, since it consists of a combined pitch and heave motion of the airfoil which sheds no vorticity and for which the energetic quantities are identically zero and the hydrodynamic efficiency is 100%. The existence of the invisible mode is a direct result of the fact that the quadratic form for the energy loss rate is positive semi definite. Since an arbitrary amount of the invisible mode is present in the solution, the latter is nonunique.

The optimum motion of a finite wing in combined pitch and heave has been analyzed rigorously for the first time. It is found that, in contrast with the two-dimensional case, here the quadratic form for the energy loss rate is positive definite. As a result, there does not exist an invisible mode for the finite rigid wing and the corresponding optimum solution is unique. Numerical results for the optimum motion of an elliptic wing are presented.

Finally, an alternate approach has been presented for the calculation of the energetic quantities in two and three dimensions, namely the use of the integral form of the conservation laws. This approach has several

advantages. i) It is quite general, being valid for arbitrary wing planform, aspect ratio, reduced frequency and mode of oscillation (small amplitudes). ii) It is physically enlightening, in that it relates the thrust and the energy loss rate to the momentum flux and the kinetic energy content of the far wake. iii) It avoids the direct calculation of the leading-edge suction force. However, the method requires the distribution of bound circulation and pressure on the wing and is found not to be well suited for optimization studies. In two dimensions, using unsteady airfoil theory, the results are obtained in closed form; although more complex shapes and motions of the airfoil give rise to tedious integrals. In three dimensions, in the absence of an exact wing theory with closed-form results, one has to resort to numerical lifting-surface theory or Reissner's theory (Reissner (1947)).

The following extensions are suggested by the present investigation. In order to take full advantage of the capabilities of the present unsteady lifting-line theory, it would be of interest to modify the present numerical schemes, which are for oscillating rigid wings, to handle spanwise-flexible wings as well. This can be accomplished by choosing a number of suitable modes for the span distribution of heave and pitch. Similarly, the present analysis of the energetics of an oscillating rigid wing can be extended to include spanwise flexibility. In turn, these calculations can be used to analyze the optimum motion of a semi-rigid wing. This would be of interest in studying wing motions of birds with small to moderate flapping amplitude and relatively large aspect ratio.

Another extension of the present theory is to determine the (aerodynamic) response of an oscillating semi-rigid finite wing to an oblique convecting sinusoidal gust, from which the response to any

arbitrary localized gust or continuous atmospheric turbulence can be obtained by Fourier superposition. This can be obtained from the present analysis by including in the lowest order inner solution the pressure field due to the interaction of a two-dimensional airfoil with the oblique gust. The latter can be obtained from the solution of Filotas (1969) by use of Green's functions (pressure doublets). This extension of the present theory might be useful in aeroacoustics as well.

Another extension is to include the effects of compressibility (using one of the existing compressible unsteady airfoil theories and Green's functions) and curvature and/or sweep of the planform. Development of a unified theory valid for all reduced frequencies would also be of interest (Section 2.1).

The present theory will also be useful in other areas, such as aeroelasticity and the analysis of energy extraction from fluid streams.

APPENDIX A

EVALUATION OF CERTAIN INTEGRALS

1. From Section 2.4

$$Q_n(\hat{\jmath},Y) = \int_{-c}^{c} \left[\frac{c+\hat{\xi}}{c-\hat{\xi}}\right]^{1/2} \frac{\hat{\xi}^n}{\hat{\xi}-\hat{\jmath}}\, d\hat{\xi} \qquad (A.1)$$

$$n = 0, 1, 2, \ldots$$

The integration is along the real axis from $\hat{x} = -c(y)$ to $\hat{x} = c(y)$ with the complex parameter $\hat{\jmath} = \hat{x} + i\,\hat{z}$.

Using the transformation

$$\eta^2 = (c+\hat{\xi})/(c-\hat{\xi}) \qquad (A.2)$$

Q_n becomes

$$Q_n(\hat{\jmath},Y) = \frac{4c^{(n+1)}}{c-\hat{\jmath}} \int_0^{\infty} \frac{(\eta^2-1)^n\,\eta^2}{(\eta^2+\alpha)(\eta^2+1)^{(n+1)}}\, d\eta \qquad (A.3)$$

where

$$\alpha = (\hat{\jmath}+c)/(\hat{\jmath}-c) \qquad (A.4)$$

For given n, Q_n can now be evaluated using the method of partial fractions which reduces (A.3) to a sum of the following integrals.

$$\int_0^{\infty} \frac{d\eta}{(\eta^2+1)^m} = \begin{cases} 1 & m = 1 \\ \dfrac{1\cdot 3\cdot 5 \cdots (2m-3)}{2\cdot 4\cdot 6 \cdots (2m-2)} \dfrac{\pi}{2} & m \geq 2 \end{cases} \qquad (A.5)$$

$$\int_0^\infty (\eta^2+\alpha)^{-1}\, d\eta = (\pi/2)\,\alpha^{-1/2} \qquad (A.6)$$

The first five Q_n's, evaluated in this manner, are listed below.

$$Q_0(\hat{\jmath},\gamma) = \pi\left[1-\Lambda\right]$$

$$Q_1(\hat{\jmath},\gamma) = \pi\left[\hat{\jmath}+c-\hat{\jmath}\,\Lambda\right]$$

$$Q_2(\hat{\jmath},\gamma) = \pi\left[\hat{\jmath}^2+c\hat{\jmath}+\tfrac{1}{2}c^2-\hat{\jmath}^2\Lambda\right]$$

$$Q_3(\hat{\jmath},\gamma) = \pi\left[\hat{\jmath}^3+c\hat{\jmath}^2+\tfrac{1}{2}c^2\hat{\jmath}+\tfrac{1}{2}c^3-\hat{\jmath}^3\Lambda\right]$$

$$Q_4(\hat{\jmath},\gamma) = \pi\left[\hat{\jmath}^4+c\hat{\jmath}^3+\tfrac{1}{2}c^2\hat{\jmath}^2+\tfrac{1}{2}c^3\hat{\jmath}+\tfrac{3}{8}c^4-\hat{\jmath}^4\Lambda\right] \qquad (A.7)$$

where

$$\Lambda = \sqrt{(\hat{\jmath}+c)/(\hat{\jmath}-c)} \qquad (A.8)$$

2. In Section 2.6, we make use of the following integrals.

$$\int_1^\infty \eta\,[\eta^2-1]^{-1/2}\, e^{-jk\eta}\, d\eta = -\frac{\pi}{2}\, H_1^{(2)}(k) \qquad (A.9)$$

$$\int_1^\infty [\eta^2-1]^{-1/2}\, e^{-jk\eta}\, d\eta = -j\,\frac{\pi}{2}\, H_0^{(2)}(k) \qquad (A.10)$$

$$\int_1^\infty \left[\eta-\sqrt{\eta^2-1}\right] e^{-jk\eta}\, d\eta = \left[1/(jk)-1/k^2\right] e^{-jk} - j\,\frac{\pi}{2}\,\frac{1}{k}\, H_1^{(2)}(k) \qquad (A.11)$$

$$\int_1^\infty \log\left[\eta+\sqrt{\eta^2-1}\right] e^{-jk\eta}\, d\eta = -\frac{\pi}{2}\frac{1}{k} H_0^{(2)}(k) \qquad (A.12)$$

$$\int_1^\infty \eta\sqrt{\eta^2-1}\; e^{-jk\eta}\; d\eta = -\frac{\pi}{k^2} H_1^{(2)}(k)$$

$$-\frac{\pi}{2}\frac{1}{k} H_0^{(2)}(k) \qquad (A.13)$$

The first two integrals are found in Watson (1966). The integral in (A.11), after an integration by parts, can be expressed in terms of (A.9). The integral in (A.12) can be obtained from (A.10) by an integration by parts. The last integral, after integrating by parts twice, can be expressed in terms of (A.9) and (A.12).

Some of the above integrals, when considered individually, are divergent for real values of k. In such cases we assign a small negative imaginary part to k. Later, for use in Section 2.6, we analytically continue the results to real values of k.

3. From Section 6.3,

$$I_1 = \int_{-c}^{c} \left[\frac{c-x}{c+x}\right]^{1/2} \frac{dx}{(x-\lambda)(\xi-x)} \qquad \xi,\lambda \gtrless c \qquad (A.14)$$

This integral can be evaluated from the following contour integral.

$$\oint_C \left[\frac{\zeta-c}{\zeta+c}\right]^{\frac{1}{2}} \frac{d\zeta}{(\zeta-\lambda)(\zeta-\xi)} = 2\pi i\left[Res(\lambda) + Res(\xi)\right]$$

$$\xi,\lambda \gtrless c \qquad (A.15)$$

where $\zeta = x + i\,z$ and the integration contour C consits of C_1, C_2, C_3 and C_R, as shown in Figure A.1. For the integrand we choose the branch cut

from $\zeta = -c$ to $\zeta = c$ defined by

$$0 \leq \arg(\zeta + c) < 2\pi$$
$$0 \leq \arg(\zeta - c) < 2\pi \qquad (A.16)$$

The integral along C_R vanishes as $R \to \infty$ and the integrals along C_2 and C_3 cancel each other out. As C_1 shrinks down to the branch cut, it can be shown, using some of the analytic properties of $\sqrt{(\zeta - c)/(\zeta + c)}$ in Table 2.1 (p. 57), that (A.15) leads to the following result.

$$I_1 = \frac{-\pi}{\lambda - \xi}\left\{\left[\frac{\lambda - c}{\lambda + c}\right]^{1/2} - \left[\frac{\xi - c}{\xi + c}\right]^{1/2}\right\} \quad \lambda, \xi \geq c \qquad (A.17)$$

4. From Section 6.3,

$$I_2 = \oint_{-c}^{c} \left[\frac{c - x}{c + x}\right]^{1/2} \frac{dx}{(x - \lambda)(\xi - x)} \quad |\lambda| \leq c \quad \xi \geq c \qquad (A.18)$$

This integral is similar to the one in the above. It can be evaluated from the following contour integral.

$$\oint_C \left[\frac{\zeta - c}{\zeta + c}\right]^{1/2} \frac{d\zeta}{(\zeta - \lambda)(\zeta - \xi)} = 2\pi i \, \mathrm{Res}(\xi) \qquad (A.19)$$
$$|\lambda| \leq c \quad \xi \geq c$$

Here, we choose the branch cut defined in (A.16). The integration contour C consists of C_1, C_2, C_3, C_ρ and C_R as shown in Figure A.2. C_R and C_ρ are circles of radius R and ρ respectively. Again, the integral along C_R vanishes as $R \to \infty$ and the integrals along C_2 and C_3 cancel each other out. The integrals along the upper and lower halves of C_ρ cancel each other out

due to the sign change of $\sqrt{(\xi - c)/(\xi + c)}$ across the branch cut (see Table 2.1). (A.19) then leads to the following result.

$$I_2 = \frac{\pi}{\lambda - \xi}\left[\frac{\xi - c}{\xi + c}\right]^{1/2} \qquad |\lambda| \leq c \qquad \xi \geq c \tag{A.20}$$

5. From Section 6.3,

$$I_3 = \int_c^\infty d\xi \oint_c^\infty d\lambda \left[\frac{\xi - c}{\xi + c}\right]^{1/2}\left[\frac{\lambda + c}{\lambda - c}\right]^{1/2} \frac{e^{j\bar{\omega}(\xi - \lambda)}}{\xi - \lambda} \tag{A.21}$$

Differentiating this equation with respect to $k = \bar{\omega} c$ uncouples the integrals.

$$\frac{dI_3}{dk} = \frac{j}{c}\int_c^\infty \left[\frac{\xi - c}{\xi + c}\right]^{1/2} e^{j\bar{\omega}\xi} d\xi \int_c^\infty \left[\frac{\lambda + c}{\lambda - c}\right]^{1/2} e^{-j\bar{\omega}\lambda} d\lambda \tag{A.22}$$

These integrals can be expressed in terms of certain known integrals (found, e.g., in Ashley and Landahl (1965)).

$$\int_c^\infty \left[\frac{\xi - c}{\xi + c}\right]^{1/2} e^{j\bar{\omega}\xi} d\xi = \frac{-\pi c}{2}\left[H_1^{(2)\circledast}(k) + j\, H_0^{(2)\circledast}(k)\right] \tag{A.23}$$

$$\int_c^\infty \left[\frac{\lambda + c}{\lambda - c}\right]^{1/2} e^{-j\bar{\omega}\lambda} d\lambda = \frac{-\pi c}{2}\left[H_1^{(2)}(k) + j\, H_0^{(2)}(k)\right] \tag{A.24}$$

Substituting these results in (A.22) and expressing the Hankel functions in terms of Bessel functions (see (2.43)), we find

$$\frac{dI_3}{dk} = \left(\frac{\pi}{2}\right)^2 c\left[-2\left(J_0 J_1 + Y_0 Y_1\right) + j\left(J_1^2 + Y_1^2 - J_0^2 - Y_0^2\right)\right] \tag{A.25}$$

where the argument of all Bessel functions is k.

I_3 is obtained from this result by integration.

$$I_3 = \left(\frac{\pi}{2}\right)^2 c \left[J_o^2 + Y_o^2 - J_o^2(0) - Y_o^2(0) + j \int_0^k (J_1^2 + Y_1^2 - J_o^2 - Y_o^2)\, dk_1 + D \right] \tag{A.26}$$

where D is the complex constant of integration and we have made use of the following identities.

$$J_o'(z) = -J_1(z)$$
$$Y_o'(z) = -Y_1(z) \tag{A.27}$$

The constant of integration is determined by evaluating I_3 in (A.21) for some value of $\bar{\omega}$ (or k) directly. Using the method of stationary phase (see, e.g., Carrier, Krook and Pearson (1966)), it can be shown that I_3 tends to zero as $\bar{\omega}$ (or k) $\to \infty$. Using this condition in (A.26), the constant of integration is found to be

$$D = J_o^2(0) + Y_o^2(0) - j \int_0^\infty (J_1^2 + Y_1^2 - J_o^2 - Y_o^2)\, dk_1 \tag{A.28}$$

Substituting this into (A.26), we obtain

$$I_3 = \left(\frac{\pi}{2}\right)^2 c \left\{ \left[J_o^2(k) + Y_o^2(k) \right] - j \int_k^\infty \left[J_1^2 + Y_1^2 - J_o^2 - Y_o^2 \right] dk_1 \right\} \tag{A.29}$$

It is seen in Section 6.3 that the imaginary part of I_3 drops out of the expression for the average thrust and, hence, there is no need to evaluate it.

APPENDIX B

NUMERICAL EVALUATION OF INDUCED DOWNWASH OF UNSTEADY LIFTING-LINE THEORY

In this appendix, we describe numerical schemes for the evaluation of the unsteady induced downwash of the present unsteady lifting-line theory given by (3.37a) and (3.37b).

From among the planforms considered in this work, we are most interested in the elliptic one. The elliptic planform, however, gives rise to infinite slopes at the tips in the spanwise variation of some of the physical quantities. This, in turn, gives rise to difficulties in the numerical evaluation of integrals containing such terms. These difficulties can be resolved by introducing the spanwise angular substitution

$$y^* = \cos\theta' \qquad |y^*| \le 1 \qquad 0 \le \theta' \le \pi$$
$$\eta^* = \cos\theta_1' \qquad |\eta^*| \le 1 \qquad 0 \le \theta_1' \le \pi \tag{B.1}$$

which transforms a planform with blunt tips into a planform with more slender tips by stretching out the tip regions. For example, the elliptic planform which has infinite slopes at the tips is transformed into one with finite slopes at the tip, as shown in Figure B.1.

In terms of the angular variables, the first integral in (3.37b) may be written as

$$A(\theta') = \fint_0^{\pi} \frac{\tilde{C}_{\ell_{2D}}(\eta^*)}{(\theta' - \theta_1')^2}\, \Pi(\mu_0 |y^* - \eta^*|)\, M_1(\theta', \theta_1')\, d\theta_1' \tag{B.2}$$

where

$$M_1(\theta', \theta_1') = \frac{(\theta' - \theta_1')^2 \sin\theta_1'}{(\cos\theta' - \cos\theta_1')^2} \tag{B.3}$$

We have introduced the factor $(\theta' - \theta_1')^2/(\theta' - \theta_1')^2$ in the integrand. As we will see later, this greatly facilitates the numerical evaluation of the integral in the neighborhood of the singularity.

Before describing the numerical integration of $A(\theta')$, we first discuss evaluation of various parts of the integrand. It follows from (3.11) and (3.36) that the strip-theory section lift coefficient is given by

$$\tilde{C}_{\ell_{2D}}(y^*) = -\pi\left(\frac{c}{c_0}\right)\left\{jk\alpha - k_0 k\left(\frac{h_0}{c_0}\right) + \left[(2+jk)\alpha + 2jk_0\left(\frac{h_0}{c_0}\right)\right]\mathbb{C}(k)\right\} \tag{B.4}$$

Numerical values of Theodorsen's function $\mathbb{C}(k)$ are obtained from (2.42) and (2.44) using library subroutines for the Bessel functions involved (1). $\mathbb{C}(k)$ is plotted as a complex vector in Figure 2.4. Listing of the primary programs used in this work are given in Appendix H.

For later use, we point out that it can be shown, using (2.62), that, near the wing tips, (B.4) has the behavior (for fixed aspect ratio)

$$\tilde{C}_{\ell_{2D}}(y^*) \sim -\pi\left(\frac{c}{c_0}\right)\left[a_1 + a_2\left(\frac{c}{c_0}\right) + a_3\left(\frac{c}{c_0}\right)\log\left(\frac{c}{c_0}\right) + O\left(\frac{c}{c_0}\right)^2\right] \quad (c/c_0) \to \tag{B.5}$$

---

(1) Numerical values of J_0, J_1, Y_0 and Y_1 are obtained respectively from subroutines DBJ0, DBJ1, DBY0 and DBY1 which are part of the IBM mathematics subroutine library SL-MATH.

where a_1, a_2 and a_3 are O(1) and well behaved near the tips. It is seen that in the vicinity of the tips, to leading order, $\tilde{C}_{\ell_{2D}}$ is proportional to the local chord. This is expected since, as we approach the tips, the local reduced frequency tends to zero and the unsteady lift takes on its quasi-steady value.

It can be shown that the function $M_1(\theta', \theta_1')$, (B.3), has the following properties (see Figure B.2):

i) $M_1 \geq 0$ for $0 \leq \theta_1' \leq \pi$;

ii) $M_1 = 0$ for $\theta_1' = 0, \pi$ and $\theta' \neq 0, \pi$;

iii) the maximum of M_1 occurs at $\theta_1' = \theta'$ and its locus is given by

$$M_1(\theta', \theta_1') = \frac{1}{\sin\theta'} = \frac{1}{\sqrt{1 - y^{*2}}} \qquad (B.6)$$

iv) for $\theta' = 0, \pi$, near the tips, to leading order,

$$M_1 \sim 4/\sin\gamma = \frac{4}{\sqrt{1 - \eta^{*2}}} \qquad (B.7)$$

where γ is the angular distance form the tips (that is, θ_1' or $\pi - \theta_1'$);

v) symmetry property: M_1 for $-y^*$ is the mirror image of that for y^* in the line $\theta_1' = \pi/2$.

Hence, M_1 has a square-root singular behavior at the tips ($\theta' = 0, \pi$). For elliptic and more slender planforms, however, the loading at the tips drops off fast enough to cancel out this singularity (see (B.5)).

The kernel function $\Pi(M)$ in (B.2) is defined in (2.155b). Numerical values of K_1 are obtained from a library subroutine (1). The rest of the

---

(1) The subroutine used is DBK1 of SL-MATH.

kernel is evaluated using the closed-form approximation derived by Watkins, Woolston and Cunningham (1959), namely

$$I_1(\mu) - L_1(\mu) \approx \frac{2}{\pi}\mu\left\{\frac{1.0085\,\mu}{1.3410+1.0050\,\mu^2}\right.$$

$$\left.+\left[\frac{\pi}{4}-.8675\,\mu\,\frac{.4648+.9159\,\mu}{1.3410+\mu^2}\right]e^{-\mu}\right\} \qquad (B.8)$$

We now describe the numerical integration of A(θ'), (B.2). First, we write the integral in the general form

$$A(\theta') = \int_0^{\pi} \frac{F(\theta';\theta_1')}{(\theta'-\theta_1')^2}\,d\theta_1' \qquad (B.9)$$

Due to the presence of the singularity at $\theta_1' = \theta'$, we break up the integral into three parts as follows.

$$A(\theta') = \left[\int_0^{\theta'-\gamma} + \int_{\theta'-\gamma}^{\theta'+\gamma} + \int_{\theta'+\gamma}^{\pi}\right]\frac{F(\theta';\theta_1')}{(\theta'-\theta_1')^2}\,d\theta_1'$$

$$= A_1(\theta') + A_\gamma(\theta') + A_2(\theta') \qquad (B.10)$$

where $\gamma > 0$ represents a small neighborhood of the singularity. The integrals $A_1(\theta')$ and $A_2(\theta')$ are nonsingular and span a finite interval. After a change of variables to transform the intervals of integration to (-1,1), they can be evaluated efficiently using Legendre-Gauss quadrature:

$$\int_a^b f(y)\,dy = (b-a)/2\int_{-1}^{1} f(y)\,dx$$

$$\approx (b-a)/2\sum_{i=1}^{n} w_i\,f(y_i) \qquad (B.11)$$

where

$$Y_i = \frac{b-a}{2} X_i + \frac{b+a}{2} \qquad (B.12)$$

The weights W_i and the abscissas X_i are listed, e.g., in Abramowitz and Stegun (1970). In the computer program, the number of integration stations n is determined through an iterative procedure aimed at achieving a prescribed level of accuracy.

We evaluate the integral $A_J(\theta)$ which contains the second order singularity using the method of Watkins, Woolston and Cunningham (1959). For completeness, the highlights of the method are discussed below. First, we approximate the function $F(\theta',\theta_1')$ with a sixth degree polynomial which can be obtained from Lagrange's interpolation formula (see, for example, Abramowitz and Stegun (1970)). With this approximation $A_J(\theta')$ becomes

$$A_J(\theta') \approx \delta^{-6} \sum_{i=0}^{4} g_i(\theta') \delta^i \int_{\theta'-J}^{\theta'+J} (\theta'-\theta_1')^{(4-i)} d\theta_1' \qquad (B.13)$$
$$+ \delta^{-1} g_5(\theta') \oint_{\theta'-J}^{\theta'+J} (\theta'-\theta_1')^{-1} d\theta_1' + g_6(\theta') \oint_{\theta'-J}^{\theta'+J} (\theta'-\theta_1')^{-2} d\theta_1'$$

where $\delta = J/3$ and $g_i(\theta')$ are linear combinations of $F(\theta',\theta_1')$ at the seven interpolation stations and can be found from Lagrange's interpolation formula. It now becomes clear that, had we not introduced the factor $(\theta' - \theta_1')^2/(\theta' - \theta_1')^2$ in (B.2), here we would have encountered the integrals

$$\int_{\theta'-J}^{\theta'+J} \frac{(\theta'-\theta_1')^n}{(\cos\theta' - \cos\theta_1')^2} d\theta_1' \qquad n = 0, 1, 2, \cdots 6$$

which are much more difficult to evaluate than those in (B.13).

It can be shown that the Cauchy principle value integral in (B.13) is

$$\oint_{\theta'-\jmath}^{\theta'+\jmath} \frac{d\theta_i'}{\theta'-\theta_i'} = \lim_{\epsilon\to 0}\left[\int_{\theta'-\jmath}^{\theta'-\epsilon} + \int_{\theta'+\epsilon}^{\theta'+\jmath}\right]\frac{d\theta_i'}{\theta'-\theta_i'} = 0 \qquad (B.14)$$

The integral with the second-order singularity in (B.13) is evaluated according to the principle value defined in (2.146). Its value can be shown to be

$$\int_{\theta'-\jmath}^{\theta'+\jmath} \frac{d\theta_i'}{(\theta'-\theta_i')^2} = \lim_{\epsilon\to 0}\left\{\left[\int_{\theta'-\jmath}^{\theta'-\epsilon} + \int_{\theta'+\epsilon}^{\theta'+\jmath}\right]\frac{d\theta_i'}{(\theta'-\theta_i')^2} - \frac{2}{\epsilon}\right\}$$

$$= -2/\jmath \qquad (B.15)$$

Substituting (B.14), (B.15) and the expressions for $g_i(\theta')$ into (B.13), we obtain the following approximation for $A_\jmath(\theta')$.

$$\begin{aligned} A_\jmath(\theta') \approx \frac{1}{100\jmath}\Big\{ & 13\left[F(\theta',\theta'-3\delta)+F(\theta',\theta'+3\delta)\right] \\ & +72\left[F(\theta',\theta'-2\delta)+F(\theta',\theta'+2\delta)\right] \\ & +495\left[F(\theta',\theta'-\delta)+F(\theta',\theta'+\delta)\right] \\ & -1360\,F(\theta',\theta')\Big\} \end{aligned} \qquad (B.16)$$

In the numerical calculations presented in this work, $\jmath$ is chosen through numerical experiments (1) to be $\jmath \approx 0.08$ to obtain three decimal places

---

(1) $\jmath$ is chosen by applying the numerical scheme for $A(\theta')$ to certain known integrals for various values of θ'.

of accuracy or better for the results.

Next, we discuss the numerical evaluation of the second integral in (3.37b) which contains a removable singularity at $\eta = y$. In terms of the angular variables, this integral may be written as

$$B(\theta') = \int_0^{\pi} \frac{\tilde{C}_{\ell 2D}(\eta^*) - \tilde{C}_{\ell 2D}(y^*)}{|\theta' - \theta_1'|} M_2(\theta', \theta_1') \, d\theta_1' \qquad (B.17)$$

where

$$M_2(\theta', \theta_1') = \frac{|\theta' - \theta_1'| \sin \theta_1'}{|\cos \theta' - \cos \theta_1'|} \qquad (B.18)$$

We have introduced the factor $|\theta' - \theta_1'|/|\theta' - \theta_1'|$ in the integrand to facilitate later evaluation of the integral in the nieghborhood of the singularity. It can be shown that $M_2(\theta', \theta_1')$ has the following properties (see Figure B.3):

i) $M_2 \sim O(1)$ for $0 \leqslant (\theta', \theta_1') \leqslant \pi$;

ii) $M_2 \geqslant 0$ for $0 \leqslant (\theta', \theta_1') \leqslant \pi$,;

iii) $M_2 = 0$ for $\theta_1' = 0, \pi$, $\theta' \neq 0, \pi$;

iv) $M_2 = 1$ is the locus of the points
$\theta_1' = \theta'$ for $0 \leqslant (\theta', \theta_1') \leqslant \pi$;

v) symmetry property: M_2 for $-y^*$ is the mirror image of that for y^* in the line $\theta_1' = \pi/2$.

The integral $B(\theta')$ is of the general form

$$B(\theta') = \int_0^{\pi} \frac{G(\theta', \theta_1')}{|\theta' - \theta_1'|} \, d\theta_1' \qquad (B.19)$$

To evaluate $B(\theta')$, we first write it as the sum of three integrals.

$$B(\theta') = \left[\int_0^{\theta'-\epsilon} + \int_{\theta'-\epsilon}^{\theta'+\epsilon} + \int_{\theta'+\epsilon}^{\pi} \right] \frac{G(\theta', \theta_1')}{|\theta' - \theta_1'|} \, d\theta_1'$$

$$= B_1(\theta') + B_\epsilon(\theta') + B_2(\theta') \qquad (B.20)$$

where $\epsilon > 0$ represents a small neighborhood of the singularity. In the integrals $B_1(\theta')$ and $B_2(\theta')$, the parts containing $\tilde{C}_{\ell_{2D}}(y^*)$ can be integrated in closed form, with respect to η^*, to obtain

$$B_1(\theta') + B_2(\theta') = \left[\int_0^{\theta'-\epsilon} + \int_{\theta'+\epsilon}^{\pi} \right] \frac{\tilde{C}_{\ell_{2D}}(\eta^*)}{|\theta' - \theta_1'|} M_2(\theta', \theta_1') \, d\theta_1'$$

$$- \tilde{C}_{\ell_{2D}}(y^*) \log\left[\frac{1 - y^{*2}}{\delta_1 \delta_2} \right] \qquad (B.21)$$

where

$$\delta_1 = y^* = \cos(\theta' + \epsilon) \qquad (B.22)$$

$$\delta_2 = \cos(\theta' - \epsilon) - y^* \qquad (B.23)$$

The latter relations are depicted graphically in Figure B.4. The remaining integrals in (B.21) are nonsingular and can be evaluated using Legendre-Gauss quadrature, (B.11) and (B.12).

The integral $B_\epsilon(\theta')$ contains the removable singularity at $\theta_1' = \theta'$. To evaluate B_ϵ, we first expand $[\tilde{C}_{\ell_{2D}}(\eta^*) - \tilde{C}_{\ell_{2D}}(y^*)]$ near $\theta_1' = \theta'$ to remove the singularity.

$$\tilde{C}_{\ell_{2D}}(\cos\theta_1') - \tilde{C}_{\ell_{2D}}(\cos\theta') = \sum_{n=1}^{\infty} \frac{1}{n!} (\theta_1' - \theta')^n \frac{\partial^n}{\partial \theta'^n} \tilde{C}_{\ell_{2D}}(\cos\theta') \qquad (B.24)$$

Using this expansion, $B_\epsilon(\theta')$ becomes

$$B_\epsilon(\theta') = \sum_{n=1}^{\infty} E_n(\theta') \frac{\partial^n}{\partial \theta'^n} \tilde{C}_{\ell_{2D}}(\cos\theta') \tag{B.25}$$

where

$$E_n(\theta') = \frac{1}{n!} \int_{\theta'-\epsilon}^{\theta'+\epsilon} M_2(\theta', \theta_1') (\theta_1' - \theta')^{(n-1)} \operatorname{sgn}(\theta_1' - \theta') \, d\theta_1'$$

$$n = 1, 2, 3, \ldots \tag{B.26}$$

The generalized function $\operatorname{sgn}(\theta_1' - \theta')$ is defined as

$$\operatorname{sgn}(\theta_1' - \theta') = \begin{cases} 1 & \theta_1' > \theta' \\ -1 & \theta_1' < \theta' \end{cases} \tag{B.27}$$

In relation to (B.25) we remark that, while the derivatives of $\tilde{C}_{\ell_{2D}}(y^*)$ with respect to y^* may become infinite at blunt wing tips (e.g., for the elliptic planform), the derivatives of $\tilde{C}_{\ell_{2D}}(\cos\theta')$ with respect to θ' are finite everywhere including at blunt tips (see (B.5) and the discussion at the beginning of this appendix).

The integrals $E_n(\theta')$, (B.26), are nonsingular, although each integrand has a finite discontinuity at $\theta_1' = \theta'$. They can be evaluated using Legendre-Gauss quadrature after breaking up each integral into two parts at the discontinuity. In the following, however, after examining the order of magnitude of $E_n(\theta')$, we will see that for a suitably small value of ϵ we may neglect $B_\epsilon(\theta')$ altogether.

Since $M_2(\theta', \theta_1')$ is well behaved near $\theta_1' = \theta'$, for θ' not very close to

the tips (see Figure B.3), we may expand M_2 near $\theta_1' = \theta'$ as

$$M_2(\theta', \theta_1') = 1 + (\theta_1' - \theta') f(\theta') + \cdots \tag{B.28}$$

where

$$f(\theta') = \frac{\partial}{\partial \theta_1'} M_2(\theta', \theta_1') \Big|_{\theta_1' = \theta'} \tag{B.29}$$

Substituting this expansion into (B.26) and integrating, we obtain

$$E_n(\theta') = \frac{1}{n!} \left\{ \frac{1}{n} \left[\epsilon^n + (-\epsilon)^n \right] + \frac{1}{n+1} \left[\epsilon^{n+1} + (-\epsilon)^{n+1} \right] f(\theta') + \cdots \right\} \tag{B.30}$$

For θ' not very close to the tips $f(\theta') \sim O(1)$ (see Figure B.3) and it follows that

$$\begin{aligned} &E_1(\theta'), E_2(\theta') \sim O(\epsilon^2) \\ &E_3(\theta'), E_4(\theta') \sim O(\epsilon^4) \\ &\vdots \end{aligned} \tag{B.31}$$

Hence,

$$B_\epsilon(\theta') \sim O(\epsilon^2) \tag{B.32}$$

As we approach the tips, for distances of $O(\epsilon)$, it can be shown that

$$E_n(\theta') \sim O(\epsilon^n) \qquad n = 1, 2, 3, \cdots \tag{B.33}$$

and, hence,

$$B_\epsilon(\theta') \sim O(\epsilon) \tag{B.34}$$

For values of θ' closer to the tips than ϵ, ϵ is redefined as the distance from the tip. Hence, $B_\epsilon(\theta')$ vanishes at the tips. Variation of $B_\epsilon(\theta')$ with θ' is depicted qualitatively in Figure B.5 for half of the span.

Therefore, if ϵ is chosen as a suitably small quantity, we can neglect $B_\epsilon(\theta')$. $B_\epsilon(\theta')$ then represents an error in the numerical evaluation of $B(\theta')$. In terms of the physical variable y^*, the maximum error, i.e., $B_\epsilon(\theta') \sim O(\epsilon)$, occurs at a distance of $O(\epsilon^2)$ from the tips, as can be seen from

$$y^* = \cos\epsilon = 1 - O(\epsilon^2) \qquad (B.35)$$

for the tip at $y^* = 1$.

In the numerical calculations presented in this work, ϵ is chosen through numerical experiments to be $\epsilon \approx 0.006$. For an elliptic wing in steady flow, using this value of ϵ, the maximum relative error was found to be approximately 0.03% occuring at a distance of about 0.01% of the semi span from the tip. This is typical of the calculations presented herein and corresponds to better than three decimal places of accuracy for the results. With the loads dropping off to zero at the tips, the effect of the above error on the overall calculations is expected to be negligible.

It should be noted that, for all practical purposes, the above schemes for the evaluation of $A(\theta')$ and $B(\theta')$ are valid for all points along the span including those very close to the tips, but exclude the tips. These schemes can be modified to accomodate the tips as well, but this is not necessary. The spanwise integrals for the calculation of the total aerodynamic quantities employ Legendre-Gauss quadrature which excludes the

end points.

APPENDIX C

NUMERICAL EVALUATION OF INDUCED DOWNWASH OF REISSNER'S THEORY

In this appendix, we describe a procedure for the numerical evaluation of the unsteady induced downwash of Reissner's theory given by (3.38a) and (3.38b). In order to accomodate blunt wing tips again we introduce the spanwise angular transformation (B.1), in terms of which (3.38b) may be written as

$$C(\theta') = \oint_0^{\pi} \frac{E(\gamma^*, \eta^*)}{(\theta' - \theta_1')} \; M_3(\theta', \theta_1') \; d\theta_1' \qquad (C.1)$$

where

$$E(\gamma^*, \eta^*) = \frac{d\tilde{\Omega}^*}{d\eta^*} \; \overline{K}(\mu_0 |\gamma^* - \eta^*|) \qquad (C.2)$$

$$M_3(\theta', \theta_1') = \frac{\theta' - \theta_1'}{\cos\theta' - \cos\theta_1'} \; \sin\theta_1' \qquad (C.3)$$

For given wing displacements, $d\tilde{\Omega}^*/d\eta^*$ can be evaluated from (3.29) using the following derivative formulae from Abramowitz and Stegun (1970).

$$A_\nu'(z) = A_{\nu-1}(z) - \frac{\nu}{z} A_\nu(z) \qquad (C.4)$$

$$A_\nu'(z) = -A_{\nu+1}(z) + \frac{\nu}{z} A_\nu(z) \qquad C.5)$$

where A_ν denotes Bessel functions of the first and second kind, J_ν and Y_ν, or Hankel functions of the first and second kind, $H_\nu^{(1)}$ and $H_\nu^{(2)}$.

Numerical values of the modified kernel function $\bar{K}(q)$ are obtained from polynomial approximations which are obtained from the tabular data in Table 3.1 (p. 339) using a least square criterion (1). Different polynomials are used for different ranges of values of the argument q. The accuracy of the numerical values is three decimal places. The real and imaginary parts of $\bar{K}$ are shown in Figure 3.4.

The function $M_3(\theta',\theta_1')$ is the negative of $M_2(\theta',\theta_1')$. Hence, apart from a minus sign, M_3 has all the properties of M_2 mentioned in Appendix B (see the discussion following (B.18) and Figure B.3).

The integral $C(\theta')$ is of the general form

$$C(\theta') = \oint_0^{\pi} \frac{H(\theta',\theta_1')}{(\theta'-\theta_1')}\, d\theta_1' \qquad (C.6)$$

In order to evaluate $C(\theta')$ numerically, we first write it as the sum of three integrals.

$$C(\theta') = \left[\int_0^{\theta'-\delta} + \int_{\theta'-\delta}^{\theta'+\delta} + \int_{\theta'+\delta}^{\pi} \right] \frac{H(\theta',\theta_1')}{(\theta'-\theta_1')}\, d\theta_1'$$

$$= C_1(\theta') + C_\epsilon(\theta') + C_2(\theta') \qquad (C.7)$$

where $\delta > 0$ represents a small neighborhood of the singularity. The integrals $C_1(\theta')$ and $C_2(\theta')$ are nonsingular and span a finite interval. They can be evaluated using Legendre-Gauss quadrature, (B.11) and (B.12).

The integral $C_\epsilon(\theta')$, which contains the Cauchy singularity, can be

---

(1) The subroutine employed is LSFIT which is currently part of the library MATHOBS at the MIT-IPS.

evaluated in a manner similar to that for $A_\epsilon(\theta')$ in Appendix B. The method is summarized below. We approximate the function $H(\theta',\theta_1')$ with a sixth degree polynomial, using Lagrange's interpolation formula, in terms of which $C_\epsilon(\theta')$ becomes

$$C_\epsilon(\theta') \approx \delta^{-6} \sum_{i=0}^{5} g_i(\theta')\, \delta^i \int_{\theta'-\gamma}^{\theta'+\gamma} (\theta'-\theta_1')^{(5-i)}\, d\theta_1' + g_6(\theta') \oint_{\theta'-\gamma}^{\theta'+\gamma} (\theta'-\theta_1')^{-1}\, d\theta_1' \qquad (C.8)$$

where $\delta = \gamma/3$ and $g_i(\theta')$ are linear combinations of $H(\theta',\theta_1')$ at the seven interpolation stations and can be found from Lagrange's interpolation formula. According to (B.14), the last integral in (C.8) is identically zero. Carrying out the remaining integrals and substituting for $g_i(\theta')$, we obtain the following approximation for $C_\epsilon(\theta')$.

$$C_\epsilon(\theta') \approx \frac{1}{200}\Big\{ 23\left[H(\theta',\theta'-3\delta) - H(\theta',\theta'+3\delta)\right] - 42\left[H(\theta',\theta'-2\delta) - H(\theta',\theta'+2\delta)\right] + 615\left[H(\theta',\theta'-\delta) - H(\theta',\theta'+\delta)\right]\Big\} \qquad (C.9)$$

The above procedure for evaluating $C(\theta')$, like those for $A(\theta')$ and $B(\theta')$ in Appendix B, are valid for any point along the span except for the wing tips. However, for reasons already mentioned in relation to $A(\theta')$ and $B(\theta')$, the above scheme is adequate for the present purposes.

The numerical examples of Reissner's unsteady induced downwash presented in this work are carried out using an earlier numerical scheme which, although different in some of the details, is similar in overall

features to the one described in the above which is a more efficient one. The accuracy of the results are three decimal places or better.

APPENDIX D

DETERMINATION OF FAR-FIELD INTEGRALS IN TWO DIMENSIONS

In this appendix we show that the following far-field integrals which arise in the momentum-theorem approach to calculating the thrust in two dimensions (Section 6.2) tend to zero as the far boundary S is removed to infinity (see Figure 6.1).

$$\int_{S_1} (w^2 - u^2)\, dS$$

$$\int_{S_2} uw\, dS \qquad (D.1)$$

$$\int_{S_4} uw\, dS$$

In order to determine an upper bound for these integrals, it sufficies to study the following simplified model. Consider a cylindrical far boundary S' of radius R, centered at the origin, representing S_1, S_2 and S_4, as shown in Figure D.1. As R tends to infinity, using multipole expansions, we can represent the airfoil and wake vorticity as a series of vortex multipoles located at the origin and along the wake. If the problem contains a steady lifting component, the leading term of the multipole expansion for the airfoil will be a vortex, otherwise a vortex dipole which produces even smaller distrubance in the far field. This is what we expect on physical grounds, since a steady lifting airfoil produces larger distrubances in the far field than its purely unsteady (small amplitude)

counterpart.

Hence, to find an upper bound for the integrals in the above, it suffices to consider a concentrated vortex at the origin for which the velocity potential is given by

$$\phi \sim \theta \tag{D.2}$$

and the perturbation velocity component in the θ direction, say w_θ, on S' is given by

$$w_\theta (R,\theta) = \frac{1}{r} \frac{\partial \phi}{\partial \theta}\Big|_{r=R} \sim O(R^{-1}) \tag{D.3}$$

The polar coordinate system (r,θ) is shown in Figure D.1. The perturbation velocity components u and w (also $\vec{q} = u\,\vec{i} + w\,\vec{k}$) on S' are of the same order as w_θ. Hence, the integrals in question are of the order

$$\int_{S'} |\vec{q}|^2 \, dS \sim \int_{S'} \frac{1}{R^2} R \, d\theta \sim O(R^{-1}) \tag{D.4}$$

and, hence, vanish as R tends to infinity.

APPENDIX E

CALCULATION OF PERTURBATION VELOCITIES IN THE FAR WAKE IN TWO DIMENSIONS

In this appendix, we calculate the perturbation velocities u and w in the far wake of a harmonically oscillating airfoil. These are needed for calculating the average thrust, see (6.29). Since u and w appear only in quadratic form, it suffices to calculate them from a linearized (planar) wake model. The effects of the lateral displacement of the wake have already been taken into account in deriving (6.29).

Here, the contribution of the airfoil to u and w is negligible, since the airfoil is located infinitely far uptstream. We consider a wake extending infinitely far upstream and downstream of the Trefftz plane. For convenience, we employ a cartesian coordinate system (x_1,z) which is attached to the Trefftz plane at the plane of the wake and is stationary in the (x,z) frame. The trefftz plane is given by $x_1 = 0$. The strength of the wake vorticity is given by (see (6.23))

$$\tilde{\gamma}_w(x) = g(k)\, e^{-j\bar{\omega}x_1} \tag{E.1}$$

where

$$g(k) = -jk\tilde{\Omega} \tag{E.2}$$

The perturbation velocity potential in the far wake is given by

$$\tilde{\phi}(x_1,z) = \frac{-1}{2\pi} g \int_{-\infty}^{\infty} e^{-j\bar{\omega}\xi} \tan^{-1}\left(\frac{z}{x_1-\xi}\right) d\xi \tag{E.3}$$

Making the change of variables

$$\eta = x_1 - \xi \tag{E.4}$$

and integrating by parts once, we find

$$\tilde{\phi}(x_1, z) = \frac{-1}{2\pi} g z \frac{e^{-j\bar{\omega}x_1}}{j\bar{\omega}} \int_{-\infty}^{\infty} \frac{e^{j\bar{\omega}\eta}}{z^2+\eta^2} d\eta \tag{E.5}$$

The imaginary part of the integral is identically zero due to symmetry. The real part is the known integral

$$2\int_0^{\infty} \frac{\cos(\bar{\omega}\eta)}{z^2+\eta^2} d\eta = \frac{\pi}{|z|} e^{-\bar{\omega}|z|} \qquad z \neq 0 \tag{E.6}$$

which is found in Dwight (1961). The perturbation potential then becomes

$$\tilde{\phi}(x_1, z) = c\tilde{\Omega} e^{-j\bar{\omega}x_1} e^{-\bar{\omega}|z|} \operatorname{sgn}(z) \qquad z \neq 0 \tag{E.7}$$

where the sgn function is defined in (B.27).

The perturbation velocity components in the far wake are obtained from (E.7) by differentiation.

$$\tilde{u}(x_1, z) = \frac{\partial}{\partial x_1} \tilde{\phi}(x_1, z) \qquad z \neq 0$$

$$= -\frac{1}{2} jk \tilde{\Omega} e^{-j\bar{\omega}x_1} e^{-\bar{\omega}|z|} \operatorname{sgn}(z) \tag{E.8}$$

and

$$\tilde{w}(x_1, z) = \frac{\partial}{\partial z} \tilde{\phi}(x_1, z) \qquad z \neq 0$$

$$= -\frac{1}{2} k \tilde{\Omega} e^{-j\bar{\omega}x_1} e^{-\bar{\omega}|z|} \tag{E.9}$$

As a check we note that, as $z \to 0\pm$,

$$\tilde{u} = \mp \frac{1}{2} j k \tilde{\Omega} \, e^{-j\bar{\omega}x_1}$$
$$\tilde{w} = -\frac{1}{2} k \tilde{\Omega} \, e^{-j\bar{\omega}x_1} \qquad (E.10)$$

which are consistent with the symmetry properties of vortex sheets in unsteady motion.

The average of the square of the perturbation velocities in the far wake is determined by applying the averaging rule (4.4) to the above results.

$$\overline{u^2}(x_1, z) = \overline{w^2}(x_1, z) = \frac{1}{8}|g|^2 e^{-2\bar{\omega}|z|} \qquad (E.11)$$

It is noteworthy that, in the far wake, $\overline{u^2}$ and $\overline{w^2}$, with reprect to the body frame, are independent of x.

APPENDIX F

DETERMINATION OF FAR-FIELD INTEGRALS IN THREE DIMENSIONS

In Section 6.5, in calculating the thrust from the momentum theorem in three dimensions, we encountered the following far-field integrals

$$I_1 = \int_{S_1} (v^2 + w^2 - u^2)\, dS \qquad (F.1)$$

$$I_2 = \int_{S_2} u(v\cos\theta + w\sin\theta)\, dS \qquad (F.2)$$

(see Figure 6.8). In this appendix, we show that the above integrals vanish as the far boundary S is removed to infinity.

Since the far-field disturbances caused by a wing in steady flow are stronger than those caused by a wing in small-amplitude unsteady motion, in the present case we can find an upper bound for the far-field disturbances by considering the following simplified steady case. We consider a wing with uniform loading across the span. For the far-field calculations, the wing may be represented by a horseshoe vortex of uniform strength Γ of width 2b as shown in Figure F.1. The perturbation velocity components at a field point (x,y,z), have been calculated by Glauert (1947). They are given by

$$u = \frac{\Gamma}{4\pi}\frac{z}{x^2+z^2}\left[\frac{y+b}{\sqrt{x^2+(y+b)^2+z^2}} - \frac{y-b}{\sqrt{x^2+(y-b)^2+z^2}}\right] \qquad (F.3)$$

$$v = \frac{-\Gamma}{4\pi}\frac{z}{z^2+(y-b)^2}\left[1 + \frac{x}{\sqrt{x^2+(y-b)^2+z^2}}\right]$$

$$+\frac{\Gamma}{4\pi}\frac{z}{z^2+(y+b)^2}\left[1+\frac{x}{\sqrt{x^2+(y+b)^2+z^2}}\right] \qquad (F.4)$$

$$w=\frac{-\Gamma}{4\pi}\frac{x}{x^2+z^2}\left[\frac{y+b}{\sqrt{x^2+(y+b)^2+z^2}}-\frac{y-b}{\sqrt{x^2+(y-b)^2+z^2}}\right]$$

$$+\frac{\Gamma}{4\pi}\frac{y-b}{z^2+(y-b)^2}\left[1+\frac{x}{\sqrt{x^2+(y-b)^2+z^2}}\right]$$

$$-\frac{\Gamma}{4\pi}\frac{y+b}{z^2+(y+b)^2}\left[1+\frac{x}{\sqrt{x^2+(y+b)^2+z^2}}\right] \qquad (F.5)$$

It can be shown, by suitable expansions of (F.3) - (F.5), that as S is removed to infinity, u, v and w are at most of $O(R^{-2})$ on S_1 and S_2. Accordingly, using the polar coordinate system (r,θ) in the yz-plane (see Figure 6.8), we find

$$I_1=\int_0^{2\pi}d\theta\int_0^{R}r\,dr\,(v^2+w^2-u^2)$$

$$\sim O(R^{-2}) \qquad (F.6)$$

and

$$I_2=\int_0^{2\pi}d\theta\int_{-R}^{R}u\,(v\cos\theta+w\sin\theta)\,R\,d\theta\,dx$$

$$\sim O(R^{-2}) \qquad (F.7)$$

both of which vanish as R tends to infinity.

APPENDIX G

CALCULATION OF PERTURBATION VELOCITIES IN THE FAR WAKE IN THREE DIMENSIONS

In this appendix, we calculate the perturbation velocities u, v and w in the far wake of a harmonically-oscillating finite wing. These are needed for calculating the average thrust, see (6.113). Since u, v, and w appear only in quadratic form, it suffices to consider a planar wake. The effects of the lateral displacement of the wake have already been taken into account in deriving (6.113).

As in two dimensions (Appendix E), we consider a wake extending infinitely far upstream and downwstream of the Trefftz plane and choose a cartesian coordinate system (x_1, y, z) which is stationary in the (x, y, z) frame and parallel to it. The Trefftz plane coincides with the yz-plane and the wake is the strip

$$|y| \leq b \qquad z = 0 \tag{G.1}$$

The components of wake vorticity are given by (6.109) and (6.117) for the wing in Figure 6.8.

Calculation of u

u is entirely due to γ_w. It follows from the Biot-Savart law and (6.109) that u is given by

$$\tilde{u}(x_1, y, z) = \frac{-1}{4\pi} j k_0 z \int_{-b}^{b} d\eta \int_{-\infty}^{\infty} d\xi \; \tilde{\Omega}(\eta) e^{-j\bar{\omega}\xi} R_1^{-3} \tag{G.2}$$

where

$$R_1 = \sqrt{(x_1 - \xi)^2 + (y-\eta)^2 + z^2} \qquad (G.3)$$

With the chage of variables $\gamma = x_1 - \xi$, the integral over ξ can be expressed in terms of modified Bessel function of the second kind K_1 (see Abramowitz and Stegun (1970)):

$$\int_{-\infty}^{\infty} e^{-j\bar{\omega}\xi} R_1^{-3} \, d\xi = \frac{2k_o}{c_o} e^{-j\bar{\omega}x_1} R_z^{-1} K_1(\bar{\omega} R_z) \qquad (G.4)$$

where

$$R_z = \sqrt{(y-\eta)^2 + z^2} \qquad (G.5)$$

Substituting (G.4) into (G.2), we obtain

$$\tilde{u}(x_1, y, z) = \frac{-1}{2\pi c_o} j k_o^2 z \, e^{-j\bar{\omega}x_1} \int_{-b}^{b} \tilde{\Omega}(\eta) R_z^{-1} K_1(\bar{\omega} R_z) \, d\eta \qquad (G.6)$$

Calculation of v

v is entirely due to δ_w. Using the Biot-Savart law and (6.117), we find

$$\tilde{v}(x_1, y, z) = \frac{1}{4\pi} c_o z \int_{-b}^{b} d\eta \int_{-\infty}^{\infty} d\xi \, \tilde{\Omega}'(\eta) e^{-j\bar{\omega}\xi} R_1^{-3} \qquad (G.7)$$

where $(\,)'$ denotes differentiation with respect to the indicated argument. Using (G.4), (G.7) reduces to

$$\tilde{v}(x_1, y, z) = \frac{1}{2\pi} k_0 z \, e^{-j\bar{\omega} x_1} \int_{-b}^{b} \tilde{\Omega}'(\eta) \, R_z^{-1} \, K_1(\bar{\omega} R_z) d\eta \quad (G.8)$$

Using the asymptotic expansion for K_1 in (2.142), it can be shown that, as $z \to o\pm$, the integrals in (G.6) and G.8) each contain a second-order singularity $(y - \eta)^{-2}$ and must be interpreted according to the principle value in (2.146).

Calculation of w

Both components of wake vorticity contribute to w. It follows from the Biot-Savart law, and (6.109) and (6.117) that w is given by

$$\tilde{w}(x_1, y, z) = \frac{-1}{4\pi} c_0 \int_{-b}^{b} d\eta \int_{-\infty}^{\infty} d\xi \; (y-\eta) \tilde{\Omega}'(\eta) \, e^{-j\bar{\omega}\xi} \, R_1^{-3}$$
$$+ \frac{1}{4\pi} j k_0 \int_{-b}^{b} d\eta \int_{-\infty}^{\infty} d\xi \; (x_1 - \xi) \tilde{\Omega}(\eta) \, e^{-j\bar{\omega}\xi} \, R_1^{-3} \quad (G.9)$$

The integral over ξ in the first term is given by (G.4). In the second term, after the change of variables $\zeta = x_1 - \xi$, the integral over ξ can be expressed in terms of modified Bessel function of the second kind K_0 (see Abramowitz and Stegun (1970)):

$$\int_{-\infty}^{\infty} (x_1 - \xi) \, e^{-j\bar{\omega}\xi} \, R_1^{-3} \, d\xi = \frac{2jk_0}{c_0} \, e^{-j\bar{\omega} x_1} \, K_0(\bar{\omega} R_z) \quad (G.10)$$

Substituting (G.4) and (G.10) into (G.9), we obtain

$$\tilde{w}(x_1, y, z) = \frac{-1}{2\pi} k_0 \, e^{-j\bar{\omega} x_1} \int_{-b}^{b} (y-\eta) \tilde{\Omega}'(\eta) \, R_z^{-1} \, K_1(\bar{\omega} R_z) d\eta$$
$$- \frac{1}{2\pi c_0} k_0^2 \, e^{-j\bar{\omega} x_1} \int_{-b}^{b} \tilde{\Omega}(\eta) \, K_0(\bar{\omega} R_z) \, d\eta \quad (G.11)$$

Using the asymptotic expansion for K_1 in (2.142), it can be shown that, as $z \to 0\pm$, the integral in (G.11) which contains K_1 has a first-order singularity $(y - \eta)^{-1}$ and must be interpreted in accordance with the Cauchy principle value (see (B.14)).

It follows from (G.6), (G.8) and (G.11), and the averaging rule in (4.4) that

$$\overline{u^2} = \frac{1}{2} |u(x_1, y, z)|^2 \qquad (G.12)$$

$$\overline{v^2} = \frac{1}{2} |v(x_1, y, z)|^2 \qquad (G.13)$$

$$\overline{w^2} = \frac{1}{2} |w(x_1, y, z)|^2 \qquad (G.14)$$

It is seen from the results of this appendix that in the far wake u, v and w have a sinusoidal dependence on x but $\overline{u^2}$, $\overline{v^2}$ and $\overline{w^2}$ are independent of x. For actual numerical calculations, for high-aspect-ratio wings, we may replace the three-dimensional reduced circulation $\tilde{\Omega}$ with its strip-theory counterpart Ω, (3.29) (see the discussion preceding (3.29)). Also, in the limit of steady flow ($\omega \to 0$), the above results for u, v and w reduce to the known steady results.

APPENDIX H

LISTING OF FORTRAN PROGRAMS

This appendix consists of the primary computer programs used in this work for the applications of the present unsteady lifting-line theory. The programs are for a rigid finite wing oscillating in combined pitch and heave. For additional details regarding the programs see Chapters III - V and Appendix B. A list of the primary symbols for the programs are given below. All coding is in FORTRAN IV. The programs were executed on the IBM 370 - 168 of the Information Processing Services at M.I.T.

The following programs are listed (1):

i) Program 1 calculates the optimum motion of a finite wing in combined pitch and heave. The listing for this program includes the subprograms DNWASH, FN2, LG2, FN1, FN3, LG3 , L2, FN5, STHEOD, KER, CL1, CM1 and RROOTS. Subroutine DNWASH calculates the unsteady induced downwash. Program 1 also generates the spanwise distribution of the energetic quantities at 8 stations along the semi span and the propulsive performance of a wing in several non-optimum modes of oscillation.

ii) Program 2 calculates spanwise distribution of unsteady induced downwash and section lift and moment coefficients for the wing at 11 stations along the semi span.

iii) Program 3 calculates total lift and moment coefficients for the wing.

---

(1)
Duplicate subprograms are not listed.

LIST OF PRIMARY SYMBOLS

ALPHP	α_p
AR	A
B	B
CCO	$c(y)/c_o$
CE	C_ε
$\tilde{C}_\ell$	= CL3DR + J CL3DI
	= (CL00P + j CL00DP) ξ_o + (CL11P + j CL11DP) ξ_1
	+ (CL22P + j CL22DP) ξ_2
$\tilde{C}_{\ell_{2D}}$	= CL2DR + j CL2DI (strip-theory value)
	= (CL0P + j CL0DP) ξ_o + (CL1P + j CL1DP) ξ_1
	+ (CL2P + j CL2DP) ξ_2
$\tilde{C}_{\ell_{Sears}}$	= (CLS0P + j CLS0DP) ξ_o + (CLS1P + j CLS1DP) ξ_1
	+ (CLS2P + j CLS2DP) ξ_2
$\tilde{C}_L$	= TCL3DR + j TCL3DI
$\tilde{C}_{L_{2D}}$	= TCL2DR + j TCL2DI (strip-theory value)

(similar notation is used for sectional and total moment coefficients)

CP	$C_\mathcal{P}$
CT	$C_\mathcal{T}$
CT0B	$\overline{C}_{\mathcal{T},0}$
CTP	$C_{\mathcal{T}_P}$
CTS	$C_{\mathcal{T}_S}$
CTSCT	$C_{\mathcal{T}_S}/C_\mathcal{T}$
D	D
DELTA	δ in function FN2

DELTA1, DELTA2	δ_1 and δ_2 in function FN5
EN	k_n with b = 1 (see (3.48))
END	= 0 or 1, dummy index to indicate end of dataset
ETA	Hydrodynamic efficiency η ; argument of the kernel function $\Pi(\mu_o \mid y^* - \eta^* \mid)$
F, G	F, G
JJ = 1, 2,...6	dummy index denoting consecutively the real and imaginary parts of coefficients of ξ_o, ξ_1 and ξ_2 in the linear quantities
NN = 1,2,3	denotes elliptic, lenticular and cusp-tipped planforms respectively
PAXIS	$b_L/(c_o/A)$
PFP	θ_L
PIP, PIDP	real and imaginary parts of the kernel function $\Pi(\mu_o \mid y^* - \eta^* \mid)$
PSI10, PSI20	ξ_1/ξ_o and ξ_2/ξ_o
S, S1	y, η
SIGMA, SIGMA0	k, k_o
SR, SI	real and imaginary parts of the Sears function
T, T1	θ', θ_1'
THETA	θ'
VAMP, VPHASE	amplitude and phase of $\tilde{W}_g^*$
$\tilde{W}_g^*$	= (V0P + j V0DP) ξ_o + (V1P + j V1DP) ξ_1 + (V2P + j V2DP) ξ_2
WI(I,N)	Ith abscissa of N-point Legendre-Gauss quadrature
WT(I,N)	Ith weight of N-point Legendre-Gauss quadrature
ZP	Z_p

```
C                                                                       PGM10001
C     PROGRAM 1                                                         PGM10002
C                                                                       PGM10003
C     DETERMINATION OF OPTIMUM MOTION OF A RIGID FINITE WING IN COMBINED PGM10004
C     PITCH AND HEAVE USING UNSTEADY LIFTING-LINE THEORY                PGM10005
C                                                                       PGM10006
      IMPLICIT REAL*8 (A-Z)                                             PGM10007
      COMPLEX*16 RZ(3)                                                  PGM10008
      DIMENSION XI(24,24),WT(24,24),A(4),P(3,3),R(3,3),K(3,3),T(3,3),   PGM10009
     &   E(3,3),DENOM(3),PSI10(3),PSI20(3),XX1(3),XX2(3),XX3(3),LAM(3), PGM10010
     &   CT0B(3),ETA(3),ZP(3),ALPHP(3),CTSCT(3)                         PGM10011
      INTEGER AR,END,I,N,NN,S,NFR,J1,J2,JJ                              PGM10012
      COMMON/AREA1/XI,WT/AREA3/GAMMA,EN/AREA4/SIGMA0,PI,NN,AR           PGM10013
      PI=3.1415926535897900                                             PGM10014
      GAMMA=.5772156649015340                                           PGM10015
      PIINV=1.D0/PI                                                     PGM10016
      PIINV2=PIINV*PIINV                                                PGM10017
      READ401,((XI(I,N),I=1,N),N=4,24,4)                                PGM10018
      READ401,((WT(I,N),I=1,N),N=4,24,4)                                PGM10019
  401 FORMAT(20X,F20.15,32X)                                            PGM10020
   88 READ402,SIGMA0,AR,END,NN                                          PGM10021
  402 FORMAT(F9.6,I2,8X,I1,4X,I1)                                       PGM10022
C                                                                       PGM10023
C     IDENTIFY PLANFORM                                                 PGM10024
C                                                                       PGM10025
      GO TO (200,201,202),NN                                            PGM10026
  200 EN=4.D0/PI                                                        PGM10027
      PRINT300,SIGMA0,AR,NN                                             PGM10028
  300 FORMAT('1','SIGMA0=',F8.5,2X,'AR=',I3,2X,'NN=',I3,2X,'ELLIPTIC    PGM10029
     &WING')                                                            PGM10030
      GO TO 303                                                         PGM10031
  201 EN=1.5D0                                                          PGM10032
      PRINT301,SIGMA0,AR,NN                                             PGM10033
  301 FORMAT('1','SIGMA0=',F8.5,2X,'AR=',I3,2X,'NN=',I3,2X,'LENTICULAR  PGM10034
     &WING')                                                            PGM10035
      GO TO 303                                                         PGM10036
```

```
  202 EN=16.D0/(3.D0*PI)                                                PGM10037
      PRINT302,SIGMA0,AR,NN                                             PGM10038
  302 FORMAT('1','SIGMA0=',F8.5,2X,'AR=',I3,2X,'NN=',I3,2X,'CUSP-TIPPED PGM10039
     &WING')                                                            PGM10040
  303 CONTINUE                                                          PGM10041
C                                                                       PGM10042
C     CALCULATION OF THE QUADRATIC FORMS REPRESENTING THE ENERGETIC     PGM10043
C     QUANTITIES                                                        PGM10044
C                                                                       PGM10045
C     SIMULTANEOUS INTEGRATION OF 18 INTEGRALS (COEFF'S OF THE QUADRATIC PGM10046
C     FORMS) USING 16-POINT LEGENDRE-GAUSS QUADRATURE                   PGM10047
C                                                                       PGM10048
      N=16                                                              PGM10049
      PRINT33,N                                                         PGM10050
   33 FORMAT('0','N=',I3)                                               PGM10051
      SUM1=0.D0                                                         PGM10052
      SUM2=0.D0                                                         PGM10053
      SUM3=0.D0                                                         PGM10054
      SUM4=0.D0                                                         PGM10055
      SUM5=0.D0                                                         PGM10056
      SUM6=0.D0                                                         PGM10057
      SUM7=0.D0                                                         PGM10058
      SUM8=0.D0                                                         PGM10059
      SUM9=0.D0                                                         PGM10060
      SUM10=0.D0                                                        PGM10061
      SUM11=0.D0                                                        PGM10062
      SUM12=0.D0                                                        PGM10063
      SUM13=0.D0                                                        PGM10064
      SUM14=0.D0                                                        PGM10065
      SUM15=0.D0                                                        PGM10066
      SUM16=0.D0                                                        PGM10067
      SUM17=0.D0                                                        PGM10068
      SUM18=0.D0                                                        PGM10069
      E=E/2                                                             PGM10070
      DO 10 I=1,N                                                       PGM10071
      THETA=.5D0*PI*(1.D0+XI(I,N))                                      PGM10072
```

```
      S=DCOS(THETA)                                                     PGM10073
      CC0=(1.D0-S*S)**(NN/2.D0)                                         PGM10074
      SIGMA=SIGMA0*CC0                                                  PGM10075
      SIG2=SIGMA*SIGMA                                                  PGM10076
      CALL STHECD(SIGMA,F,G,D,B,SR,SI)                                  PGM10077
      S2=SR*SR+SI*SI                                                    PGM10078
      CALL DWWASH(S,V0P,V0DP,V1P,V1DP,V2P,V2DP)                         PGM10079
      CALL       CL1(S,V0P,V0DP,V1P,V1DP,V2P,V2DP,                      PGM10080
     &              CL0P,CL0DP,CL1P,CL1DP,CL2P,CL2DP,                  PGM10081
     &              CLS0P,CLS0DP,CLS1P,CLS1DP,CLS2P,CLS2DP,            PGM10082
     &              CL00P,CL00DP,CL11P,CL11DP,CL22P,CL22DP)            PGM10083
      CALL       CM1(S,V0P,V0DP,V1P,V1DP,V2P,V2DP,                      PGM10084
     &              CM0P,CM0DP,CM1P,CM1DP,CM2P,CM2DP,                  PGM10085
     &              CMS0P,CMS0DP,CMS1P,CMS1DP,CMS2P,CMS2DP,            PGM10086
     &              CM00P,CM00DP,CM11P,CM11DP,CM22P,CM22DP)            PGM10087
      QQ=DSIN(THETA)                                                    PGM10088
C                                                                       PGM10089
C     NUMBERS ON CP, CTP, CTS AND CT CORRESPOND TO MATRIX POSITIONS     PGM10090
C     (1,1), (2,2), (3,3), (1,2), (1,3), (2,3) RESPECTIVELY            PGM10091
C                                                                       PGM10092
C     SECTIONAL POWER REQUIRED                                          PGM10093
C                                                                       PGM10094
      AC1=-SIGMA0*PIINV                                                 PGM10095
      CP1=CL00DP*AC1                                                    PGM10096
      CP2=-4.D0*CM11DP*AC1                                              PGM10097
      CP3=4.D0*CM22P*AC1                                                PGM10098
      CP4=(CL11DP-4.D0*CM00DP)*.5D0*AC1                                 PGM10099
      CP5=(CL22DP+4.D0*CM00P)*.5D0*AC1                                  PGM10100
      CP6=2.D0*(CM11P-CM22DP)*AC1                                       PGM10101
      PRINT17                                                           PGM10102
   17 FORMAT('0','SECTIONAL POWER REQUIRED IS:')                        PGM10103
      PRINT20,S,CP1,CP2,CP3,CP4,CP5,CP6                                 PGM10104
   20 FORMAT('0','S=',F6.3,1X,'CP1=',D10.4,1X,'CP2=',D10.4,1X,'CP3=',   PGM10105
     &   D10.4,1X,'CP4=',D10.4,1X,'CP5=',D10.4,1X,'CP6=',D10.4)         PGM10106
C                                                                       PGM10107
C     SECTIONAL THRUST FROM NORMAL FORCE AT THE WING                    PGM10108
```

```
C                                                                       PGM10109
      AC2=2.D0*PIINV                                                    PGM10110
      CTP1=0.D0                                                         PGM10111
      CTP2=CL11P*AC2                                                    PGM10112
      CTP3=CL22DP*AC2                                                   PGM10113
      CTP4=CL00P*.5D0*AC2                                               PGM10114
      CTP5=CL00DP*.5D0*AC2                                              PGM10115
      CTP6=(CL11DP+CL22P)*.5D0*AC2                                      PGM10116
C                                                                       PGM10117
C     SECTIONAL LEADING-EDGE SUCTION FORCE                              PGM10118
C                                                                       PGM10119
      A1=G*SIGMA0                                                       PGM10120
      A2=G*SIGMA-2.D0*F                                                 PGM10121
      A3=2.D0*G+SIGMA*(F-1.D0)                                          PGM10122
      B1=-F*SIGMA0                                                      PGM10123
      B2=-(2.D0*G+F*SIGMA-SIGMA)                                        PGM10124
      B3=-2.D0*F+SIGMA* G                                               PGM10125
      C1=SR*V0P-SI*V0DP                                                 PGM10126
      C2=SR*V1P-SI*V1DP                                                 PGM10127
      C3=SR*V2P-SI*V2DP                                                 PGM10128
      D1=SR*V0DP+SI*V0P                                                 PGM10129
      D2=SR*V1DP+SI*V1P                                                 PGM10130
      D3=SR*V2DP+SI*V2P                                                 PGM10131
      CTS1=CC0*(SIGMA0*SIGMA0*D                                +4.D0*(A1*C1 PGM10132
     &      +B1*D1))                                                    PGM10133
      CTS2=CC0*(SIG2+(4.D0+SIG2)*D-2.D0*SIG2*F-4.D0*SIGMA*G             PGM10134
     &                  +4.D0*(A2*C2+B2*D2))                            PGM10135
      CTS3=CC0*(SIG2+(4.D0+SIG2)*D-2.D0*SIG2*F-4.D0*SIGMA*G             PGM10136
     &                  +4.D0*(A3*C3+B3*D3))                            PGM10137
      CTS4=CC0*(-SIGMA*SIGMA0*B                                +2.D0*   PGM10138
     &      (A1*C2+A2*C1+B1*D2+B2*D1))                                  PGM10139
      CTS5=CC0*(2.D0*SIGMA0*D-SIGMA*SIGMA0*G                            PGM10140
     &      +2.D0*(A1*C3+A3*C1+B1*D3+B3*D1))                            PGM10141
      CTS6=CC0*(                    2.D0*(A2*C3+A3*C2+B2*D3             PGM10142
     &      +B3*D2))                                                    PGM10143
      PRINT18                                                           PGM10144
```

```
   18 FORMAT('0','SECTIONAL LE SUCTION IS:')                                PGM10145
      PRINT21,S,CTS1,CTS2,CTS3,CTS4,CTS5,CTS6                               PGM10146
   21 FORMAT('0','S=',F6.3,1X,'CTS1=',D10.4,1X,'CTS2=',D10.4,1X,'CTS3=',   PGM10147
     6    D10.4,1X,'CTS4=',D10.4,1X,'CTS5=',D10.4,1X,'CTS6=',D10.4)         PGM10148
C                                                                           PGM10149
C     SECTIONAL THRUST                                                      PGM10150
C                                                                           PGM10151
      CT1=CTP1+CTS1                                                         PGM10152
      CT2=CTP2+CTS2                                                         PGM10153
      CT3=CTP3+CTS3                                                         PGM10154
      CT4=CTP4+CTS4                                                         PGM10155
      CT5=CTP5+CTS5                                                         PGM10156
      CT6=CTP6+CTS6                                                         PGM10157
      PRINT19                                                               PGM10158
   19 FORMAT('0','SECTIONAL THRUST IS:')                                    PGM10159
      PRINT22,S,CT1,CT2,CT3,CT4,CT5,CT6                                     PGM10160
   22 FORMAT('0','S=',F6.3,1X,'CT1=',D10.4,1X,'CT2=',D10.4,1X,'CT3=',      PGM10161
     6    D10.4,1X,'CT4=',D10.4,1X,'CT5=',D10.4,1X,'CT6=',D10.4)           PGM10162
      SUM1=SUM1+QQ*WT(I,N)*CP1                                              PGM10163
      SUM2=SUM2+QQ*WT(I,N)*CP2                                              PGM10164
      SUM3=SUM3+QQ*WT(I,N)*CP3                                              PGM10165
      SUM4=SUM4+QQ*WT(I,N)*CP4                                              PGM10166
      SUM5=SUM5+QQ*WT(I,N)*CP5                                              PGM10167
      SUM6=SUM6+QQ*WT(I,N)*CP6                                              PGM10168
      SUM7=SUM7+QQ*WT(I,N)*CTP1                                             PGM10169
      SUM8=SUM8+QQ*WT(I,N)*CTP2                                             PGM10170
      SUM9=SUM9+QQ*WT(I,N)*CTP3                                             PGM10171
      SUM10=SUM10+QQ*WT(I,N)*CTP4                                           PGM10172
      SUM11=SUM11+QQ*WT(I,N)*CTP5                                           PGM10173
      SUM12=SUM12+QQ*WT(I,N)*CTP6                                           PGM10174
      SUM13=SUM13+QQ*WT(I,N)*CTS1                                           PGM10175
      SUM14=SUM14+QQ*WT(I,N)*CTS2                                           PGM10176
      SUM15=SUM15+QQ*WT(I,N)*CTS3                                           PGM10177
      SUM16=SUM16+QQ*WT(I,N)*CTS4                                           PGM10178
      SUM17=SUM17+QQ*WT(I,N)*CTS5                                           PGM10179
   10 SUM18=SUM18+QQ*WT(I,N)*CTS6                                           PGM10180
C                                                                           PGM10181
C     MATRIX OF QUADRATIC FORM FOR TOTAL POWER REQUIRED                     PGM10182
C                                                                           PGM10183
      AB1=.5D0*PI*EN                                                        PGM10184
      P(1,1)=AB1*SUM1                                                       PGM10185
      P(2,2)=AB1*SUM2                                                       PGM10186
      P(3,3)=AB1*SUM3                                                       PGM10187
      P(1,2)=AB1*SUM4                                                       PGM10188
      P(1,3)=AB1*SUM5                                                       PGM10189
      P(2,3)=AB1*SUM6                                                       PGM10190
      P(2,1)=P(1,2)                                                         PGM10191
      P(3,1)=P(1,3)                                                         PGM10192
      P(3,2)=P(2,3)                                                         PGM10193
      PRINT23                                                               PGM10194
   23 FORMAT('0','MATRIX OF QUADRATIC FORM FOR TOTAL POWER REQUIRED:')      PGM10195
      DO 13 I=1,3                                                           PGM10196
   13 PRINT3,P(I,1),P(I,2),P(I,3)                                           PGM10197
    3 FORMAT('0',3(2X14.8,3X))                                              PGM10198
C                                                                           PGM10199
C     MATRIX OF QUADRATIC FORM FOR TOTAL THRUST FROM NORMAL FORCE AT        PGM10200
C     THE WING                                                              PGM10201
C                                                                           PGM10202
      R(1,1)=AB1*SUM7                                                       PGM10203
      R(2,2)=AB1*SUM8                                                       PGM10204
      R(3,3)=AB1*SUM9                                                       PGM10205
      R(1,2)=AB1*SUM10                                                      PGM10206
      R(1,3)=AB1*SUM11                                                      PGM10207
      R(2,3)=AB1*SUM12                                                      PGM10208
      R(2,1)=R(1,2)                                                         PGM10209
      R(3,1)=R(1,3)                                                         PGM10210
      R(3,2)=R(2,3)                                                         PGM10211
C                                                                           PGM10212
C     MATRIX OF QUADRATIC FORM FOR TOTAL LEADING-EDGE SUCTION FORCE         PGM10213
C                                                                           PGM10214
      R(1,1)=AB1*SUM13                                                      PGM10215
      R(2,2)=AB1*SUM14                                                      PGM10216
```

```
      E(3,3)=AB1*SUM15                                                  PGM10217
      K(1,2)=AB1*SUM16                                                  PGM10218
      K(1,3)=AB1*SUM17                                                  PGM10219
      K(2,3)=AB1*SUM18                                                  PGM10220
      K(2,1)=K(1,2)                                                     PGM10221
      K(3,1)=K(1,3)                                                     PGM10222
      K(3,2)=K(2,3)                                                     PGM10223
      PRINT24                                                           PGM10224
   24 FORMAT('0','MATRIX OF QUADRATIC FORM FOR TOTAL LE SUCTION:')      PGM10225
      DO 14 I=1,3                                                       PGM10226
   14 PRINT3,K(I,1),K(I,2),K(I,3)                                       PGM10227
C                                                                       PGM10228
C     MATRIX OF QUADRATIC FORM FOR TOTAL THRUST                         PGM10229
C                                                                       PGM10230
      T(1,1)=R(1,1)+K(1,1)                                              PGM10231
      T(2,2)=R(2,2)+K(2,2)                                              PGM10232
      T(3,3)=R(3,3)+K(3,3)                                              PGM10233
      T(1,2)=R(1,2)+K(1,2)                                              PGM10234
      T(1,3)=R(1,3)+K(1,3)                                              PGM10235
      T(2,3)=R(2,3)+K(2,3)                                              PGM10236
      T(2,1)=T(1,2)                                                     PGM10237
      T(3,1)=T(1,3)                                                     PGM10238
      T(3,2)=T(2,3)                                                     PGM10239
      PRINT25                                                           PGM10240
   25 FORMAT('0','MATRIX OF QUADRATIC FORM FOR TOTAL THRUST:')          PGM10241
      DO 15 I=1,3                                                       PGM10242
   15 PRINT3,T(I,1),T(I,2),T(I,3)                                       PGM10243
C                                                                       PGM10244
C     MATRIX OF QUADRATIC FORM FOR TOTAL ENERGY LOSS RATE               PGM10245
C                                                                       PGM10246
      Z(1,1)=P(1,1)-T(1,1)                                              PGM10247
      Z(2,2)=P(2,2)-T(2,2)                                              PGM10248
      Z(3,3)=P(3,3)-T(3,3)                                              PGM10249
      Z(1,2)=P(1,2)-T(1,2)                                              PGM10250
      Z(1,3)=P(1,3)-T(1,3)                                              PGM10251
      Z(2,3)=P(2,3)-T(2,3)                                              PGM10252
      Z(2,1)=Z(1,2)                                                     PGM10253
      Z(3,1)=Z(1,3)                                                     PGM10254
      Z(3,2)=Z(2,3)                                                     PGM10255
      PRINT26                                                           PGM10256
   26 FORMAT('0','MATRIX OF QUADRATIC FORM FOR TOTAL ENERGY LOSS RATE:') PGM10257
      DO 16 I=1,3                                                       PGM10258
   16 PRINT3,Z(I,1),Z(I,2),Z(I,3)                                       PGM10259
C                                                                       PGM10260
C     CHARACTERISTICS OF A RIGID ELLIPTIC WING IN PURE PITCH AND PURE   PGM10261
C     HEAVE                                                             PGM10262
C                                                                       PGM10263
      CZH=Z(1,1)                                                        PGM10264
      CPH=P(1,1)                                                        PGM10265
      CZP=Z(2,2)                                                        PGM10266
      CPP=P(2,2)                                                        PGM10267
      PRINT188,CZH,CPH,CZP,CPP                                          PGM10268
  188 FORMAT('0','CZH=',D10.3,2X,'CPH=',D10.3,2X,'CZP=',D10.3,2X,       PGM10269
     &       'CPP=',D10.3)                                              PGM10270
      CTH=T(1,1)                                                        PGM10271
      CTP=T(2,2)                                                        PGM10272
      CTSH=K(1,1)                                                       PGM10273
      CTSP=K(2,2)                                                       PGM10274
      CTSCTH=K(1,1)/T(1,1)                                              PGM10275
      CTSCTP=K(2,2)/T(2,2)                                              PGM10276
      PRINT199,CTH,CTP,CTSH,CTSP,CTSCTH,CTSCTP                          PGM10277
  199 FORMAT('0','CTH=',D10.3,2X,'CTP=',D10.3,2X,'CTSH=',D10.3,2X,      PGM10278
     &       'CTSP=',D10.3,2X,'CTSCTH=',F10.3,2X,'CTSCTP=',F10.3)       PGM10279
      ETAH=1.D0-Z(1,1)/P(1,1)                                           PGM10280
      ETAP=1.D0-Z(2,2)/P(2,2)                                           PGM10281
      PRINT177,ETAH,ETAP                                                PGM10282
  177 FORMAT('0','ETAH=',F10.3,2X,'ETAP=',F10.3)                        PGM10283
C                                                                       PGM10284
C     DETERMINATION OF THE OPTIMUM MOTION                               PGM10285
C                                                                       PGM10286
C     COEF'S OF SECULAR EQ                                              PGM10287
C     A(1)*Z**3+A(2)*Z**2+A(3)*Z+A(4)=0                                 PGM10288
```

```
C                                                                       PGM10289
      A(1)=-P(1,1)*P(2,2)*P(3,3)-2.D0*P(1,2)*P(1,3)*P(2,3)+P(1,1)*      PGM10290
     &    P(2,3)*P(2,3)+P(1,3)*P(1,3)*P(2,2)+P(1,2)*P(1,2)*P(3,3)       PGM10291
      A(2)=P(1,1)*P(2,2)*E(3,3)+E(1,1)*P(2,2)*P(3,3)+P(1,1)*E(2,2)*     PGM10292
     &    P(3,3)+2.D0*P(1,2)*P(1,3)*E(2,3)+2.D0*P(1,2)*E(1,3)*P(2,3)+   PGM10293
     &    2.D0*E(1,2)*P(1,3)*P(2,3)-E(1,1)*P(2,3)*P(2,3)-2.D0*P(1,1)*   PGM10294
     &    E(2,3)*P(2,3)-P(1,3)*P(1,3)*E(2,2)-2.D0*E(1,3)*P(1,3)*P(2,2)  PGM10295
     &    -P(1,2)*P(1,2)*E(3,3)-2.D0*E(1,2)*P(1,2)*P(3,3)               PGM10296
      A(3)=-E(1,1)*E(2,2)*P(3,3)-E(1,1)*P(2,2)*E(3,3)-P(1,1)*E(2,2)*    PGM10297
     &    E(3,3)-2.D0*P(1,2)*E(1,3)*E(2,3)-2.D0*E(1,2)*P(1,3)*E(2,3)-   PGM10298
     &    2.D0*E(1,2)*E(1,3)*P(2,3)+P(1,1)*E(2,3)*E(2,3)+2.D0*E(1,1)*   PGM10299
     &    E(2,3)*P(2,3)+E(1,3)*E(1,3)*P(2,2)+2.D0*E(1,3)*P(1,3)*E(2,2)  PGM10300
     &    +E(1,2)*E(1,2)*P(3,3)+2.D0*E(1,2)*P(1,2)*E(3,3)               PGM10301
      A(4)=E(1,1)*E(2,2)*E(3,3)+2.D0*E(1,2)*E(1,3)*E(2,3)-E(1,1)*E(2,3)* PGM10302
     &    E(2,3)-E(2,2)*E(1,3)*E(1,3)-E(1,2)*E(1,2)*E(3,3)              PGM10303
C                                                                       PGM10304
C     DETERMINATION OF THE ROOTS OF THE SECULAR EQ. AND THE SOLUTION FOR PGM10305
C     EACH ROOT                                                         PGM10306
C                                                                       PGM10307
      J1=1                                                              PGM10308
      CALL REGOTS(A,BZ,NRR)                                             PGM10309
      DO 444 I=1,NRR                                                    PGM10310
      LAM(I)=BZ(I)                                                      PGM10311
      DENOM(I)=(E(1,2)-LAM(I)*P(1,2))*(E(2,3)-LAM(I)*P(2,3))-           PGM10312
     &         (E(1,3)-LAM(I)*P(1,3))*(E(2,2)-LAM(I)*P(2,2))            PGM10313
      PSI10(I)=((E(1,2)-LAM(I)*P(1,2))*(E(1,3)-LAM(I)*P(1,3))           PGM10314
     &        -(E(2,3)-LAM(I)*P(2,3))*(E(1,1)-LAM(I)*P(1,1)))/DENOM(I)  PGM10315
      PSI20(I)=((E(2,2)-LAM(I)*P(2,2))*(E(1,1)-LAM(I)*P(1,1))           PGM10316
     &        -(E(1,2)-LAM(I)*P(1,2))*(E(1,2)-LAM(I)*P(1,2)))/DENOM(I)  PGM10317
      XX1(I)=PSI10(I)*PSI10(I)                                          PGM10318
      XX2(I)=PSI20(I)*PSI20(I)                                          PGM10319
      XX3(I)=PSI10(I)*PSI20(I)                                          PGM10320
      CTOB(I)=T(1,1)+T(2,2)*XX1(I)+T(3,3)*XX2(I)+2.D0*T(1,2)*PSI10(I)+  PGM10321
     &        2.D0*T(1,3)*PSI20(I)+2.D0*T(2,3)*XX3(I)                   PGM10322
      PRINT1,I,PSI10(I),PSI20(I),CTOB(I)                                PGM10323
    1 FORMAT('0','I=',I1,1X,'PSI10(I)=',D10.4,2X,'PSI20(I)=',D10.4,2X,  PGM10324
     &    'CTOB(I)=',D10.4)                                             PGM10325
      IF(CTOB(I))  112,113,113                                          PGM10326
  113 ETA(I)=1.D0-((E(1,1)+E(2,2)*XX1(I)+E(3,3)*XX2(I)+2.D0*E(1,2)*     PGM10327
     &        PSI10(I)+2.D0*E(1,3)*PSI20(I)+2.D0*E(2,3)*XX3(I))/(P(1,1)+ PGM10328
     &        P(2,2)*XX1(I)+P(3,3)*XX2(I)+2.D0*P(1,2)*PSI10(I)+2.D0*     PGM10329
     &        P(1,3)*PSI20(I)+2.D0*P(2,3)*XX3(I)))                       PGM10330
      ZP(I)=DSQRT(XX1(I)+XX2(I))                                        PGM10331
      ALPHP(I)=DATAN2(PSI20(I),PSI10(I))                                PGM10332
      IF(ALPHP(I))  217,218,218                                         PGM10333
  217 ALPHP(I)=2.D0*PI+ALPHP(I)                                         PGM10334
  218 ALPHP(I)=180.D0*ALPHP(I)/PI                                       PGM10335
      CISCT(I)=(K(1,1)+K(2,2)*XX1(I)+K(3,3)*XX2(I)+2.D0*K(1,2)*PSI10(I)+ PGM10336
     &        2.D0*K(1,3)*PSI20(I)+2.D0*K(2,3)*XX3(I))/CTOB(I)          PGM10337
      GO TO (110,220,330),J1                                            PGM10338
  110 LAM1=LAM(I)                                                       PGM10339
      CTOB1=CTOB(I)                                                     PGM10340
      ETA1=ETA(I)                                                       PGM10341
      ZP1=ZP(I)                                                         PGM10342
      ALPHP1=ALPHP(I)                                                   PGM10343
      CTSCT1=CTSCT(I)                                                   PGM10344
      J1=J1+1                                                           PGM10345
      GO TO 444                                                         PGM10346
  220 LAM2=LAM(I)                                                       PGM10347
      CTOB2=CTOB(I)                                                     PGM10348
      ETA2=ETA(I)                                                       PGM10349
      ZP2=ZP(I)                                                         PGM10350
      ALPHP2=ALPHP(I)                                                   PGM10351
      CTSCT2=CTSCT(I)                                                   PGM10352
      J1=J1+1                                                           PGM10353
      GO TO 444                                                         PGM10354
  330 LAM3=LAM(I)                                                       PGM10355
      CTOB3=CTOB(I)                                                     PGM10356
      ETA3=ETA(I)                                                       PGM10357
      ZP3=ZP(I)                                                         PGM10358
      ALPHP3=ALPHP(I)                                                   PGM10359
      CTSCT3=CTSCT(I)                                                   PGM10360.
```

```
      J1=J1+1                                                          PGM10361
      GO TO 444                                                        PGM10362
  112 PRINT114,NEL,I                                                   PGM10363
  114 FORMAT('0','NO OPT. FOR THIS LAMBDA, CTOBAR IS NEG.',2X,'NEL=',I1,PGM10364
     &   2X,'I=',I1)                                                   PGM10365
  444 CONTINUE                                                         PGM10366
C                                                                      PGM10367
C     PICK OUT THE OPT. SOLUTION                                       PGM10368
C                                                                      PGM10369
      J2=J1-1                                                          PGM10370
      IF(J2.EQ.0) GO TO 666                                            PGM10371
      GO TO (109,219,329),J2                                           PGM10372
  109 BLAM=LAM1                                                        PGM10373
      BCTOB=CTOB1                                                      PGM10374
      BETA=ETA1                                                        PGM10375
      BZP=ZP1                                                          PGM10376
      BALPHP=ALPHP1                                                    PGM10377
      BCTSCT=CTSCT1                                                    PGM10378
      GO TO 555                                                        PGM10379
  219 IF(ETA1-ETA2) 208,208,109                                        PGM10380
  208 BLAM=LAM2                                                        PGM10381
      BCTOB=CTOB2                                                      PGM10382
      BETA=ETA2                                                        PGM10383
      BZP=ZP2                                                          PGM10384
      BALPHP=ALPHP2                                                    PGM10385
      BCTSCT=CTSCT2                                                    PGM10386
      GO TO 555                                                        PGM10387
  329 IF(ETA1-ETA2) 408,408,409                                        PGM10388
  408 IF(ETA2-ETA3) 407,407,208                                        PGM10389
  407 BLAM=LAM3                                                        PGM10390
      BCTOB=CTOB3                                                      PGM10391
      BETA=ETA3                                                        PGM10392
      BZP=ZP3                                                          PGM10393
      BALPHP=ALPHP3                                                    PGM10394
      BCTSCT=CTSCT3                                                    PGM10395
      GO TO 555                                                        PGM10396
```

```
  409 IF(ETA1-ETA3) 407,407,109                                        PGM10397
  555 PRINT511                                                         PGM10398
  511 FORMAT('0','THE OPTIMUM SOLUTION IS:')                           PGM10399
      PRINT210,BLAM,BCTOB,BETA                                         PGM10400
  210 FORMAT('0','LAM=',D10.3,2X,'CTOB=',D10.3,2X,'ETA=',F10.3)        PGM10401
      PRINT211,BZP,BALPHP,BCTSCT                                       PGM10402
  211 FORMAT('0','ZP=',D10.3,2X,'ALPHP=',F10.3,2X,'CTSCT=',F10.3)      PGM10403
C                                                                      PGM10404
C     OPTIMUM IN LIGHTHILL'S NOTATION                                  PGM10405
C                                                                      PGM10406
      BALPHP=PI*BALPHP/180.D0                                          PGM10407
      PAXIS=(-.5D0*DCOS(BALPHP))/BZP                                   PGM10408
      PFP=-2.D0*BZP/(SIGMA0*DSIN(BALPHP))                              PGM10409
      PRINT2,PFP,PAXIS                                                 PGM10410
    2 FORMAT('0','OPT IN LIGHTHILL NOTATION:  PROPORTIONAL-FEATHERING PA PGM10411
     &RAMETER=',D10.3,1X,'PITCH AXIS PER SEMI ROOT CHORD=',D10.3)      PGM10412
C                                                                      PGM10413
C     PROPULSIVE PERFORMANCE OF A FINITE WING IN COMBINED PITCH AND    PGM10414
C     HEAVE IN LIGHTHILL'S NOTATION, PITCH AXIS LOCATED AT 3/4 CHORD.  PGM10415
C                                                                      PGM10416
      PRINT4                                                           PGM10417
    4 FORMAT('0','A FAMILY OF SOLUTIONS IN LIGHTHILL'S NOTATION')      PGM10418
      PAXIS=.5D0                                                       PGM10419
      PFP=.2D0                                                         PGM10420
    5 DDD=1.D0/(SIGMA0*SIGMA0*PFP*PFP)                                 PGM10421
      PAXIS2=PAXIS*PAXIS                                               PGM10422
      DD=PAXIS2+DDD                                                    PGM10423
      CPSI10=-.5D0*PAXIS/DD                                            PGM10424
      CPSI20=-.5D0/(DD*SIGMA0*PFP)                                     PGM10425
      CXX1=CPSI10*CPSI10                                               PGM10426
      CXX2=CPSI20*CPSI20                                               PGM10427
      CXX3=CPSI10*CPSI20                                               PGM10428
      CETA=1.D0-((E(1,1)+E(2,2)*CXX1+E(3,3)*CXX2+2.D0*E(1,2)*CPSI10+2.D0 PGM10429
     &   *E(1,3)*CPSI20+2.D0*E(2,3)*CXX3)/(P(1,1)+P(2,2)*CXX1+P(3,3)*  PGM10430
     &   CXX2+2.D0*P(1,2)*CPSI10+2.D0*P(1,3)*CPSI20+2.D0*P(2,3)*CXX3)) PGM10431
      CCTOB=T(1,1)+T(2,2)*CXX1+T(3,3)*CXX2+2.D0*T(1,2)*CPSI10+2.D0*    PGM10432
```

```
     &    T(1,3)*CPSI20+2.D0*T(2,3)*CXX3                                    PGM10433
      CCTSCT=(K(1,1)+K(2,2)*CXX1+K(3,3)*CXX2+2.D0*K(1,2)*CPSI10+2.D0*       PGM10434
     &    K(1,3)*CPSI20+2.D0*K(2,3)*CXX3)/CCT08                             PGM10435
      CT2=4.D0*PI*CCT08                                                     PGM10436
      PRINT9,PAXIS, PFP, CETA, CT2,CCTSCT,CPSI10,CPSI20                     PGM10437
    9 FORMAT('0','PAXIS=',D10.3,1X,'PFP=',D10.3,1X,'ETA=',D10.3,1X,        PGM10438
     &    'CT2=',D10.3,1X,'CTSCT=',D11.3,1X,'PSI10=',D10.3,1X,'PSI20=',     PGM10439
     &    D10.3)                                                            PGM10440
      IF(PFP.GT..995D0) GO TO 666                                           PGM10441
      IF(PFP.GT..95D0) GO TO 7                                              PGM10442
      IF(PFP.GT..7D0) GO TO 6                                               PGM10443
      PFP=PFP+.2D0                                                          PGM10444
      GO TO 5                                                               PGM10445
    6 PFP=PFP+.06D0                                                         PGM10446
      GO TO 5                                                               PGM10447
    7 PFP=PFP+.01D0                                                         PGM10448
      GO TO 5                                                               PGM10449
  666 IF(END.NE.1) GO TO 88                                                 PGM10450
      STOP                                                                  PGM10451
      END                                                                   PGM10452
```

```
      SUBROUTINE DNWASH(S,V0P,V0DP,V1P,V1DP,V2P,V2DP)                       ULLT0001
C                                                                           ULLT0002
C     CALCULATION OF UNSTEADY INDUCED DOWNWASH OF UNSTEADY LIFTING-LINE     ULLT0003
C     THEORY                                                                ULLT0004
C                                                                           ULLT0005
      REAL*8 S,V0P,V0DP,V1P,V1DP,V2P,V2DP,SIGMA0,EPSLN,GAMMA,PISQR,TERM1     ULLT0006
     &    ,TERM2,TERM3,CONST,FN2,L1,VEL,FN3,PI,FN5,CC0,SIGMA,EN,T           ULLT0007
      INTEGER AR                                                            ULLT0008
      COMMON/AREA2/SIGMA,CC0,JJ/AREA3/GAMMA,EN/AREA4/SIGMA0,PI,NN,AR        ULLT0009
      CC0=(1.D0-S*S)**(NN/2.D0)                                             ULLT0010
      SIGMA=SIGMA0*CC0                                                      ULLT0011
      T=DACOS(S)                                                            ULLT0012
      DO 9 JJ=1,6                                                           ULLT0013
C                                                                           ULLT0014
C     FOR PURE HEAVE, TO SAVE COMPUTATION TIME, REPLACE DO 9 JJ=1,6 BY      ULLT0015
C                                                                           ULLT0016
      V1P=0.D0                                                              ULLT0017
      V1DP=0.D0                                                             ULLT0018
      V2P=0.D0                                                              ULLT0019
      V2DP=0.D0                                                             ULLT0020
      DO 9 JJ=1,2                                                           ULLT0021
C                                                                           ULLT0022
C     FOR PURE PITCH, TO SAVE COMUTATION TIME, REPLACE DO 9 JJ=1,6 BY       ULLT0023
C                                                                           ULLT0024
      V0P=0.D0                                                              ULLT0025
      V0DP=0.D0                                                             ULLT0026
      V2P=0.D0                                                              ULLT0027
      V2DP=0.D0                                                             ULLT0028
      DO 9 JJ=3,4                                                           ULLT0029
C                                                                           ULLT0030
      TERM1=-EN*FN2(T)/(4.D0*AR)                                            ULLT0031
      TERM3=-SIGMA0*FN3(T,EPSLN)/4.D0                                       ULLT0032
      TERM2=.5D0*SIGMA0*FN5(T,EPSLN)                                        ULLT0033
      VEL=TERM1+TERM2+TERM3                                                 ULLT0034
      GO TO (1,2,3,4,5,6),JJ                                                ULLT0035
    1 V0P=VEL                                                               ULLT0036
```

```
      GO TO 9                                                          ULLT0037
    2 V0DP=VEL                                                         ULLT0038
      GO TO 9                                                          ULLT0039
    3 V1P=VEL                                                          ULLT0040
      GO TO 9                                                          ULLT0041
    4 V1DP=VEL                                                         ULLT0042
      GO TO 9                                                          ULLT0043
    5 V2P=VEL                                                          ULLT0044
      GO TO 9                                                          ULLT0045
    6 V2DP=VEL                                                         ULLT0046
    9 CONTINUE                                                         ULLT0047
      RETURN                                                           ULLT0048
      END                                                              ULLT0049
```

```
      DOUBLE PRECISION FUNCTION FN2(T)                                 ULLT0001
C                                                                      ULLT0002
C     NUMERICAL INTEGRATION OF THE INTEGRAL WITH SECOND-ORDER SPAN     ULLT0003
C     SINGULARITY W.R.T. SPANWISE ANGULAR VARIABLE T.                  ULLT0004
C     ZETA DENOTES THE SIZE OF THE REGION NEAR THE SINGULARITY         ULLT0005
C                                                                      ULLT0006
      REAL*8 S,EPSLN,ZETA,DELTA,LG2,INTEG1,INTEG2,INTEG3,FN1,X1,A1,A2, ULLT0007
     &   DELA,SUM,T,PI,DELX                                            ULLT0008
      PI=3.14159265358979D0                                            ULLT0009
      EPSLN=PI/200.D0                                                  ULLT0010
      ZETA=(PI/20.D0)*.5D0                                             ULLT0011
C                                                                      ULLT0012
C     IS T NEAR THE WING TIPS OR AWAY FROM THE TIPS                    ULLT0013
C                                                                      ULLT0014
      IF(T-ZETA)11,11,13                                               ULLT0015
   13 IF(T-ZETA.LE.EPSLN)GO TO 11                                      ULLT0016
      IF(PI-T-ZETA)10,10,16                                            ULLT0017
   16 IF(PI-T-ZETA.LE.EPSLN) GO TO 10                                  ULLT0018
C                                                                      ULLT0019
C     FOR T NOT NEAR 0 OR PI (AWAY FROM WING TIPS)                     ULLT0020
C                                                                      ULLT0021
      DELTA=ZETA/3.D0                                                  ULLT0022
      X1=T-ZETA                                                        ULLT0023
      IF(DABS(X1).LE.PI/3.D0) GO TO 500                                ULLT0024
      INTEG1=LG2(0.D0,.5D0*X1,T,N11)+LG2(.5D0*X1,X1,T,N12)             ULLT0025
      GO TO 501                                                        ULLT0026
  500 INTEG1=LG2(0.D0,X1,T,N11)                                        ULLT0027
      N12=0                                                            ULLT0028
  501 CONTINUE                                                         ULLT0029
      X1=T+ZETA                                                        ULLT0030
      DELX=(PI-X1)*.5D0                                                ULLT0031
      IF(DABS(PI-X1).LE.PI/3.D0) GO TO 502                             ULLT0032
      INTEG2=LG2(X1,X1+DELX,T,N22)+LG2(X1+DELX,PI,T,N21)               ULLT0033
      GO TO 503                                                        ULLT0034
  502 INTEG2=LG2(X1,PI,T,N21)                                          ULLT0035
      N22=0                                                            ULLT0036
```

```
  503 CONTINUE                                                          ULLT0037
      INTEG3=(1.D0/(300.D0*DELTA))*(13.D0*FN1(T,T-3.D0*DELTA)+72.D0*FN1 ULLT0038
     &    (T,T-2.D0*DELTA)+495.D0*FN1(T,T-DELTA)-1360.D0*FN1(T,T)+495.D0 ULLT0039
     &    *FN1(T,T+DELTA)+72.D0*FN1(T,T+2.D0*DELTA)+13.D0*FN1(T,T+3.D0*  ULLT0040
     &    DELTA))                                                        ULLT0041
      FN2=INTEG1+INTEG2+INTEG3                                          ULLT0042
      RETURN                                                            ULLT0043
C                                                                       ULLT0044
C     FOR T NEAR PI (NEAR ONE WING TIP)                                 ULLT0045
C                                                                       ULLT0046
   10 INTEG2=0.D0                                                       ULLT0047
      ZETA=PI-T                                                         ULLT0048
      DELTA =ZETA /3.D0                                                 ULLT0049
      INTEG3=(1.D0/(300.D0*DELTA))*(13.D0*FN1(T,T-3.D0*DELTA)+72.D0*FN1 ULLT0050
     &    (T,T-2.D0*DELTA)+495.D0*FN1(T,T-DELTA)-1360.D0*FN1(T,T)+495.D0 ULLT0051
     &    *FN1(T,T+DELTA)+72.D0*FN1(T,T+2.D0*DELTA)+13.D0*FN1(T,T+3.D0*  ULLT0052
     &    DELTA))                                                        ULLT0053
      X1=T-ZETA                                                         ULLT0054
      INTEG1=LG2(0.D0,X1-PI/20.D0,T,N1)                                 ULLT0055
     &      +LG2(X1-PI/20.D0,X1-PI/200.D0,T,N11)+                       ULLT0056
     &       LG2(X1-PI/200.D0,X1,T,N12)                                 ULLT0057
      FN2=INTEG1+INTEG2+INTEG3                                          ULLT0058
      RETURN                                                            ULLT0059
C                                                                       ULLT0060
C     FOR T NEAR 0 (NEAR THE OTHER WING TIP)                            ULLT0061
C                                                                       ULLT0062
   11 INTEG1=0.D0                                                       ULLT0063
      ZETA=T                                                            ULLT0064
      DELTA =ZETA /3.D0                                                 ULLT0065
      INTEG3=(1.D0/(300.D0*DELTA))*(13.D0*FN1(T,T-3.D0*DELTA)+72.D0*FN1 ULLT0066
     &    (T,T-2.D0*DELTA)+495.D0*FN1(T,T-DELTA)-1360.D0*FN1(T,T)+495.D0 ULLT0067
     &    *FN1(T,T+DELTA)+72.D0*FN1(T,T+2.D0*DELTA)+13.D0*FN1(T,T+3.D0*  ULLT0068
     &    DELTA))                                                        ULLT0069
      X1=T+ZETA                                                         ULLT0070
      INTEG2=LG2(X1,X1+PI/200.D0,T,N22)+                                ULLT0071
     &       LG2(X1+PI/200.D0,X1+PI/20.D0,T,N21)+                       ULLT0072
     &       LG2(X1+PI/20.D0,PI,T,N2)                                   ULLT0073
      FN2=INTEG1+INTEG2+INTEG3                                          ULLT0074
      RETURN                                                            ULLT0075
      END                                                               ULLT0076
```

```
      DOUBLE PRECISION FUNCTION LG2(A ,B ,T ,N)                          ULLT0001
C                                                                        ULLT0002
C     LEGENDRE-GAUSS QUADRATURE, USED IN CALCULATING FN2(T) ONLY         ULLT0003
C     TRANSFORMS INTERVAL OF INTEGRATION FROM (A,B) TO (-1,1)            ULLT0004
C                                                                        ULLT0005
      REAL*8 AP,BP,A,B,AA,BB,SUM,THETA,S,FN4,LG2P,XI(24,24),WT(24,24)    ULLT0006
     &    ,S1,FN1,SIGMA0,PI,CC0,SIGMA,T,T1                               ULLT0007
      COMMON/AREA1/XI,WT/AREA2/SIGMA,CC0,JJ/AREA4/SIGMA0,PI,NN,AR        ULLT0008
      INTEGER AR                                                         ULLT0009
      FN4(T,T1)=FN1(T,T1)/((T-T1)*(T-T1))                                ULLT0010
      S=DCOS(T)                                                          ULLT0011
      AA=(B-A)/2.D0                                                      ULLT0012
      BB=(B+A)/2.D0                                                      ULLT0013
      LG2P=100.D0                                                        ULLT0014
C                                                                        ULLT0015
C     ITERATE ON N UNTIL DESIRED CONVERGENCE IS ACHIEVED                 ULLT0016
C                                                                        ULLT0017
      DO 11 N=4,24,4                                                     ULLT0018
      SUM=0.D0                                                           ULLT0019
      DO 10 I=1,N                                                        ULLT0020
      T1   =AA*XI(I,N)+BB                                                ULLT0021
   10 SUM=SUM+FN4(T,T1)*WT(I,N)                                          ULLT0022
      LG2=AA*SUM                                                         ULLT0023
      IF(DABS(LG2-LG2P).LE.1.D-5) RETURN                                 ULLT0024
      IF(N.EQ.24) GO TO 13                                               ULLT0025
   11 LG2P=LG2                                                           ULLT0026
   13 PRINT400                                                           ULLT0027
  400 FORMAT('0','ACCURACY OF 1.D-5 NOT ACHIEVED IN LG2')                ULLT0028
      PRINT100,A ,B ,N,LG2P,LG2,S,JJ                                     ULLT0029
  100 FORMAT('0','A =',F8.4,2X,'B =',F8.4,2X,'N=',I6,2X,'LG2P=',F18.8,   ULLT0030
     &    2X,'LG2=',F18.8,2X,'S =',F18.8,2X,'JJ=',I4)                    ULLT0031
      RETURN                                                             ULLT0032
      END                                                                ULLT0033
```

```
      DOUBLE PRECISION FUNCTION FN1(T,T1)                                ULLT0001
C                                                                        ULLT0002
C     EVALUATION OF INTEGRAND OF INTEGRAL WITH SECOND-ORDER SPAN         ULLT0003
C     SINGULARITY WITH COS SUBSTITUTION. IT CONSISTS OF STRIP-THEORY CL  ULLT0004
C     AND KERNEL FUNCTION OF UNSTEADY INDUCED DOWNWASH. MOD IS FACTOR    ULLT0005
C     INTRODUCED BY COS SUBSTITUTION,NAMELY S1(T,T1)                     ULLT0006
C                                                                        ULLT0007
      REAL*8 S,S1,C1,SIGMA1,SIGMA0,ETA,F1,G1,D1,B1,PIP,PIDP,SR1,SI1,PI,  ULLT0008
     &    CC0,SIGMA,C1C0,GAMMA,EN,T,T1,DEN,MOD                           ULLT0009
      INTEGER AR                                                         ULLT0010
      COMMON/AREA2/SIGMA,CC0,JJ/AREA3/GAMMA,EN/AREA4/SIGMA0,PI,NN,AR     ULLT0011
      S=DCOS(T)                                                          ULLT0012
      S1=DCOS(T1)                                                        ULLT0013
      C1C0=(1.D0-S1*S1)**(NN/2.D0)                                       ULLT0014
      SIGMA1=SIGMA0*C1C0                                                 ULLT0015
      CALL STHEOD(SIGMA1,F1,G1,D1,B1,SR1,SI1)                            ULLT0016
C                                                                        ULLT0017
C     ARGUMENT OF KERNEL FUNCTION OF UNSTEADY INDUCED DOWNWASH           ULLT0018
C                                                                        ULLT0019
      ETA=AR*SIGMA0*DABS(S-S1)/EN                                        ULLT0020
      CALL KER(ETA,PIP,PIDP)                                             ULLT0021
C                                                                        ULLT0022
C     CALCULATION OF MOD, S1 IS AT ONE WING TIP                          ULLT0023
C                                                                        ULLT0024
      IF(DABS(T1).LT.1.D-5) GO TO 18                                     ULLT0025
      IF(DABS(PI-T1).LT.1.D-5) GO TO 18                                  ULLT0026
C                                                                        ULLT0027
C     CALCULATION OF MOD, S1 IS AT THE SINGULARITY AT S                  ULLT0028
C                                                                        ULLT0029
      IF(DABS(T-T1).LT.1.D-5) GO TO 19                                   ULLT0030
C                                                                        ULLT0031
C     CALCULATION OF MOD FOR ALL OTHER VALUES OF S1                      ULLT0032
C                                                                        ULLT0033
      DEN=((T-T1)/(DCOS(T)-DCOS(T1)))*((T-T1)/(DCOS(T)-DCOS(T1)))        ULLT0034
      MOD=DEN*DSIN(T1)                                                   ULLT0035
      GO TO 20                                                           ULLT0036
```

```
   18 MOD=0.D0                                                          ULLT0037
      GO TO 20                                                          ULLT0038
   19 MOD=1.D0/DSIN(T1)                                                 ULLT0039
   20 CONTINUE                                                          ULLT0040
      GO TO (1,2,3,4,5,6),JJ                                            ULLT0041
    1 FN1=-(SIGMA0*(G1+.5D0*SIGMA1)*PIP+SIGMA0*F1*PIDP)*C1C0*MOD        ULLT0042
      RETURN                                                            ULLT0043
    2 FN1=(SIGMA0*F1*PIP-SIGMA0*(G1+.5D0*SIGMA1)*PIDP)*C1C0*MOD         ULLT0044
      RETURN                                                            ULLT0045
    3 FN1=((2.D0*F1-SIGMA1*G1)*PIP-(2.D0*G1+SIGMA1*(1.D0+F1))*PIDP)*C1C0 ULLT0046
     &   *MOD                                                           ULLT0047
      RETURN                                                            ULLT0048
    4 FN1=((2.D0*G1+SIGMA1*(1.D0+F1))*PIP+(2.D0*F1-SIGMA1*G1)*PIDP)*C1C0 ULLT0049
     &   *MOD                                                           ULLT0050
      RETURN                                                            ULLT0051
    5 FN1=-((2.D0*G1+SIGMA1*(1.D0+F1))*PIP+(2.D0*F1-SIGMA1*G1)*PIDP)*   ULLT0052
     &   C1C0*MOD                                                       ULLT0053
      RETURN                                                            ULLT0054
    6 FN1=((2.D0*F1-SIGMA1*G1)*PIP-(2.D0*G1+SIGMA1*(1.D0+F1))*PIDP)*C1C0 ULLT0055
     &   *MOD                                                           ULLT0056
      RETURN                                                            ULLT0057
      END                                                               ULLT0058
```

```
      DOUBLE PRECISION FUNCTION FN3(T,EPSLN)                            ULLT0001
C                                                                       ULLT0002
C     NUMERICAL INTEGRATION OF NONSINGULAR PARTS OF  THE INTEGRAL WITH  ULLT0003
C     (REMOVABLE) ABS(S-S1) SINGULARITY W.R.T. SPANWISE ANGULAR         ULLT0004
C     VARIABLE T. EPSLN DENOTES THE SIZE OF THE REGION NEAR THE SING.   ULLT0005
C                                                                       ULLT0006
      REAL*8 S,INTEG1,INTEG2,LG3,EPSLN,X1,X2,T,PI                       ULLT0007
      PI=3.1415926535897D0                                              ULLT0008
      EPSLN=(PI/400.D0)*.75D0                                           ULLT0009
C                                                                       ULLT0010
C     IS T NEAR THE WING TIPS OR AWAY FROM THE TIPS                     ULLT0011
C                                                                       ULLT0012
      IF(T-EPSLN) 310,310,313                                           ULLT0013
  313 IF(T-EPSLN.LE.PI/2000.D0) GO TO 310                               ULLT0014
      IF(PI-T-EPSLN) 311,311,316                                        ULLT0015
  316 IF(PI-T-EPSLN.LE.PI/2000.D0) GO TO 311                            ULLT0016
C                                                                       ULLT0017
C     T NOT NEAR 0 OR PI (AWAY FROM THE WING TIPS)                      ULLT0018
C                                                                       ULLT0019
      X1=T-EPSLN                                                        ULLT0020
      X2=T+EPSLN                                                        ULLT0021
      IF(X1-12.D0*PI/200.D0.GT.0.D0) GO TO 401                          ULLT0022
      INTEG1=LG3(0.D0,X1,T,N11)                                         ULLT0023
      N12=0                                                             ULLT0024
      GO TO 402                                                         ULLT0025
  401 INTEG1=LG3(0.D0,X1-PI/20.D0,T,N11)+LG3(X1-PI/20.D0,X1,T,N12)      ULLT0026
  402 IF(X2+12.D0*PI/200.D0.LT.PI) GO TO 403                            ULLT0027
      INTEG2=LG3(X2,PI,T,N21)                                           ULLT0028
      N22=0                                                             ULLT0029
      GO TO 778                                                         ULLT0030
  403 INTEG2=LG3(X2,X2+PI/20.D0,T,N22)+LG3(X2+PI/20.D0,PI,T,N21)        ULLT0031
  778 FN3=INTEG1+INTEG2                                                 ULLT0032
      RETURN                                                            ULLT0033
C                                                                       ULLT0034
C     T NEAR 0 (NEAR ONE WING TIP)                                      ULLT0035
C                                                                       ULLT0036
```

```
  310 INTEG1=0.D0                                                       ULLT0037
      EPSLN=T                                                           ULLT0038
      X2=T+EPSLN                                                        ULLT0039
      INTEG2=LG3(X2,X2+PI/200.D0,T,N23)+LG3(X2+PI/200.D0,X2+PI/20.D0,   ULLT0040
     &   T,N22)+LG3(X2+PI/20.D0,PI,T,N21)                               ULLT0041
      FN3=INTEG1+INTEG2                                                 ULLT0042
      RETURN                                                            ULLT0043
C                                                                       ULLT0044
C     T NEAR PI (NEAR THE OTHER WING TIP)                               ULLT0045
C                                                                       ULLT0046
  311 INTEG2=0.D0                                                       ULLT0047
      EPSLN=PI-T                                                        ULLT0048
      X1=T-EPSLN                                                        ULLT0049
      INTEG1=LG3(0.D0,X1-PI/20.D0,T,N11)+LG3(X1-PI/20.D0,X1-PI/200.D0,  ULLT0050
     &   T,N12)+LG3(X1-PI/200.D0,X1,T,N13)                              ULLT0051
      FN3=INTEG1+INTEG2                                                 ULLT0052
      RETURN                                                            ULLT0053
      END                                                               ULLT0054
```

```
      DOUBLE PRECISION FUNCTION LG3(A ,B ,T,N)                          ULLT0001
C                                                                       ULLT0002
C     LEGENDRE-GAUSS QUADRATURE, USED IN CALCULATING FN3(T,EPSLN) ONLY  ULLT0003
C     TRANSFORMS INTERVAL OF INTEGRATION FROM (A,B) TO (-1,1)           ULLT0004
C                                                                       ULLT0005
      COMMON/AREA1/XI,WT/AREA2/SIGMA,CC0,JJ/AREA4/SIGMA0,PI,NN,AB       ULLT0006
      REAL*8 AP,BP,A,B,AA,BB,SUM,THETA,S,L2P ,LG3P,XI(24,24),WT(24,24)  ULLT0007
     &   ,L2,S1,SIGMA0,PI,CC0,SIGMA,T,T1                                ULLT0008
      INTEGER AB                                                        ULLT0009
      L2P(T,T1)=L2(T,T1)/DABS(T-T1)                                     ULLT0010
      S=DCOS(T)                                                         ULLT0011
      AA=(B-A)*.5D0                                                     ULLT0012
      BB=(B+A)*.5D0                                                     ULLT0013
      LG3P=100.D0                                                       ULLT0014
C                                                                       ULLT0015
C     ITERATE ON N UNTIL DESIRED CONVERGENCE IS ACHIEVED                ULLT0016
C                                                                       ULLT0017
      DO 11 N=4,24,4                                                    ULLT0018
      SUM=0.D0                                                          ULLT0019
      DO 10 I=1,N                                                       ULLT0020
      T1   =AA*XI(I,N)+BB                                               ULLT0021
   10 SUM=SUM+L2P(T,T1)            *WT(I,N)                             ULLT0022
      LG3=AA*SUM                                                        ULLT0023
      IF(DABS(LG3-LG3P).LE.1.D-5) RETURN                                ULLT0024
      IF(N.EQ.24) GO TO 13                                              ULLT0025
   11 LG3P=LG3                                                          ULLT0026
   13 PRINT400                                                          ULLT0027
  400 FORMAT('0','ACCURACY OF 1.D-5 NOT ACHIEVED IN LG3')               ULLT0028
      PRINT100,A,B,N,LG3P,LG3,S,JJ                                      ULLT0029
  100 FORMAT('0','A =',F8.4,2X,'B =',F8.4,2X,'N=',I6,2X,'LG3P=',F18.8,  ULLT0030
     &   2X,'LG3=',F18.8,2X,'S =',F18.8,2X,'JJ=',I4)                    ULLT0031
      RETURN                                                            ULLT0032
      END                                                               ULLT0033
```

```
      DOUBLE PRECISION FUNCTION L2(T,T1)                                    ULLT0001
C                                                                           ULLT0002
C     SIMP-THEORY SECTION CL TIMES J (SQRT OF -1), USED IN CALCULATING      ULLT0003
C     FNJ(T,EPSLN) CALL. MOD2 IS FACTOR INTRODUCED BY COS SUB., M2(T,T1)    ULLT0004
C                                                                           ULLT0005
      REAL*8 S1,LT,SIGMA0,SIGMA,SIGMA1,CC0,C1C0,PI,F1,G1,D1,B1,SB1,SI1      ULLT0006
     &   ,T,T1,MOD2                                                         ULLT0007
      COMMON/AREA2/SIGMA,CC0,JJ/AREA4/SIGMA0,PI,NN,AP                       ULLT0008
      INTEGER AR                                                            ULLT0009
      S1=DCOS(T1)                                                           ULLT0010
      C1C0=(1.D0-S1*S1)**(NN/2.D0)                                          ULLT0011
      SIGMA1=SIGMA0*C1C0                                                    ULLT0012
      CALL STHEOD(SIGMA1,F1,G1,D1,B1,SB1,SI1)                               ULLT0013
C                                                                           ULLT0014
C     CALCULATION OF MOD2, T1 IS AT ONE WING TIP                            ULLT0015
C                                                                           ULLT0016
      IF(DABS(T1).LT.1.D-5) GO TO 19                                        ULLT0017
      IF(DABS(PI-T1).LT.1.D-5) GO TO 19                                     ULLT0018
C                                                                           ULLT0019
C     CALCULATION OF MOD2, T1 IS ANY OTHER POINT                            ULLT0020
C                                                                           ULLT0021
      MOD2=DABS((T-T1)/(DCOS(T)-DCOS(T1)))*DSIN(T1)                         ULLT0022
      GO TO 20                                                              ULLT0023
   19 MOD2=0.D0                                                             ULLT0024
   20 CONTINUE                                                              ULLT0025
      GO TO (11,12,13,14,15,16),JJ                                          ULLT0026
   11 L2=SIGMA0*F1*C1C0*MOD2                                                ULLT0027
      RETURN                                                                ULLT0028
   12 L2=SIGMA0*(G1+.5D0*SIGMA1)*C1C0*MOD2                                  ULLT0029
      RETURN                                                                ULLT0030
   13 L2=(2.D0*G1+SIGMA1*(1.D0+F1))*C1C0*MOD2.                              ULLT0031
      RETURN                                                                ULLT0032
   14 L2=(SIGMA1*G1-2.D0*F1)*C1C0*MOD2                                      ULLT0033
      RETURN                                                                ULLT0034
   15 L2=(2.D0*F1-SIGMA1*G1)*C1C0*MOD2                                      ULLT0035
      RETURN                                                                ULLT0036
   16 L2=(2.D0*G1+SIGMA1*(1.D0+F1))*C1C0*MOD2                               ULLT0037
      RETURN                                                                ULLT0038
      END                                                                   ULLT0039
```

```
      DOUBLE PRECISION FUNCTION FN5(T,EPSLN)                                ULLT0001
C                                                                           ULLT0002
C     EVALUATION OF TERM2, THE NONINTEGRAL PART OF UNSTEADY INDUCED         ULLT0003
C     DOWNWASH, INCLUDES STEIF-THEORY SECTION CL TIMES J (SQRT OF -1)       ULLT0004
C                                                                           ULLT0005
      REAL*8 SIGMA,SIGMA0,C,S,EPSLN,GAMMA,PI,A1,A2,F,G,D,B,SR,SI,CC0,EN     ULLT0006
     &    ,T,DELTA1,DELTA2                                                  ULLT0007
      INTEGER AR                                                            ULLT0008
      COMMON/AREA2/SIGMA,CC0,JJ/AREA3/GAMMA,EN/AREA4/SIGMA0,PI,NN,AR        ULLT0009
      CALL STHEOD(SIGMA,F,G,D,B,SR,SI)                                      ULLT0010
      S=DCOS(T)                                                             ULLT0011
      DELTA1=S-DCOS(T+EPSLN)                                                ULLT0012
      DELTA2=DCOS(T-EPSLN)-S                                                ULLT0013
      A1=1.D0-GAMMA-DLOG(2.D0*DSQRT(DELTA1*DELTA2)*AR*SIGMA0/EN)            ULLT0014
      A2=-.5D0*PI                                                           ULLT0015
      GO TO (1,2,3,4,5,6),JJ                                                ULLT0016
    1 FN5=  (-A2*SIGMA0*(G+.5D0*SIGMA)+A1*SIGMA0*F)*CC0                     ULLT0017
      RETURN                                                                ULLT0018
    2 FN5=  (A2*SIGMA0*F+A1*SIGMA0*(G+.5D0*SIGMA))*CC0                      ULLT0019
      RETURN                                                                ULLT0020
    3 FN5=  (A2*(2.D0*F-SIGMA*G)+A1*(2.D0*G+SIGMA*(1.D0+F)))*CC0            ULLT0021
      RETURN                                                                ULLT0022
    4 FN5=  (A2*(2.D0*G+SIGMA*(1.D0+F))-A1*(2.D0*F-SIGMA*G))*CC0            ULLT0023
      RETURN                                                                ULLT0024
    5 FN5=  (-A2*(2.D0*G+SIGMA*(1.D0+F))+A1*(2.D0*F-SIGMA*G))*CC0           ULLT0025
      RETURN                                                                ULLT0026
    6 FN5=  (A2*(2.D0*F-SIGMA*G)+A1*(2.D0*G+SIGMA*(1.D0+F)))*CC0            ULLT0027
      RETURN                                                                ULLT0028
      END                                                                   ULLT0029
```

```
      SUBROUTINE STHEOD(SIGMA,F,G,D,B,SR,SI)                                ULLT0001
C                                                                           ULLT0002
C     CALCULATION OF THE REAL AND IMAGINARY PARTS OF THEODORSEN'S FN.       ULLT0003
C     AND THE SEARS FN.                                                     ULLT0004
C                                                                           ULLT0005
      IMPLICIT REAL*8 (A-Z)                                                 ULLT0006
      INTEGER IER,JJ,AR,NN                                                  ULLT0007
      DATA PI/3.141592653589793/                                            ULLT0008
      IER=0                                                                 ULLT0009
      IF(SIGMA.LT.1.D-11)    GO TO 55                                       ULLT0010
      CALL DBJY0 (SIGMA,J0,Y0,IER)                                          ULLT0011
      IF(IER.NE.0) WRITE(6,100) IER                                         ULLT0012
  100 FORMAT(' ERROR IN DBJY0, IER= ',I5)                                   ULLT0013
      CALL DBJY1 (SIGMA,J1,Y1,IER)                                          ULLT0014
      IF(IER.NE.0) WRITE(6,200) IER                                         ULLT0015
  200 FORMAT (' ERROR IN DBJY1, IER= ',I5)                                  ULLT0016
      AA=(J1+Y0)*(J1+Y0)+(J0-Y1)*(J0-Y1)                                    ULLT0017
      BB=J1*J1+Y1*Y1+2.D0/(PI*SIGMA)                                        ULLT0018
      CC=-(J0*J1+Y0*Y1)                                                     ULLT0019
      F=BB/AA                                                               ULLT0020
      G=CC/AA                                                               ULLT0021
      SF=J0*F+J1*G                                                          ULLT0022
      SI=J1+J0*G-J1*F                                                       ULLT0023
      D=F*F+G*G                                                             ULLT0024
      B=F-D                                                                 ULLT0025
      RETURN                                                                ULLT0026
   55 F=1.D0                                                                ULLT0027
      G=0.D0                                                                ULLT0028
      SR=1.D0                                                               ULLT0029
      SI=0.D0                                                               ULLT0030
      D=1.D0                                                                ULLT0031
      B=0.D0                                                                ULLT0032
      RETURN                                                                ULLT0033
      END                                                                   ULLT0034
```

```
      SUBROUTINE KER(ETA,PIP,PIDP)                                      ULLT0001
C                                                                       ULLT0002
C     CALCULATION OF THE KERNEL FN. OF UNSTEADY INDUCED DOWNWASH OF     ULLT0003
C     UNSTEADY LIFTING-LINE THEORY                                      ULLT0004
C                                                                       ULLT0005
      IMPLICIT REAL*8 (A-Z)                                             ULLT0006
      COMMON/AREA2/SIGMA,CC0,JJ/AREA4/SIGMA0,PI,NN,AR                   ULLT0007
      INTEGER IER,JJ,AR,NN                                              ULLT0008
      IER=0                                                             ULLT0009
      IF(ETA.LT.1.D-11) GO TO 65                                        ULLT0010
      CALL DBK1 (ETA,K1,IER)                                            ULLT0011
      IF(IER.NE.0) WRITE(6,100) IER                                     ULLT0012
  100 FORMAT(' ERROR IN DBK1, IER= ',I5)                                ULLT0013
      PIP=ETA*K1                                                        ULLT0014
      B=(PI/4.D0-.8675D0*ETA*((.4648D0+.9159D0*ETA)/(1.3410D0+ETA*      ULLT0015
     &   ETA)))*DEXP(-ETA)                                              ULLT0016
      C=B+(1.0385D0*ETA)/(1.3410D0+1.3050D0*ETA*ETA)                    ULLT0017
      I1L1=((2.D0/PI)*ETA)*C                                            ULLT0018
      PIDP=(PI/2.D0)*ETA*I1L1                                           ULLT0019
      RETURN                                                            ULLT0020
   65 PIP=1.D0                                                          ULLT0021
      PIDP=0.D0                                                         ULLT0022
      RETURN                                                            ULLT0023
      END                                                               ULLT0024
```

```
      SUBROUTINE CL1(S,V0P,V0DP,V1P,V1DP,V2P,V2DP,                      3DCL0001
     &               CL0P,CL0DP,CL1P,CL1DP,CL2P,CL2DP,                  3DCL0002
     &               CLS0P,CLS0DP,CLS1P,CLS1DP,CLS2P,CLS2DP,            3DCL0003
     &               CL00P,CL00DP,CL11P,CL11DP,CL22P,CL22DP)            3DCL0004
C                                                                       3DCL0005
C     UNIVERSAL COEF'S OF STRIP-THEORY AND 3D SECTION CL AND THE 3D     3DCL0006
C     (SEARS) CORRECTION                                                3DCL0007
C                                                                       3DCL0008
      REAL*8       S,V0P,V0DP,V1P,V1DP,V2P,V2DP,                        3DCL0009
     &               CL0P,CL0DP,CL1P,CL1DP,CL2P,CL2DP,                  3DCL0010
     &               CLS0P,CLS0DP,CLS1P,CLS1DP,CLS2P,CLS2DP,            3DCL0011
     &               SIGMA0,SIGMA,C,F,G,D,B,SR,SI,PI,CC0,               3DCL0012
     &               CL00P,CL00DP,CL11P,CL11DP,CL22P,CL22DP             3DCL0013
      INTEGER AR                                                        3DCL0014
      COMMON/AREA4/SIGMA0,PI,NN,AR                                      3DCL0015
      CC0=(1.D0-S*S)**(NN/2.D0)                                         3DCL0016
      SIGMA=SIGMA0*CC0                                                  3DCL0017
      CALL STHEOD (SIGMA,F,G,D,B,SR,SI)                                 3DCL0018
C                                                                       3DCL0019
C     STRIP-THEORY SECTION CL                                           3DCL0020
C                                                                       3DCL0021
      CL0P=PI*SIGMA0*(G+.5D0*SIGMA)*CC0                                 3DCL0022
      CL0DP=-PI*SIGMA0*F*CC0                                            3DCL0023
      CL1P=-PI*(2.D0*F-SIGMA*G)*CC0                                     3DCL0024
      CL1DP=-PI*(2.D0*G+SIGMA*(1.D0+F))*CC0                             3DCL0025
      CL2P=PI*(2.D0*G+SIGMA*(1.D0+F))*CC0                               3DCL0026
      CL2DP=-PI*(2.D0*F-SIGMA*G)*CC0                                    3DCL0027
C                                                                       3DCL0028
C     3D SECTIONAL (SEARS) CORRECTION                                   3DCL0029
C                                                                       3DCL0030
      CLS0P=2.D0*PI*(V0P*SR-V0DP*SI)*CC0                                3DCL0031
      CLS0DP=2.D0*PI*(V0DP*SR+V0P*SI)*CC0                               3DCL0032
      CLS1P=2.D0*PI*(V1P*SR-V1DP*SI)*CC0                                3DCL0033
      CLS1DP=2.D0*PI*(V1DP*SR+V1P*SI)*CC0                               3DCL0034
      CLS2P=2.D0*PI*(V2P*SR-V2DP*SI)*CC0                                3DCL0035
      CLS2DP=2.D0*PI*(V2DP*SR+V2P*SI)*CC0                               3DCL0036
```

```
C                                                                       3DCL0037
C     3D SECTION CL                                                     3DCL0038
C                                                                       3DCL0039
      CL0GP=CL0P+CLS0P                                                  3DCL0040
      CL00DP=CL0DP+CLS0DP                                               3DCL0041
      CL11P=CL1P+CLS1P                                                  3DCL0042
      CL11DP=CL1DP+CLS1DP                                               3DCL0043
      CL22P=CL2P+CLS2P                                                  3DCL0044
      CL22DP=CL2DP+CLS2DP                                               3DCL0045
      RETURN                                                            3DCL0046
      END                                                               3DCL0047
```

```
      SUBROUTINE CM1(S,V0P,V0DP,V1P,V1DP,V2P,V2DP,                      3DCM0001
     &               CM0P,CM0DP,CM1P,CM1DP,CM2P,CM2DP,                  3DCM0002
     &               CMS0P,CMS0DP,CMS1P,CMS1DP,CMS2P,CMS2DP,            3DCM0003
     &               CM00P,CM00DP,CM11P,CM11DP,CM22P,CM22DP)            3DCM0004
C                                                                       3DCM0005
C     UNIVERSAL COEF'S OF STRIP-THEORY AND 3D SECTION CM AND THE 3D     3DCM0006
C     (SEARS) CORRECTION                                                3DCM0007
C                                                                       3DCM0008
      REAL*8       S,V0P,V0DP,V1P,V1DP,V2P,V2DP,                        3DCM0009
     &               CM0P,CM0DP,CM1P,CM1DP,CM2P,CM2DP,                  3DCM0010
     &               CMS0P,CMS0DP,CMS1P,CMS1DP,CMS2P,CMS2DP,            3DCM0011
     &               SIGMA,SIGMA0,C,F,G,D,B,SR,SI,PI,CC0,CC02,          3DCM0012
     &               CM00P,CM00DP,CM11P,CM11DP,CM22P,CM22DP             3DCM0013
      INTEGER AR                                                        3DCM0014
      COMMON/AREA4/SIGMA0,PI,NN,AR                                      3DCM0015
      CC0=(1.D0-S*S)**(NN/2.D0)                                         3DCM0016
      SIGMA=SIGMA0*CC0                                                  3DCM0017
      CC02=CC0*CC0                                                      3DCM0018
      CALL STHEOD (SIGMA,F,G,D,B,SR,SI)                                 3DCM0019
C                                                                       3DCM0020
C     STRIP-THEORY SECTION CM                                           3DCM0021
C                                                                       3DCM0022
      CM0P=.25D0*PI*SIGMA0*G*CC02                                       3DCM0023
      CM0DP=-.25D0*PI*SIGMA0*F*CC02                                     3DCM0024
      CM1P=.25D0*PI*(SIGMA*G-2.D0*F-.25D0*SIGMA*SIGMA)*CC02             3DCM0025
      CM1DP=.25D0*PI*(SIGMA-SIGMA*F-2.D0*G)*CC02                        3DCM0026
      CM2P=.25D0*PI*(SIGMA*F+2.D0*G-SIGMA)*CC02                         3DCM0027
      CM2DP=.25D0*PI*(SIGMA*G-2.D0*F-.25D0*SIGMA*SIGMA)*CC02            3DCM0028
C                                                                       3DCM0029
C     3D SECTIONAL (SEARS) CORRECTION                                   3DCM0030
C                                                                       3DCM0031
      CMS0P=.5D0*PI*(V0P*SR-V0DP*SI)*CC02                               3DCM0032
      CMS0DP=.5D0*PI*(V0DP*SR+V0P*SI)*CC02                              3DCM0033
      CMS1P=.5D0*PI*(V1P*SR-V1DP*SI)*CC02                               3DCM0034
      CMS1DP=.5D0*PI*(V1DP*SR+V1P*SI)*CC02                              3DCM0035
      CMS2P=.5D0*PI*(V2P*SR-V2DP*SI)*CC02                               3DCM0036
```

```
      CMS2DP=.5D0*PI*(V2DP*SR+V2P*SI)+CC02                              3DCM0037
C                                                                       3DCM0038
C     3D SECTION CM                                                     3DCM0039
C                                                                       3DCM0040
      CM00P=CM0P+CMS0P                                                  3DCM0041
      CM00DP=CM0DP+CMS0DP                                               3DCM0042
      CM11P=CM1P+CMS1P                                                  3DCM0043
      CM11DP=CM1DP+CMS1DP                                               3DCM0044
      CM22P=CM2P+CMS2P                                                  3DCM0045
      CM22DP=CM2DP+CMS2DP                                               3DCM0046
      RETURN                                                            3DCM0047
      END                                                               3DCM0048
```

```
      SUBROUTINE RROOTS(A,RZ,NER)                                       ROOT0001
C                                                                       ROOT0002
C     CALCULATION OF THE REAL ROOTS OF THE CUBIC SECULAR EQ. IN 3D OPT. ROOT0003
C     THE ROOTS ARE DETERMINED USING SUBROUTINE ZRPOLY OF IMSL          ROOT0004
C                                                                       ROOT0005
      REAL*8 A(4),AA,BB,CC                                              ROOT0006
      COMPLEX*16 Z(3),RZ(3)                                             ROOT0007
C                                                                       ROOT0008
C     THE GIVEN CUBIC SECULAR EQUATION                                  ROOT0009
C                                                                       ROOT0010
      PRINT147                                                          ROOT0011
  147 FORMAT('0','SECULAR EQ IS:')                                      ROOT0012
      PRINT148,A(1),A(2),A(3),A(4)                                      ROOT0013
  148 FORMAT('0',D10.4,'Z**3+',D10.4,'Z**2+',D10.4,'Z+',D10.4,'=0')     ROOT0014
      AA=DABS(A(1))                                                     ROOT0015
      IF(AA.LT.1.D-12)GO TO 151                                         ROOT0016
      NDEG=3                                                            ROOT0017
      CALL ZRPOLY(A,NDEG,Z,IER)                                         ROOT0018
      IF(IER.NE.0)  GO TO 103                                           ROOT0019
C                                                                       ROOT0020
C     PRINT ROOTS OF CUBIC, SELECT REAL ROOTS                           ROOT0021
C                                                                       ROOT0022
      DO 161 I=1,3                                                      ROOT0023
  161 PRINT162,Z(I)                                                     ROOT0024
  162 FORMAT('0','ROOT OF SECULAR EQ., Z=',2(D10.4,2X))                 ROOT0025
      J=1                                                               ROOT0026
      DO 163 I=1,3                                                      ROOT0027
      BB=DIMAG(Z(I))                                                    ROOT0028
      CC=DABS(BB)                                                       ROOT0029
      IF(CC.GT.1.D-12)GO TO 163                                         ROOT0030
      RZ(J)=Z(I)                                                        ROOT0031
      NER=J                                                             ROOT0032
      PRINT164,RZ(J)                                                    ROOT0033
  164 FORMAT('0','REAL ROOT OF SECULAR EQ, RZ=',2(D10.4,2X))            ROOT0034
      J=J+1                                                             ROOT0035
  163 CONTINUE                                                          ROOT0036
```

```
      PRINT 167,NRR                                                     ROOT0037
  167 FORMAT('0','NUMBER OF REAL ROOTS OF CUBIC SECULAR EQ, NRR=',I1)   ROOT0038
      RETURN                                                            ROOT0039
C                                                                       ROOT0040
C     IF LEADING TERM OF CUBIC IS ZERO, CONSIDER IT AS A QUADRATIC      ROOT0041
C                                                                       ROOT0042
  151 A(1)=A(2)                                                         ROOT0043
      A(2)=A(3)                                                         ROOT0044
      A(3)=A(4)                                                         ROOT0045
      AA=DABS(A(1))                                                     ROOT0046
      IF(AA.LT.1.D-12) GO TO 152                                        ROOT0047
      NDEG=2                                                            ROOT0048
      CALL ZEPOLY(A,NDEG,Z,IER)                                         ROOT0049
      IF(IER.NE.0) GO TO 103                                            ROOT0050
C                                                                       ROOT0051
C     PRINT ROOTS OF QUADRATIC, SELECT REAL ROOTS                       ROOT0052
C                                                                       ROOT0053
      DO 165 I=1,2                                                      ROOT0054
  165 PRINT162,Z(I)                                                     ROOT0055
      J=1                                                               ROOT0056
      DO 166 I=1,2                                                      ROOT0057
      BB=DIMAG(Z(I))                                                    ROOT0058
      CC=DABS(BB)                                                       ROOT0059
      IF(CC.GT.1.D-12) GO TO 166                                        ROOT0060
      RZ(J)=Z(I)                                                        ROOT0061
      NRR=J                                                             ROOT0062
      PRINT164,RZ(J)                                                    ROOT0063
      J=J+1                                                             ROOT0064
  166 CONTINUE                                                          ROOT0065
      PRINT167,NRR                                                      ROOT0066
      RETURN                                                            ROOT0067
C                                                                       ROOT0068
C     IF LEADING TERM OF QUADRATIC IS ZERO, CONSIDER IT AS A LINEAR EQ. ROOT0069
C                                                                       ROOT0070
  152 A(1)=A(2)                                                         ROOT0071
      A(2)=A(3)                                                         ROOT0072
      RZ(1)=-A(2)/A(1)                                                  ROOT0073
      NRR=1                                                             ROOT0074
      PRINT164,RZ(1)                                                    ROOT0075
      PRINT167,NRR                                                      ROOT0076
      RETURN                                                            ROOT0077
  103 PRINT101,IER                                                      ROOT0078
  101 FORMAT('0','ERROR IN ZEPOLY, IER=',I6)                            ROOT0079
      RETURN                                                            ROOT0080
      END                                                               ROOT0081
```

```
C                                                                       PGM20001
C     PROGRAM 2                                                         PGM20002
C                                                                       PGM20003
C     CALCULATION OF SPANWISE DISTRIBUTION OF UNSTEADY INDUCED DOWNWASH, PGM20004
C     SECTION LIFT AND SECTION MOMENT USING UNSTEADY LIFTING-LINE THEORY PGM20005
C                                                                       PGM20006
      REAL*8 XI(24,24),WT(24,24),SIGMA0,PI,    THETA,PSI0,PSI1,PSI2,V0P,PGM20007
     &   V0DP,V1P,V1DP,V2P,V2DP,VP,VDP,VAMP,VPHASE,S,DEL1,DEL2,         PGM20008
     &   CL0P,CL0DP,CL1P,CL1DP,CL2P,CL2DP,                             PGM20009
     &   CLS0P,CLS0DP,CLS1P,CLS1DP,CLS2P,CLS2DP,                       PGM20010
     &   CM0P,CM0DP,CM1P,CM1DP,CM2P,CM2DP,                             PGM20011
     &   CMS0P,CMS0DP,CMS1P,CMS1DP,CMS2P,CMS2DP,                       PGM20012
     &   CL2DR,CL2DI,CL3DP,CL3DI,CM2DR,CM2DI,CM3DR,CM3DI,GAMMA,CC0,    PGM20013
     &   SIGMA,EN,CL00P,CL00DP,CL11P,CL11DP,CL22P,CL22DP,CM00P,CM00DP, PGM20014
     &   CM11P,CM11DP,CM22P,CM22DP                                     PGM20015
      COMMON/AREA1/XI,WT/AREA2/SIGMA,CC0,JJ/AREA3/GAMMA,EN/AREA4/SIGMA0,PGM20016
     &PI,NN,AR                                                         PGM20017
      INTEGER AR,END                                                    PGM20018
      PI=3.14159265358979D0                                             PGM20019
      GAMMA=.57721566490 1534D0                                         PGM20020
      READ401,((XI(I,N),I=1,N),N=4,24,4)                                PGM20021
      READ401,((WT(I,N),I=1,N),N=4,24,4)                                PGM20022
  401 FORMAT(20X,F20.15,32X)                                            PGM20023
      DEL1=PI/60.D0                                                     PGM20024
      DEL2=8.7D0*PI/180.D0                                              PGM20025
   88 READ402,SIGMA0,AR,END,NN                                          PGM20026
  402 FORMAT(F9.6,I2,8X,I1,4X,I1)                                       PGM20027
C                                                                       PGM20028
C     IDENTIFY PLANFORM                                                 PGM20029
C                                                                       PGM20030
      GO TO (200,201,202),NN                                            PGM20031
  200 EN=4.D0/PI                                                        PGM20032
      PRINT300,SIGMA0,AR,NN                                             PGM20033
  300 FORMAT('1','SIGMA0=',F8.5,2X,'AR=',I3,2X,'NN=',I3,2X,'ELLIPTIC    PGM20034
     &WING')                                                            PGM20035
      GO TO 303                                                         PGM20036

  201 EN=1.5D0                                                          PGM20037
      PRINT301,SIGMA0,AR,NN                                             PGM20038
  301 FORMAT('1','SIGMA0=',F8.5,2X,'AR=',I3,2X,'NN=',I3,2X,'LENTICULAR  PGM20039
     &WING')                                                            PGM20040
      GO TO 303                                                         PGM20041
  202 EN=16.D0/(3.D0*PI)                                                PGM20042
      PRINT302,SIGMA0,AR,NN                                             PGM20043
  302 FORMAT('1','SIGMA0=',F8.5,2X,'AR=',I3,2X,'NN=',I3,2X,'CUSP-TIPPED PGM20044
     &WING')                                                            PGM20045
  303 CONTINUE                                                          PGM20046
      THETA=DEL1                                                        PGM20047
      DO 191 II=1,11                                                    PGM20048
      S=DCOS(THETA)                                                     PGM20049
      CALL DNWASH(S,V0P,V0DP,V1P,V1DP,V2P,V2DP)                         PGM20050
C                                                                       PGM20051
C     FOR PURE HEAVE SET (NON-D. W.R.T. NEGATIVE OF HEAVE ANGLE)        PGM20052
C                                                                       PGM20053
      VP=2.D0*V0DP/SIGMA0                                               PGM20054
      VDP=-2.D0*V0P/SIGMA0                                              PGM20055
C                                                                       PGM20056
C     FOR PURE PITCH SET                                                PGM20057
C                                                                       PGM20058
      VP=V1P                                                            PGM20059
      VDP=V1DP                                                          PGM20060
C                                                                       PGM20061
      VAMP=DSQRT(VP*VP+VDP*VDP)                                         PGM20062
      VPHASE=DATAN2(VDP,VP)                                             PGM20063
      IF(VPHASE) 41,42,42                                               PGM20064
   41 VPHASE=2.D0*PI+VPHASE                                             PGM20065
   42 VPHASE=180.D0*VPHASE/PI                                           PGM20066
      PRINT400,S,V0P,V1P,V2P,V0DP,V1DP,V2DP                             PGM20067
  400 FORMAT('0','S=',F8.3,2X,'V0P=',F10.7,2X,'V1P=',F10.7,2X,'V2P=',   PGM20068
     &   F10.7,2X,'V0DP=',F10.7,2X,'V1DP=',F10.7,2X,'V2DP=',F10.7)      PGM20069
      PRINT500,S,VP,VDP,VAMP,VPHASE                                     PGM20070
  500 FORMAT('0','S=',F8.3,2X,'VP=',F10.7,2X,'VDP=',F10.7,2X,'VAMP=',   PGM20071
     &   F10.7,2X,'VPHASE=',F13.8)                                      PGM20072
```

```
      CALL       CL1(S,V0P,V0DP,V1P,V1DP,V2P,V2DP,                    PGM20073
     &              CL0P,CL0DP,CL1P,CL1DP,CL2P,CL2DP,                 PGM20074
     &              CLS0P,CLS0DP,CLS1P,CLS1DP,CLS2P,CLS2DP,           PGM20075
     &              CL00P,CL00DP,CL11P,CL11DP,CL22P,CL22DP)           PGM20076
      CALL       CM1(S,V0P,V0DP,V1P,V1DP,V2P,V2DP,                    PGM20077
     &              CM0P,CM0DP,CM1P,CM1DP,CM2P,CM2DP,                 PGM20078
     &              CMS0P,CMS0DP,CMS1P,CMS1DP,CMS2P,CMS2DP,           PGM20079
     &              CM00P,CM00DP,CM11P,CM11DP,CM22P,CM22DP)           PGM20080
C                                                                     PGM20081
C     FOR PURE HEAVE SET                                              PGM20082
C                                                                     PGM20083
      CL2DR=CL0P                                                      PGM20084
      CL2DI=CL0DP                                                     PGM20085
      CL3DR=CL0P                                                      PGM20086
      CL3DI=CL0DP                                                     PGM20087
      CM2DR=CM0P                                                      PGM20088
      CM2DI=CM0DP                                                     PGM20089
      CM3DR=CM00P                                                     PGM20090
      CM3DI=CM00DP                                                    PGM20091
C                                                                     PGM20092
C     FOR PURE PITCH SET                                              PGM20093
C                                                                     PGM20094
      CL2DR=CL1P                                                      PGM20095
      CL2DI=CL1DP                                                     PGM20096
      CL3DR=CL11P                                                     PGM20097
      CL3DI=CL11DP                                                    PGM20098
      CM2DR=CM1P                                                      PGM20099
      CM2DI=CM1DP                                                     PGM20100
      CM3DR=CM11P                                                     PGM20101
      CM3DI=CM11DP                                                    PGM20102
C                                                                     PGM20103
      PRINT 600,S,CL2DR,CL2DI,CL3DR,CL3DI                             PGM20104
  600 FORMAT('0','S=',F8.3,2X,'CL2DR=',F10.5,2X,'CL2DI=',F10.5,2X,    PGM20105
     &                        'CL3DR=',F10.5,2X,'CL3DI=',F10.5)       PGM20106
      PRINT 700,S,CM2DR,CM2DI,CM3DR,CM3DI                             PGM20107
  700 FORMAT('0','S=',F8.3,2X,'CM2DR=',F10.5,2X,'CM2DI=',F10.5,2X,    PGM20108
     &                        'CM3DR=',F10.5,2X,'CM3DI=',F10.5)       PGM20109
  191 THETA=THETA+DEL2                                                PGM20110
      IF(END.NE.1) GO TO 88                                           PGM20111
      STOP                                                            PGM20112
      END                                                             PGM20113
```

```
C                                                                       PGM30001
C     PROGRAM 3                                                         PGM30002
C                                                                       PGM30003
C     CALCULATION OF TOTAL CL AND CM FOR AN OSCILLATING FINITE WING     PGM30004
C     USING UNSTEADY LIFTING-LINE THEORY                                PGM30005
C                                                                       PGM30006
      REAL*8 XI(24,24),WT(24,24),SIGMA0,PI,     THETA,PSI0,PSI1,PSI2,V0P,PGM30007
     &   V0DP,V1P,V1DP,V2P,V2DP,VP,VDP,VAMP,VPHASE,S,DEL1,DEL2,         PGM30008
     &   CL0P,CL0DP,CL1P,CL1DP,CL2P,CL2DP,                              PGM30009
     &   CLS0P,CLS0DP,CLS1P,CLS1DP,CLS2P,CLS2DP,                        PGM30010
     &   CM0P,CM0DP,CM1P,CM1DP,CM2P,CM2DP,                              PGM30011
     &   CMS0P,CMS0DP,CMS1P,CMS1DP,CMS2P,CMS2DP,                        PGM30012
     &   CL2DR,CL2DI,CL3DR,CL3DI,CM2DR,CM2DI,CM3DR,CM3DI,GAMMA,CC0,     PGM30013
     &   SIGMA,EN,CC,SUM1,SUM2,SUM3,SUM4,SUM5,SUM6,SUM7,SUM8,           PGM30014
     &   TCL2DR,TCL2DI,TCL3DR,TCL3DI,TCM2DR,TCM2DI,TCM3DR,TCM3DI,FACT,  PGM30015
     &   CL00P,CL00DP,CL11P,CL11DP,CL22P,CL22DP,CM00P,CM00DP,CM11P,     PGM30016
     &   CM11DP,CM22P,CM22DP                                            PGM30017
      COMMON/AREA1/XI,WT/AREA3/GAMMA,EN/AREA4/SIGMA0,PI,NN,AR           PGM30018
      INTEGER AR,END                                                    PGM30019
      PI=3.1415926535897900                                             PGM30020
      GAMMA=.57721566490153400                                          PGM30021
      READ401,((XI(I,N),I=1,N),N=4,24,4)                                PGM30022
      READ401,((WT(I,N),I=1,N),N=4,24,4)                                PGM30023
  401 FORMAT(20X,F20.15,32X)                                            PGM30024
   88 READ402,SIGMA0,AR,END,NN                                          PGM30025
  402 FORMAT(F9.6,I2,8X,I1,4X,I1)                                       PGM30026
C                                                                       PGM30027
C     IDENTIFY PLANFORM                                                 PGM30028
C                                                                       PGM30029
      GO TO (200,201,202),NN                                            PGM30030
  200 EN=4.D0/PI                                                        PGM30031
      PRINT300,SIGMA0,AR,NN                                             PGM30032
  300 FORMAT('1','SIGMA0=',F8.5,2X,'AR=',I3,2X,'NN=',I3,2X,'ELLIPTIC    PGM30033
     &WING')                                                            PGM30034
      GO TO 303                                                         PGM30035
  201 EN=1.5D0                                                          PGM30036
      PRINT301,SIGMA0,AR,NN                                             PGM30037
  301 FORMAT('1','SIGMA0=',F8.5,2X,'AR=',I3,2X,'NN=',I3,2X,'LENTICULAR  PGM30038
     &WING')                                                            PGM30039
      GO TO 303                                                         PGM30040
  202 EN=16.D0/(3.D0*PI)                                                PGM30041
      PRINT302,SIGMA0,AR,NN                                             PGM30042
  302 FORMAT('1','SIGMA0=',F8.5,2X,'AR=',I3,2X,'NN=',I3,2X,'CUSP-TIPPED PGM30043
     &WING')                                                            PGM30044
  303 CONTINUE                                                          PGM30045
C                                                                       PGM30046
C     INTEGRATION OF SECTION LIFT AND MOMENT COEFF'S, USING 16-POINT    PGM30047
C     LEGENDRE-GAUSS QUADRATURE, TO FIND TOTAL COEFF'S                  PGM30048
C                                                                       PGM30049
      N=16                                                              PGM30050
      SUM1=0.D0                                                         PGM30051
      SUM2=0.D0                                                         PGM30052
      SUM3=0.D0                                                         PGM30053
      SUM4=0.D0                                                         PGM30054
      SUM5=0.D0                                                         PGM30055
      SUM6=0.D0                                                         PGM30056
      SUM7=0.D0                                                         PGM30057
      SUM8=0.D0                                                         PGM30058
      E=N/2                                                             PGM30059
      DO 10 I=1,N                                                       PGM30060
      THETA=.5D0*PI*(1.D0+XI(I,N))                                      PGM30061
      S=DCOS(THETA)                                                     PGM30062
      CALL DNWASH(S,V0P,V0DP,V1P,V1DP,V2P,V2DP)                         PGM30063
      CALL       CL1(S,V0P,V0DP,V1P,V1DP,V2P,V2DP,                      PGM30064
     &              CL0P,CL0DP,CL1P,CL1DP,CL2P,CL2DP,                  PGM30065
     &              CLS0P,CLS0DP,CLS1P,CLS1DP,CLS2P,CLS2DP,            PGM30066
     &              CL00P,CL00DP,CL11P,CL11DP,CL22P,CL22DP)            PGM30067
      CALL       CM1(S,V0P,V0DP,V1P,V1DP,V2P,V2DP,                      PGM30068
     &              CM0P,CM0DP,CM1P,CM1DP,CM2P,CM2DP,                  PGM30069
     &              CMS0P,CMS0DP,CMS1P,CMS1DP,CMS2P,CMS2DP,            PGM30070
     &              CM00P,CM00DP,CM11P,CM11DP,CM22P,CM22DP)            PGM30071
C                                                                       PGM30072
```

```
C     FOR PURE HEAVE SET                                                    PGM30073
C                                                                           PGM30074
      CL2DR=CL0P                                                            PGM30075
      CL2DI=CL0DP                                                           PGM30076
      CL3DR=CL00P                                                           PGM30077
      CL3DI=CL00DP                                                          PGM30078
      CM2DR=CM0P                                                            PGM30079
      CM2DI=CM0DP                                                           PGM30080
      CM3DR=CM00P                                                           PGM30081
      CM3DI=CM00DP                                                          PGM30082
C                                                                           PGM30083
C     FOR PURE PITCH SET                                                    PGM30084
C                                                                           PGM30085
      CL2DR=CL1P                                                            PGM30086
      CL2DI=CL1DP                                                           PGM30087
      CL3DR=CL11P                                                           PGM30088
      CL3DI=CL11DP                                                          PGM30089
      CM2DR=CM1P                                                            PGM30090
      CM2DI=CM1DP                                                           PGM30091
      CM3DR=CM11P                                                           PGM30092
      CM3DI=CM11DP                                                          PGM30093
C                                                                           PGM30094
      CC=DSIN(THETA)                                                        PGM30095
      SUM1=SUM1+CL2DR*CC*WT(I,N)                                            PGM30096
      SUM2=SUM2+CL2DI*CC*WT(I,N)                                            PGM30097
      SUM3=SUM3+CL3DR*CC*WT(I,N)                                            PGM30098
      SUM4=SUM4+CL3DI*CC*WT(I,N)                                            PGM30099
      SUM5=SUM5+CM2DR*CC*WT(I,N)                                            PGM30100
      SUM6=SUM6+CM2DI*CC*WT(I,N)                                            PGM30101
      SUM7=SUM7+CM3DR*CC*WT(I,N)                                            PGM30102
   10 SUM8=SUM8+CM3DI*CC*WT(I,N)                                            PGM30103
C                                                                           PGM30104
C     TOTAL CL AND CM                                                       PGM30105
C                                                                           PGM30106
C     FOR HEAVE SET (NORMALIZED W.R.T. NEGATIVE OF HEAVE ANGLE)             PGM30107
C                                                                           PGM30108
```

```
      FACT=4.D0/SIGMA0                                                      PGM30109
      TCL2DR=SUM2*FACT                                                      PGM30110
      TCL2DI=-SUM1*FACT                                                     PGM30111
      TCL3DR=SUM4*FACT                                                      PGM30112
      TCL3DI=-SUM3*FACT                                                     PGM30113
      TCM2DR=SUM6*FACT                                                      PGM30114
      TCM2DI=-SUM5*FACT                                                     PGM30115
      TCM3DR=SUM8*FACT                                                      PGM30116
      TCM3DI=-SUM7*FACT                                                     PGM30117
C                                                                           PGM30118
C     FOR PITCH SET                                                         PGM30119
C                                                                           PGM30120
      TCL2DR=SUM1*2.D0                                                      PGM30121
      TCL2DI=SUM2*2.D0                                                      PGM30122
      TCL3DR=SUM3*2.D0                                                      PGM30123
      TCL3DI=SUM4*2.D0                                                      PGM30124
      TCM2DR=SUM5*2.D0                                                      PGM30125
      TCM2DI=SUM6*2.D0                                                      PGM30126
      TCM3DR=SUM7*2.D0                                                      PGM30127
      TCM3DI=SUM8*2.D0                                                      PGM30128
      PRINT800  ,TCL2DR,TCL2DI,TCL3DR,TCL3DI                                PGM30129
  800 FORMAT('0',10X          ,'TCL2DR=',F10.5,2X,'TCL2DI=',F10.5,2X,       PGM30130
     &                         'TCL3DR=',F10.5,2X,'TCL3DI=',F10.5)          PGM30131
      PRINT900  ,TCM2DR,TCM2DI,TCM3DR,TCM3DI                                PGM30132
  900 FORMAT('0',10X          ,'TCM2DR=',F10.5,2X,'TCM2DI=',F10.5,2X,       PGM30133
     &                         'TCM3DR=',F10.5,2X,'TCM3DI=',F10.5)          PGM30134
      IF(END.NE.1) GO TO 88                                                 PGM30135
      STOP                                                                  PGM30136
      END                                                                   PGM30137
```

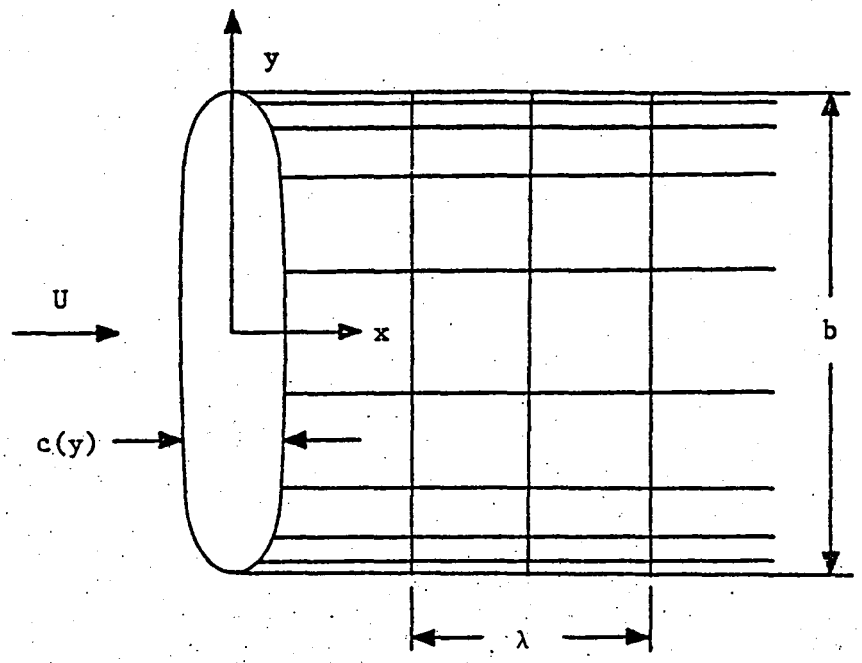

Figure 2.1. The three characteristic length scales for a harmonically-oscillating wing.

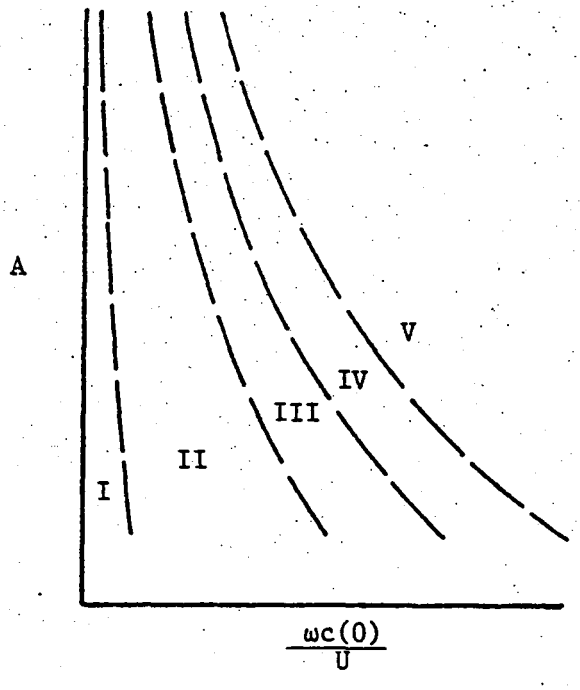

Figure 2.2. The five domains of unsteady three-dimensional effects.

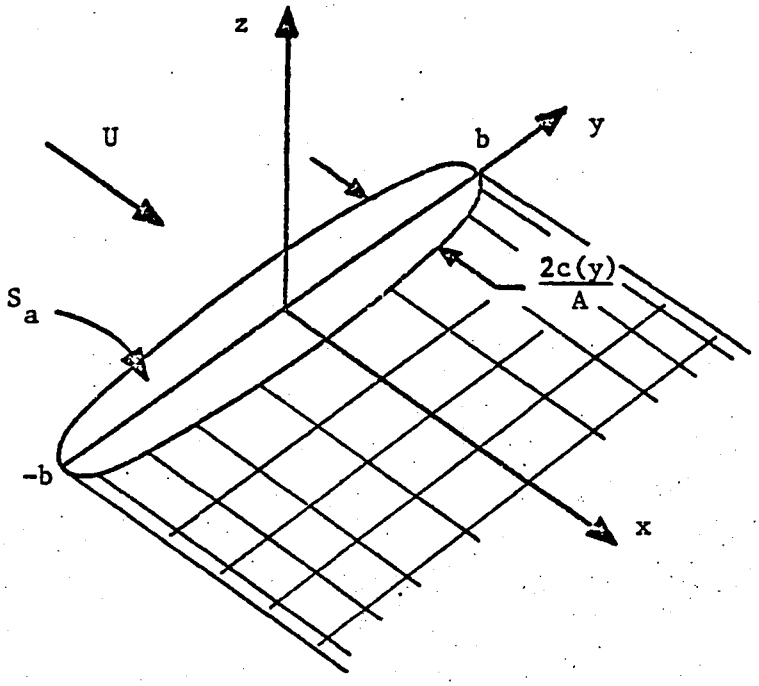

Figure 2.3a. Schematic of a wing in unsteady motion.

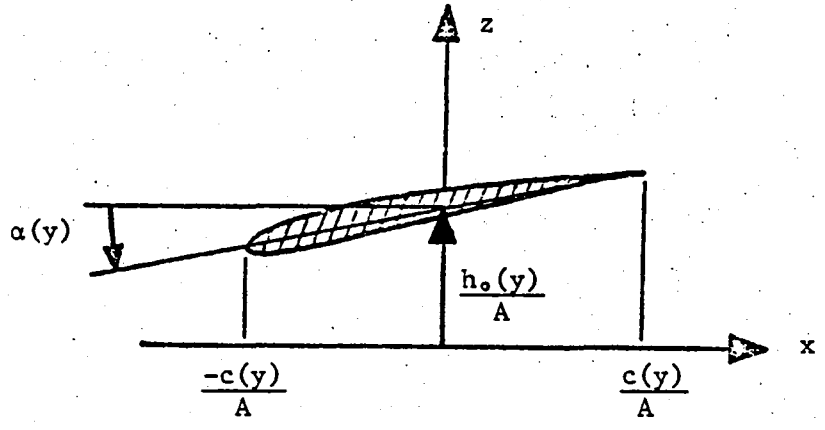

Figure 2.3b. Positive directions of pitch and heave for a wing section.

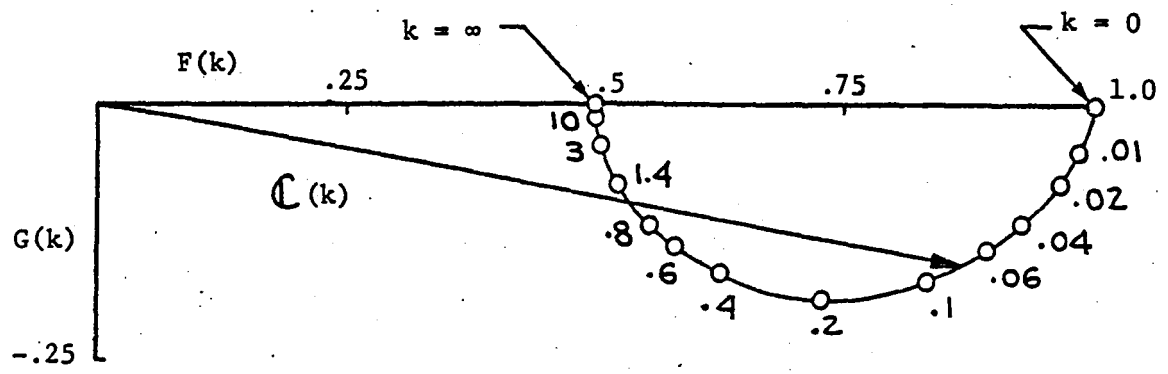

Figure 2.4. Theodorsen's function plotted as a complex vector, $\mathbb{C}(k) = F(k) + j\,G(k)$.

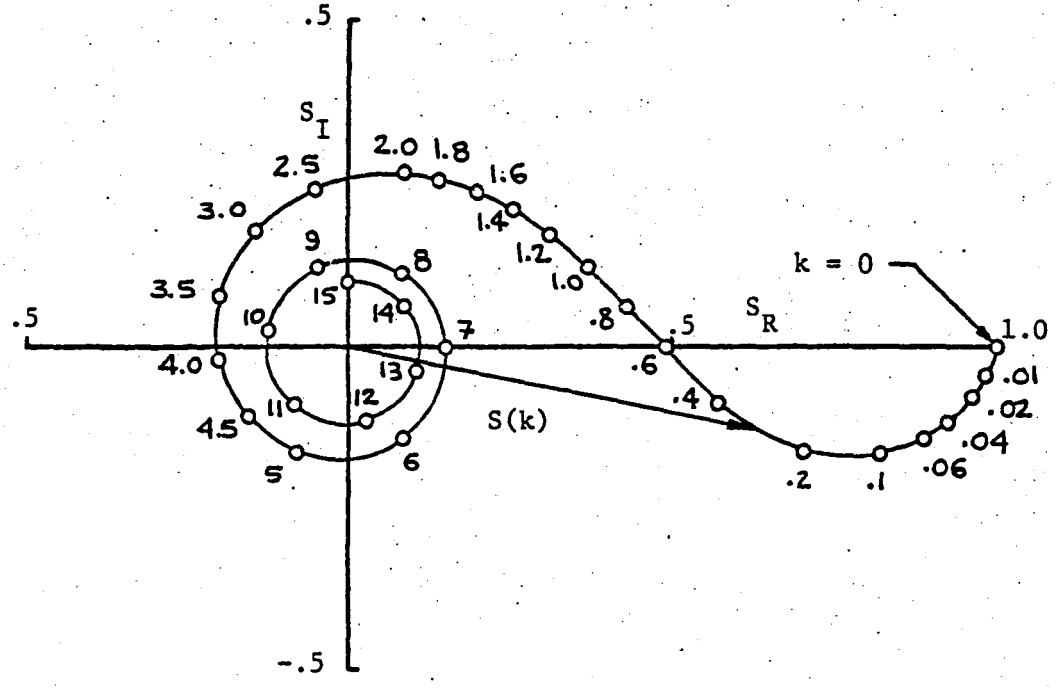

Figure 2.5. The Sears function plotted as a complex vector, $S(k) = S_R(k) + j\,S_I(k)$.

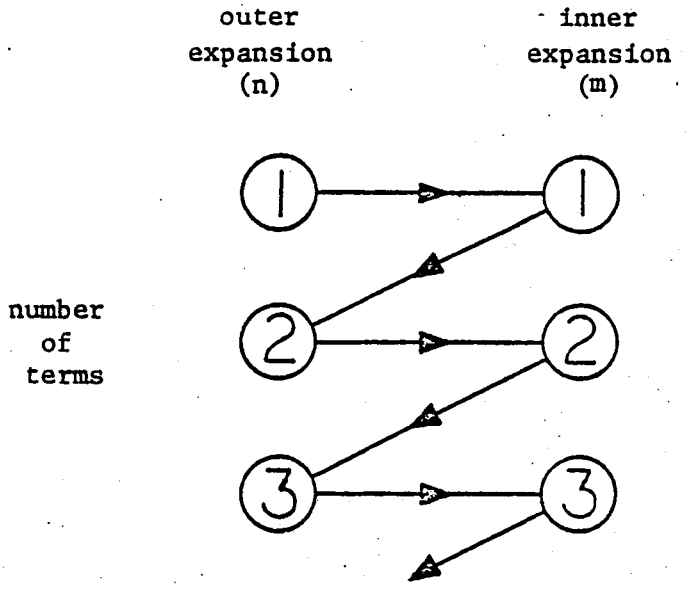

Figure 2.6. Schematic of matching order for inner and outer expansions.

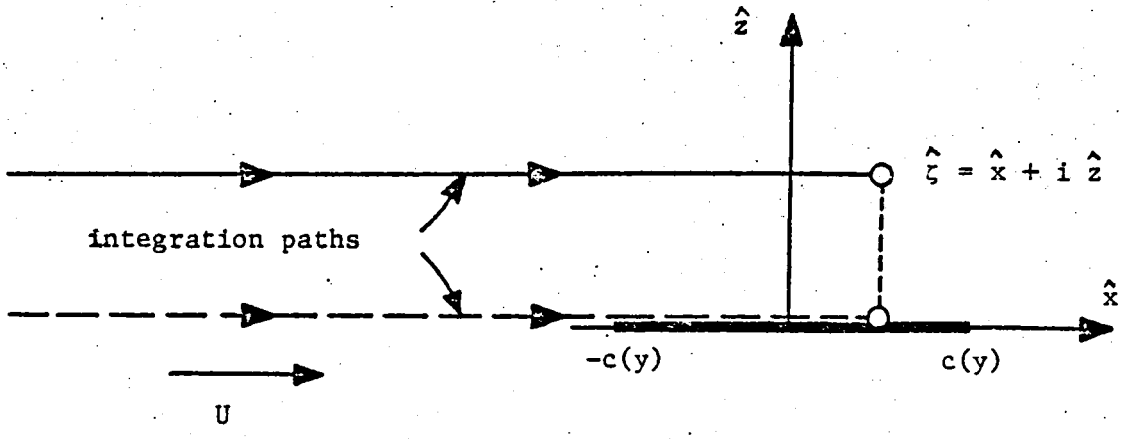

Figure 2.7. Linearized paths of integration for calculating downwash at the wing.

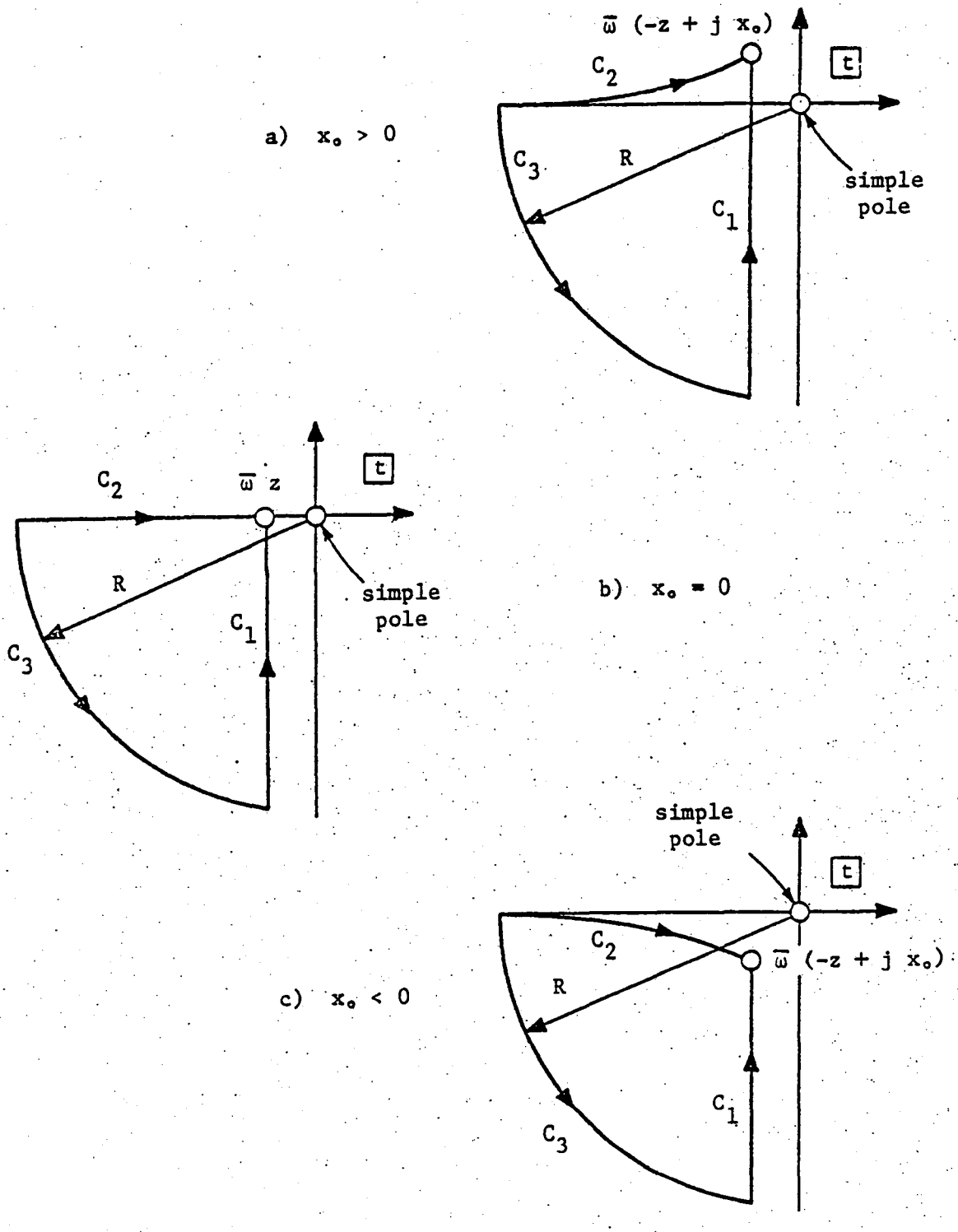

Figure 2.8. Integration contours for the first integral in (2.166).

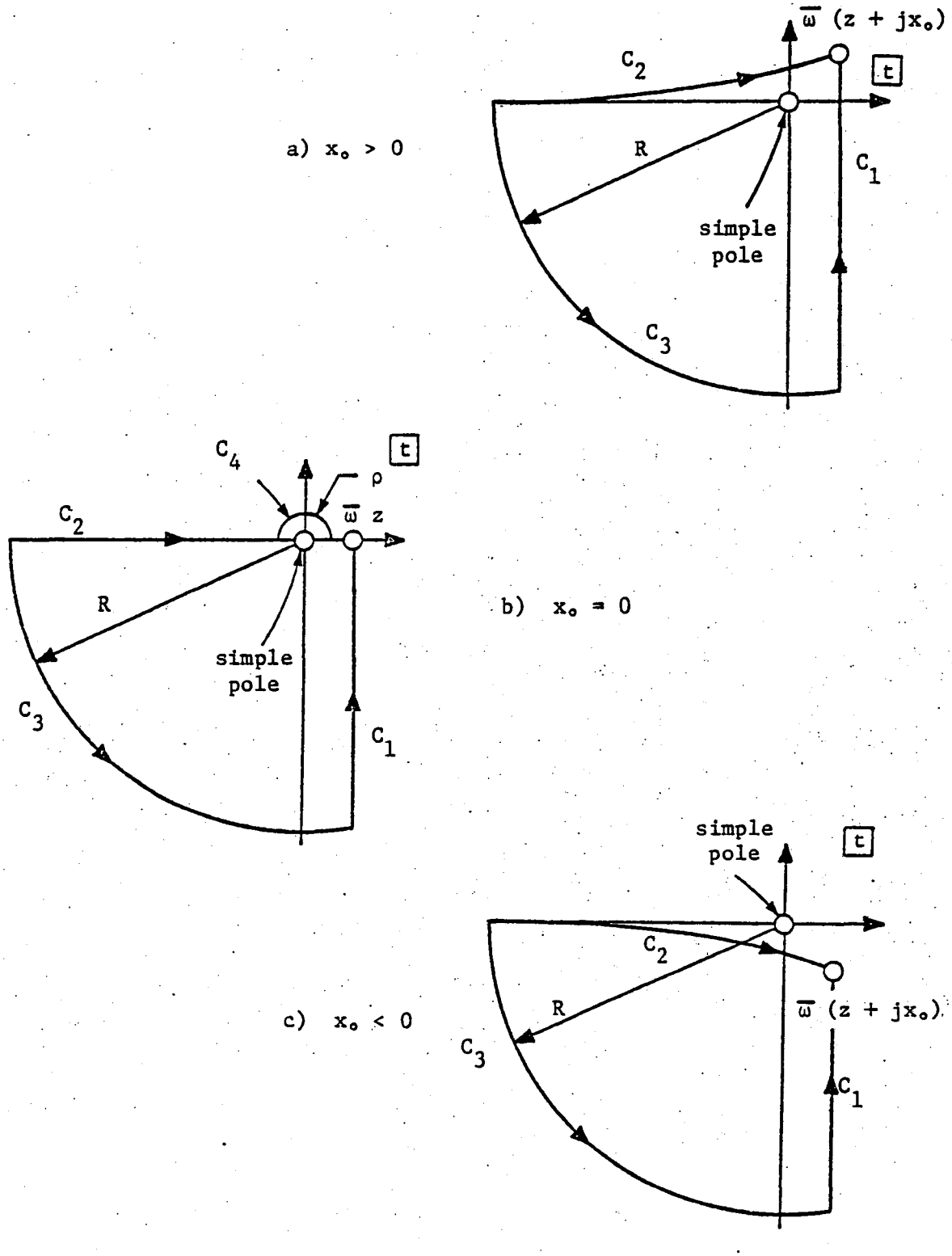

Figure 2.9. Integration contours for the second integral in (2.166).

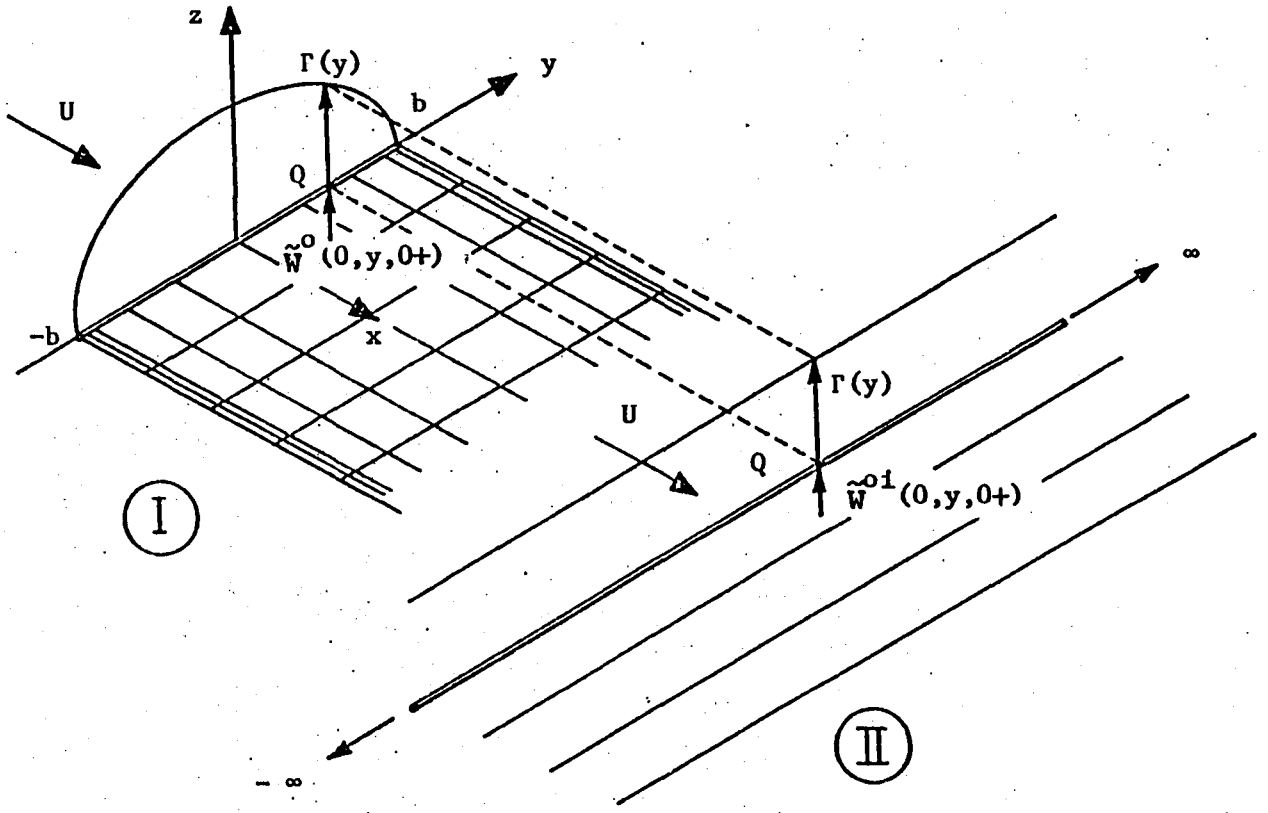

Figure 3.1. Physical interpretation of unsteady induced downwash (after Van Holten (1976)).

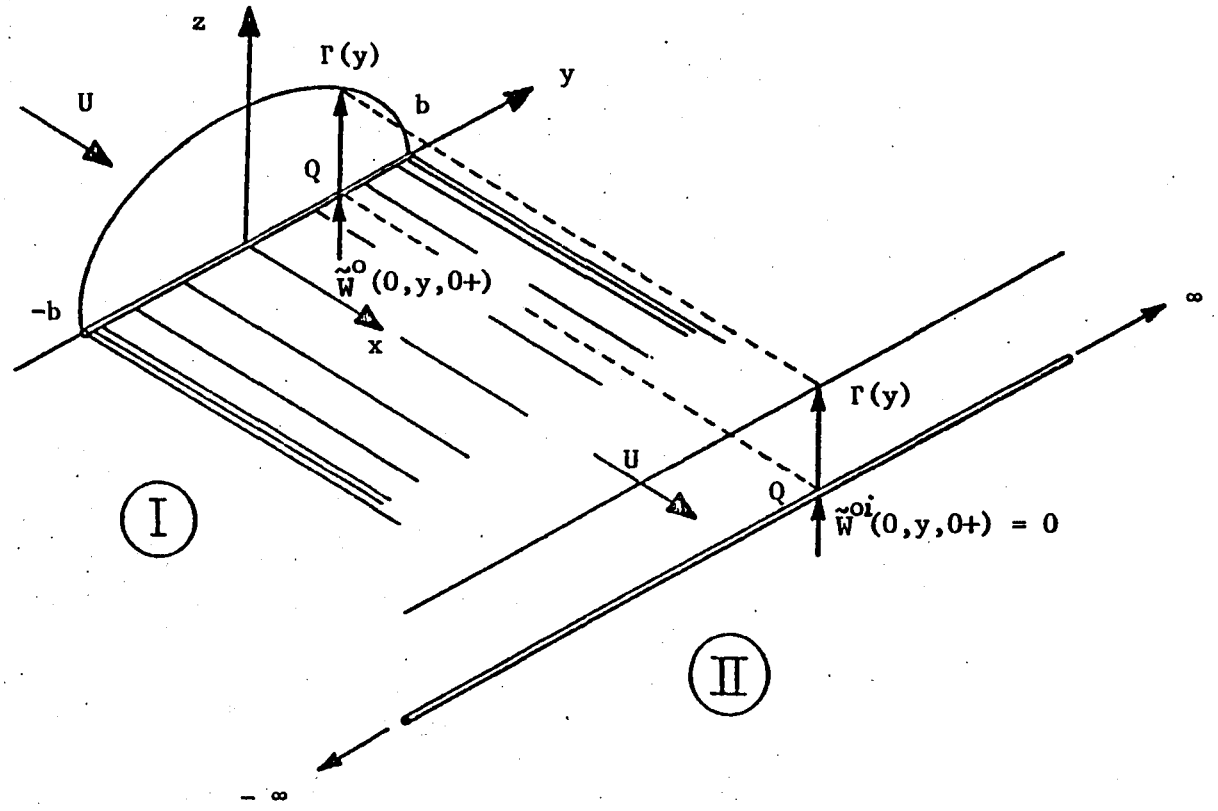

Figure 3.2. Physical interpretation of steady induced downwash (after Van Holten (1976)).

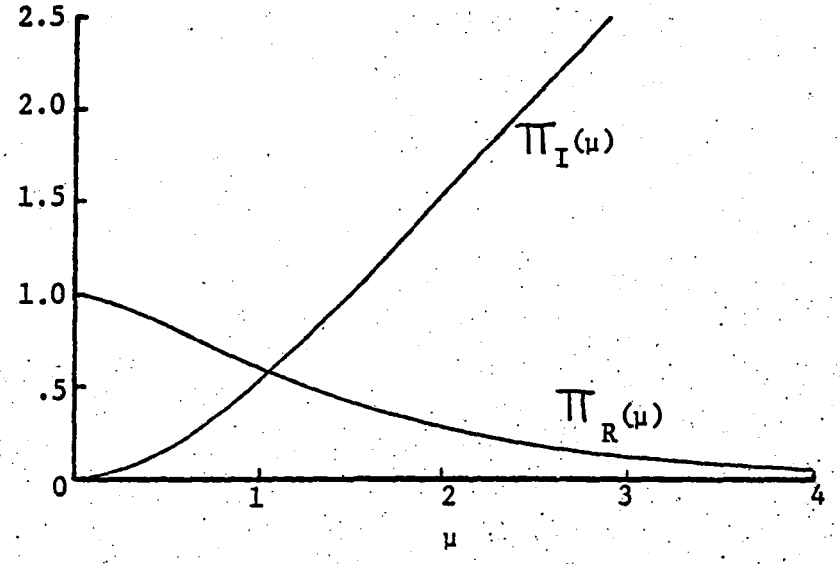

Figure 3.3. The real and imaginary parts of the kernel function of unsteady lifting-line theory $\Pi(\mu) = \Pi_R(\mu) + j\,\Pi_I(\mu)$.

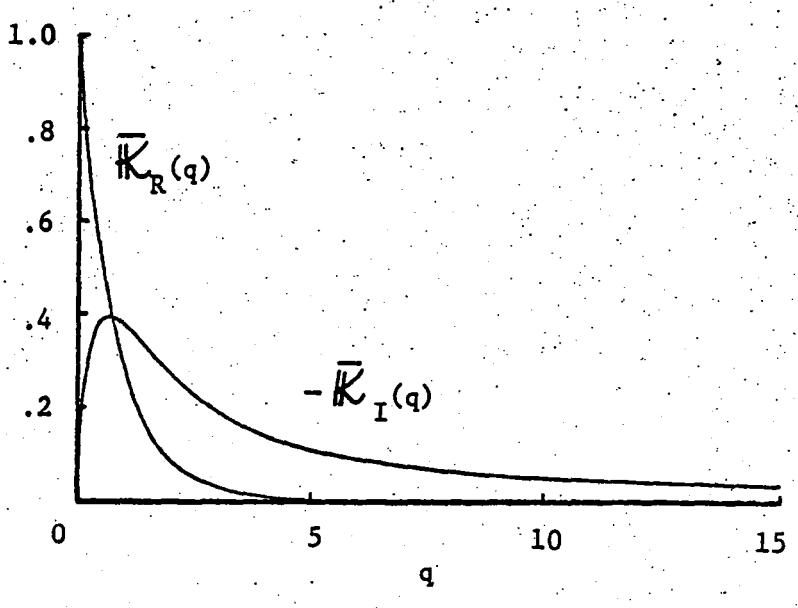

Figure 3.4. The real and imaginary parts of the modified kernel function of Reissner $\bar{K}(q) = \bar{K}_R(q) + j\,\bar{K}_I(q)$.

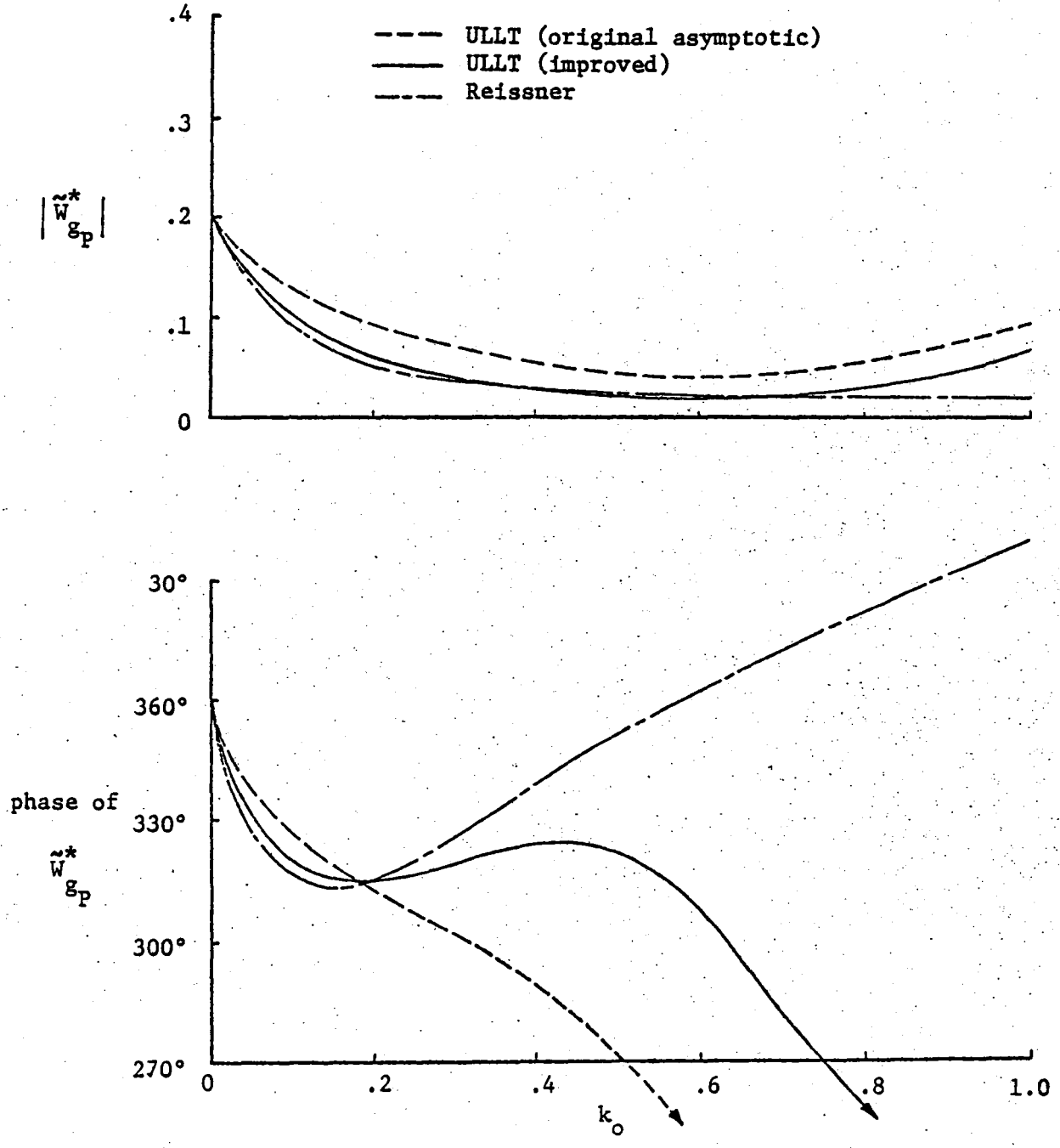

Figure 3.5. Amplitude and phase of $\tilde{W}^*_{g_p}$ for an elliptic wing in pitch (A = 10, y* = 0).

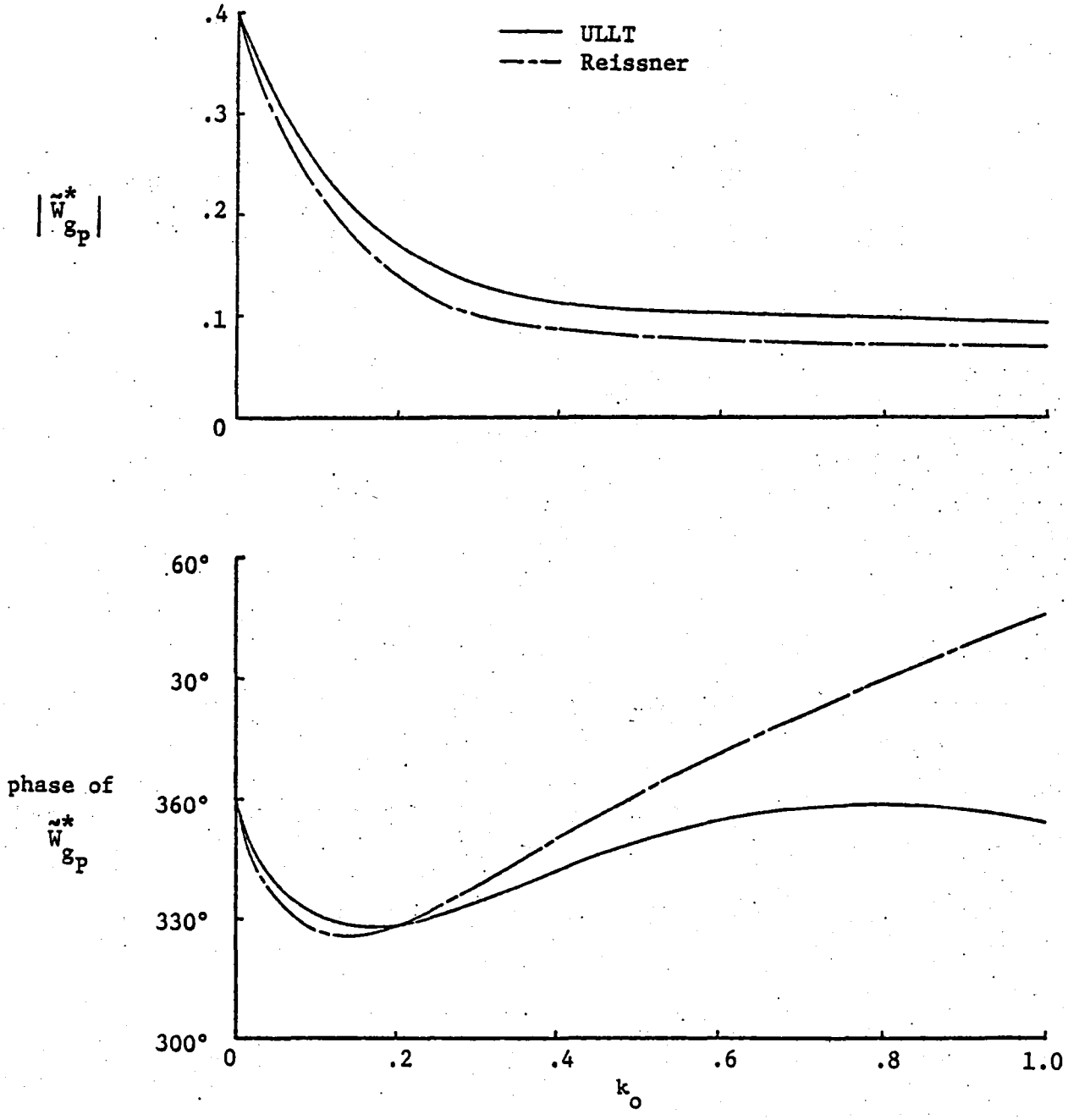

Figure 3.6. Amplitude and phase of $\tilde{W}^*_{g_p}$ for an elliptic wing in pitch (A = 5, y* = 0).

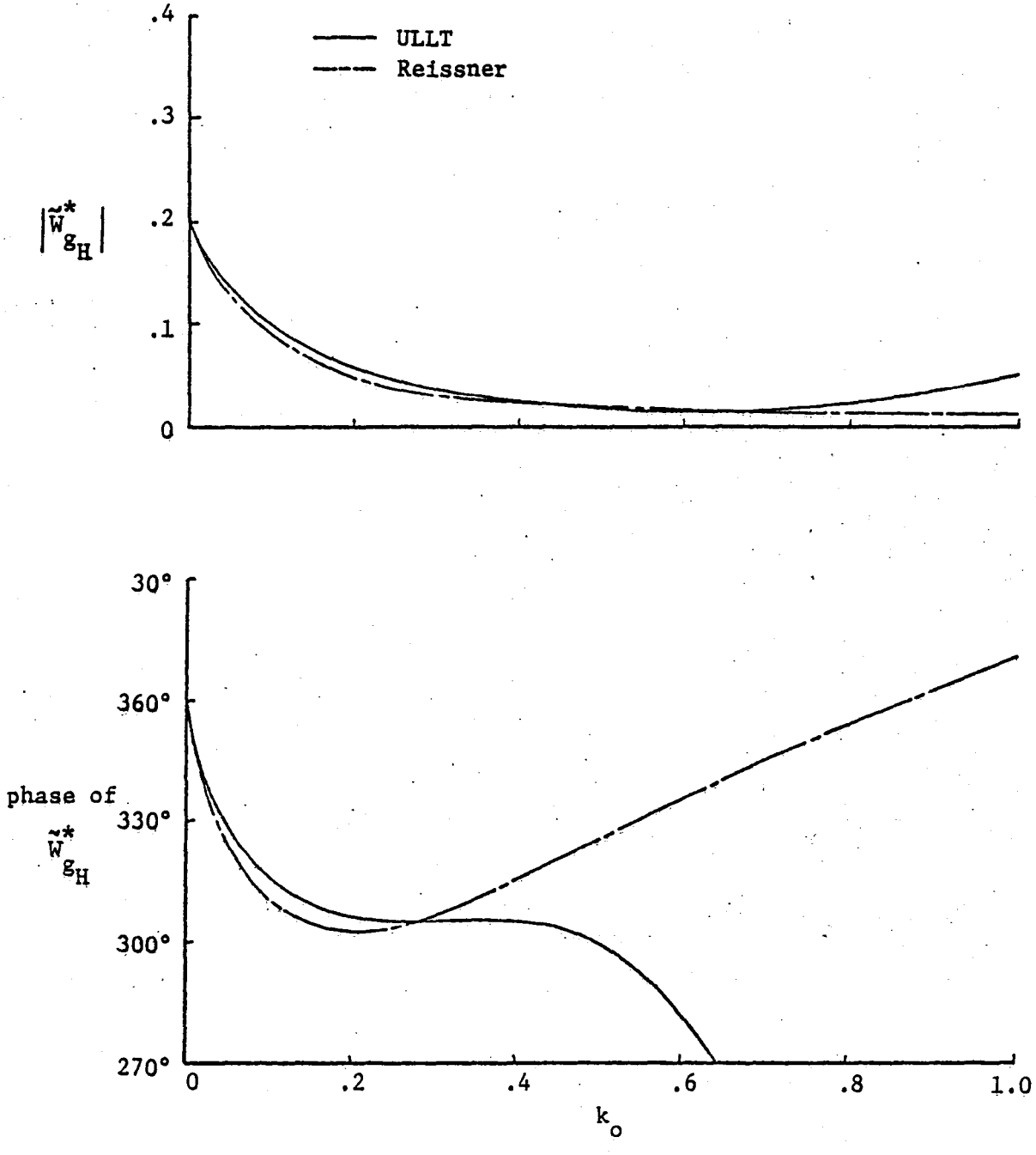

Figure 3.7. Amplitude and phase of $\tilde{W}^*_{g_H}$ for an elliptic wing in heave (A = 10, y* = 0).

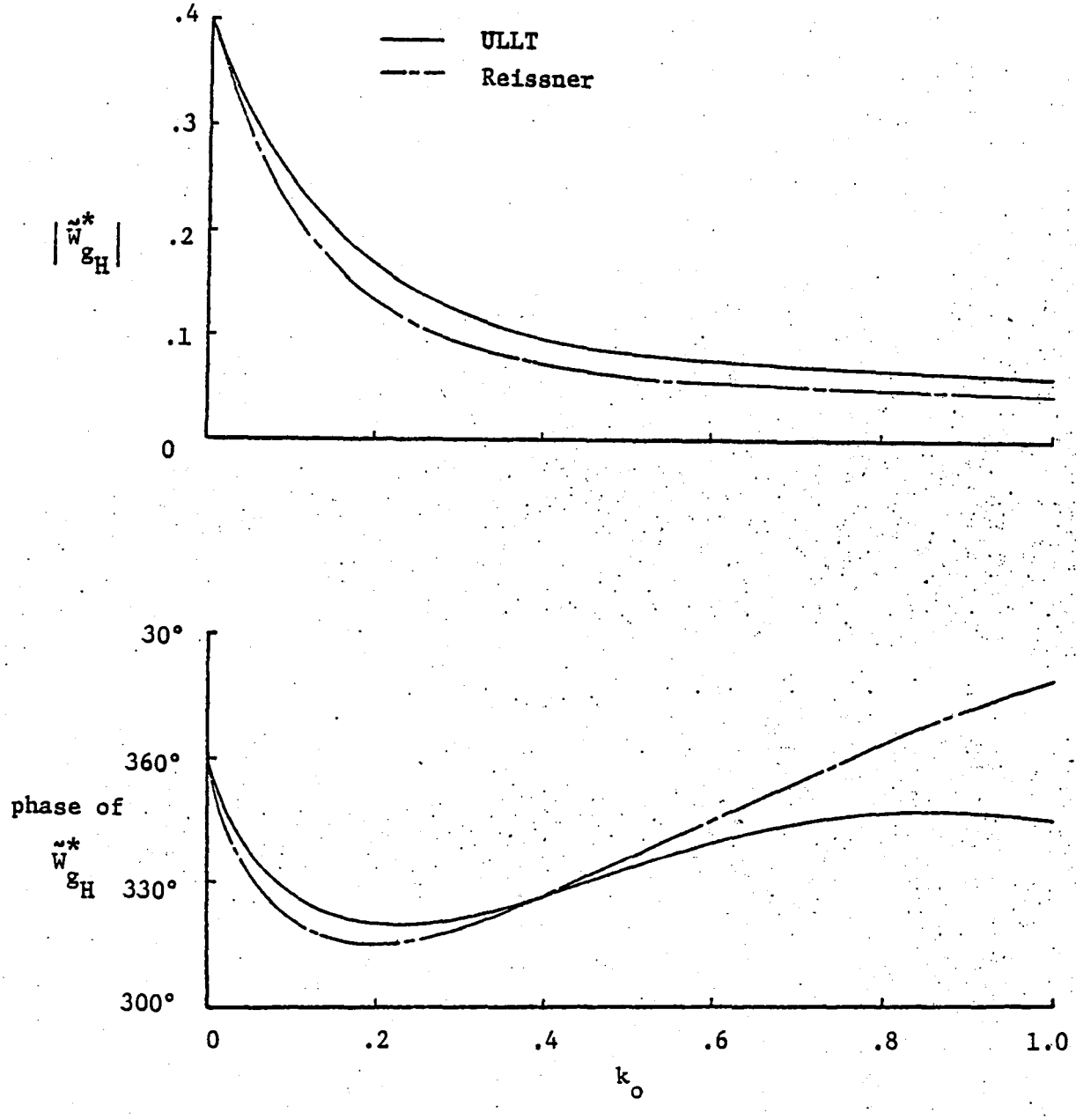

Figure 3.8. Amplitude and phase of $\tilde{w}^*_{g_H}$ for an elliptic wing in heave (A = 5, y* = 0).

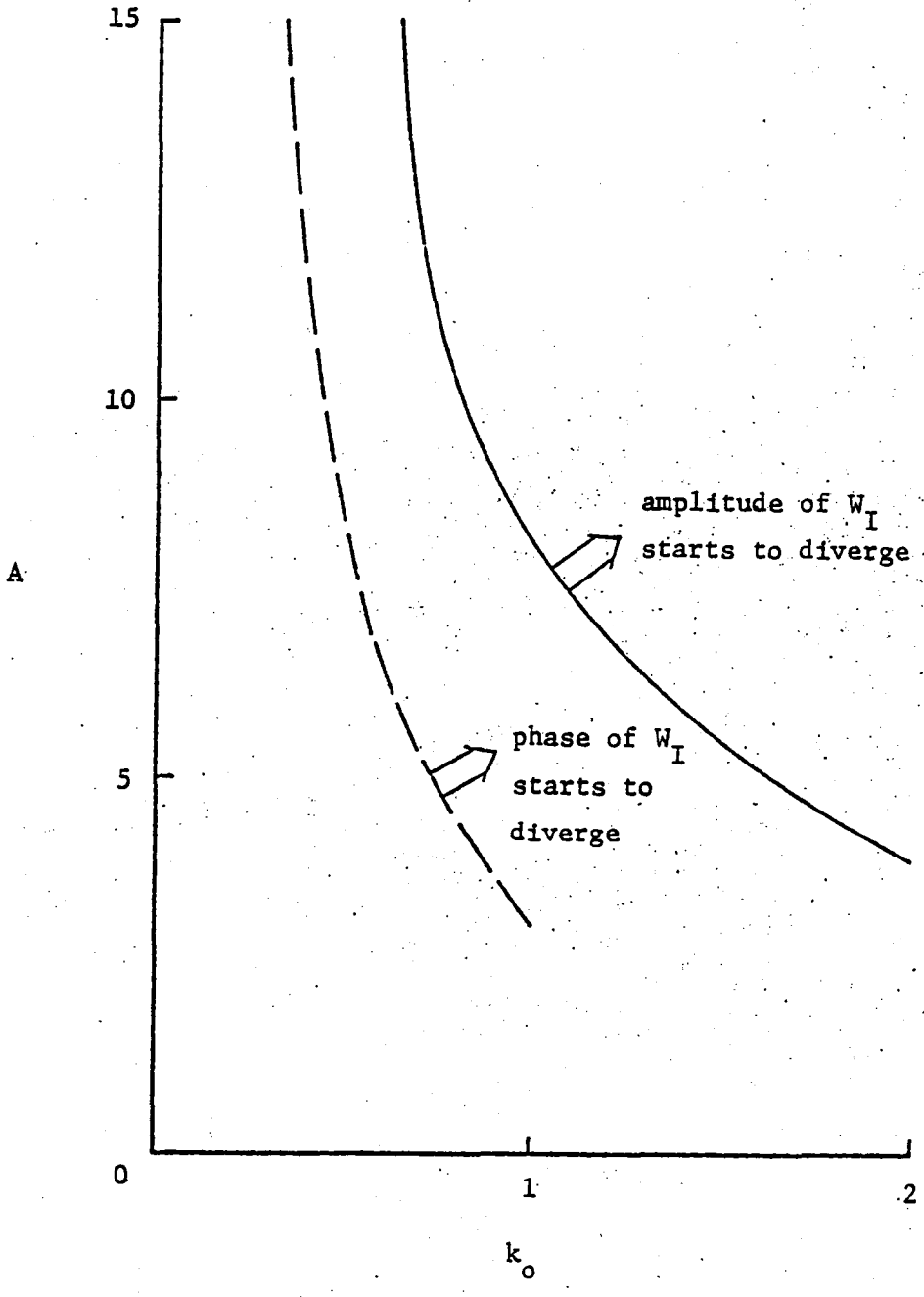

Figure 3.9. Region of validity of the present unsteady lifting-line theory.

a) rectangular

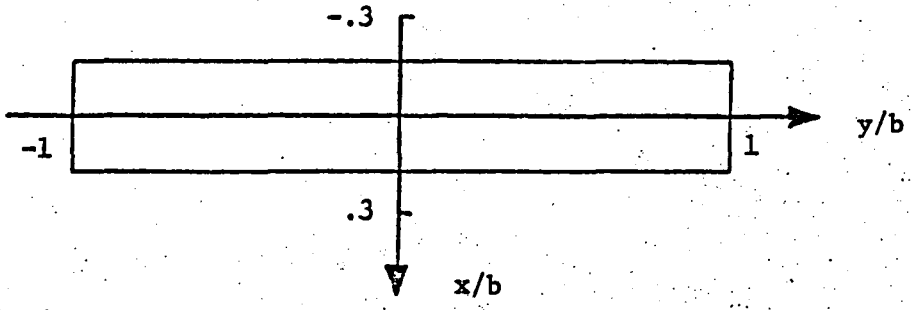

b) elliptic

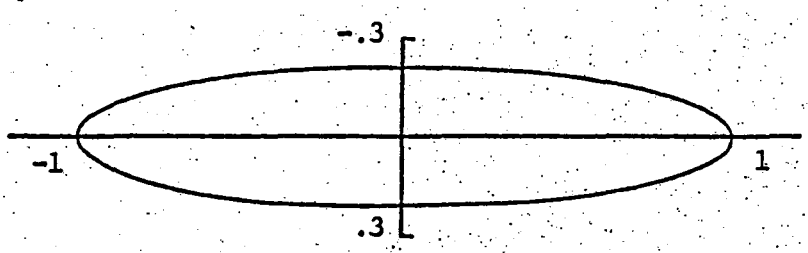

c) lenticular

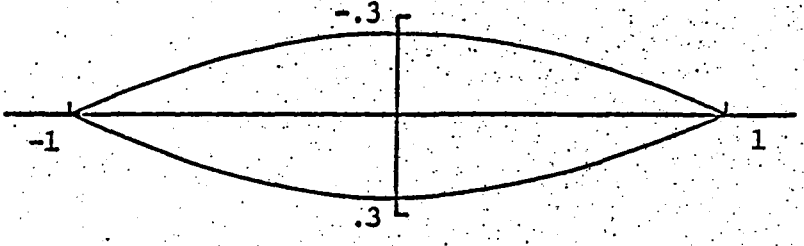

d) cusp tipped

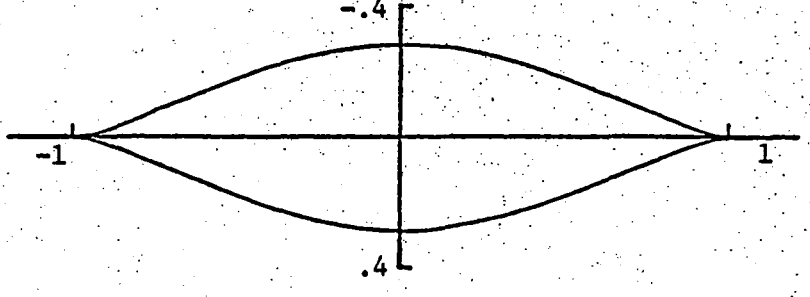

Figure 3.10. A family of wing planforms (A = 6).

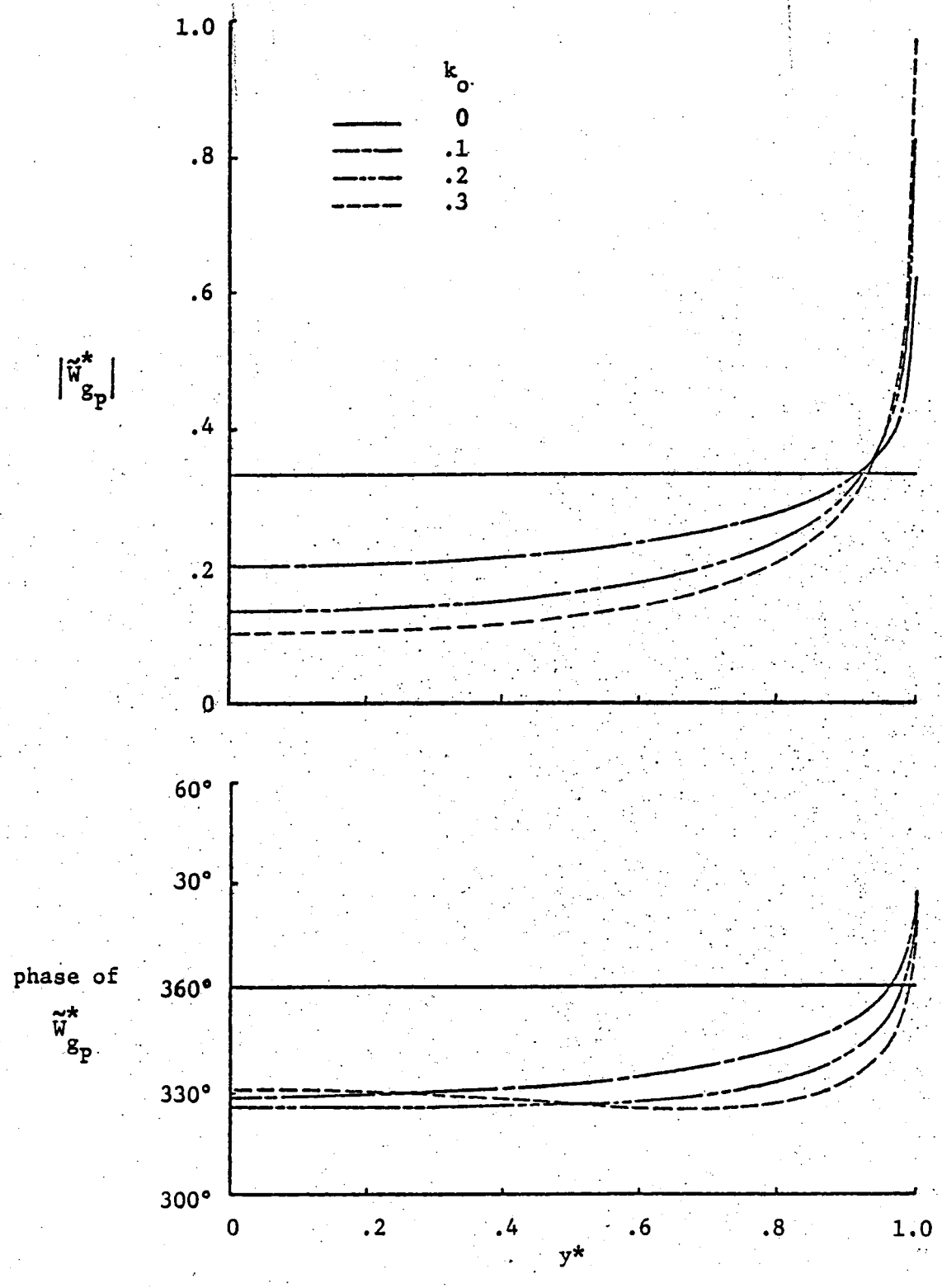

Figure 3.11. Amplitude and phase of $\tilde{W}^*_{g_p}$ for an elliptic wing in pitch (A = 6).

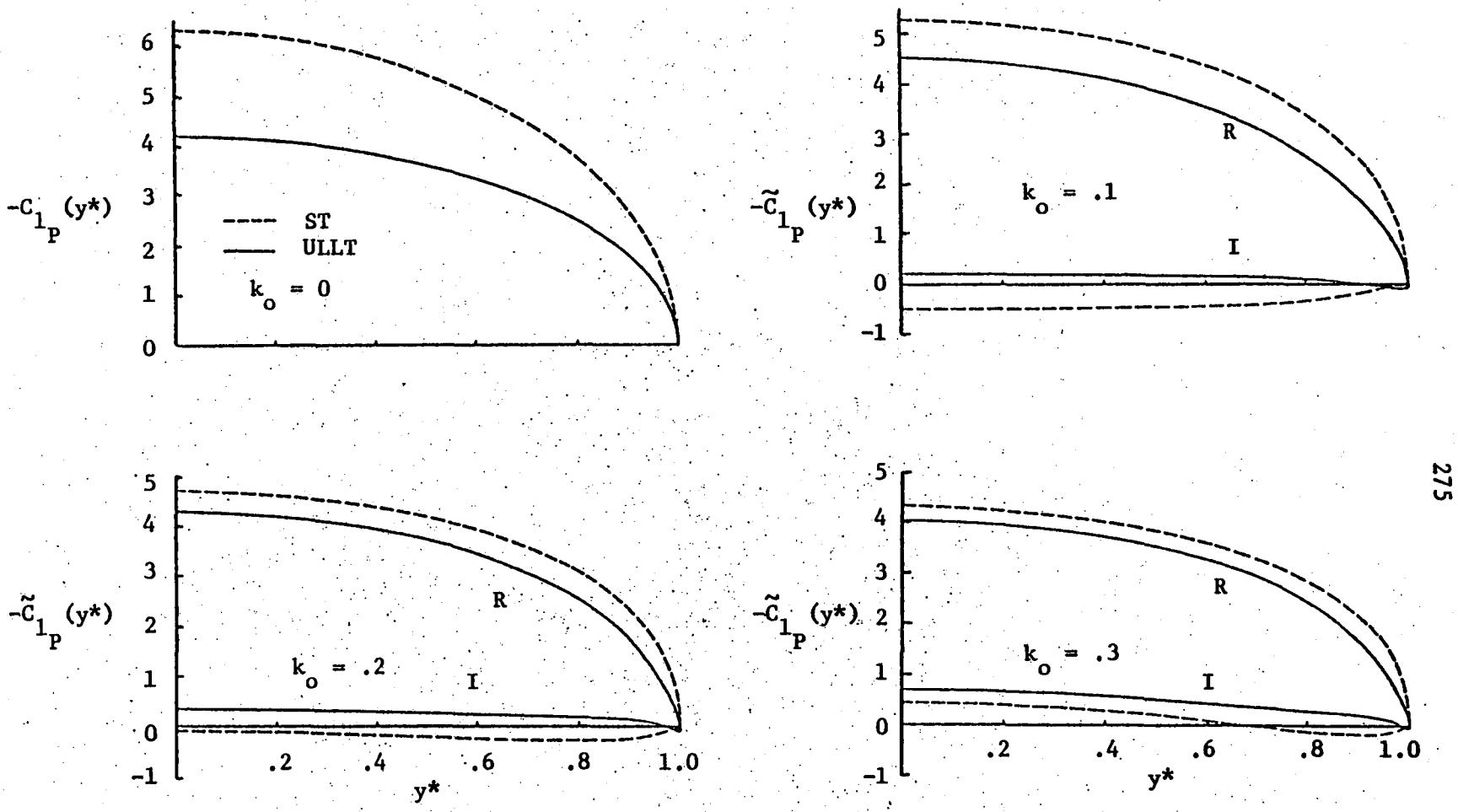

Figure 3.12. Spanwise lift distribution for an elliptic wing in pitch (A = 6).

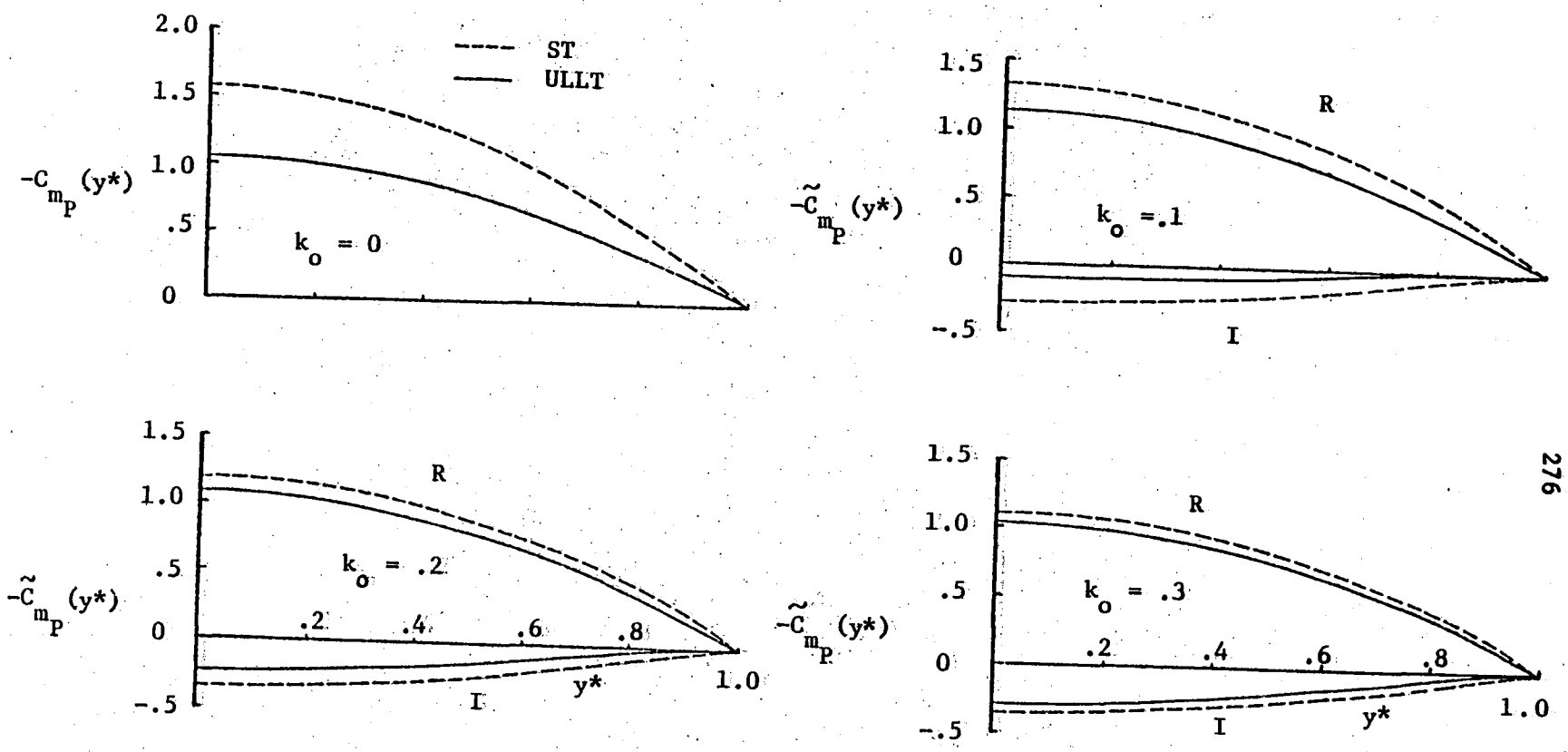

Figure 3.13. Spanwise moment distribution for an elliptic wing in pitch (A = 6).

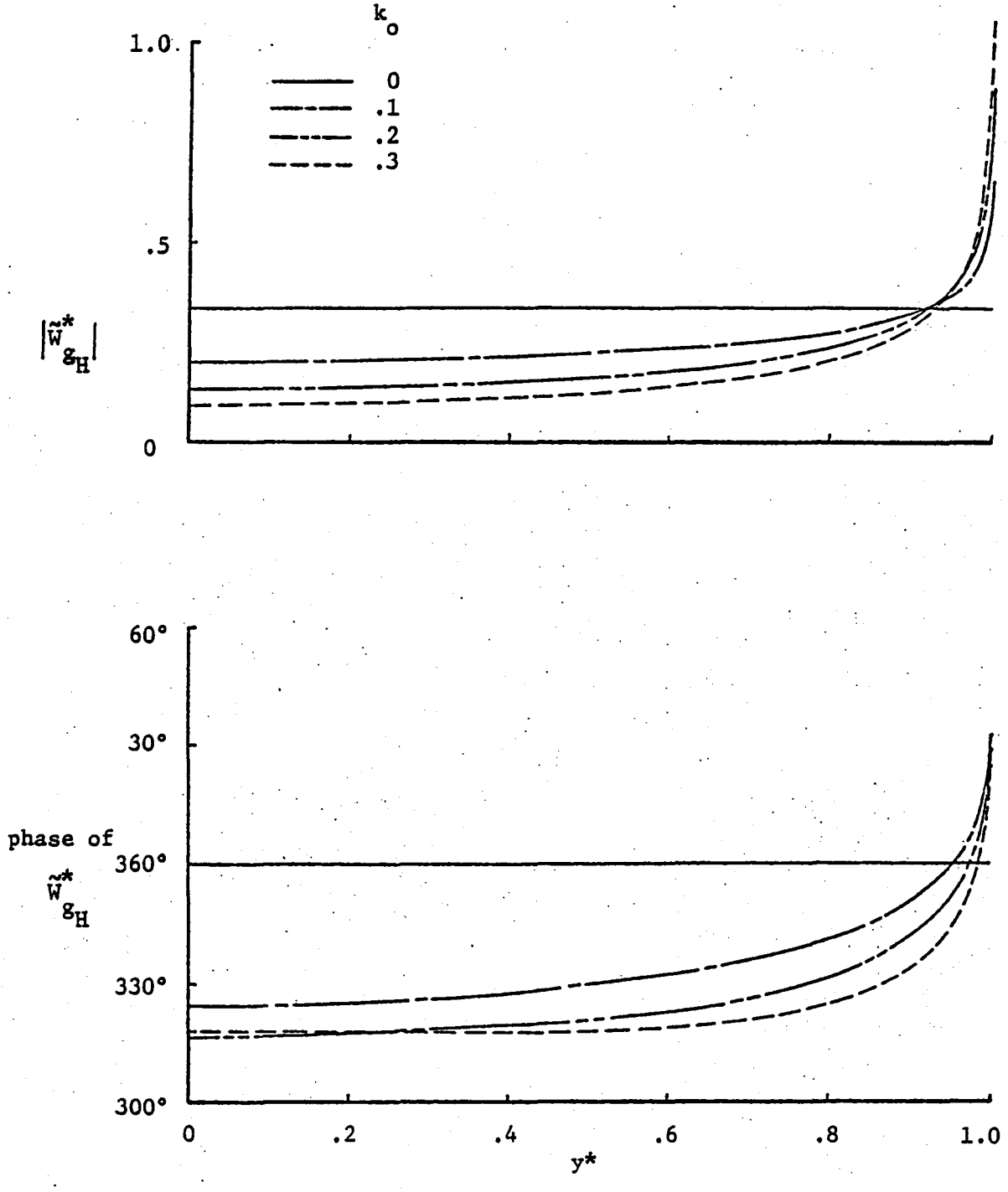

Figure 3.14. Amplitude and phase of $\tilde{\tilde{w}}^*_{g_H}$ for an elliptic wing in heave (A = 6).

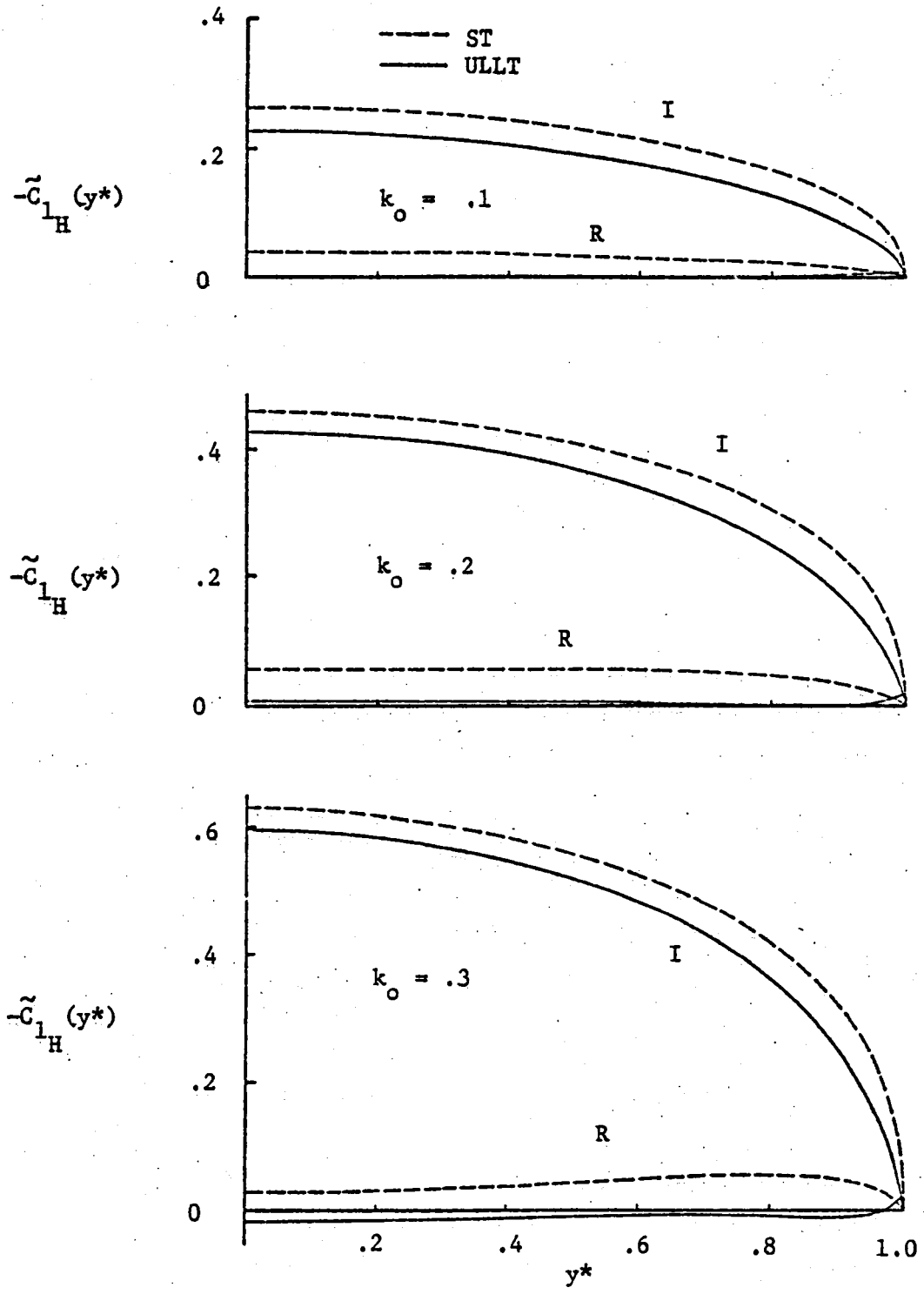

Figure 3.15. Spanwise lift distribution for an elliptic wing in heave (A = 6).

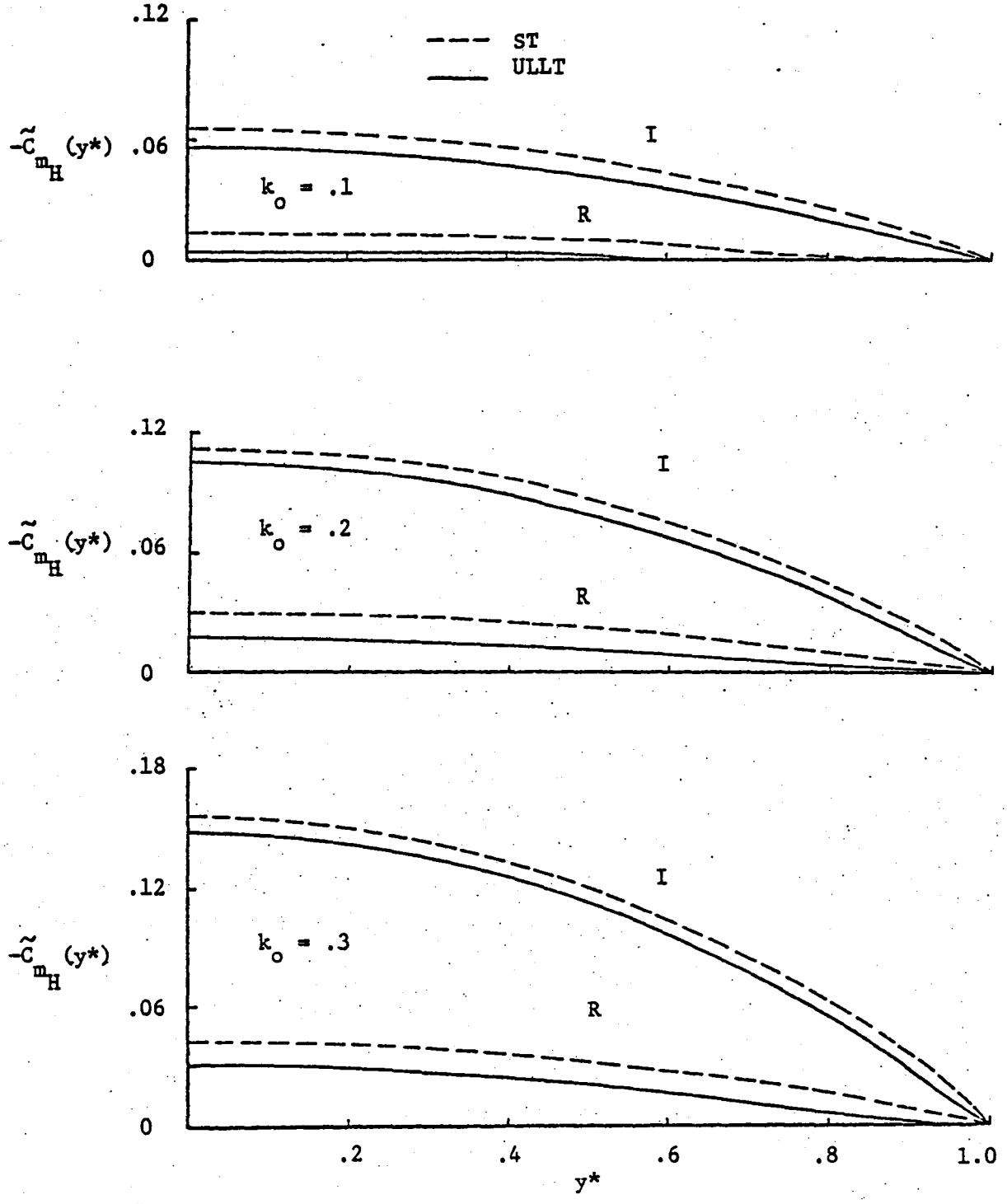

Figure 3.16. Spanwise moment distribution for an elliptic wing in heave (A = 6).

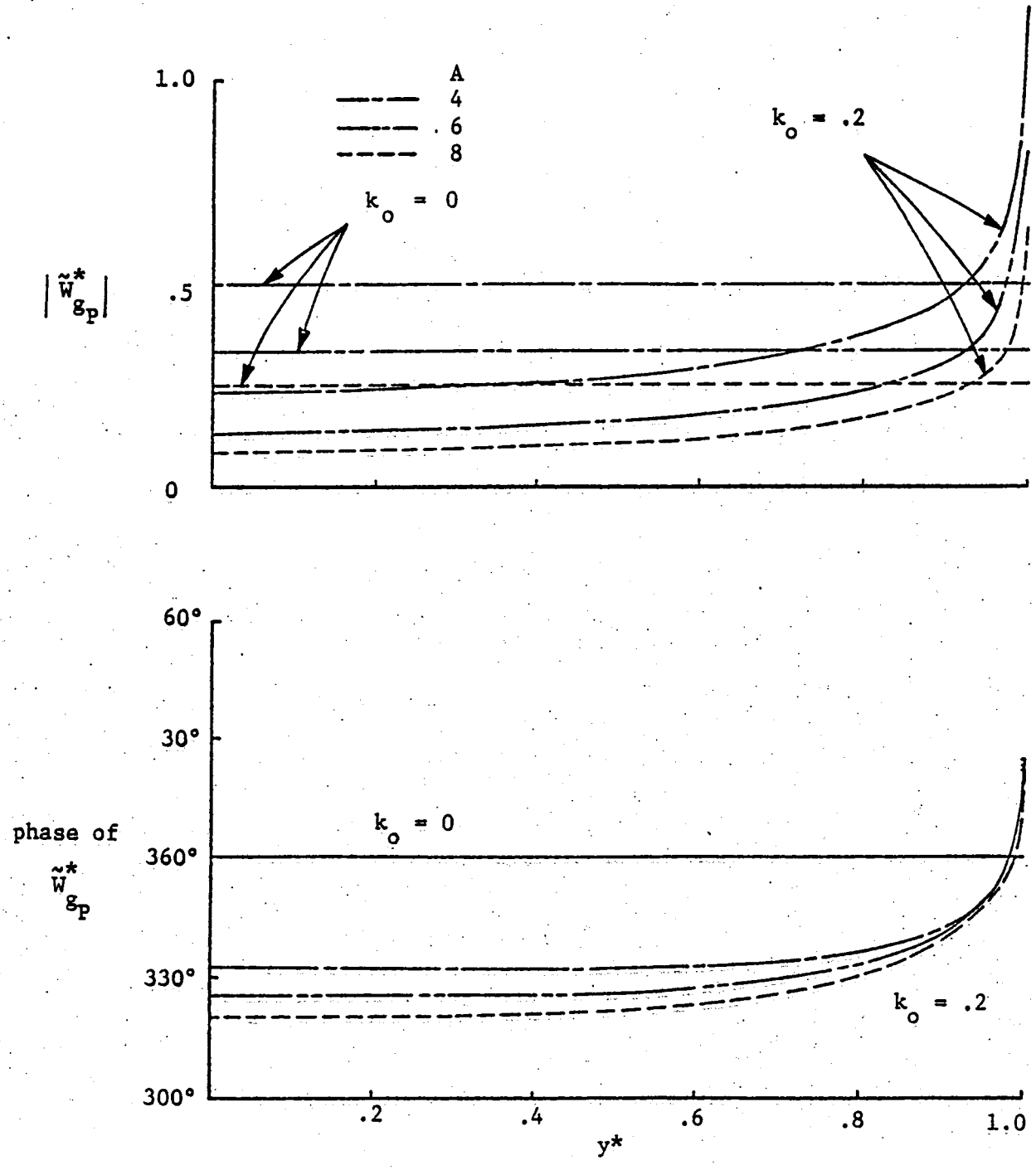

Figure 3.17. Amplitude and phase of $\tilde{W}^*_{g_p}$ for an elliptic wing in pitch (k_o = 0, .2).

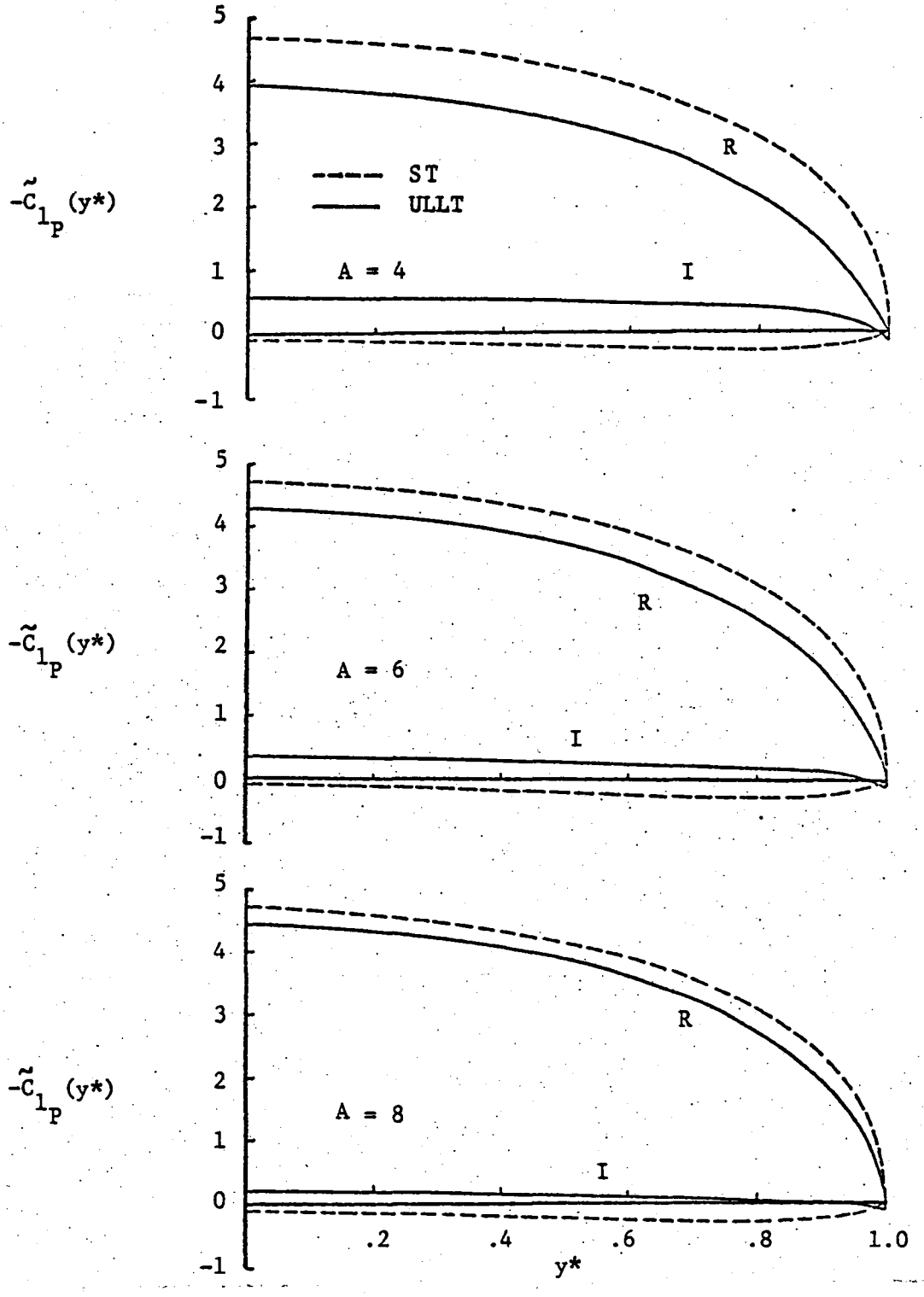

Figure 3.18. Spanwise lift distribution for an elliptic wing in pitch (k_o = .2).

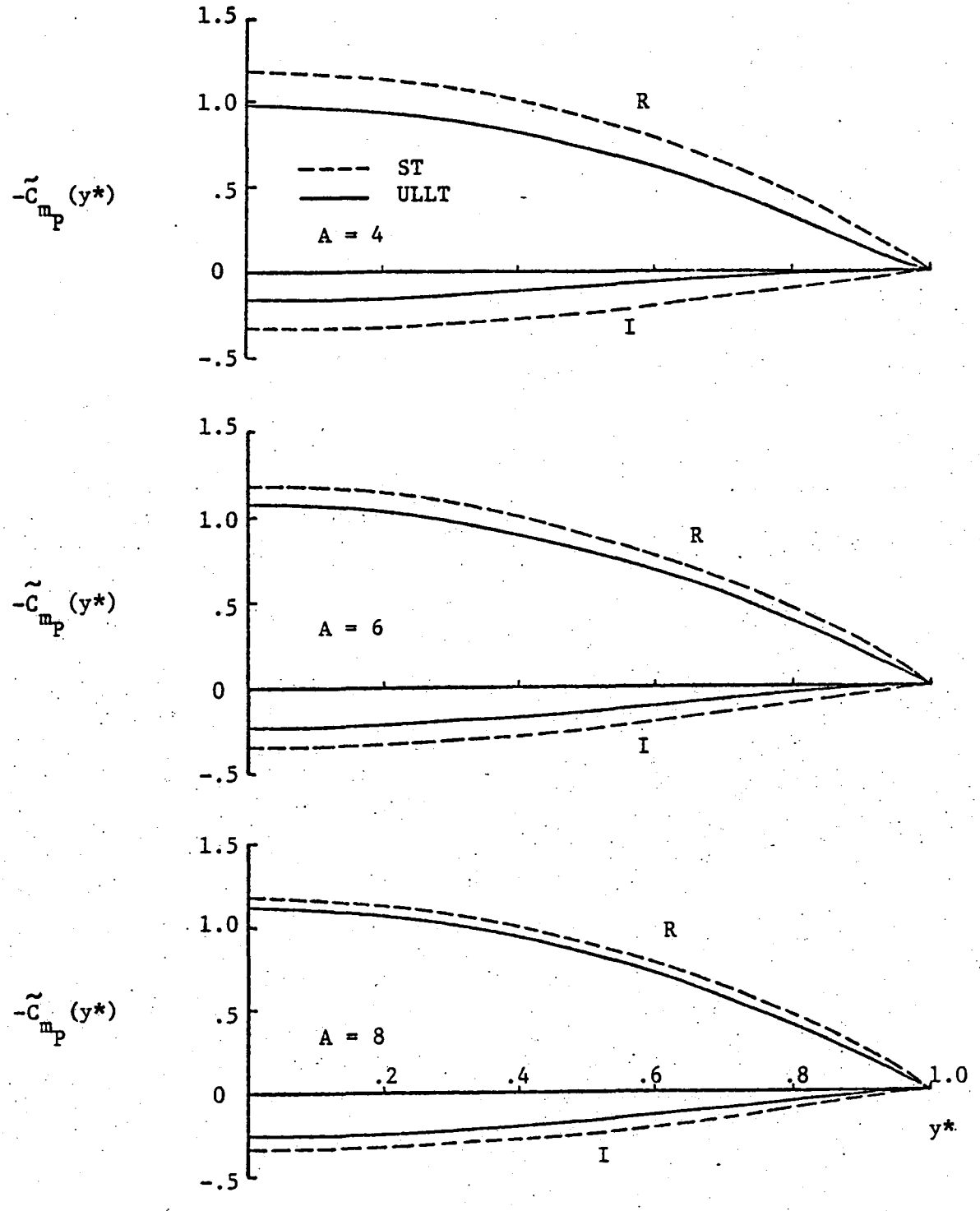

Figure 3.19. Spanwise moment distribution for an elliptic wing in pitch (k_o = .2).

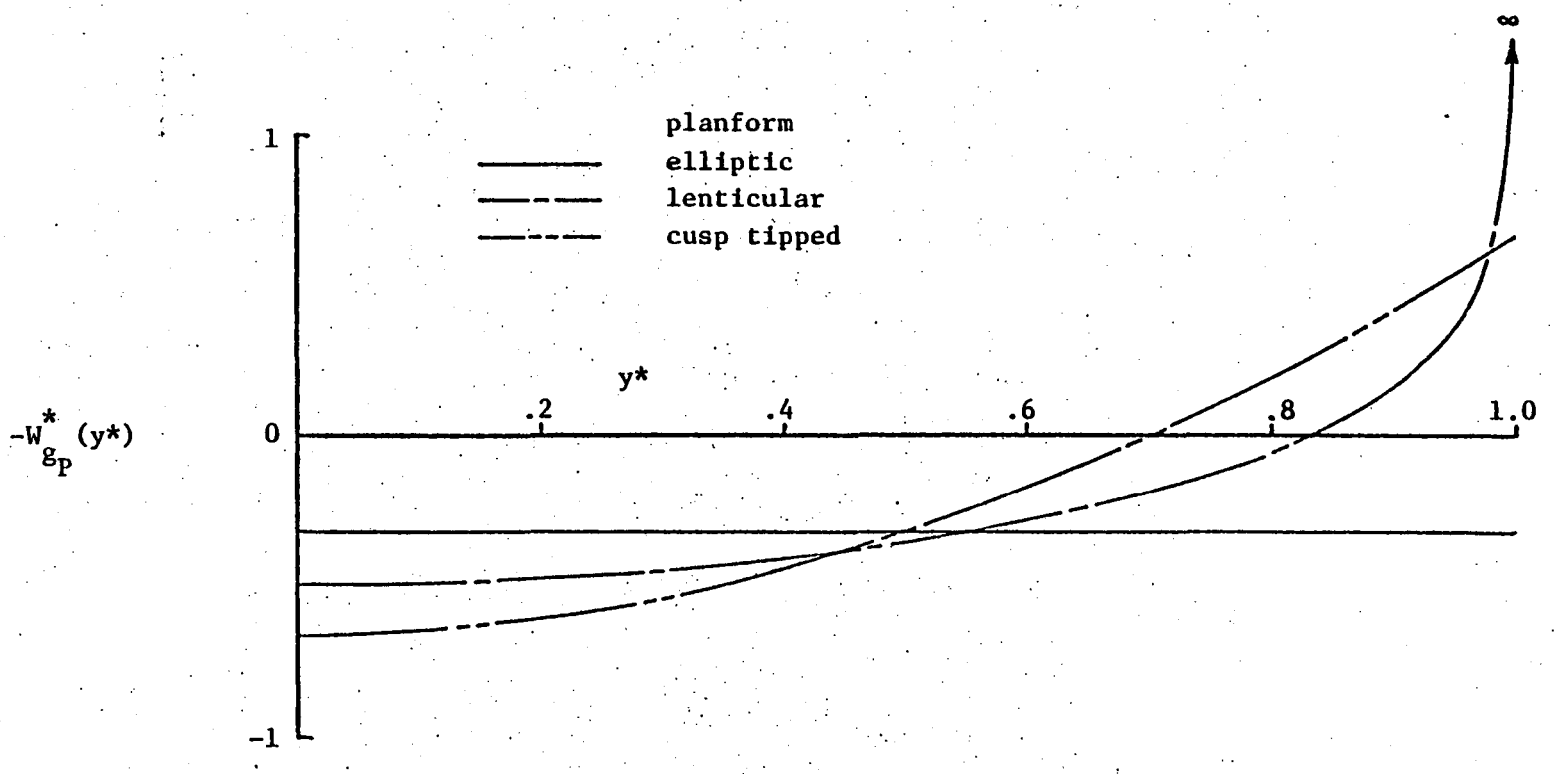

Figure 3.20. Spanwise distribution of induced downwash for a family of planforms in steady flow.

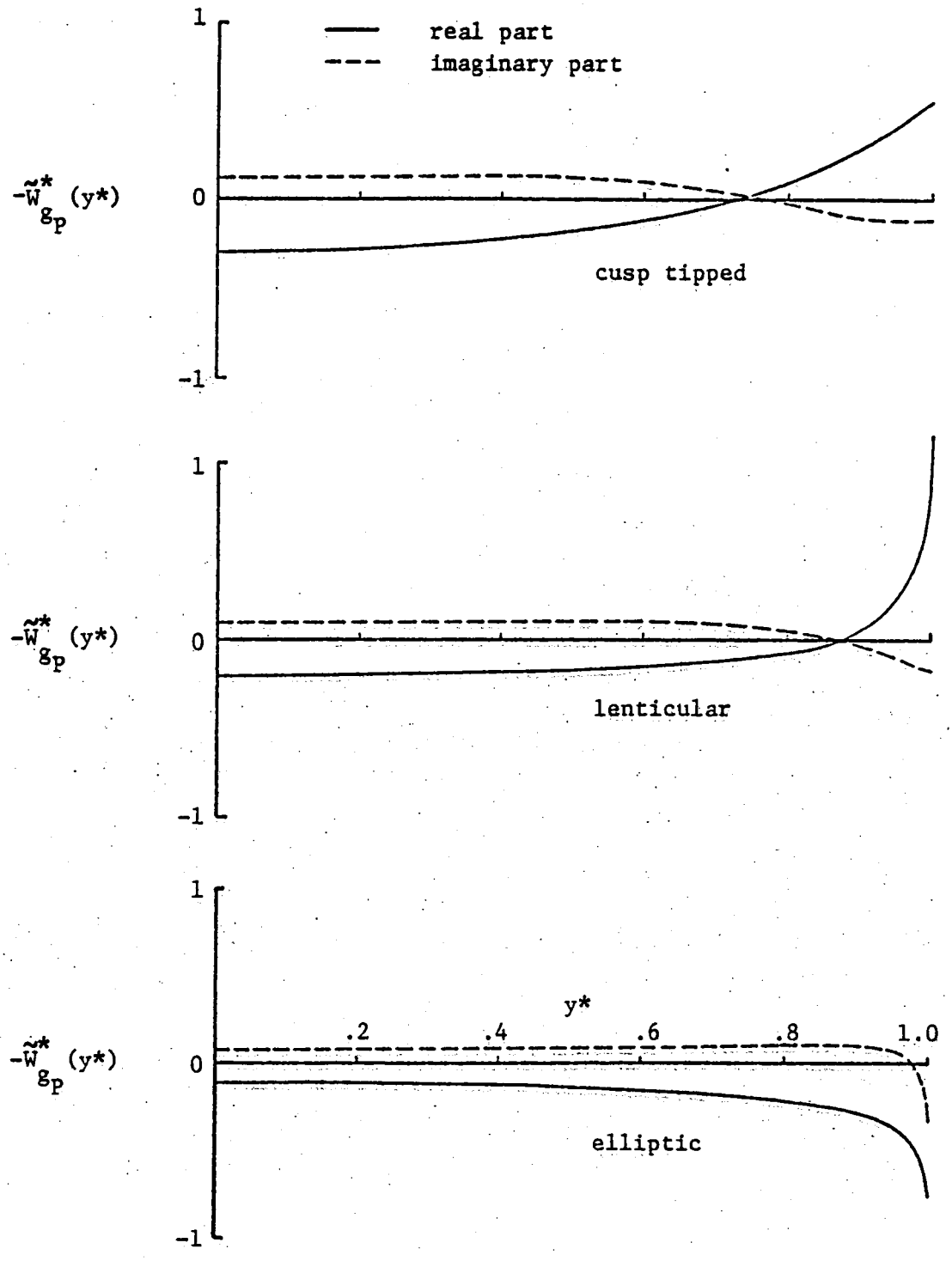

Figure 3.21. Spanwise distribution of $\tilde{W}^*_{g_p}$ for a wing in pitch (A = 6, k_o = .2).

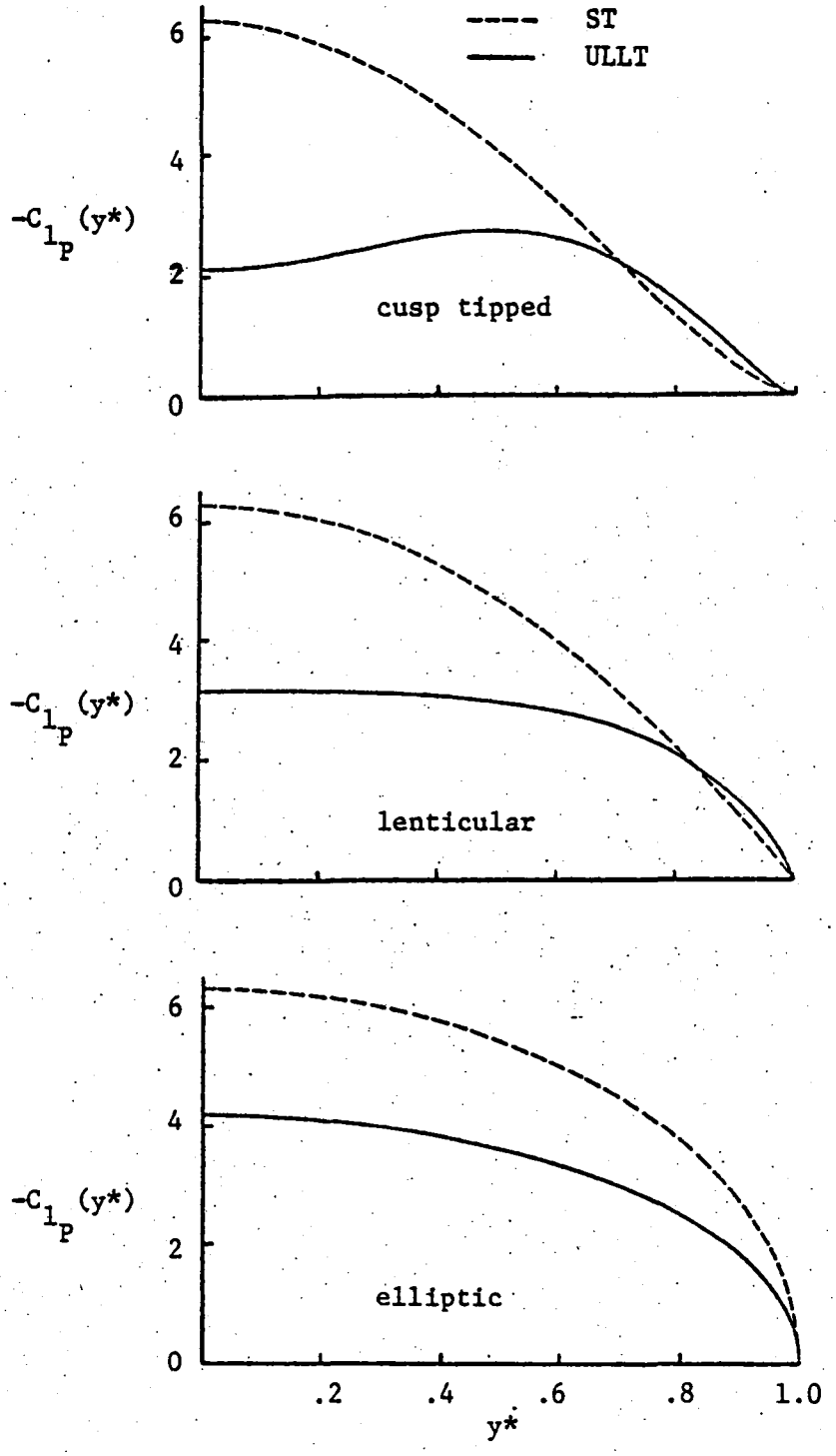

Figure 3.22. Spanwise lift distribution for a wing in steady flow (A = 6).

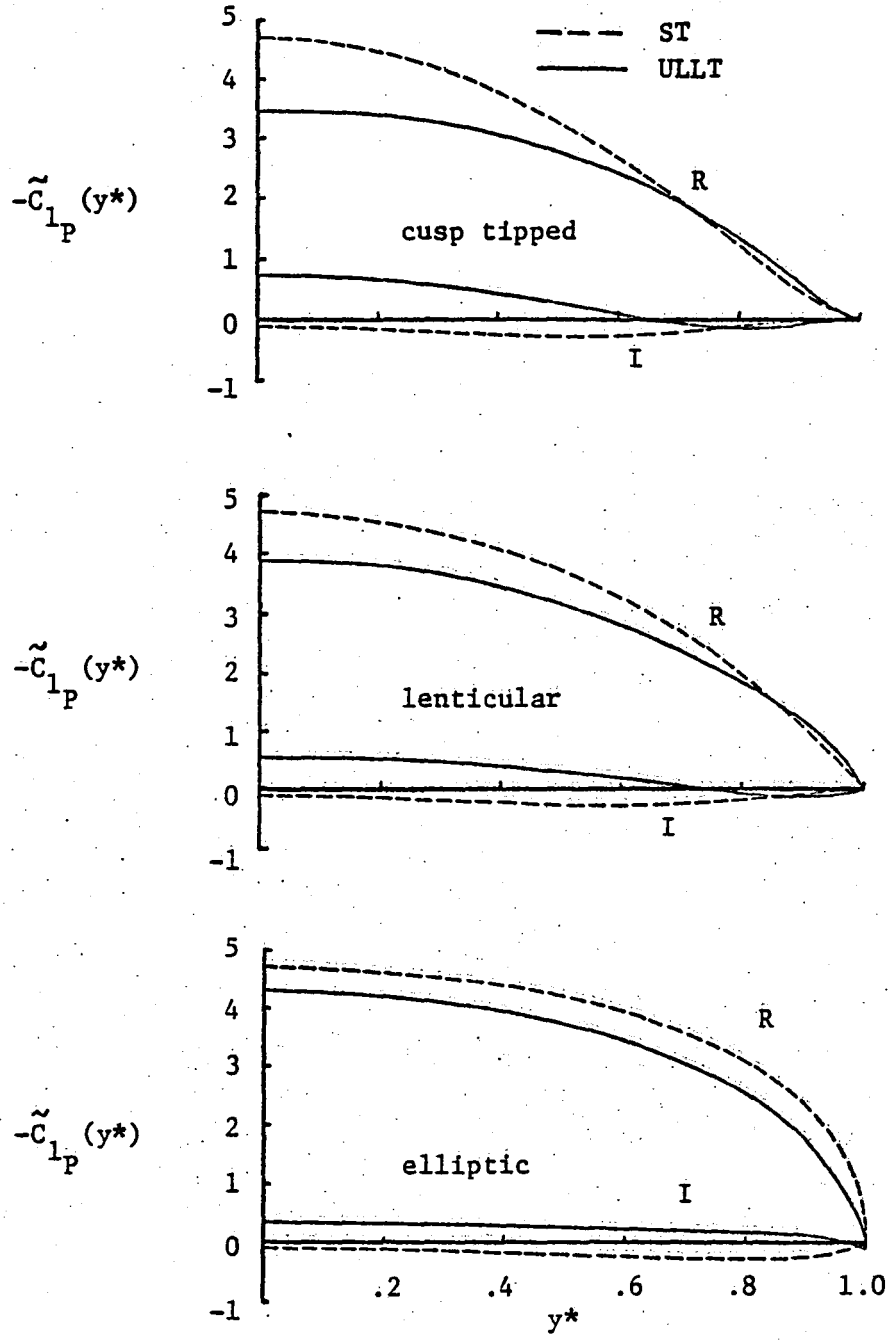

Figure 3.23. Spanwise lift distribution for a wing in pitch (A = 6, k_o = .2).

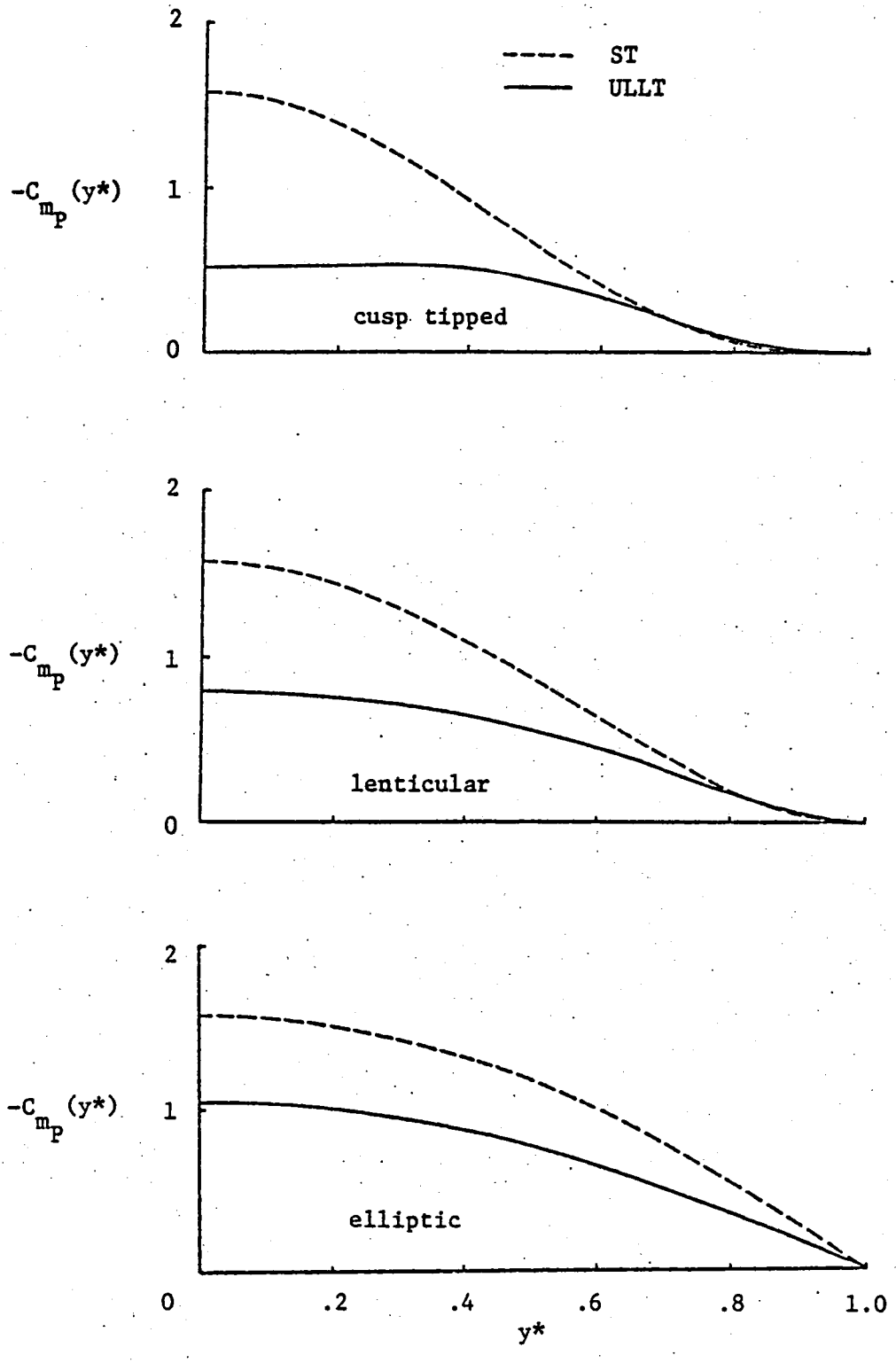

Figure 3.24. Spanwise moment distribution for a wing in steady flow (A = 6).

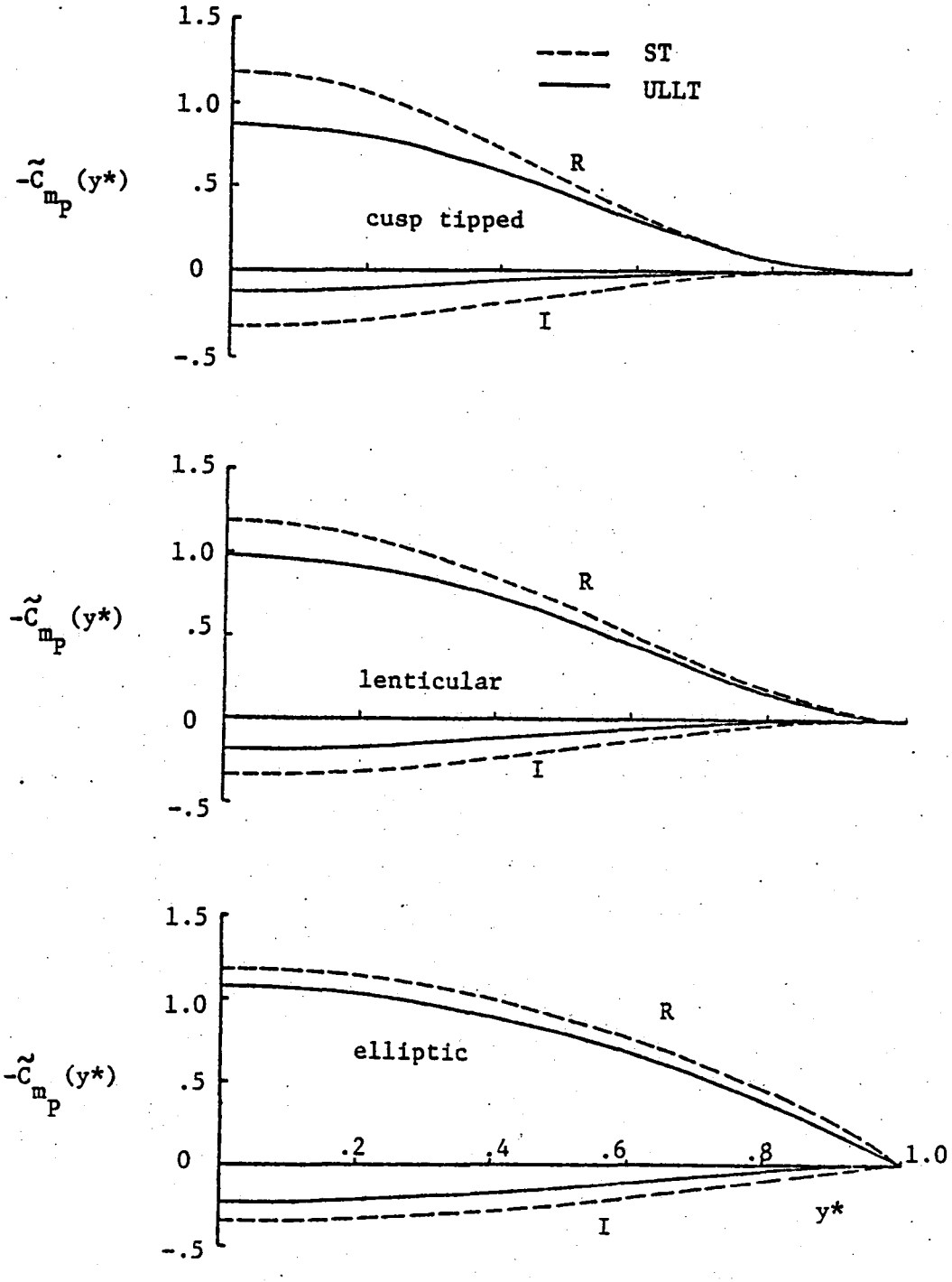

Figure 3.25. Spanwise moment distribution for a wing in pitch (A = 6, k_o = .2).

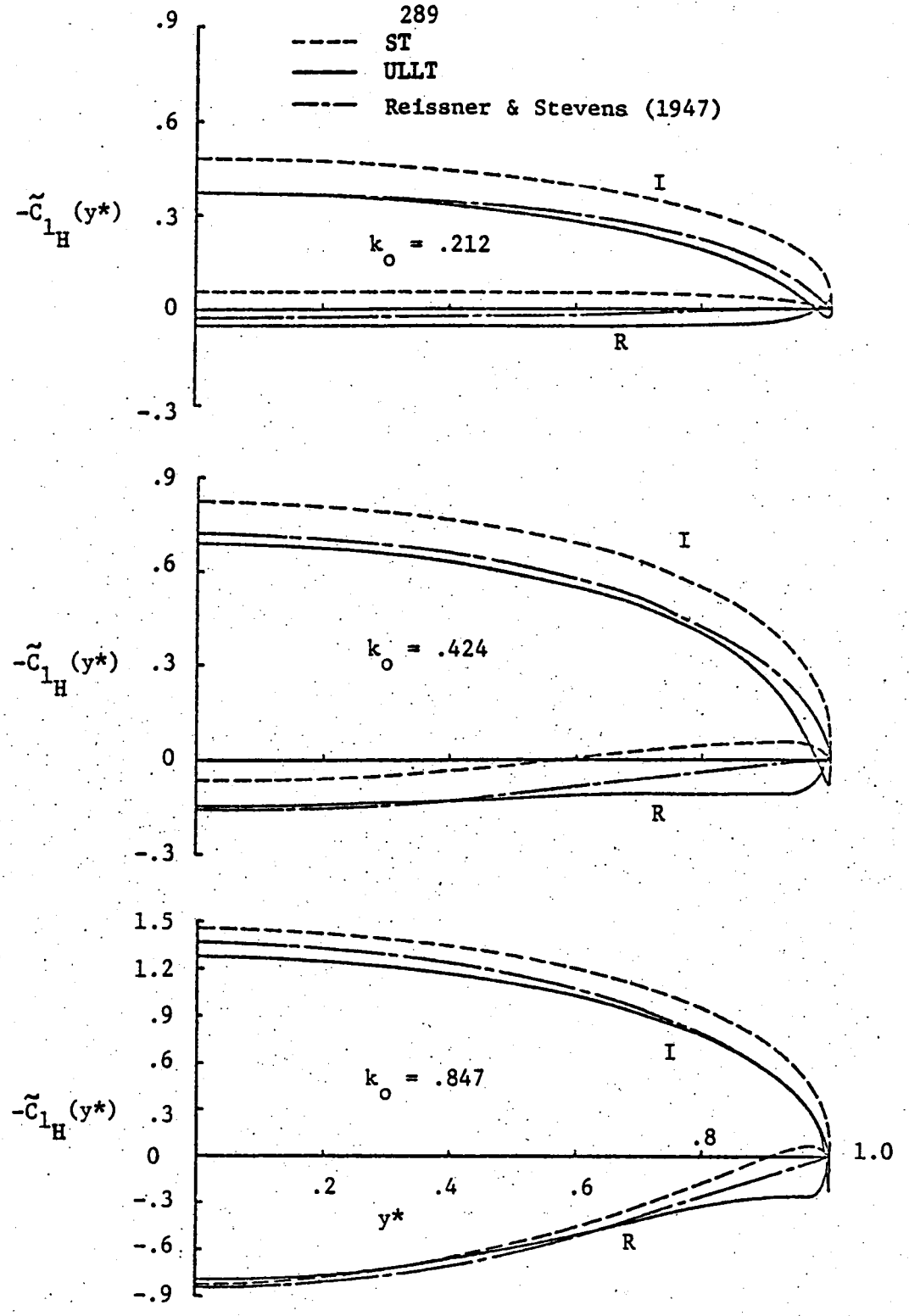

Figure 3.26. Spanwise lift distribution for an elliptic wing in heave (A = 3).

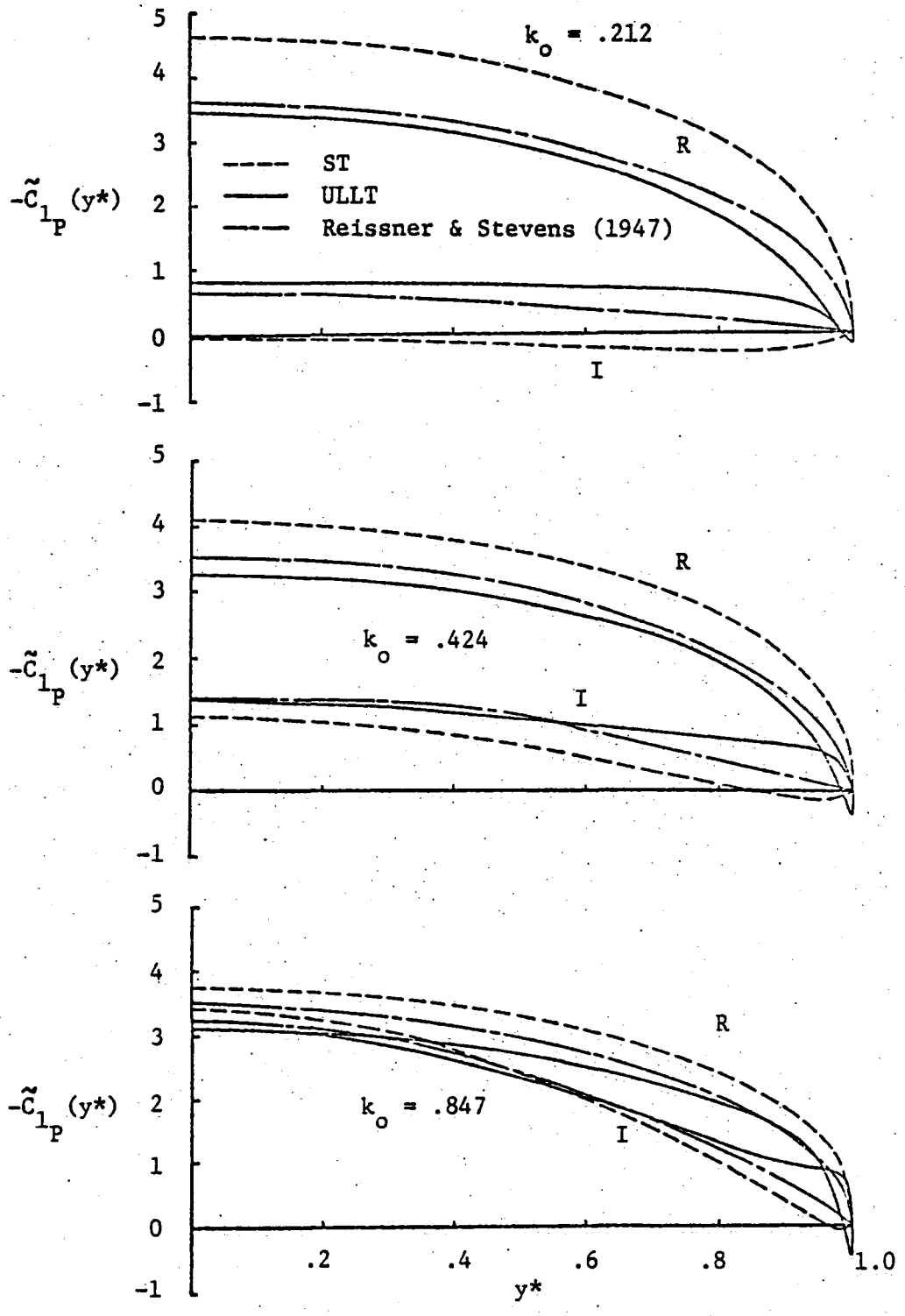

Figure 3.27. Spanwise lift distribution for an elliptic wing in pitch (A = 3 , k_o = .212, .424, .847).

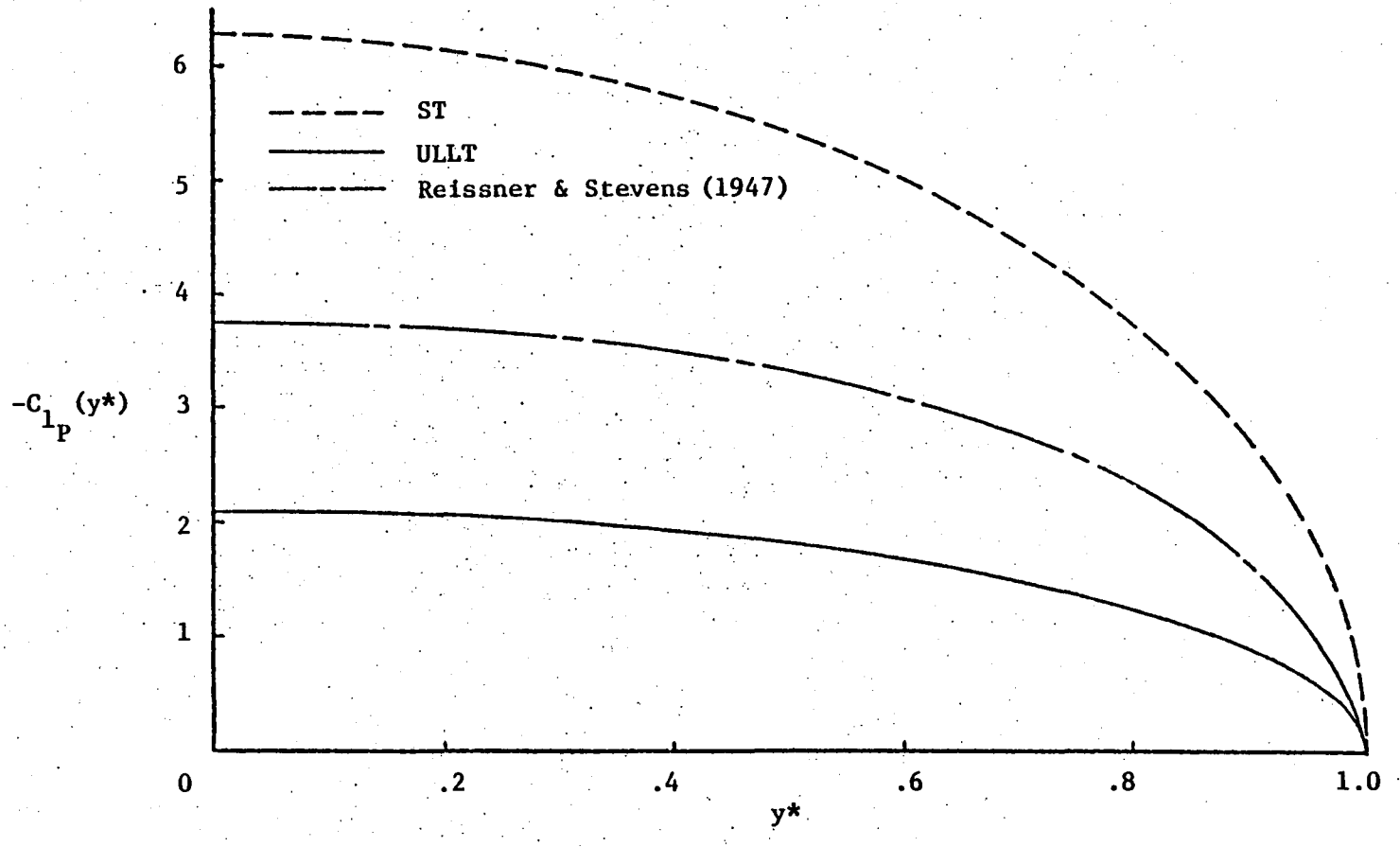

Figure 3.28. Spanwise lift distribution for an elliptic wing in steady flow (A = 3).

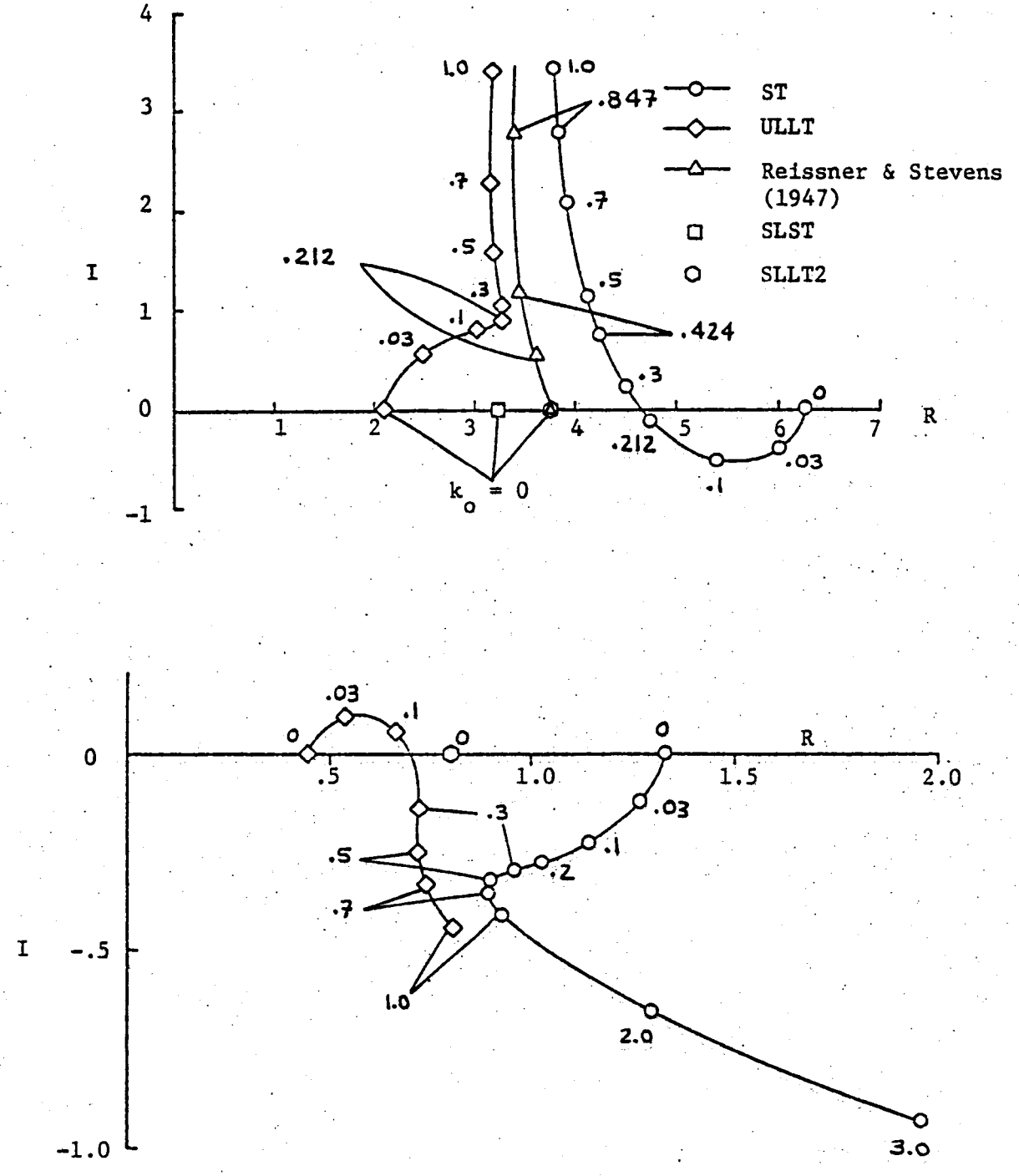

Figure 3.29. Complex vector diagram of $-\tilde{C}_{L_p}$ and $-\tilde{C}_{M_p}$ as a function of k_o for an elliptic wing in pitch (A = 3).

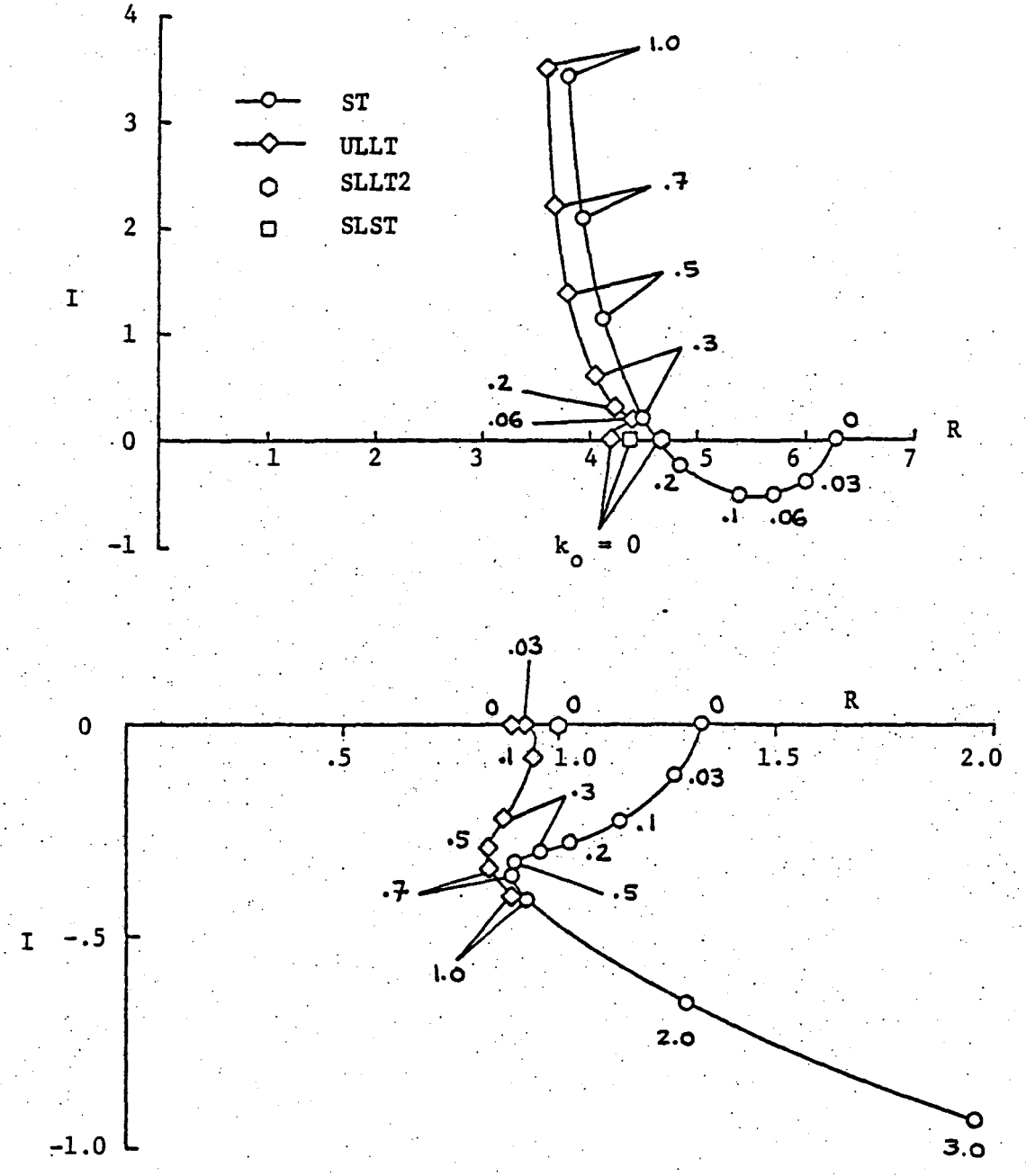

Figure 3.30. Complex vector diagram of $-\tilde{C}_{L_p}$ and $-\tilde{C}_{M_p}$ as a function of k_o for an elliptic wing in pitch (A = 6).

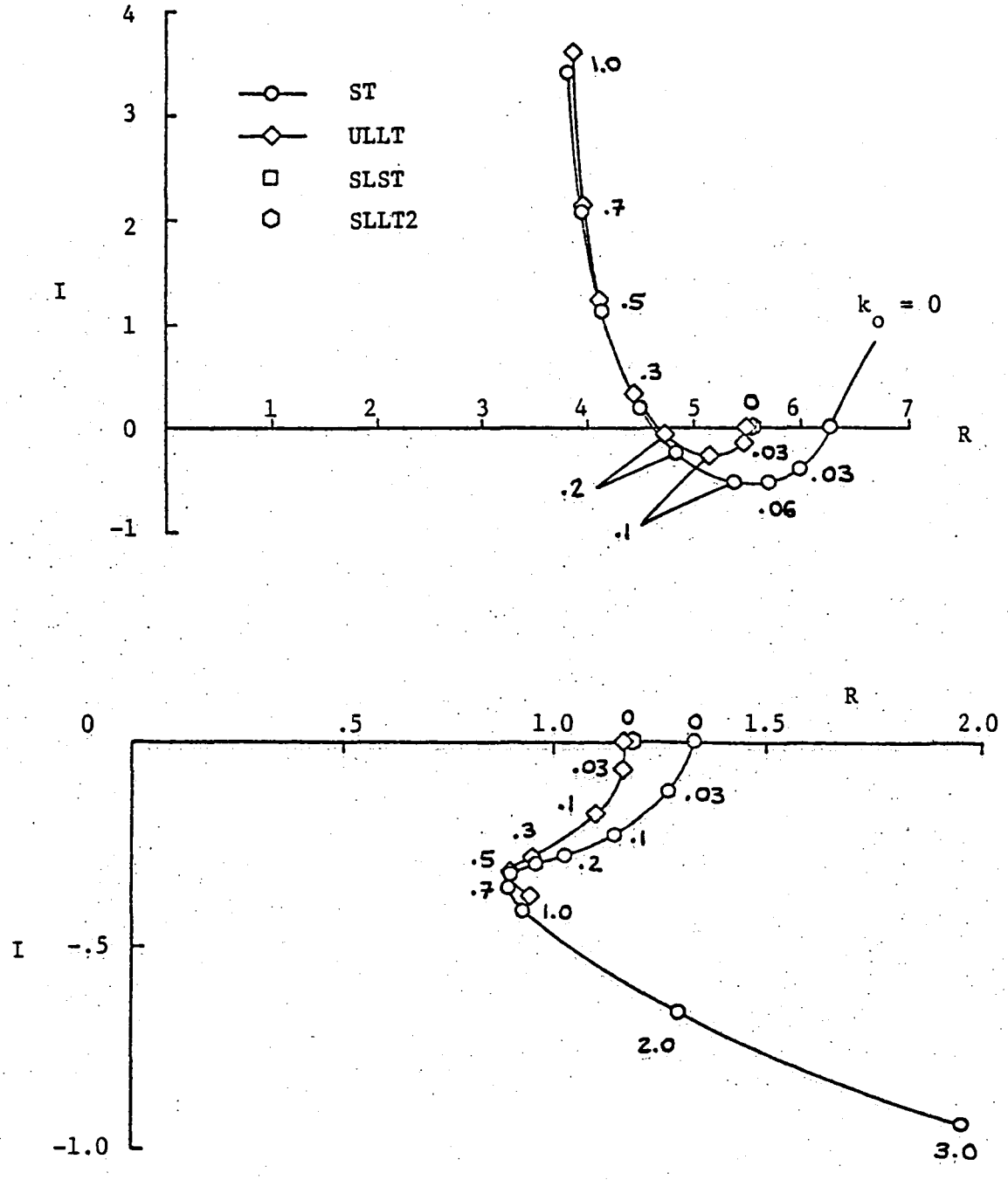

Figure 3.31. Complex vector diagram of $-\tilde{C}_{L_p}$ and $-\tilde{C}_{M_p}$ as a function of k_o for an elliptic wing in pitch (A = 16).

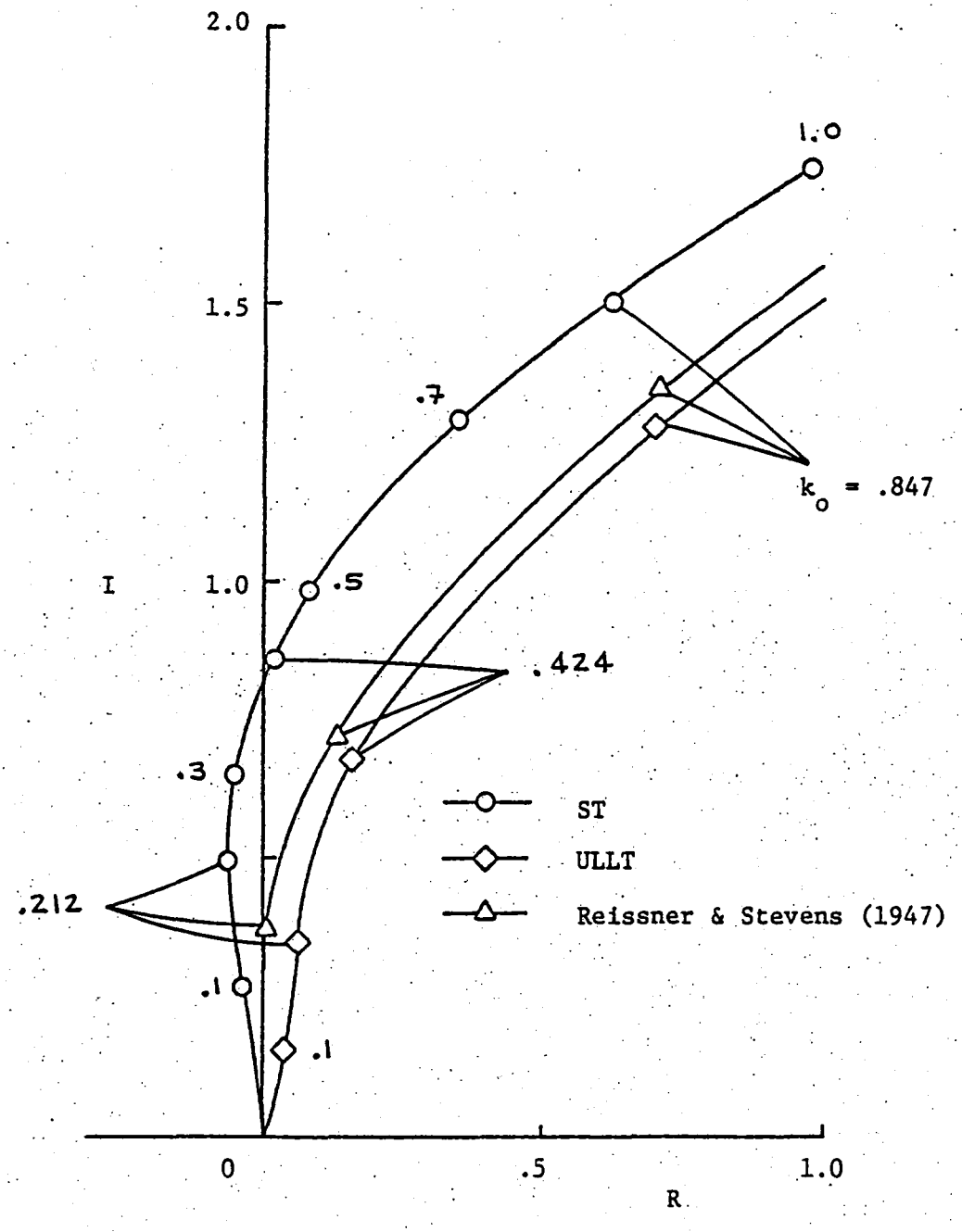

Figure 3.32. Complex vector diagram of $-\tilde{C}_{L_H}$ as a function of k_o for an elliptic wing in heave (A = 3).

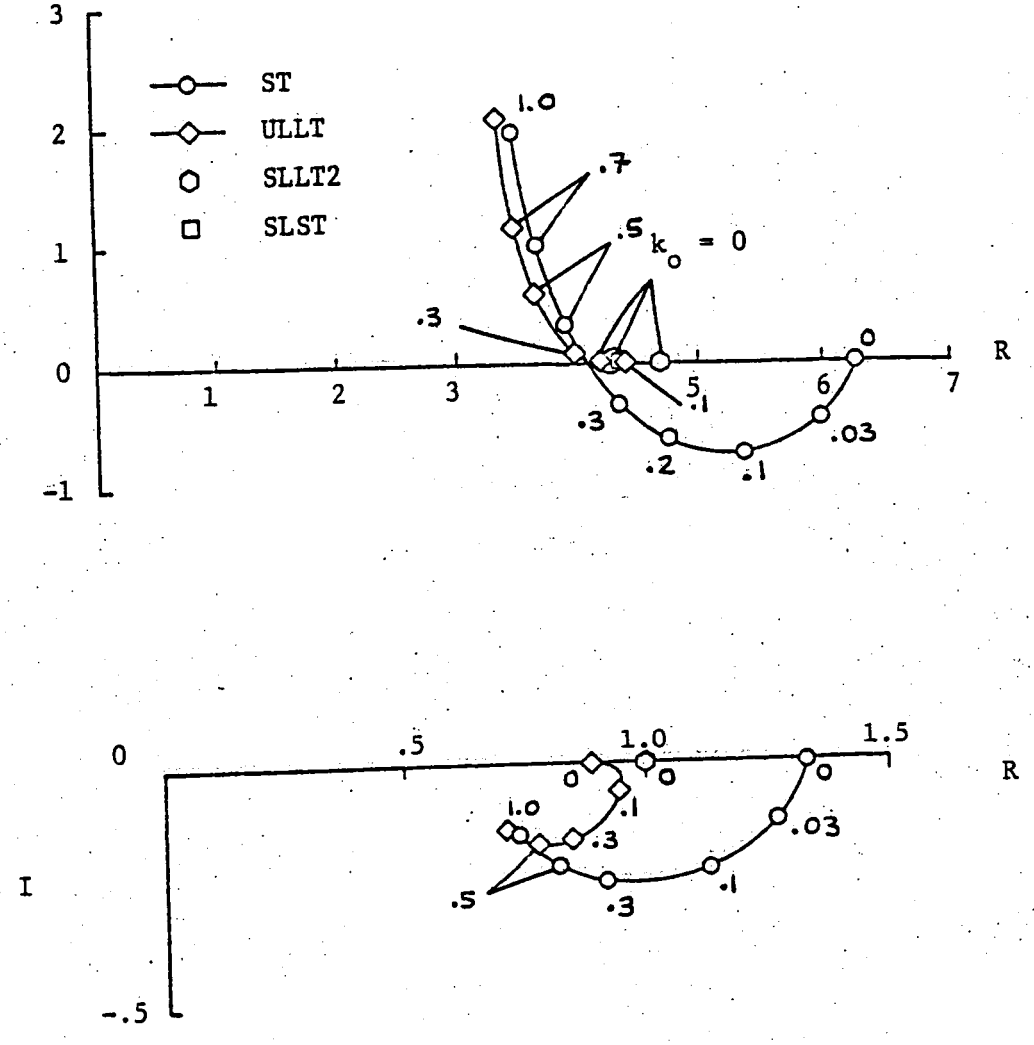

Figure 3.33. Complex vector diagram of $(-\tilde{C}_{L_H}/\frac{1}{2} j k_o)$ and $(-\tilde{C}_{M_H}/\frac{1}{2} j k_o)$ as a function of k_o for an elliptic wing in heave (A = 6).

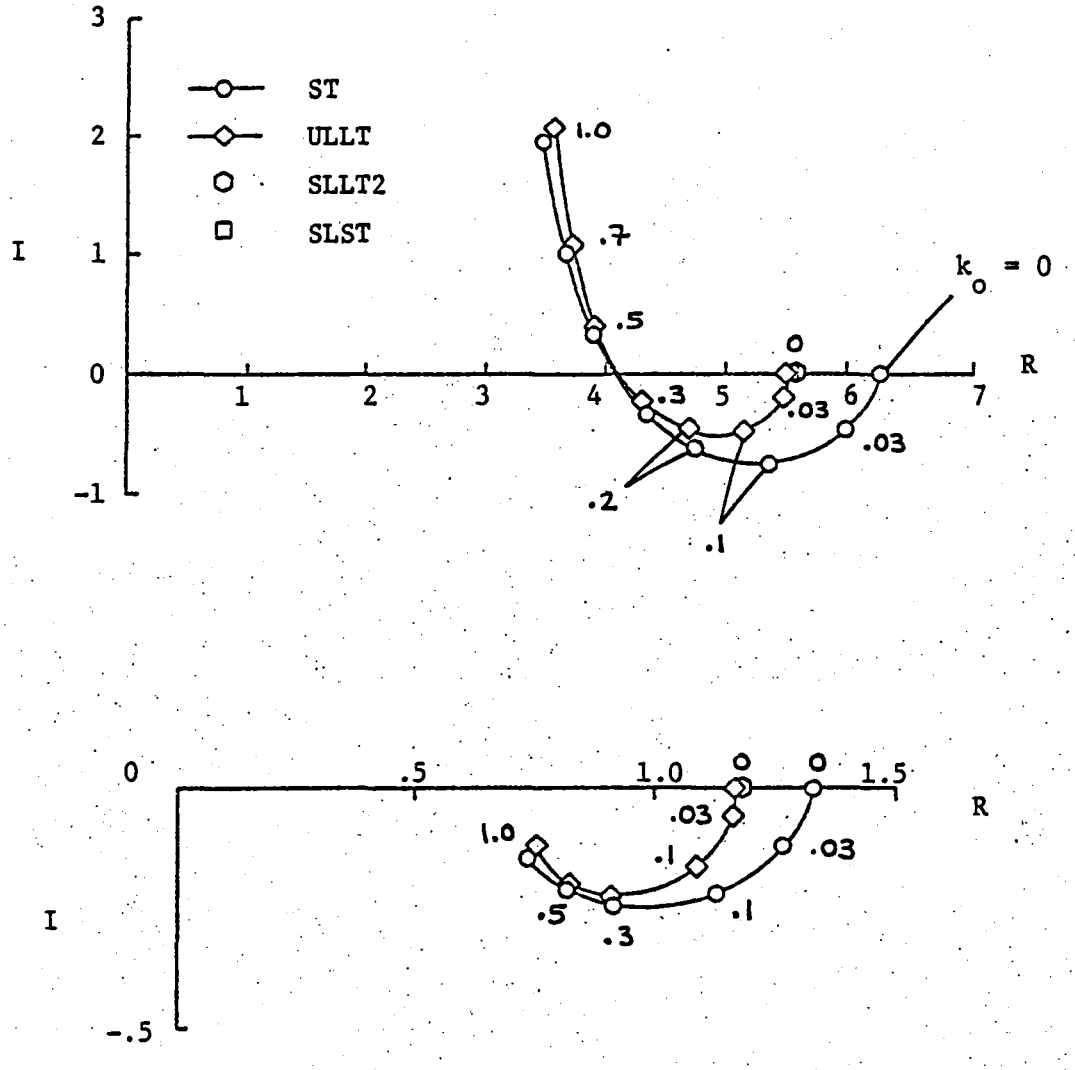

Figure 3.34. Complex vector diagram of $(-\tilde{C}_{L_H}/\frac{1}{2} j k_o)$ and $(-\tilde{C}_{M_H}/\frac{1}{2} j k_o)$ as a function of k_o for an elliptic wing in heave (A = 16).

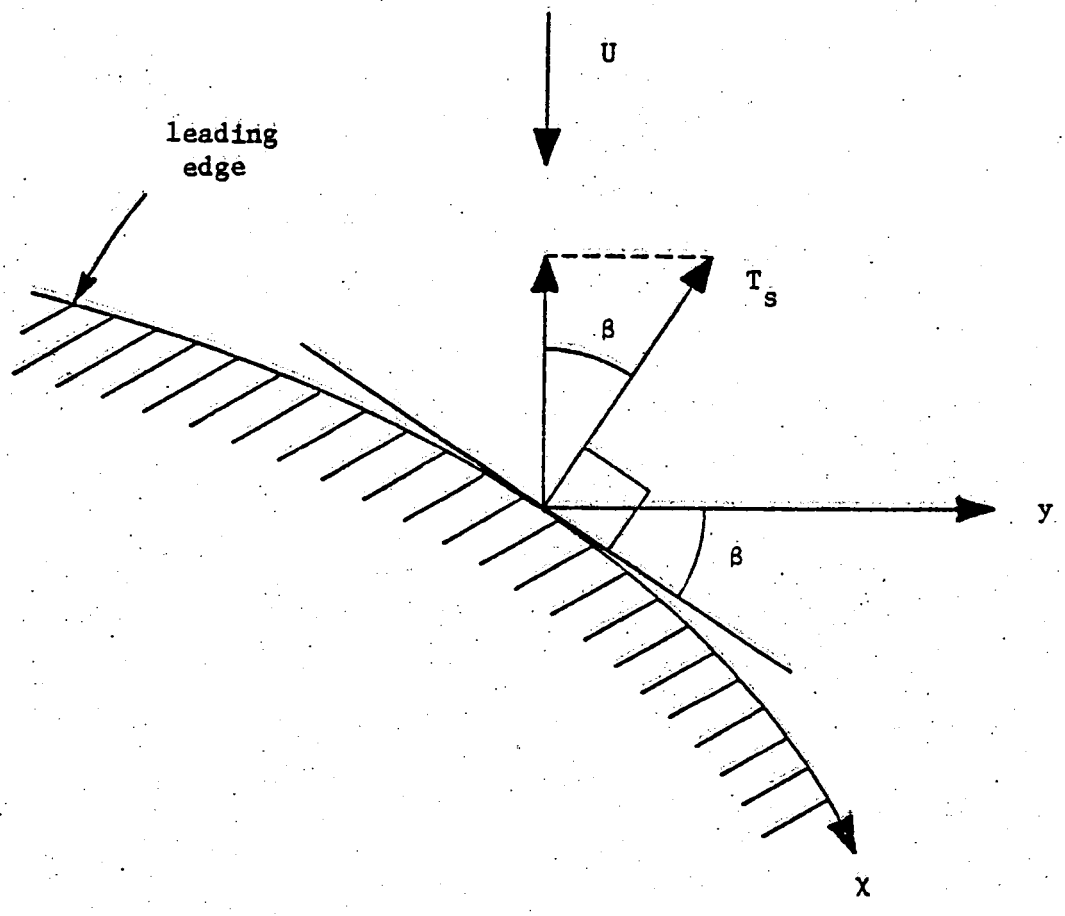

Figure 4.1. Leading-edge suction force.

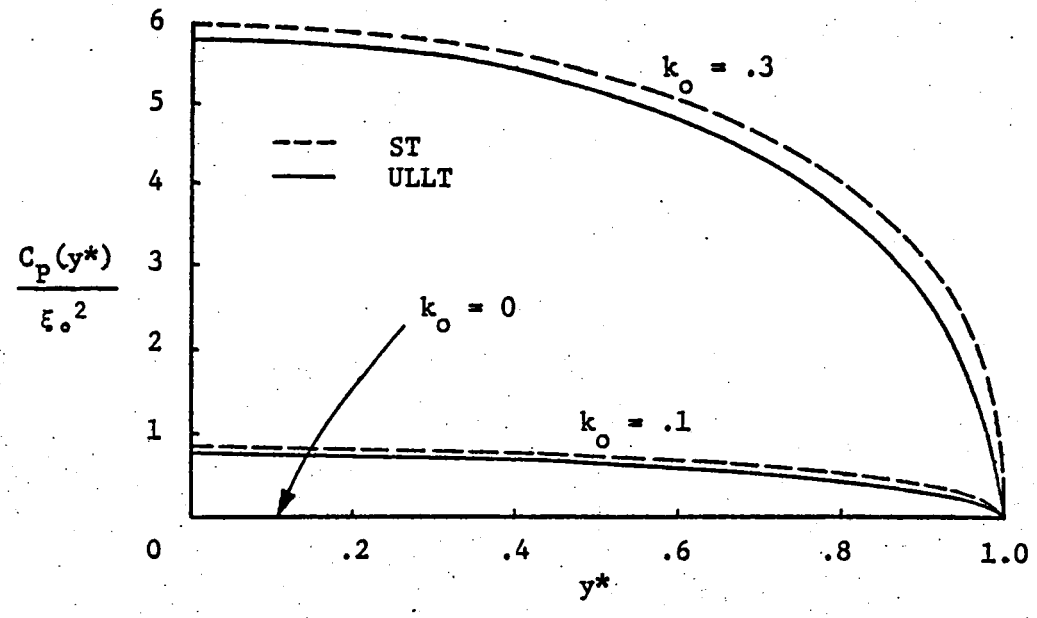

Figure 4.2. Spanwise distribution of required power for an elliptic wing in heave (A = 8).

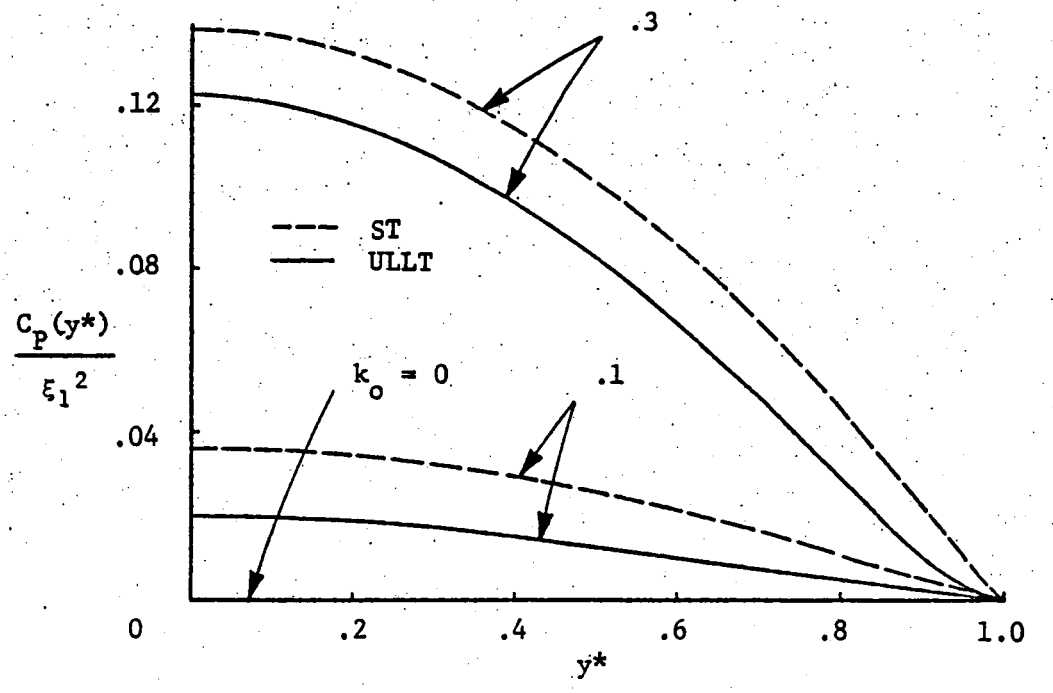

Figure 4.3. Spanwise distribution of required power for an elliptic wing in pitch (A = 8).

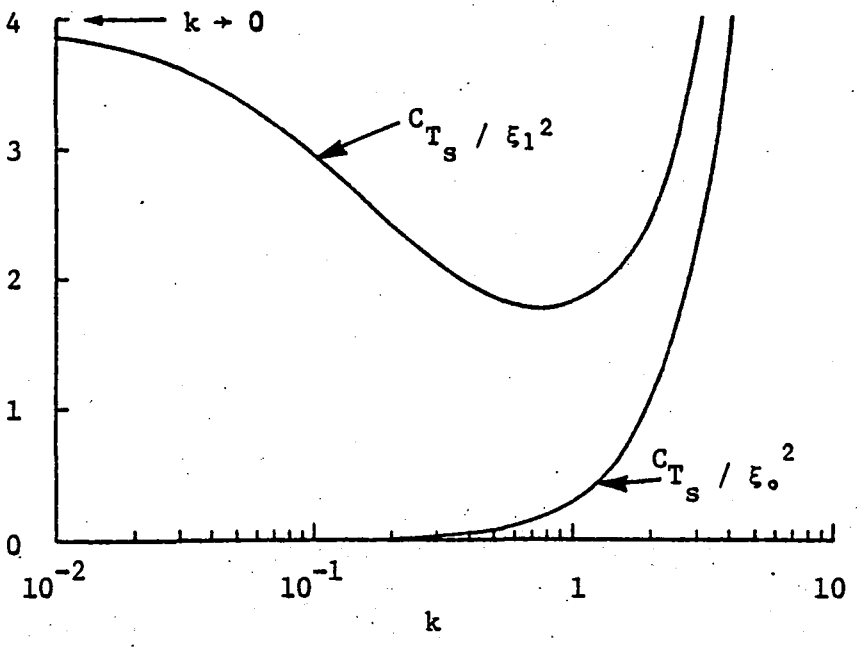

Figure 4.4. Leading-edge suction force for an airfoil in pitch and heave.

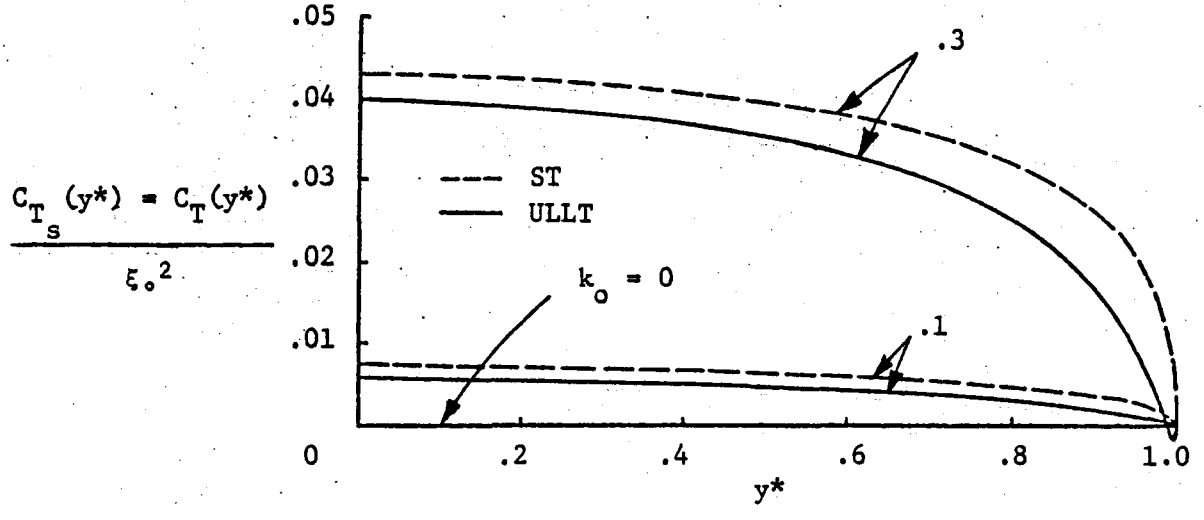

Figure 4.5. Spanwise distribution of leading-edge suction force or thrust for an elliptic wing in heave (A = 8).

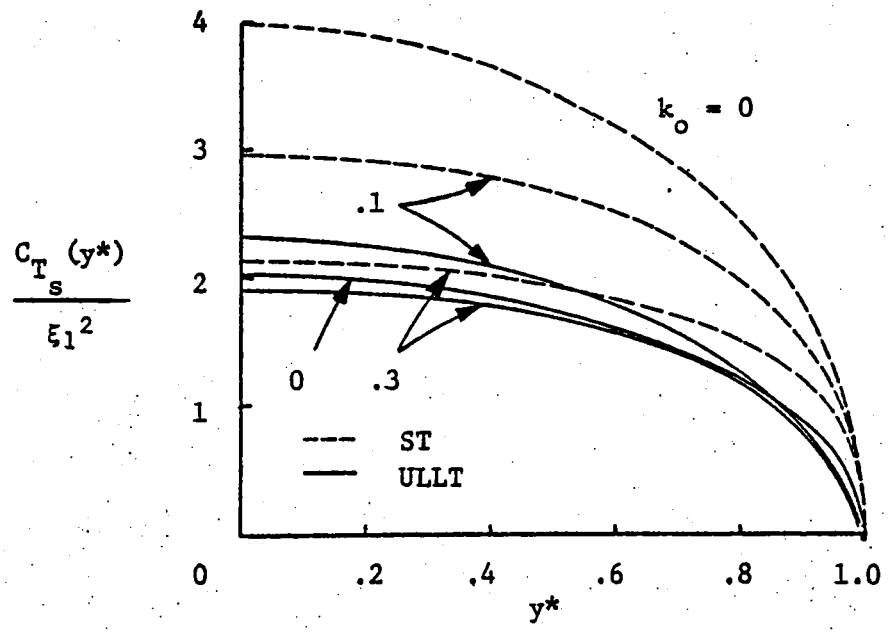

Figure 4.6. Spanwise distribution of leading-edge suction force for an elliptic wing in pitch (A = 8).

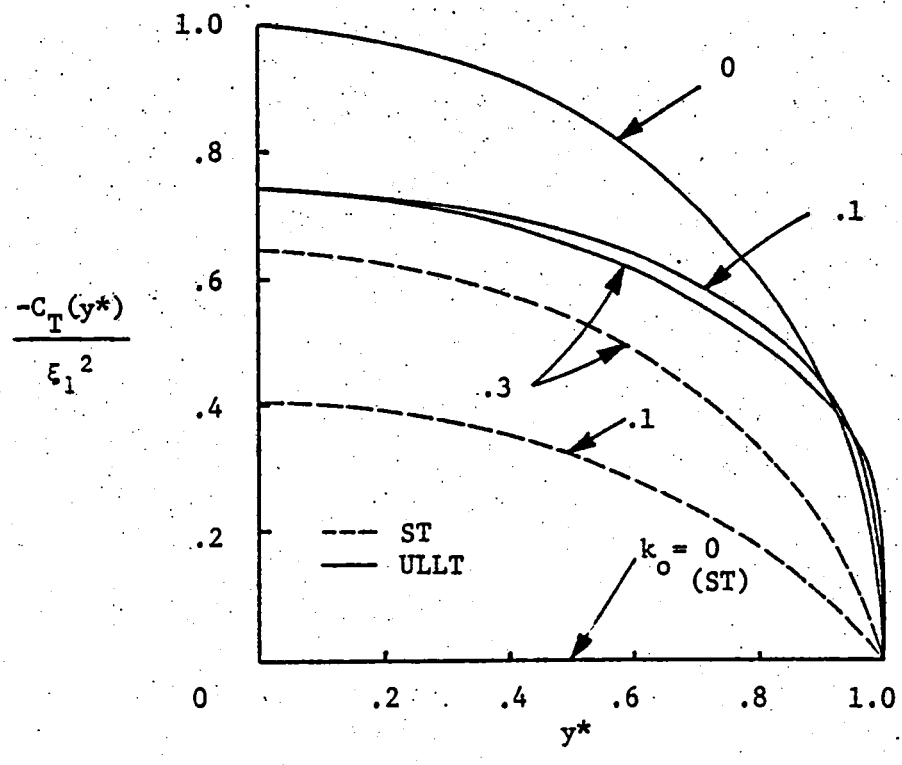

Figure 4.7. Spanwise distribution of section thrust (drag) for an elliptic wing in pitch (A = 8).

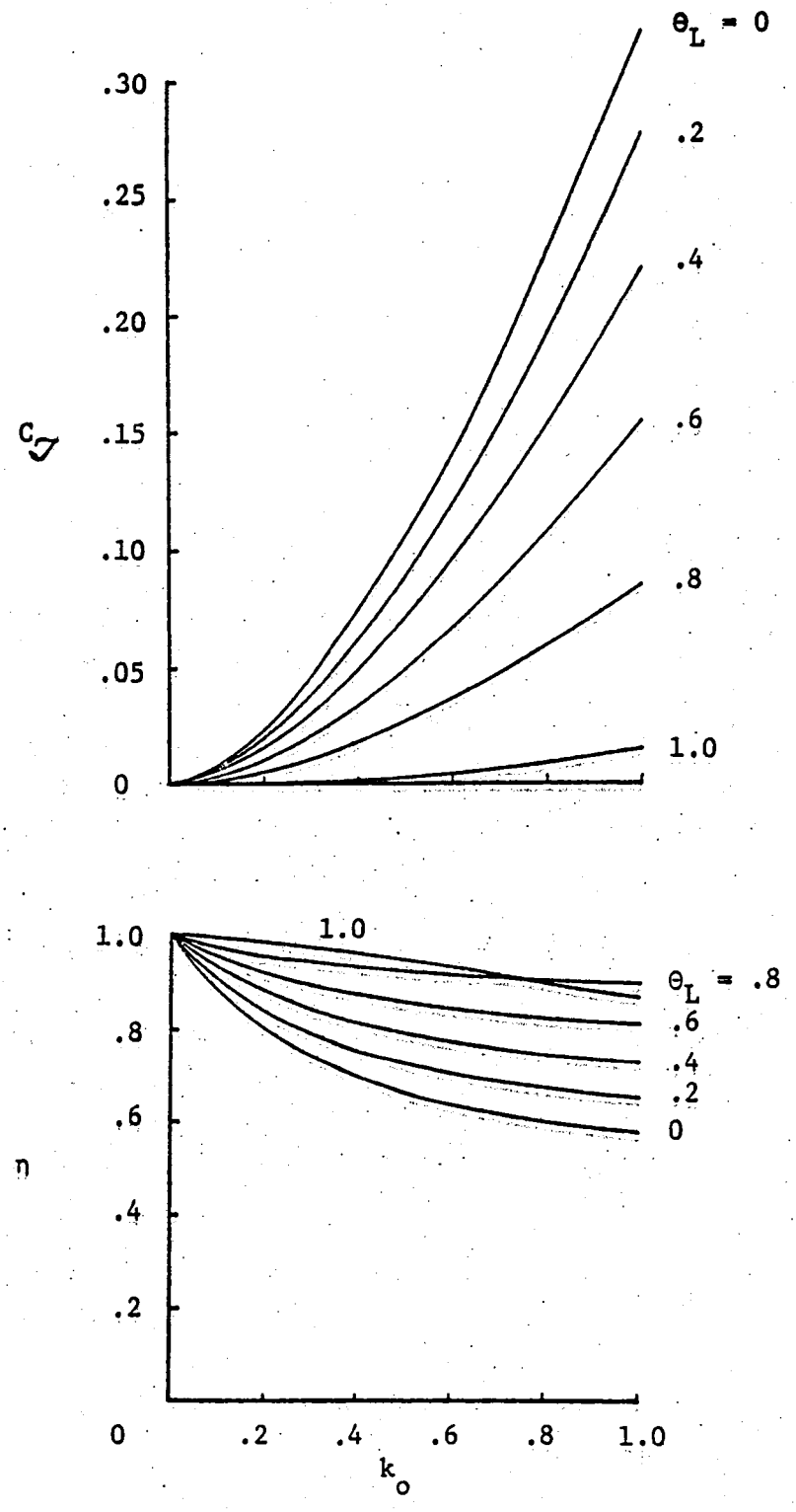

Figure 4.8. Strip-theory values of thrust coefficient and hydrodynamic efficiency for an elliptic wing for several values of feathering parameter with pitch axis located at 3/4 of center-section chord.

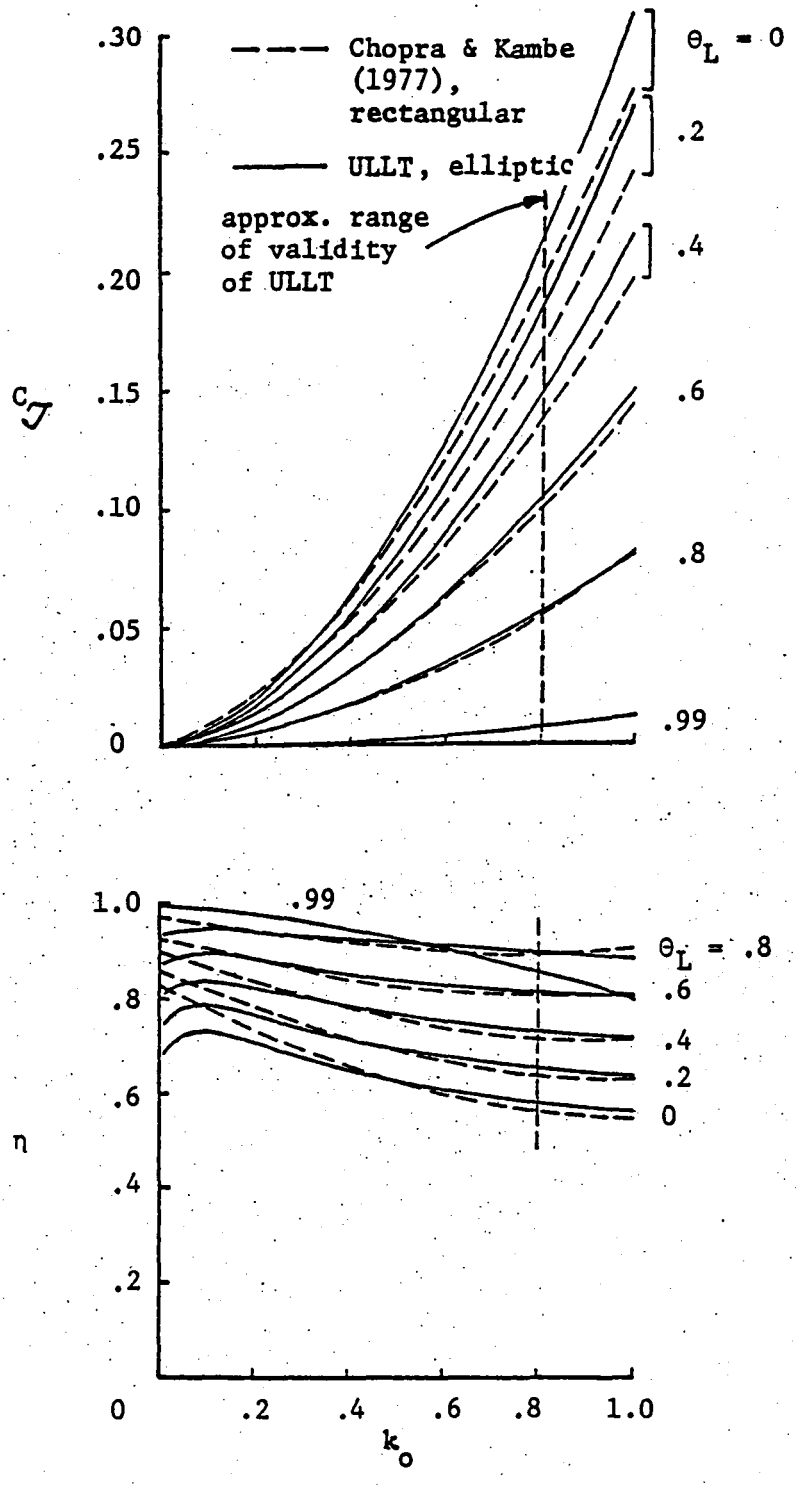

Figure 4.9. Thrust coefficient and hydrodynamic efficiency for an elliptic and a rectangular wing (A = 8) for several values of feathering parameter with axis of pitch located at 3/4 chord (at center section for elliptic wing).

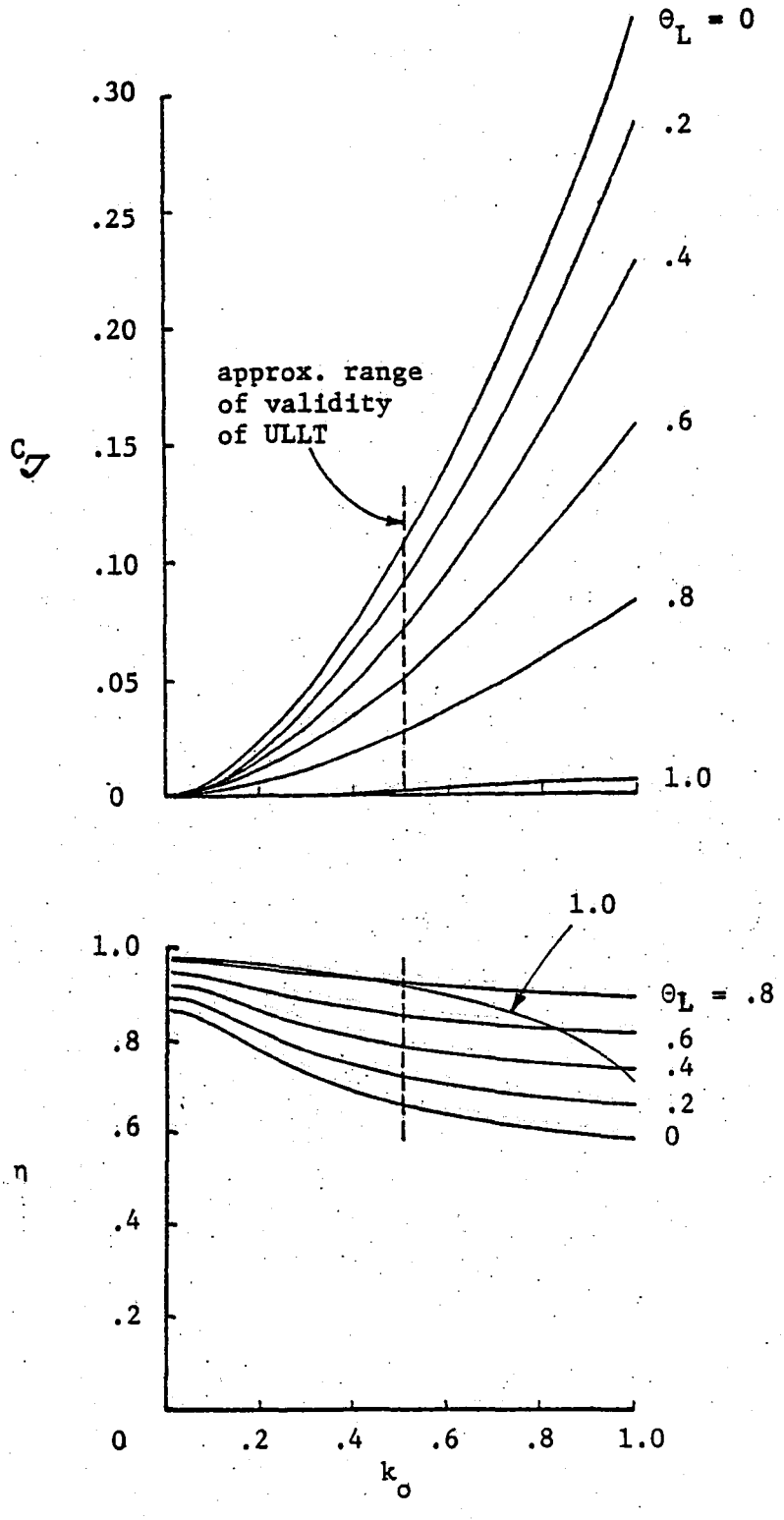

Figure 4.10. Thrust coefficient and hydrodynamic efficiency, predicted by unsteady lifting-line theory, for an elliptic wing (A = 16) for several values of feathering parameter with axis of pitch located at 3/4 of center section chord.

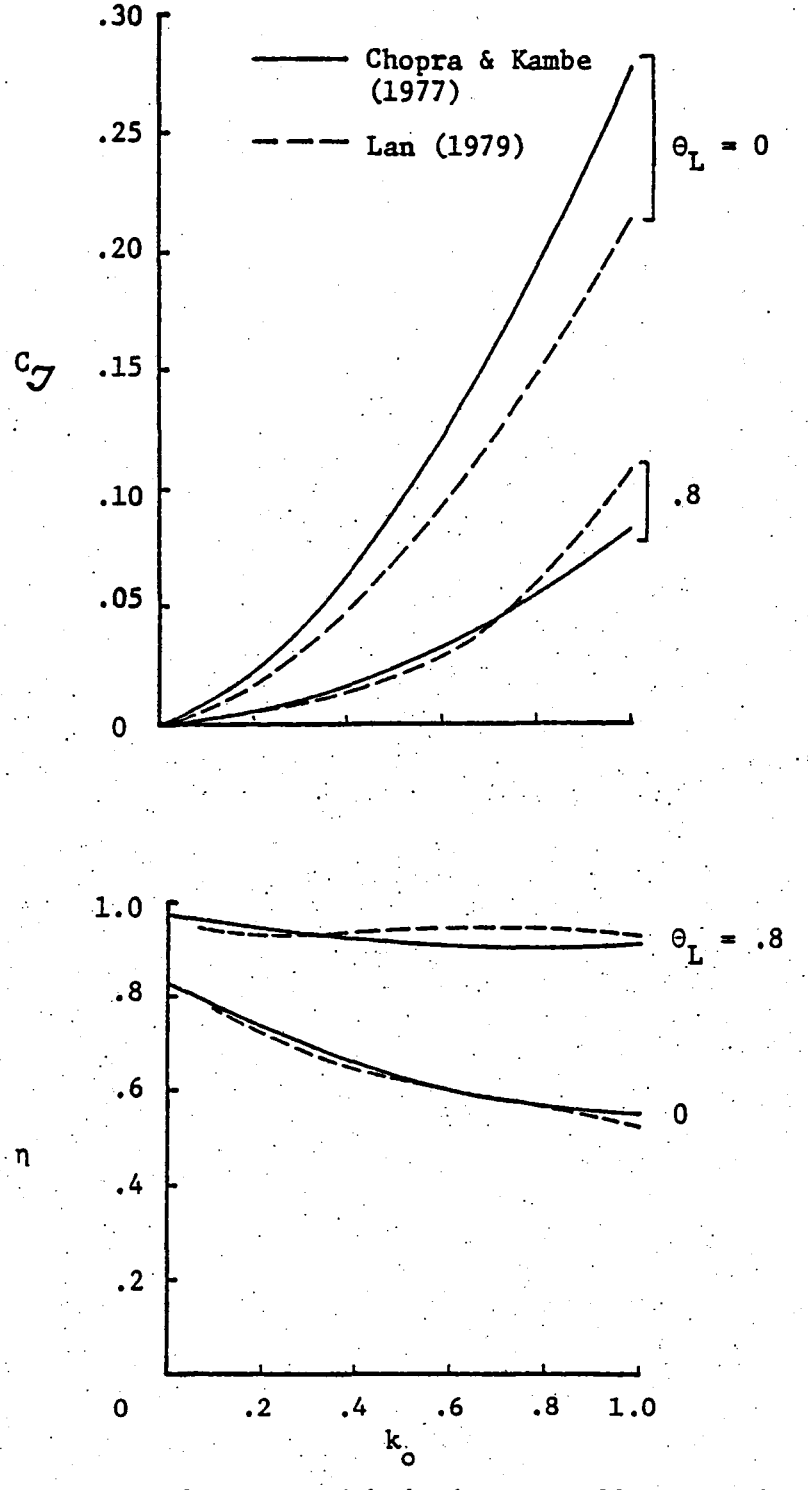

Figure 4.11. Thrust coefficient and hydrodynamic efficiency for a rectangular wing (A = 8) for θ_L = 0 and .8 with axis of pitch located at 3/4 chord (after Lan (1979)).

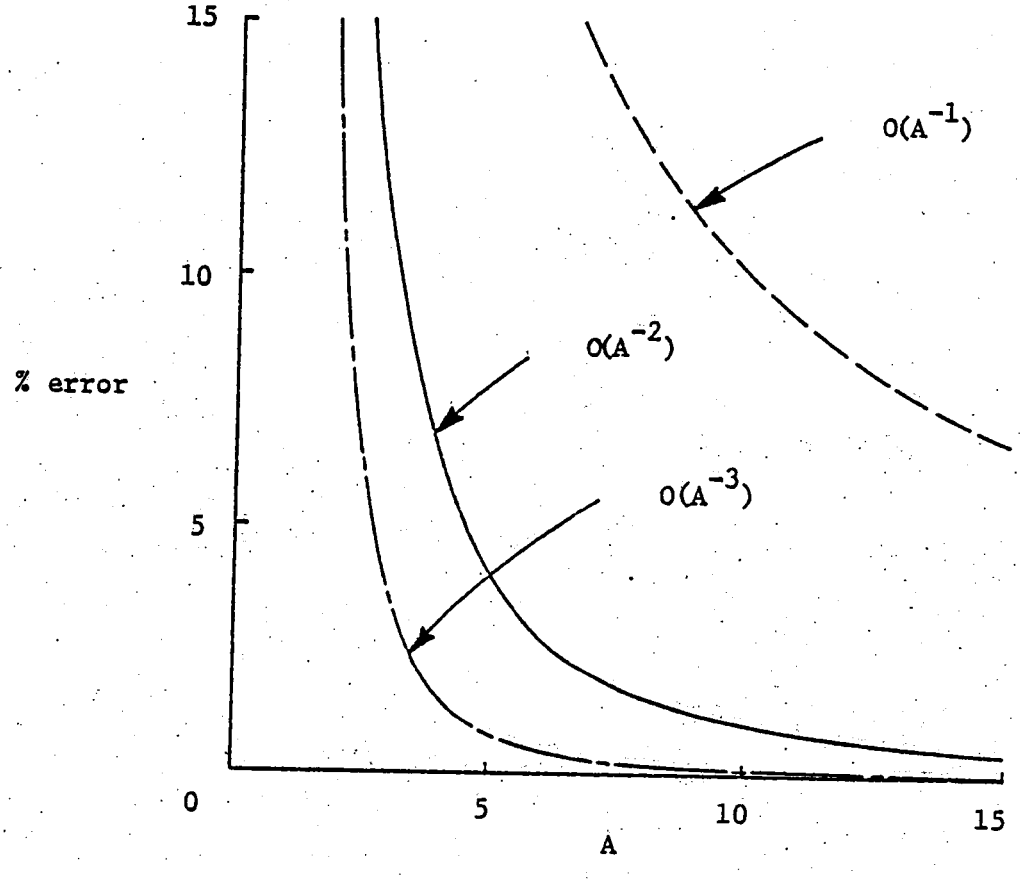

Figure 4.12. Order of magnitude of errors of unsteady lifting-line theory versus aspect ratio.

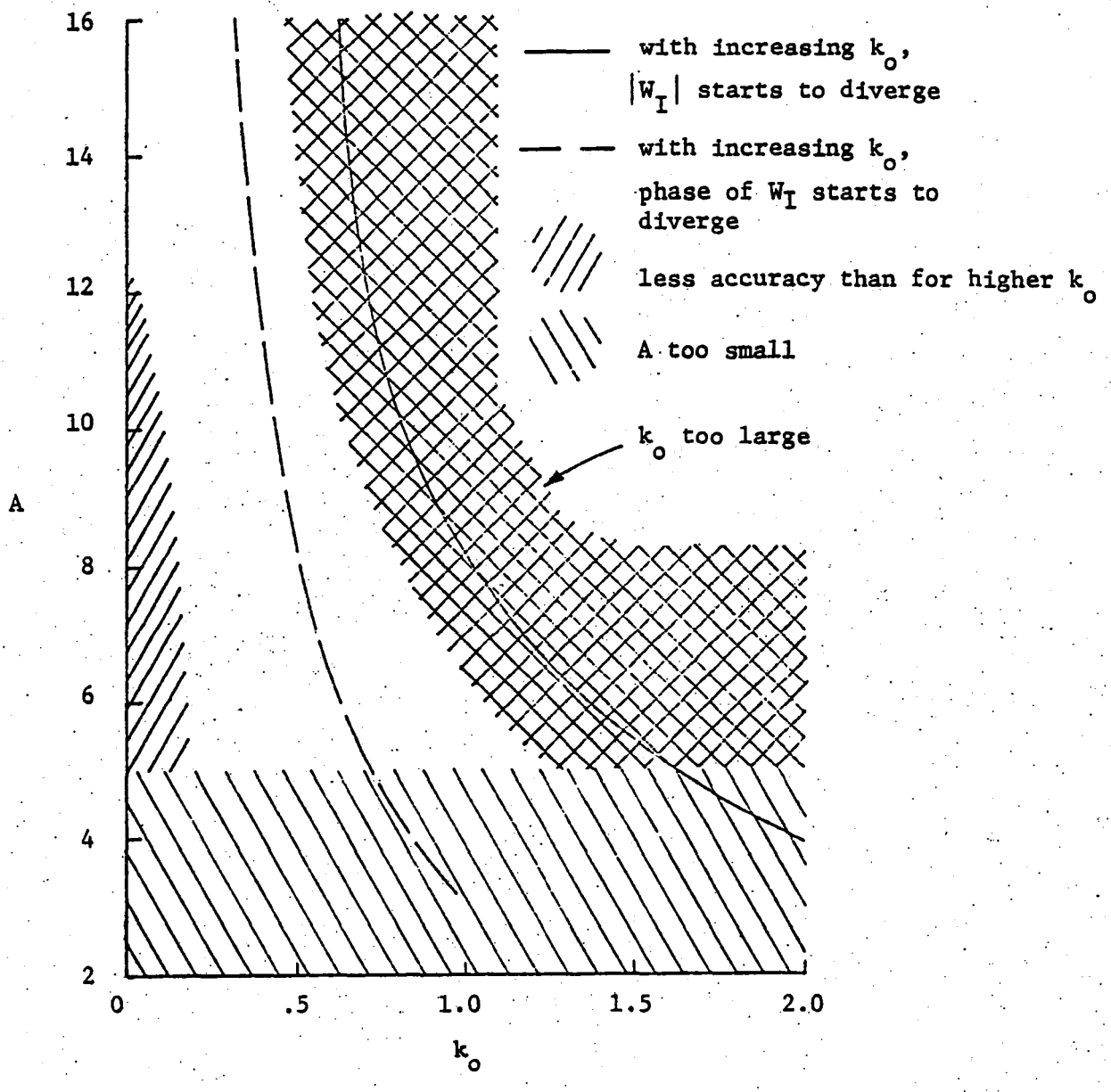

Figure 4.13. Region of validity of the present unsteady lifting-line theory.

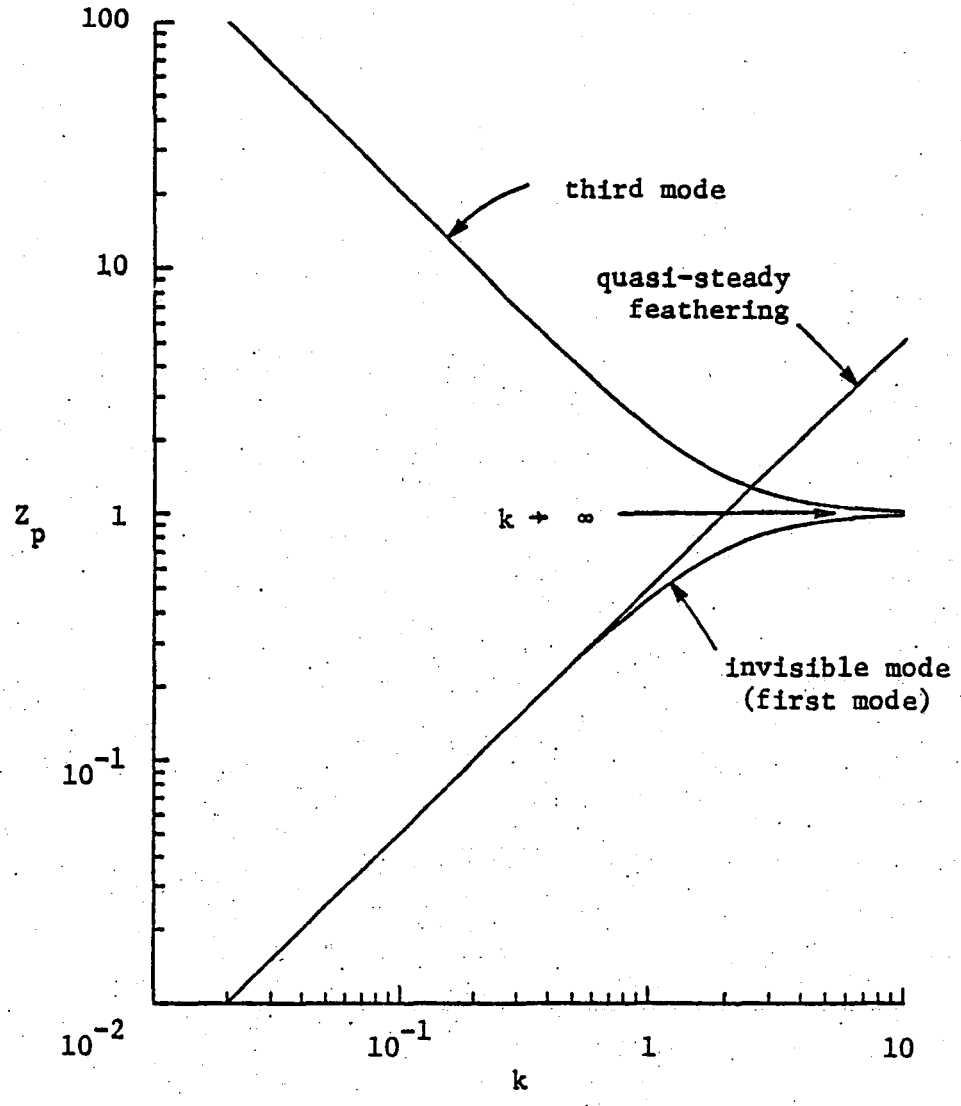

Figure 5.1. Amplitude ratio of pitch relative to heave for the normal modes of E.

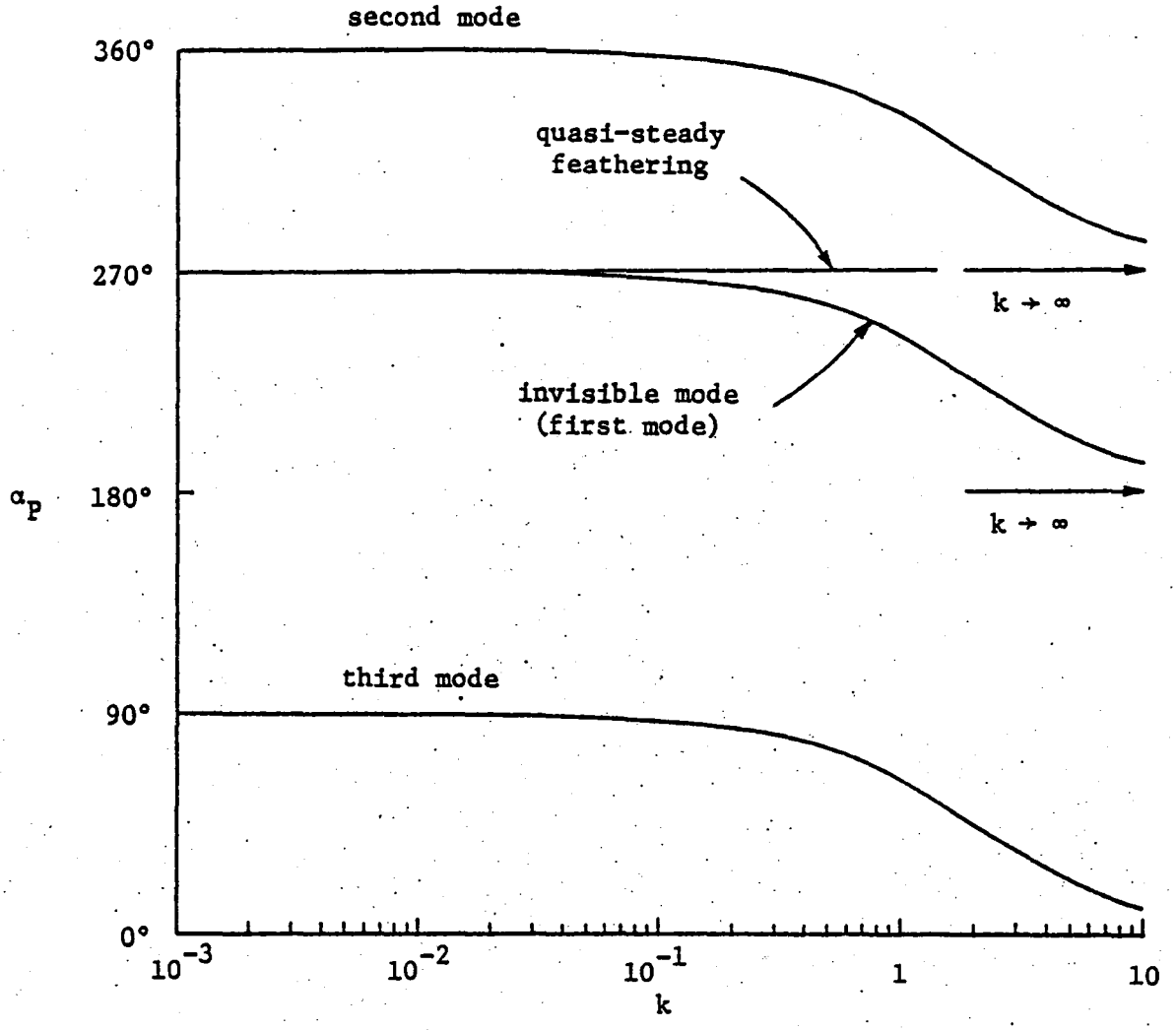

Figure 5.2. Phase advance of pitch relative to heave for the normal modes of E.

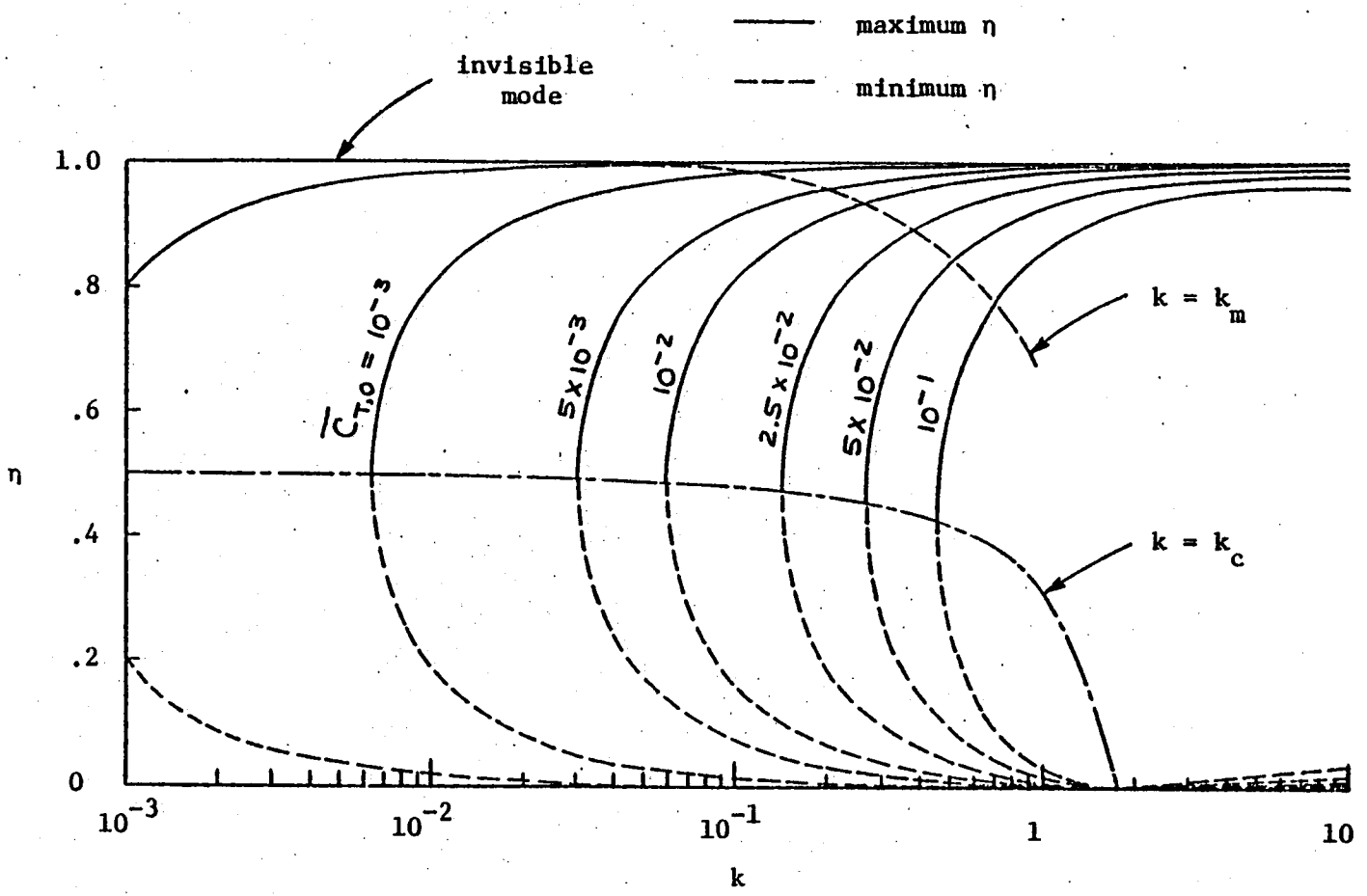

Figure 5.3. Hydrodynamic efficiency for the optimum motion.

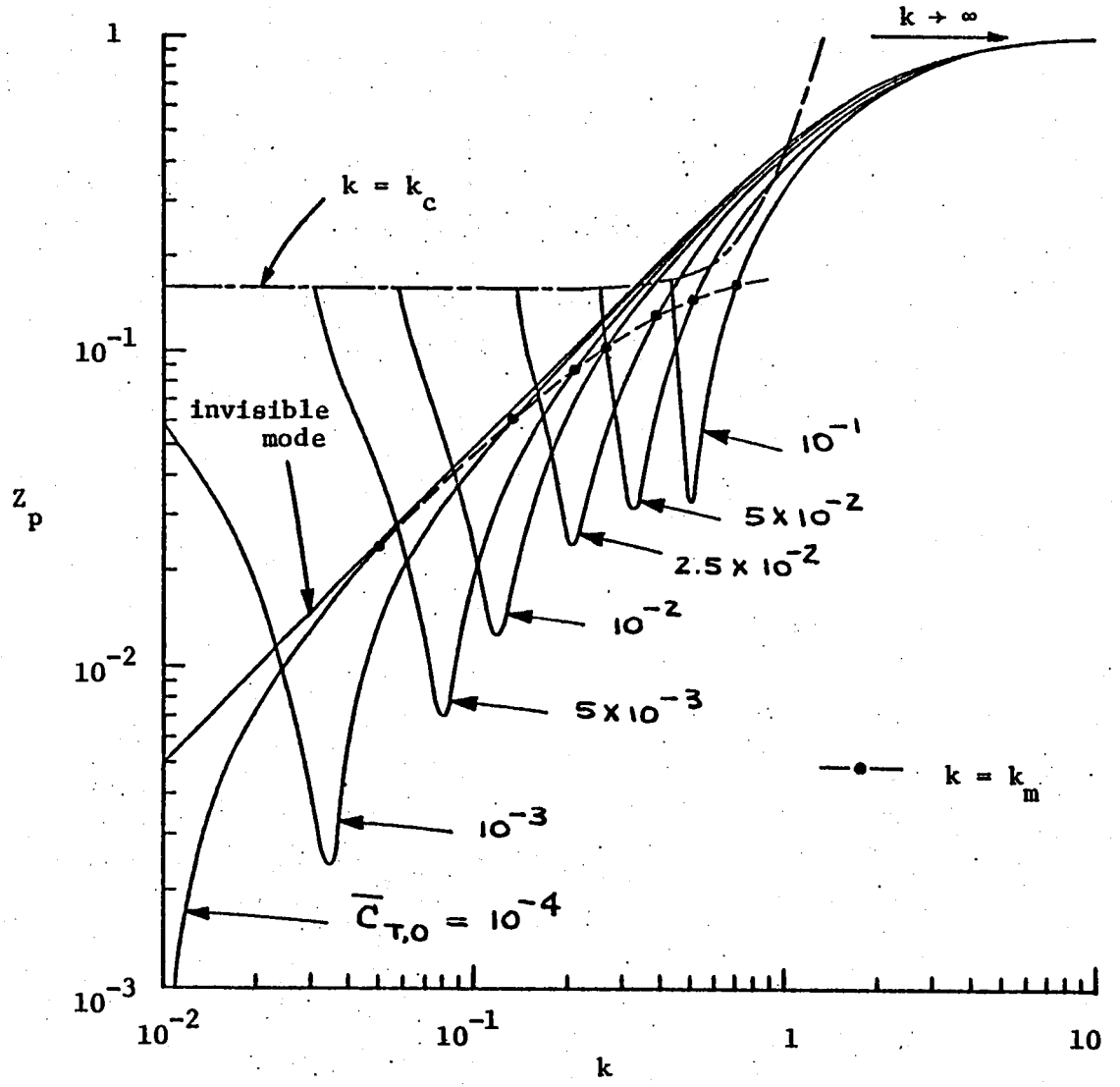

Figure 5.4. Amplitude ratio of pitch relative to heave for the optimum motion.

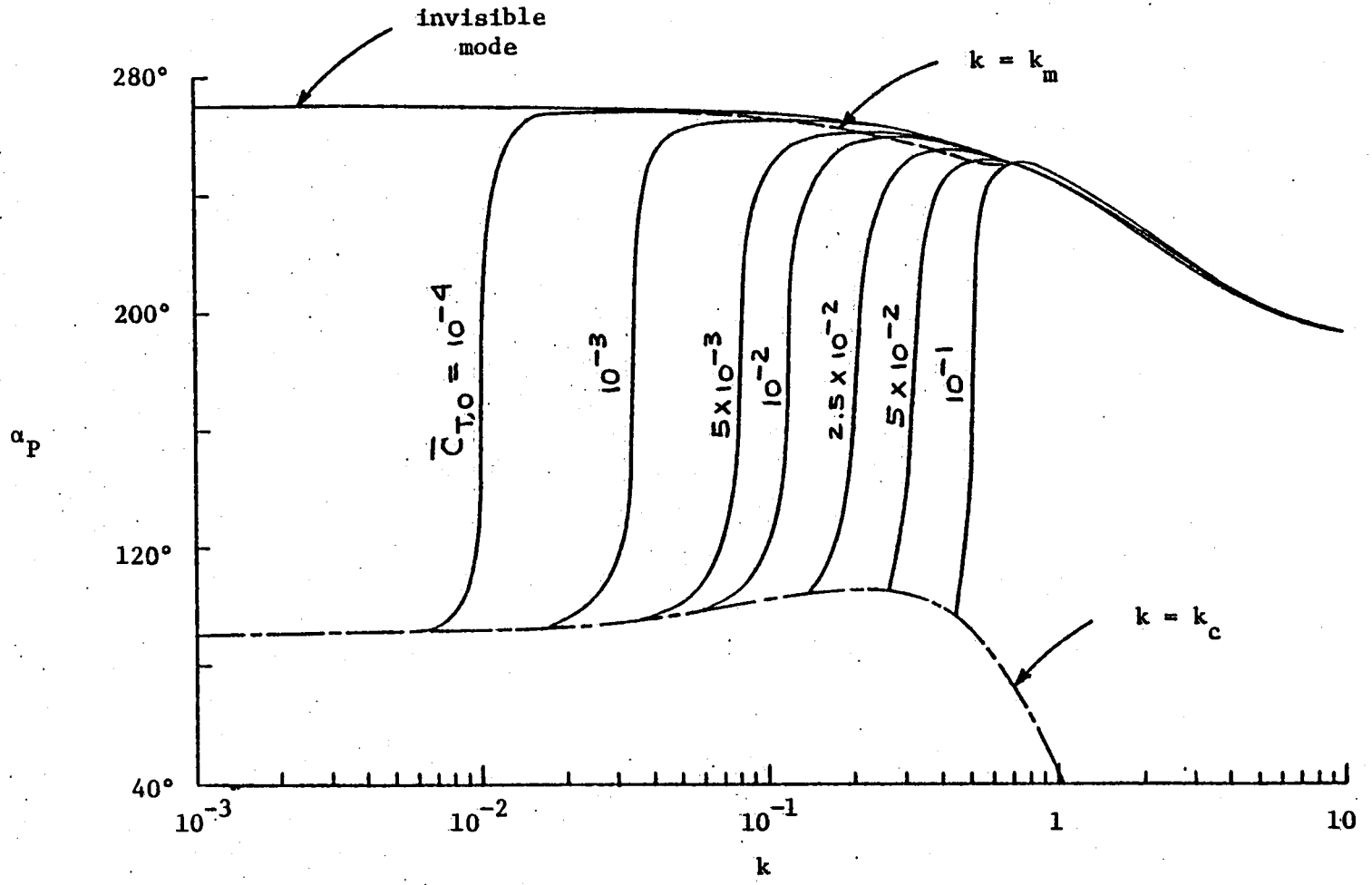

Figure 5.5. Phase advance of pitch relative to heave for the optimum motion.

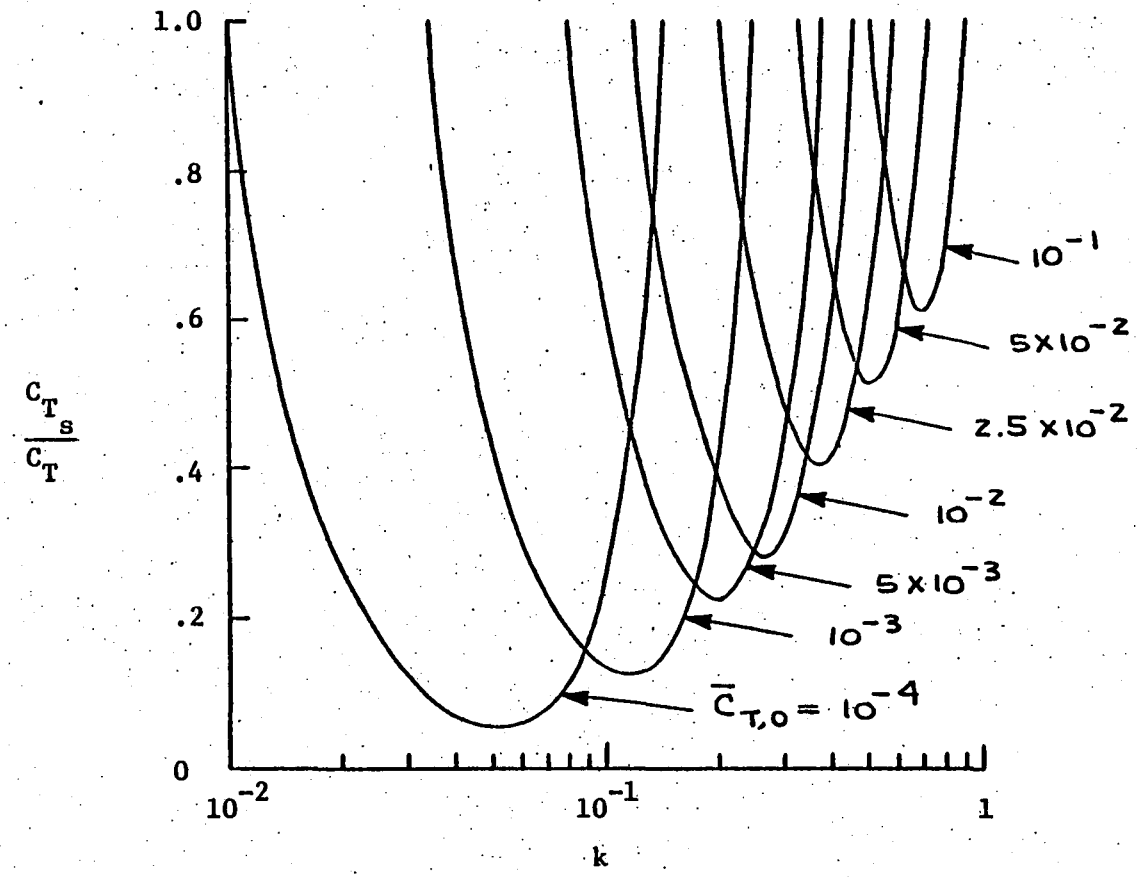

Figure 5.6. Ratio of leading-edge suction force to thrust for the optimum motion.

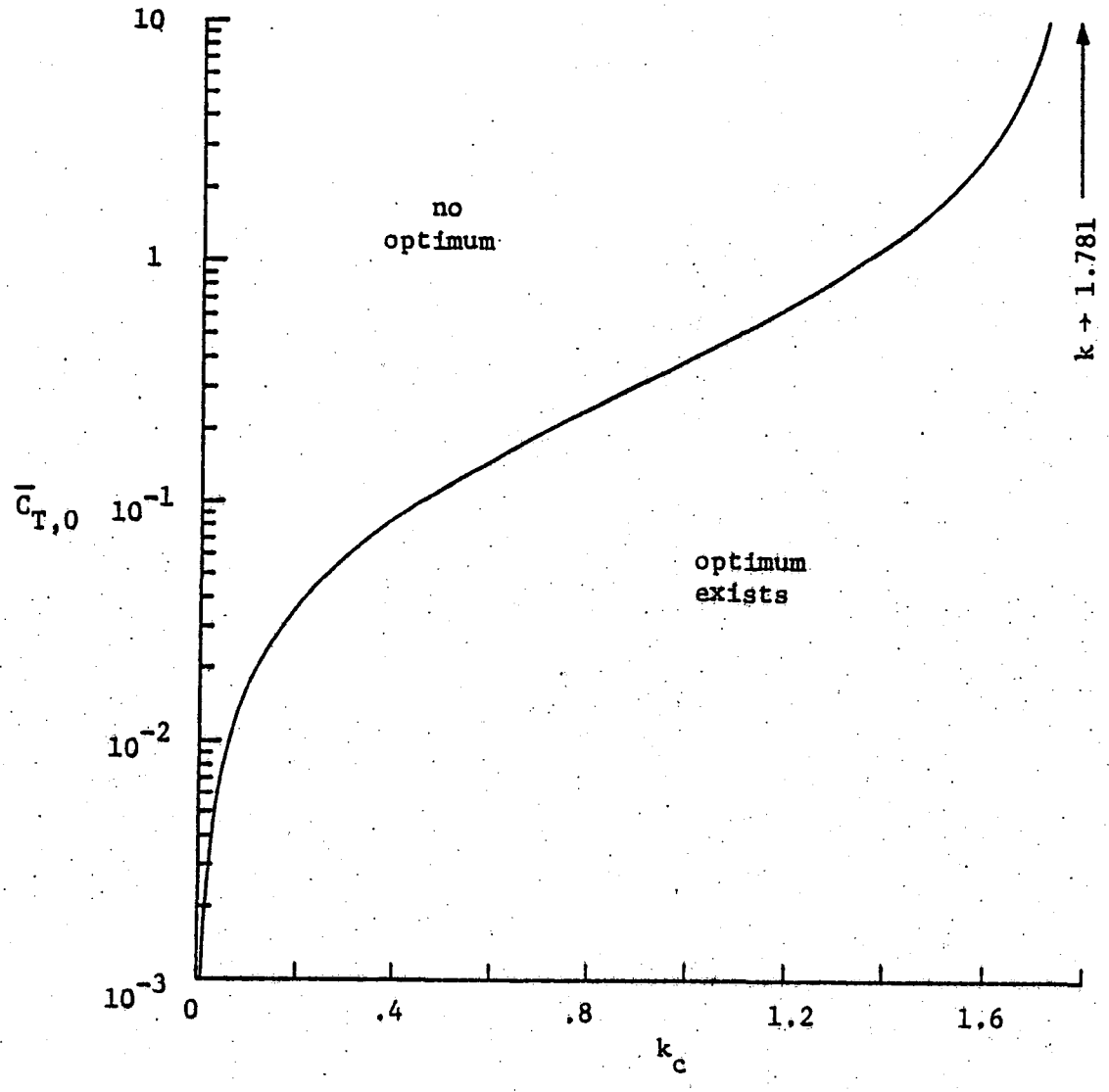

Figure 5.7. For given $\bar{C}_{T,0} > 0$, optimum exists for $k \geq k_c$.

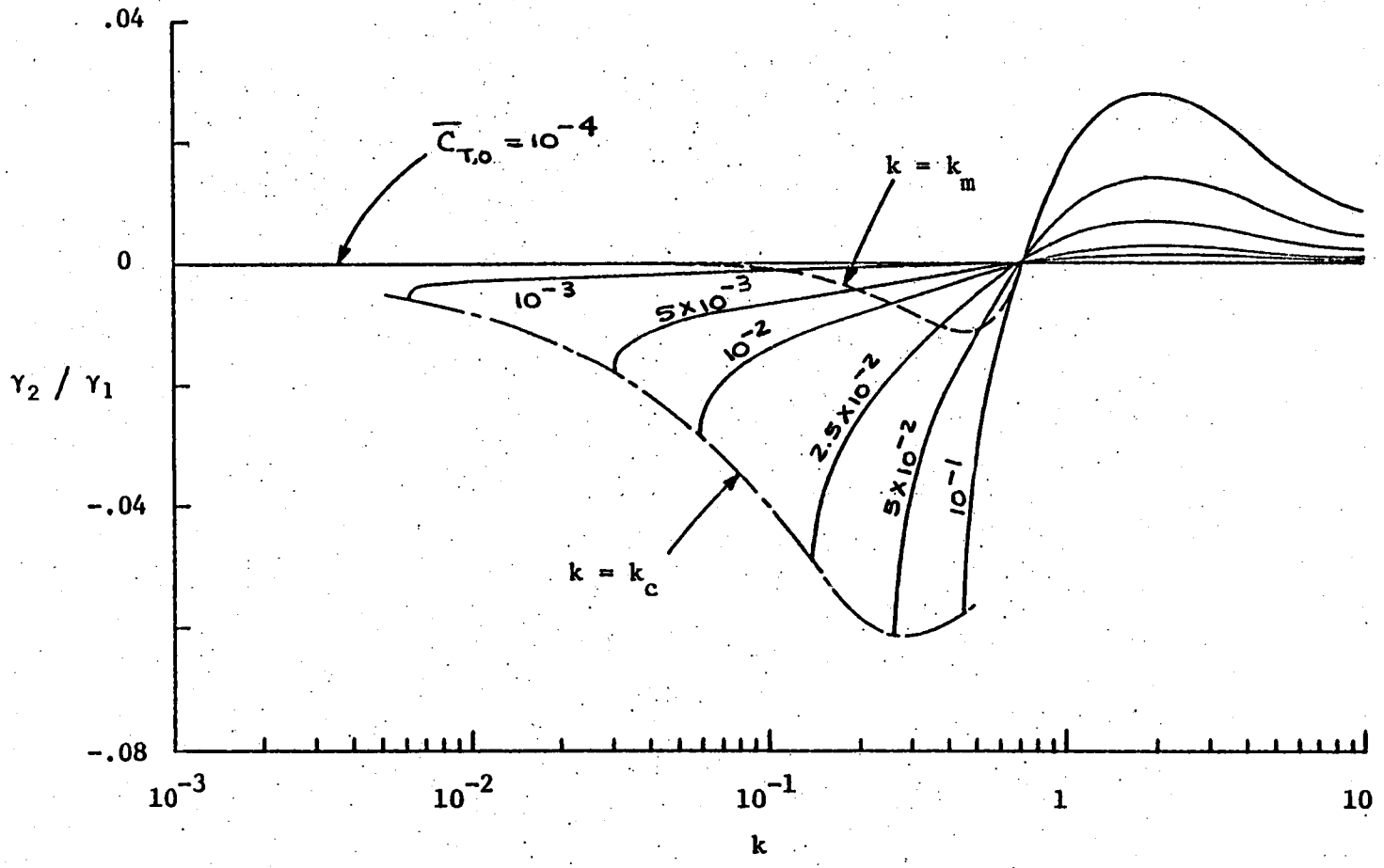

Figure 5.8. Amount of second mode relative to invisible mode in the optimum.

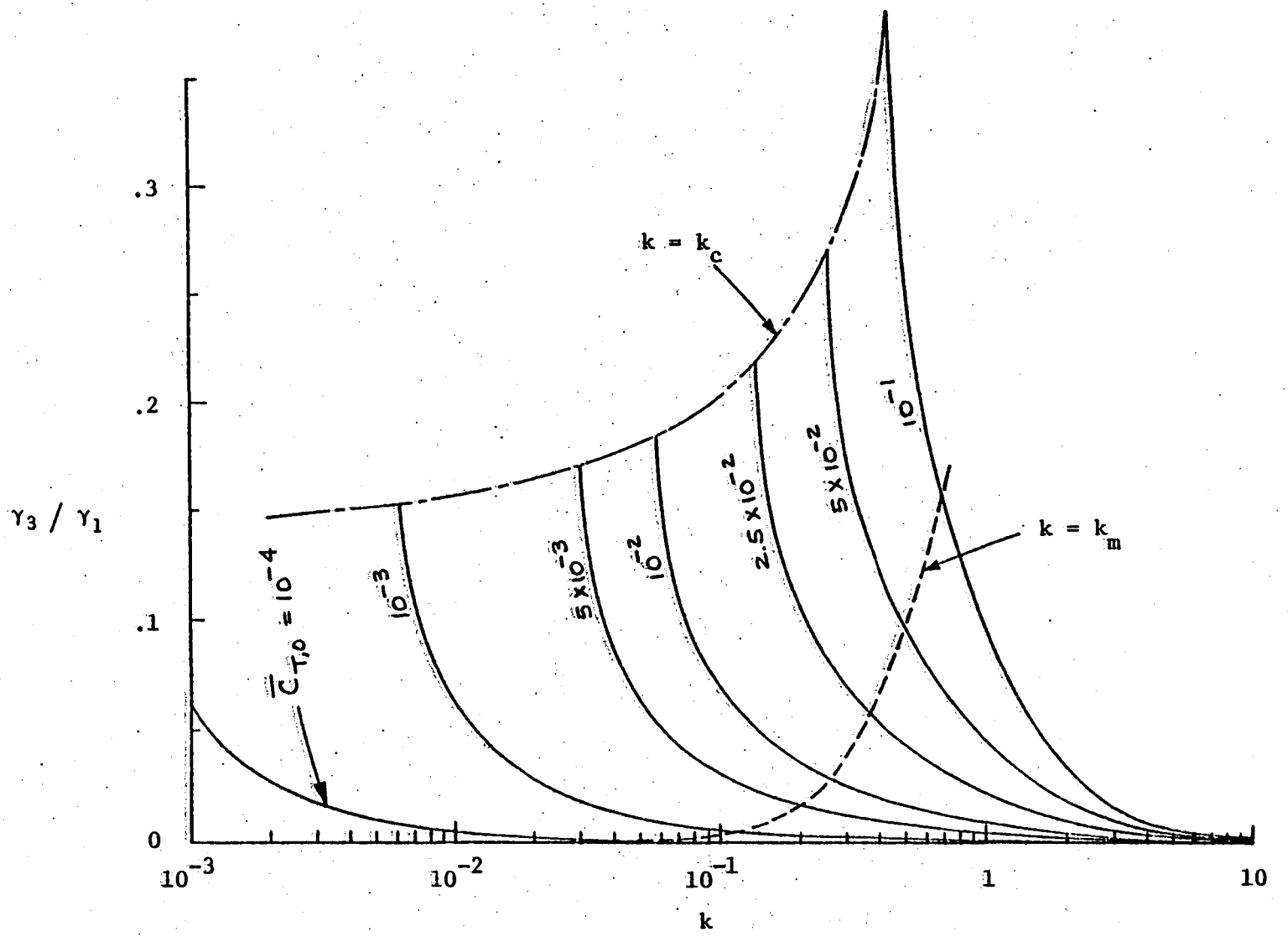

Figure 5.9. Amount of third mode relative to invisible mode in the optimum.

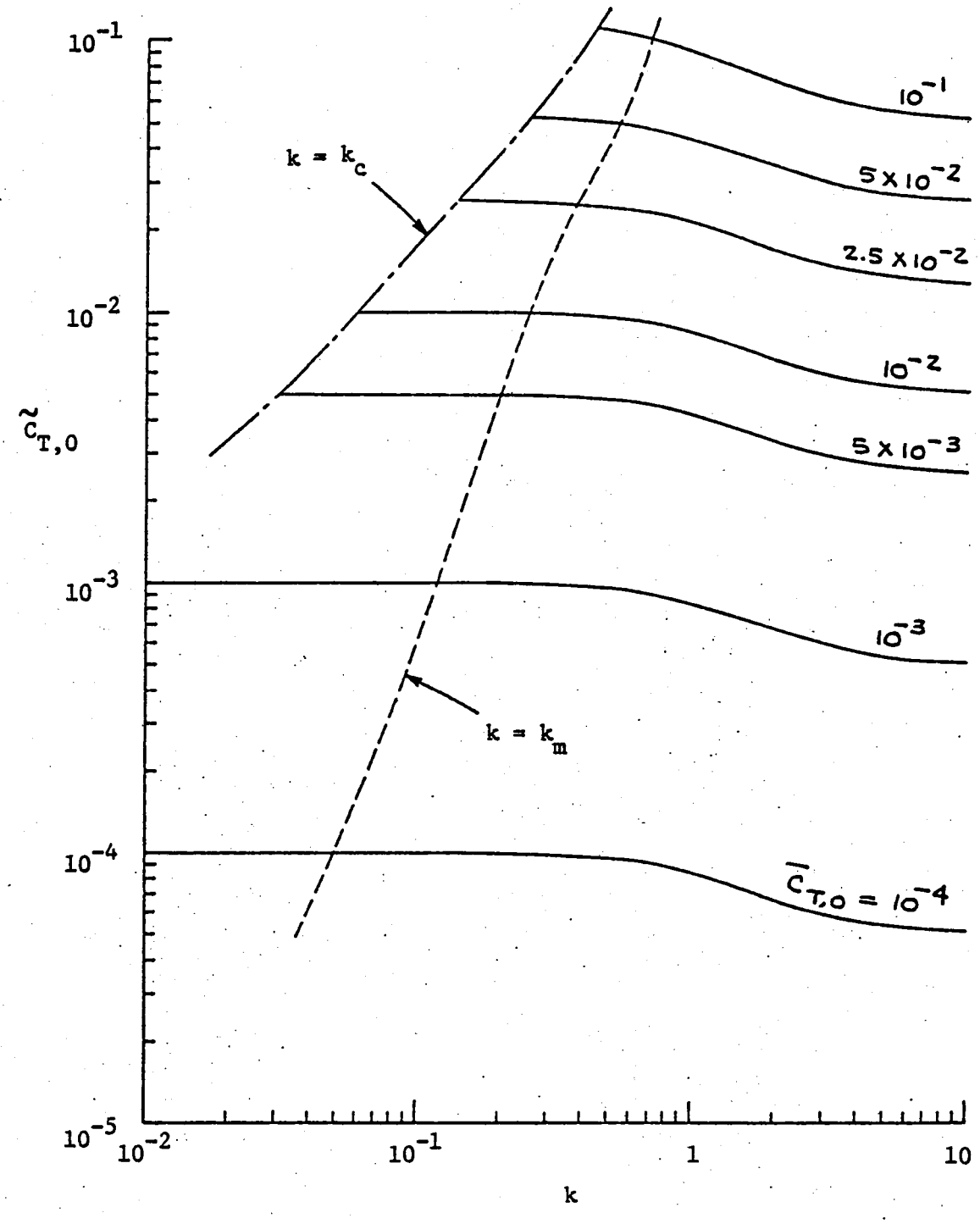

Figure 5.10. $\tilde{C}_{T,0}$ as a function of k and $\bar{C}_{T,0}$.

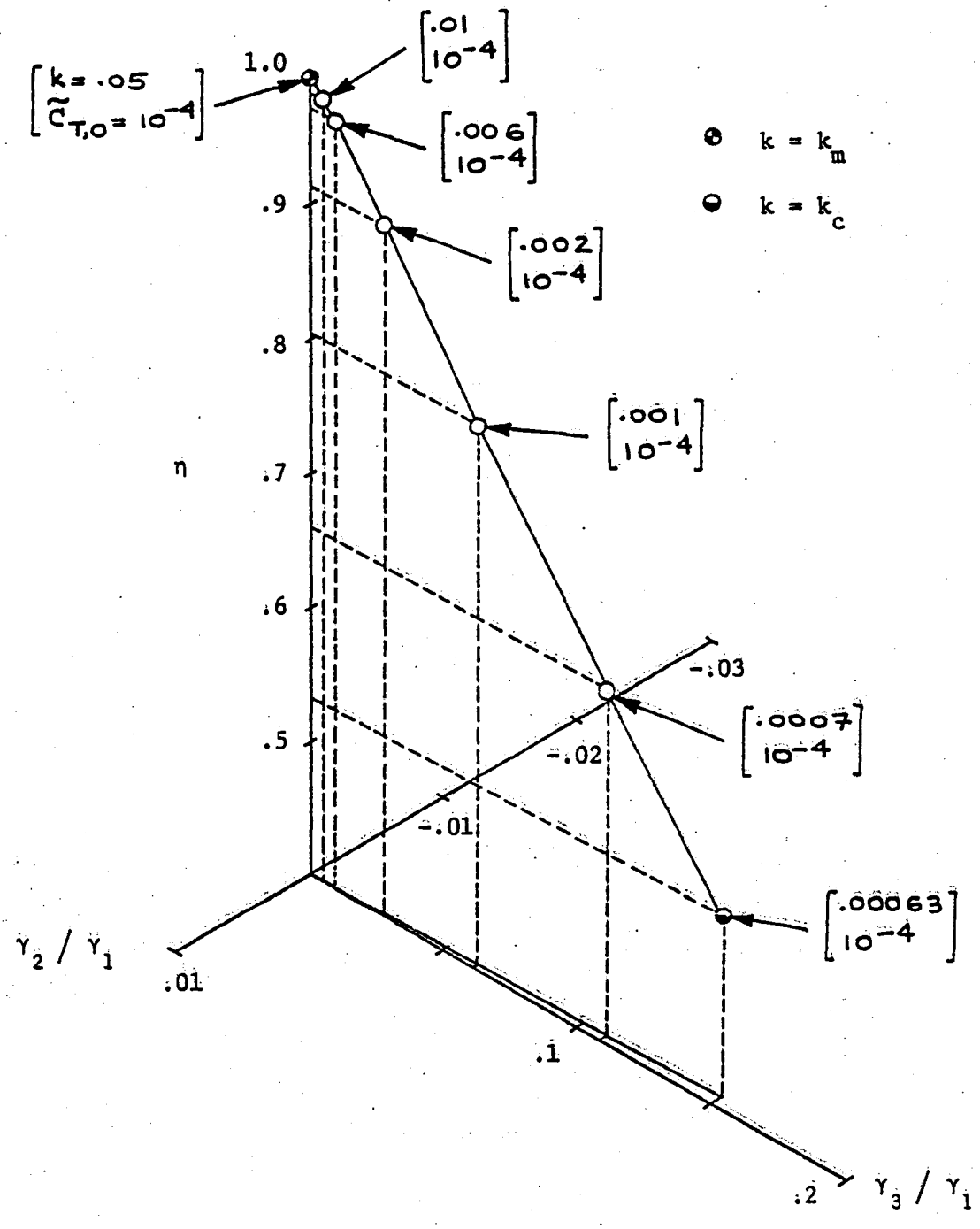

Figure 5.11. The optimum solution for $\bar{C}_{T,0} = 10^{-4}$.

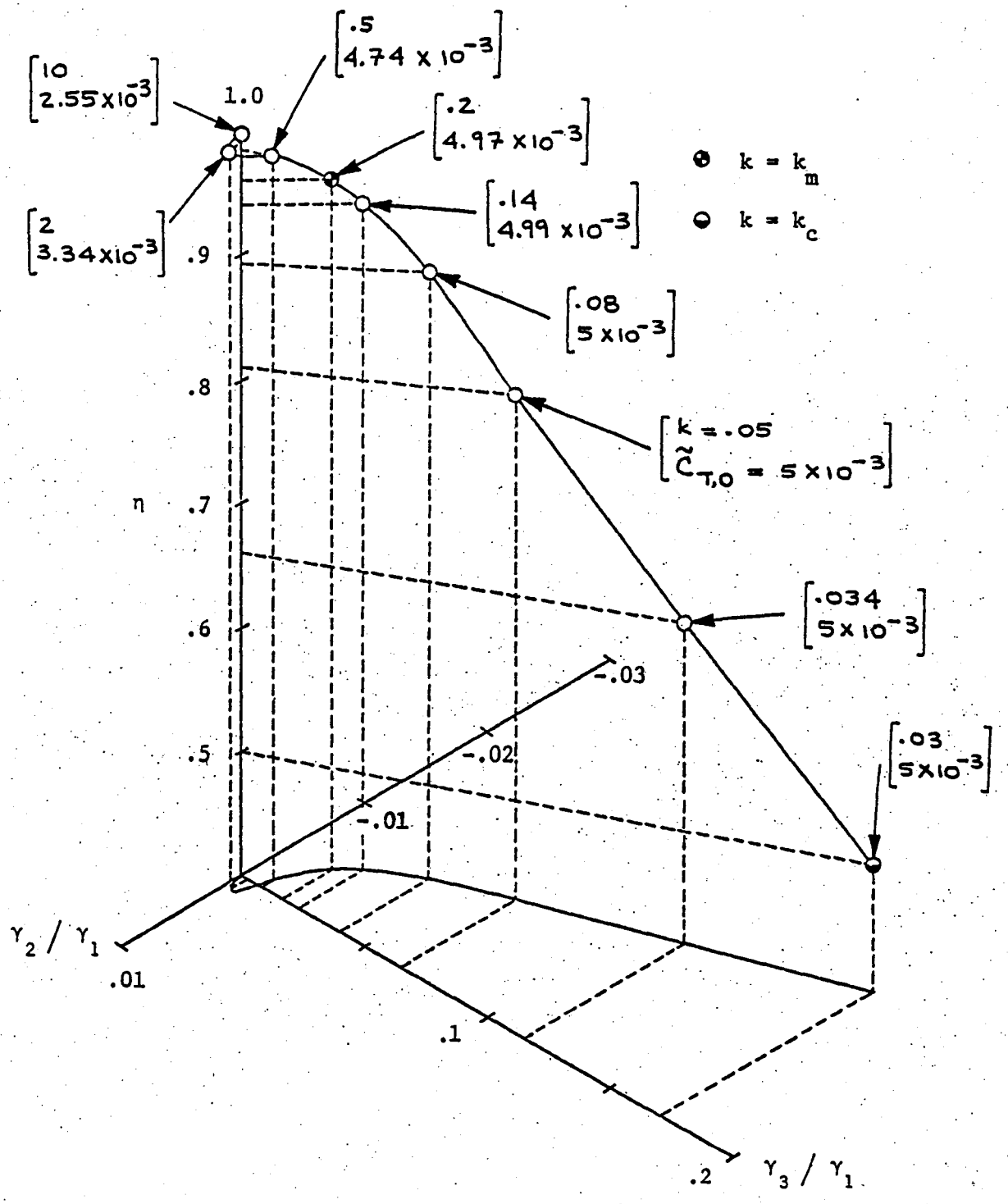

Figure 5.12. The optimum solution for $\bar{C}_{T,0} = 5 \times 10^{-3}$.

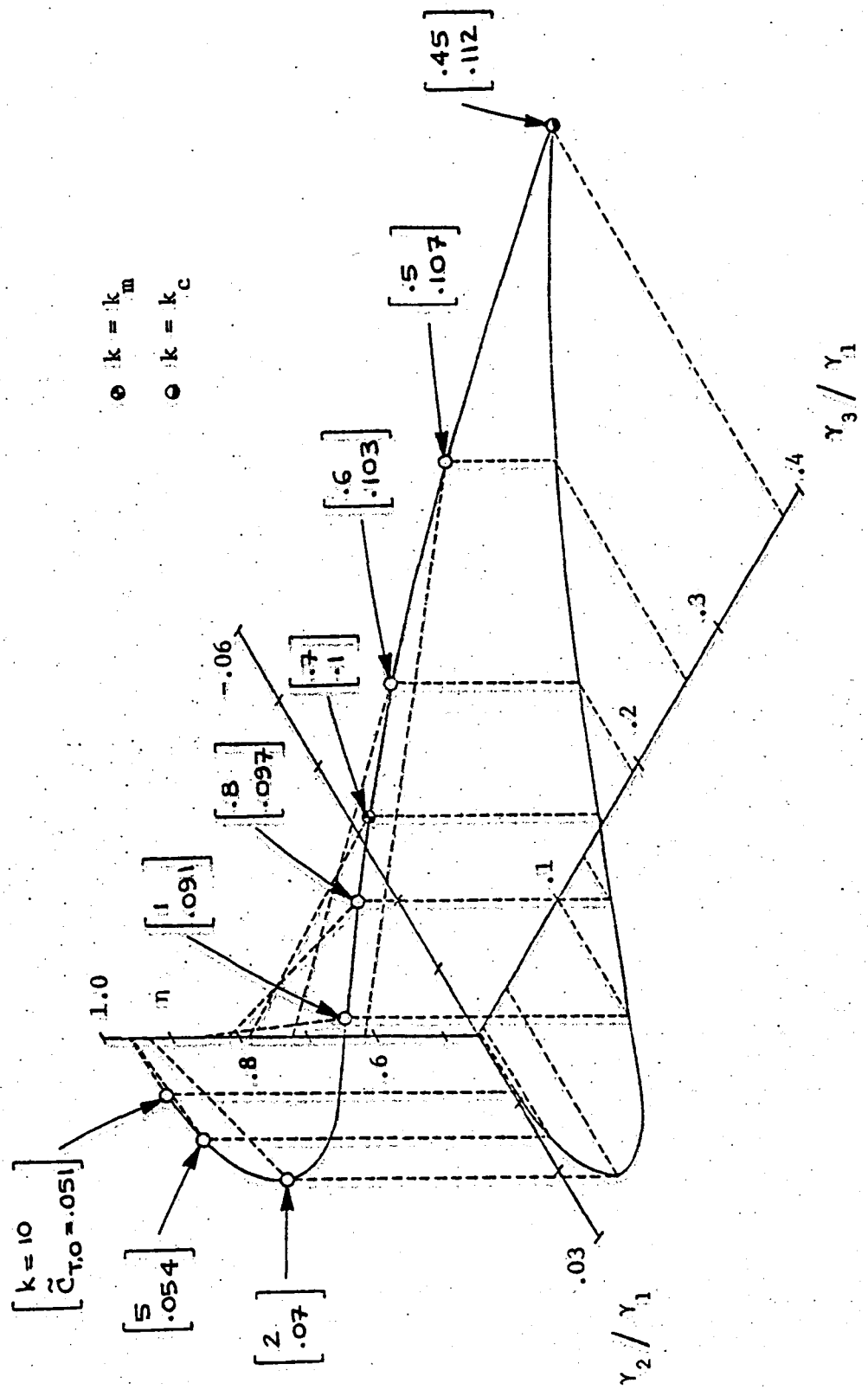

Figure 5.13. The optimum solution for $\bar{C}_{T,0} = 10^{-1}$.

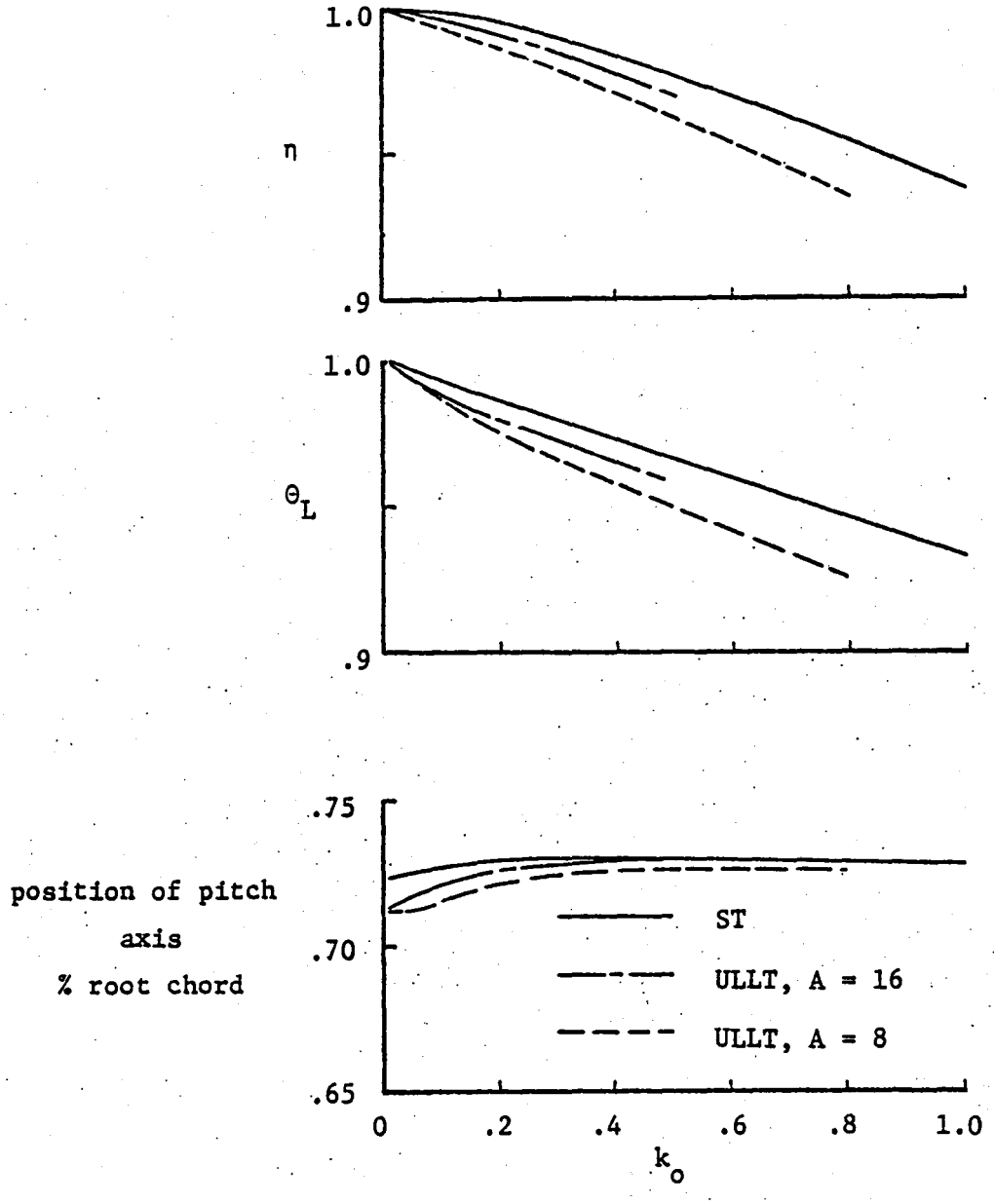

Figure 5.14. Hydrodynamic efficiency, proportional feathering parameter and location of pitch axis for optimum movement of a rigid elliptic wing.

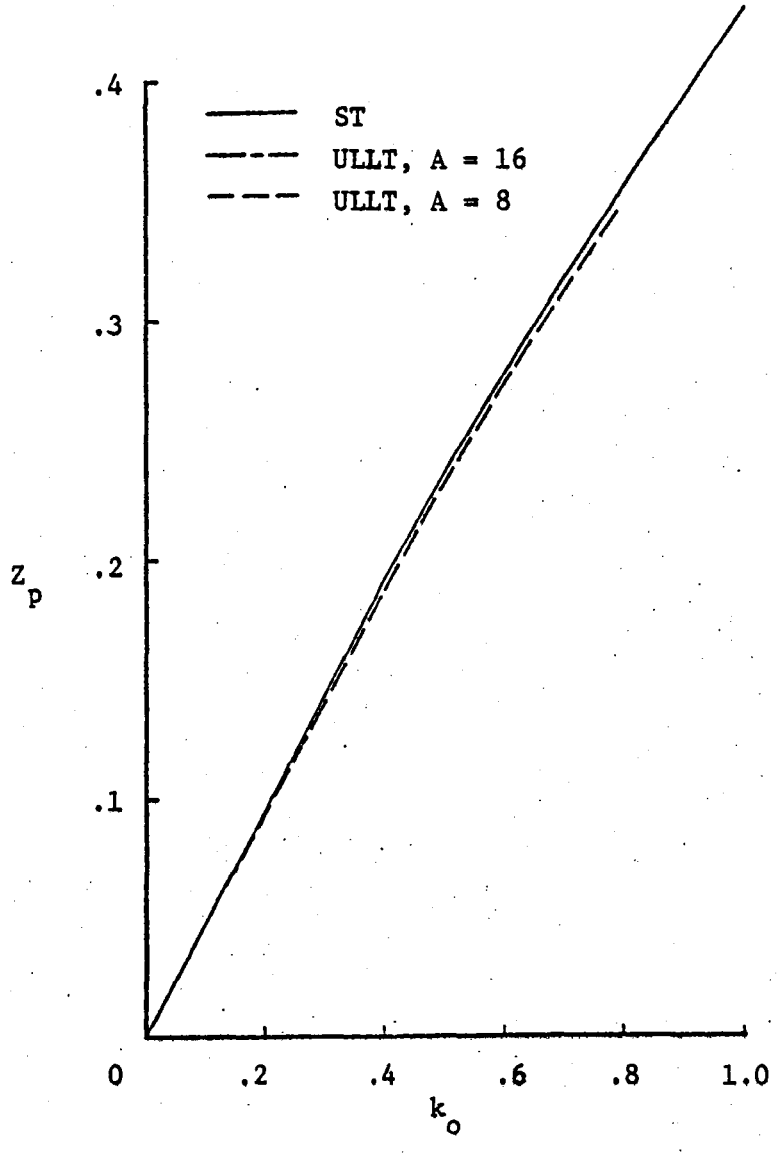

Figure 5.15. Amplitude ratio of pitch relative to heave for optimum movement of a rigid elliptic wing.

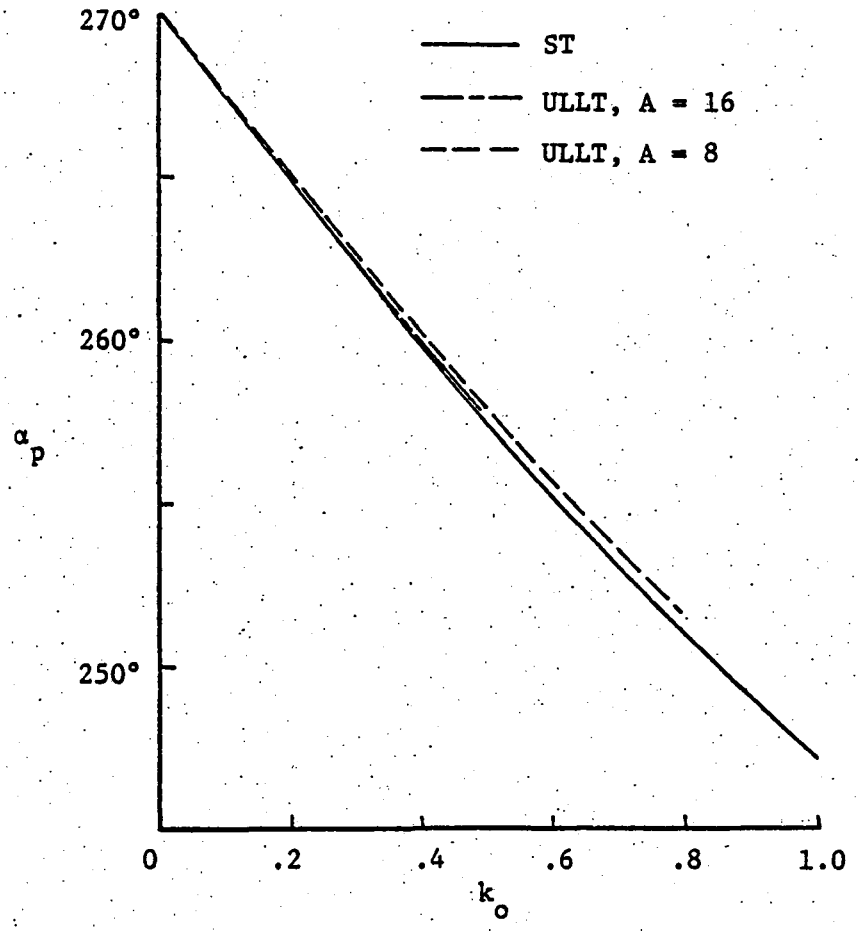

Figure 5.16. Phase advance of pitch relative to heave for optimum movement of a rigid elliptic wing.

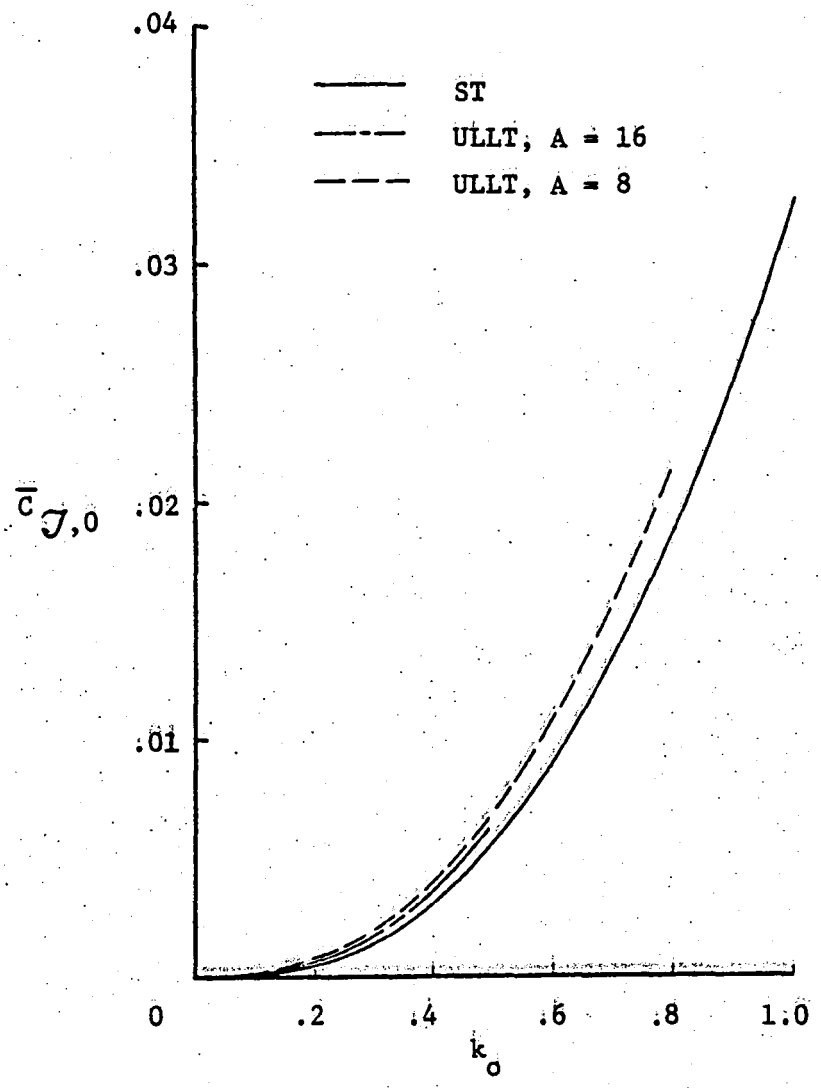

Figure 5.17. Proportional loading parameter for optimum movement of a rigid elliptic wing.

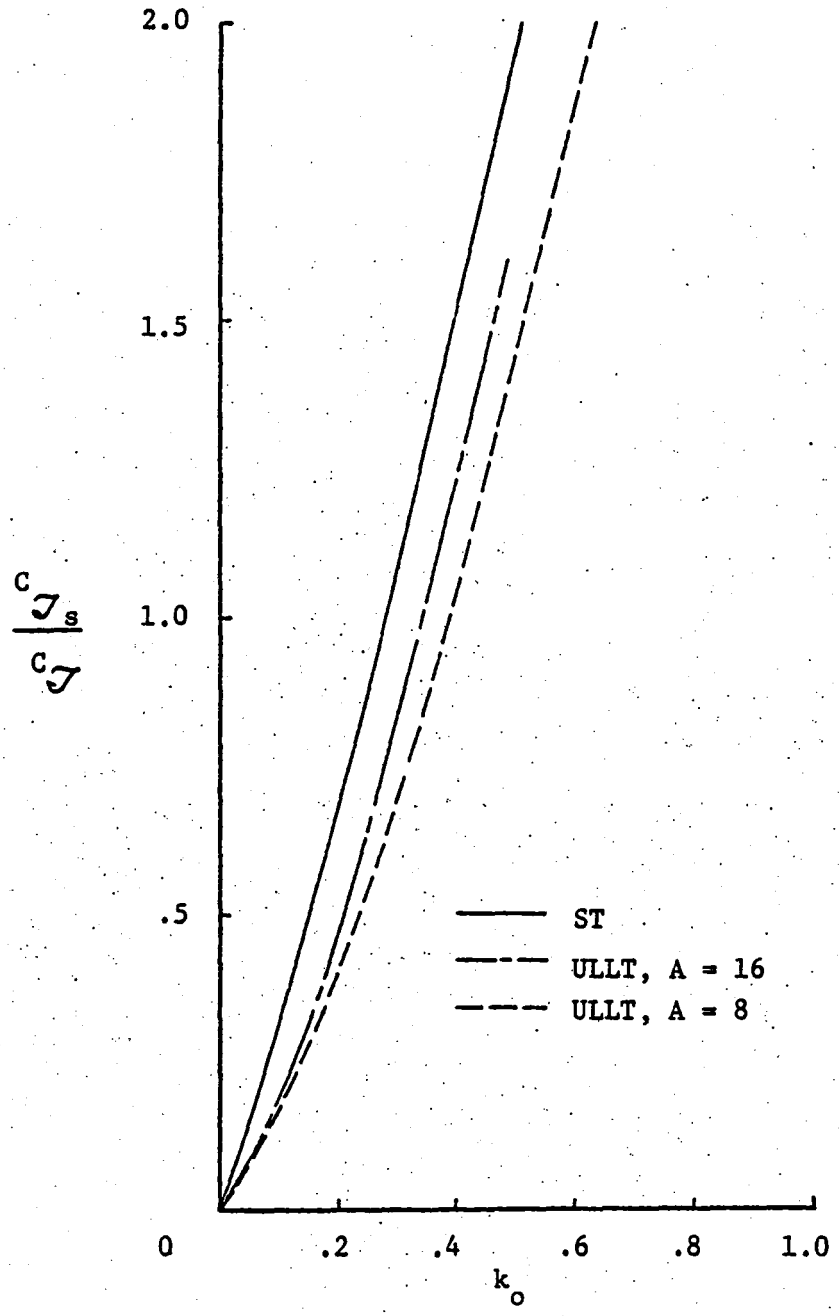

Figure 5.18. Ratio of leading-edge suction force to thrust for optimum movement of a rigid elliptic wing.

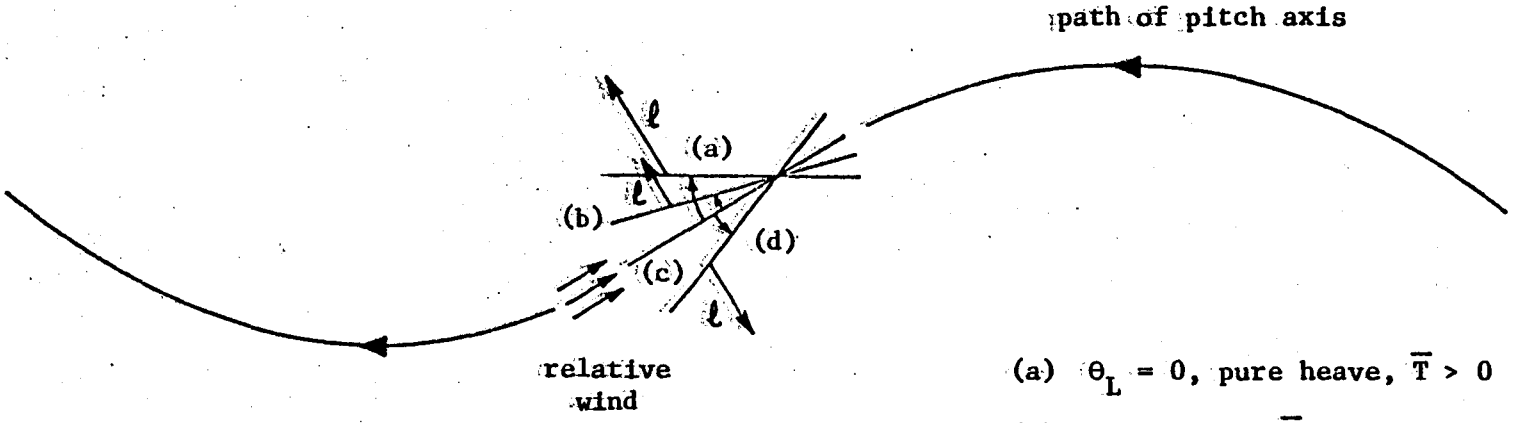

Figure 5.19. Sinusoidal motion of a flat plate airfoil under quasi-steady conditions.

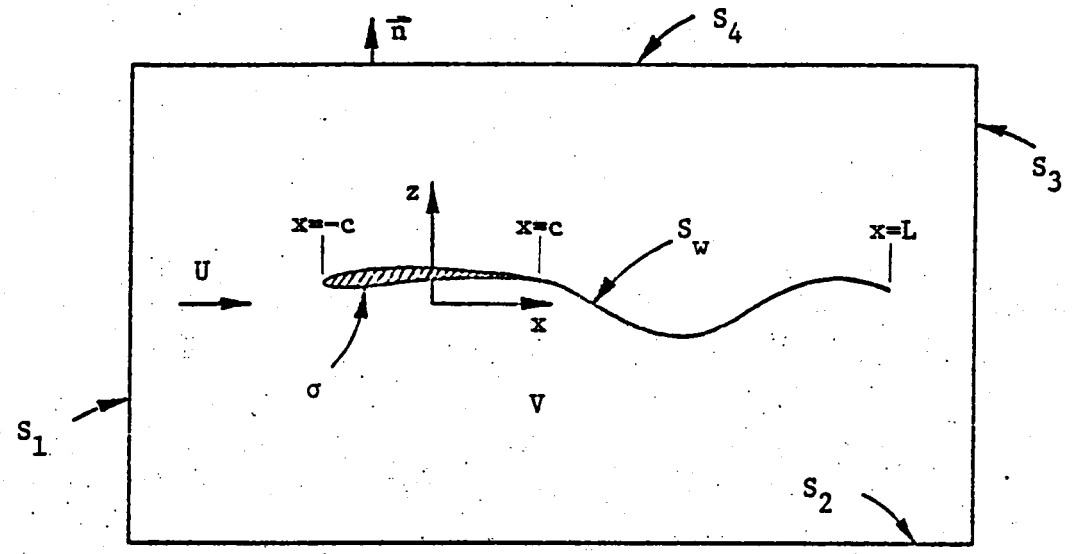

Figure 6.1. Control volume for the momentum theorem in two dimensions.

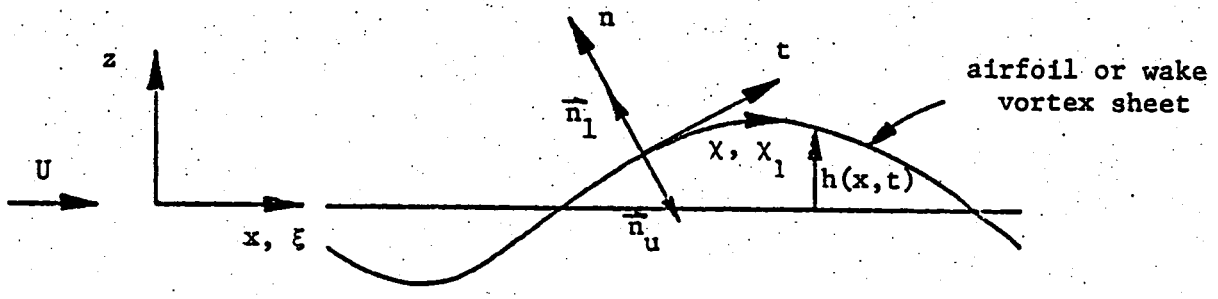

Figure 6.2. Schematic of airfoil and wake geometry.

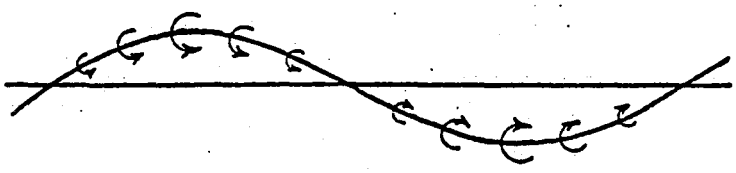

a) thrust-type wake ($\alpha - \beta = \pi$)

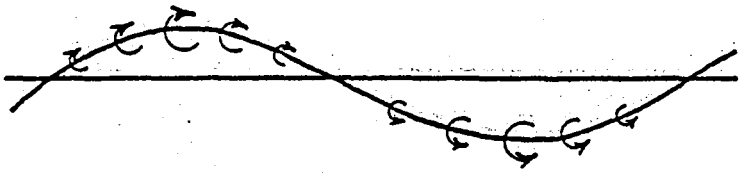

b) drag-type wake ($\alpha - \beta = 0$)

Figure 6.3. Two examples of thrust- and drag-type wakes (the strength and sense of local vorticity is indicated by curved arrows).

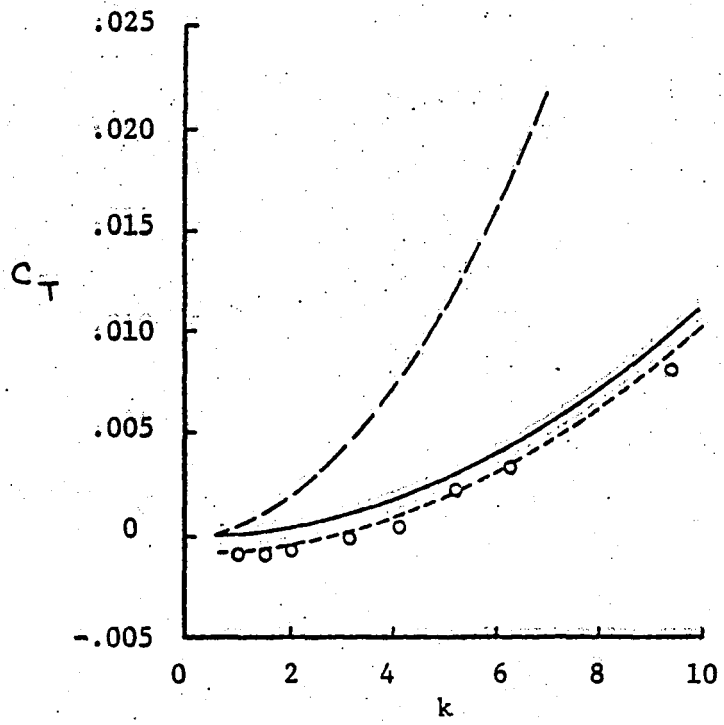

Figure 6.4. Thrust coefficient for an airfoil in heave. Unsteady theory:——; Smith and Stone (1961):– – –; turbulent boundary layer drag added to results of unsteady theory:-----; experiment: o (after Kelly, et al. (1964)).

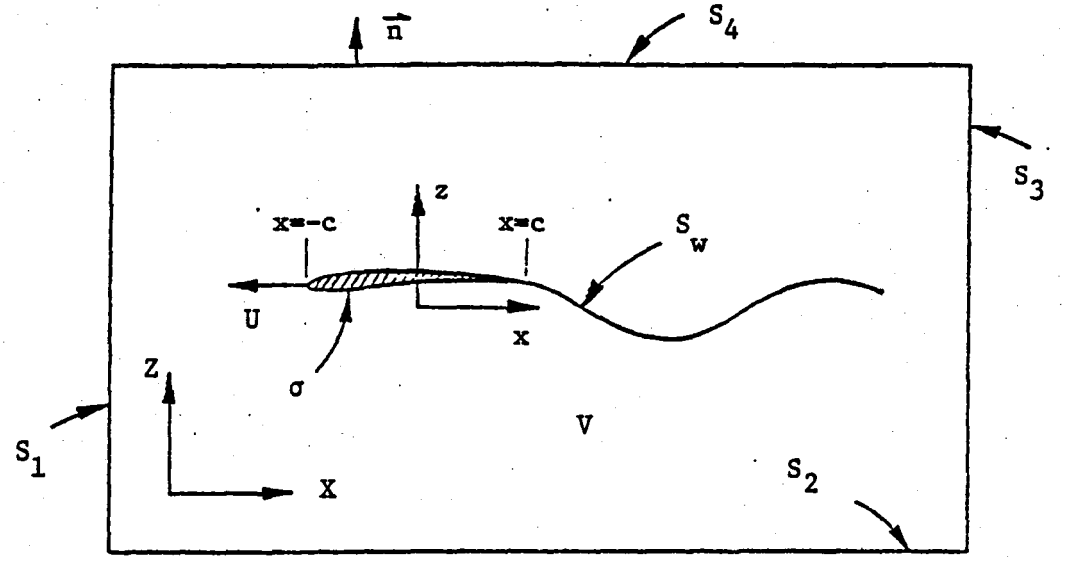

Figure 6.5. Control volume for conservation of energy in two dimensions.

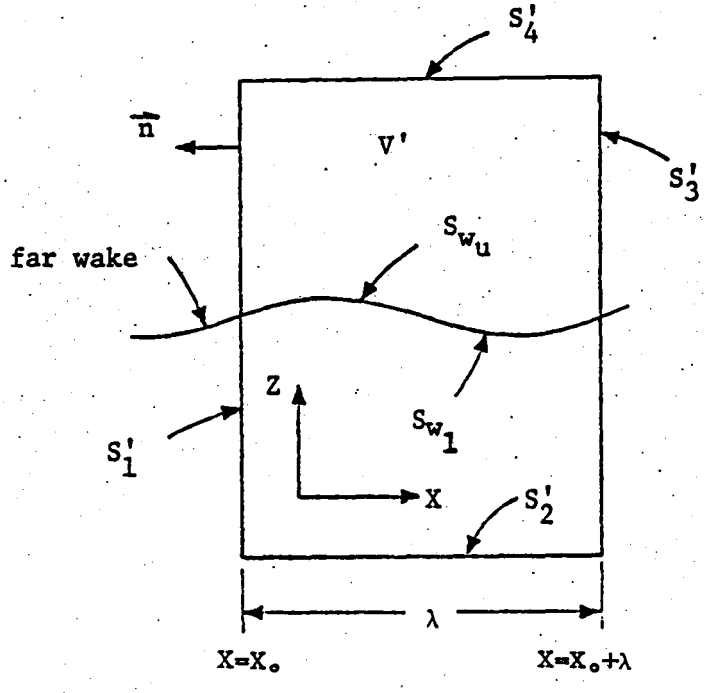

Figure 6.6. Control volume for calculation of wake energy.

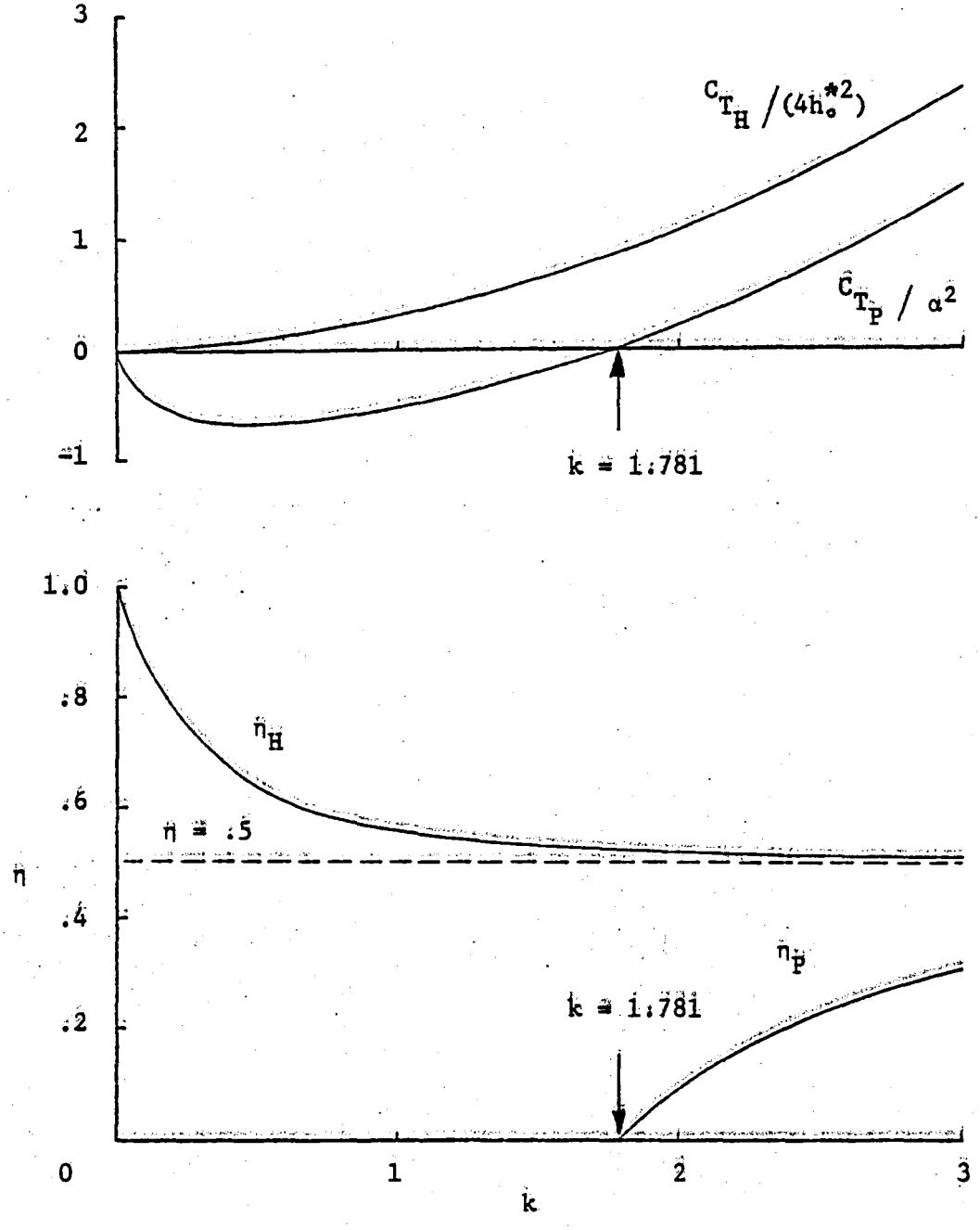

Figure 6.7. Thrust coefficient and hydrodynamic efficiency for an airfoil in pitch and heave.

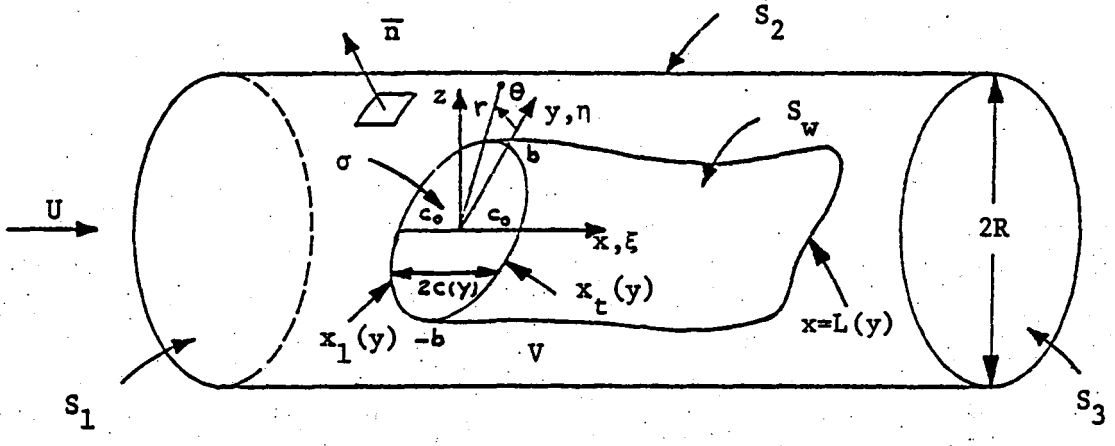

Figure 6.8. Control volume for the momentum theorem in three dimensions.

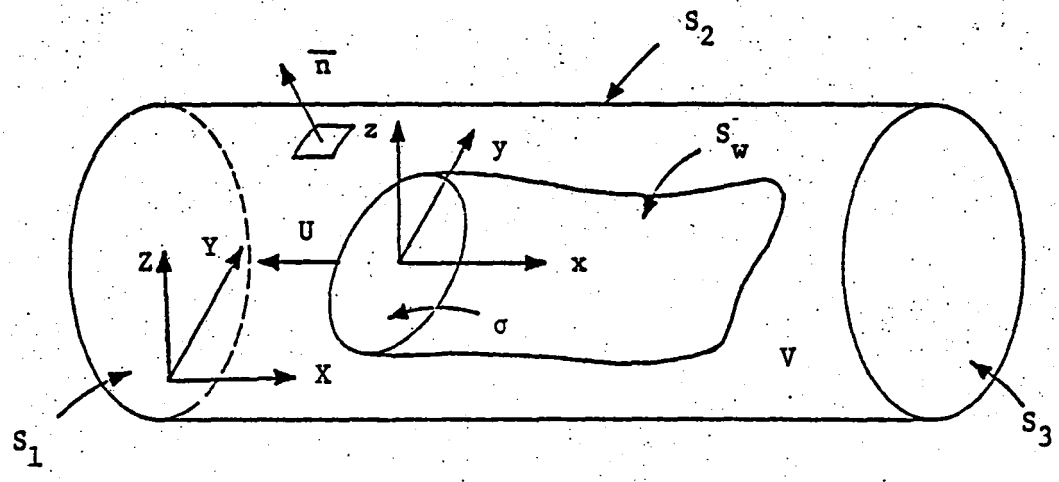

Figure 6.9. Control volume for conservation of energy in three dimensions.

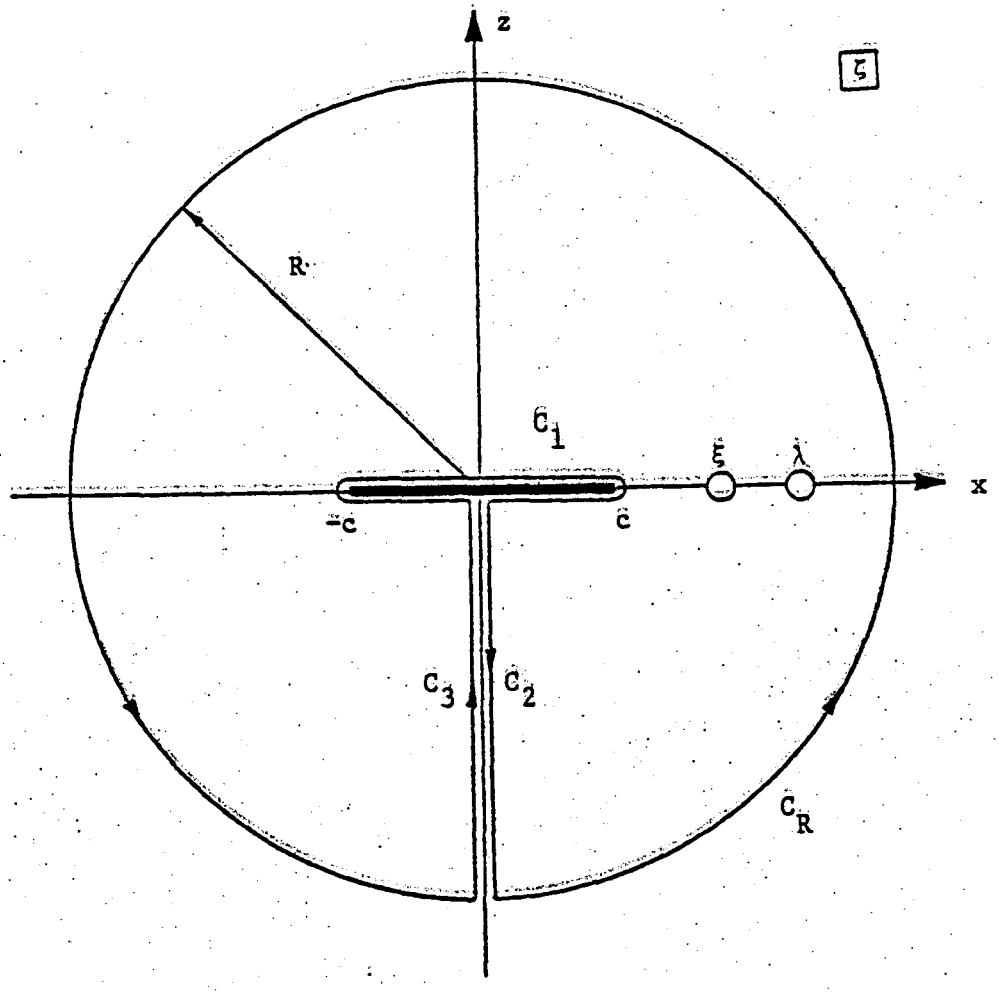

Figure A.1. Integration contour for (A.15).

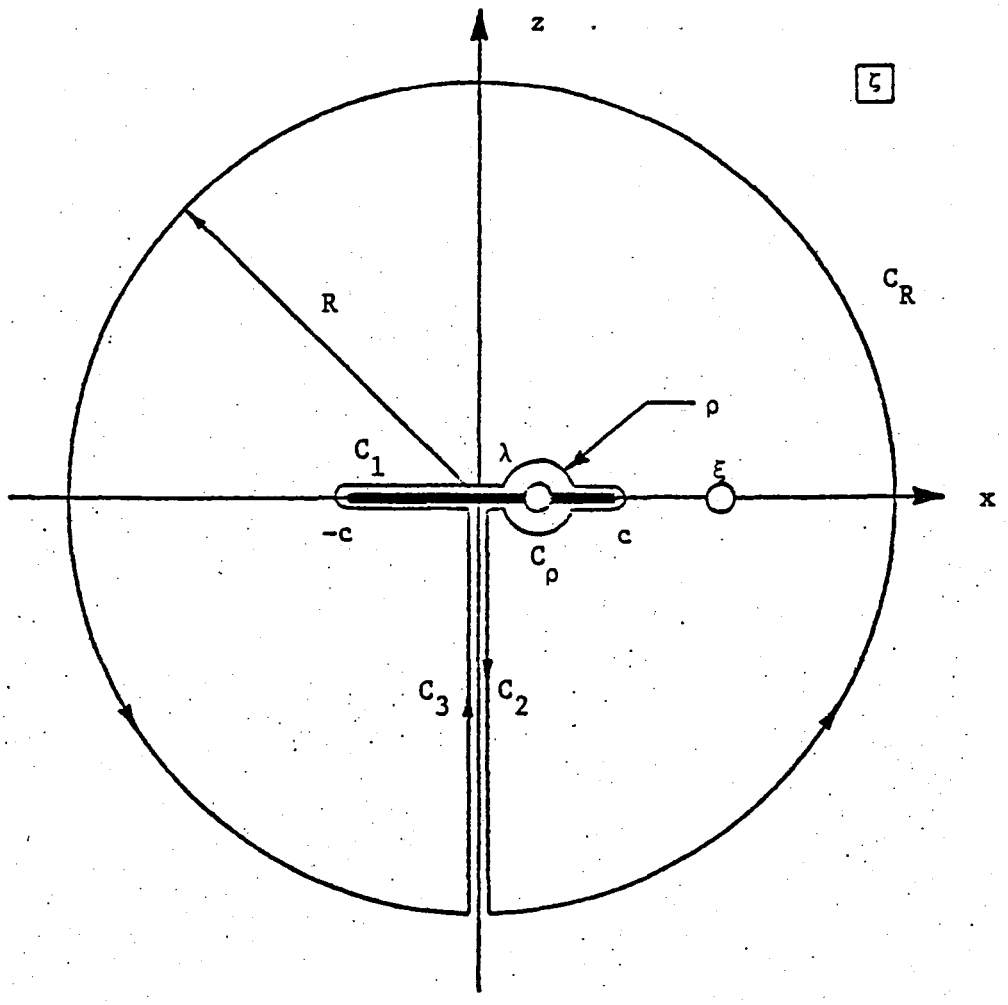

Figure A.2. Integration contour for (A.20).

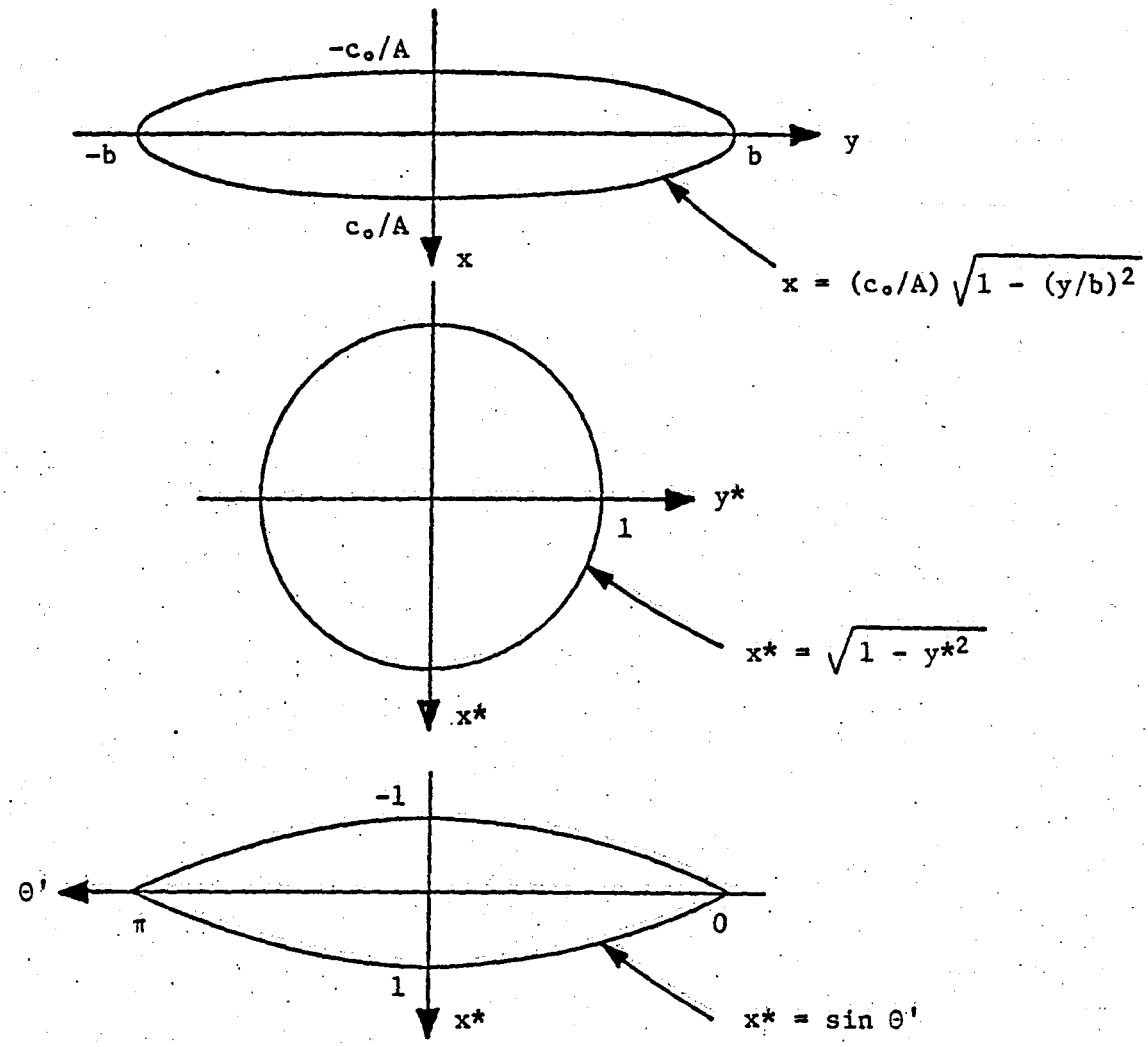

Figure B.1. Transformation of the elliptic planform using $y^* = \cos \theta'$.

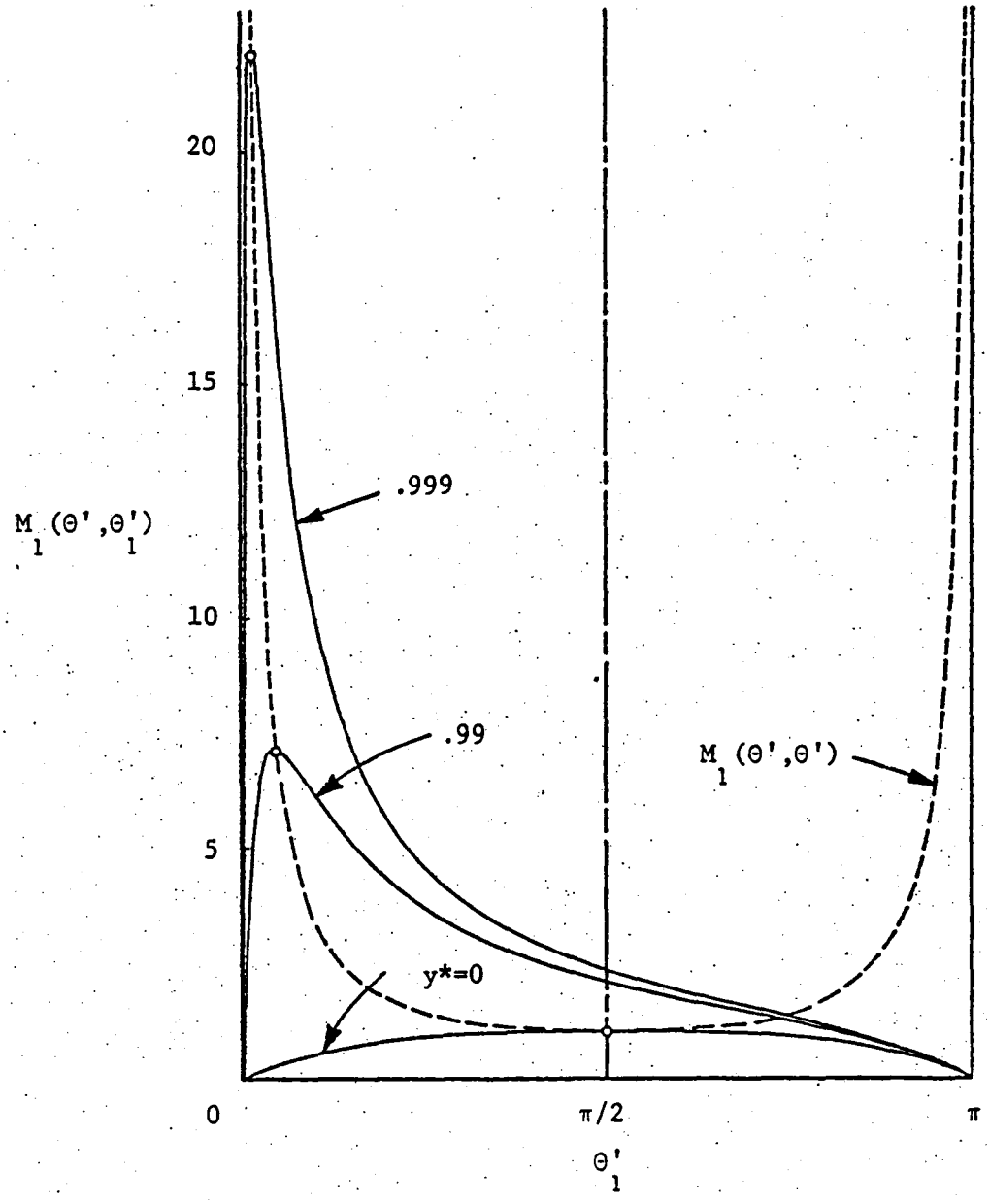

Figure B.2. The function $M_1(\theta',\theta_1') \equiv (\theta' - \theta_1')^2 \sin\theta_1' / (\cos\theta' - \cos\theta_1')^2$ versus θ_1' for several values of $y^* = \cos\theta'$.

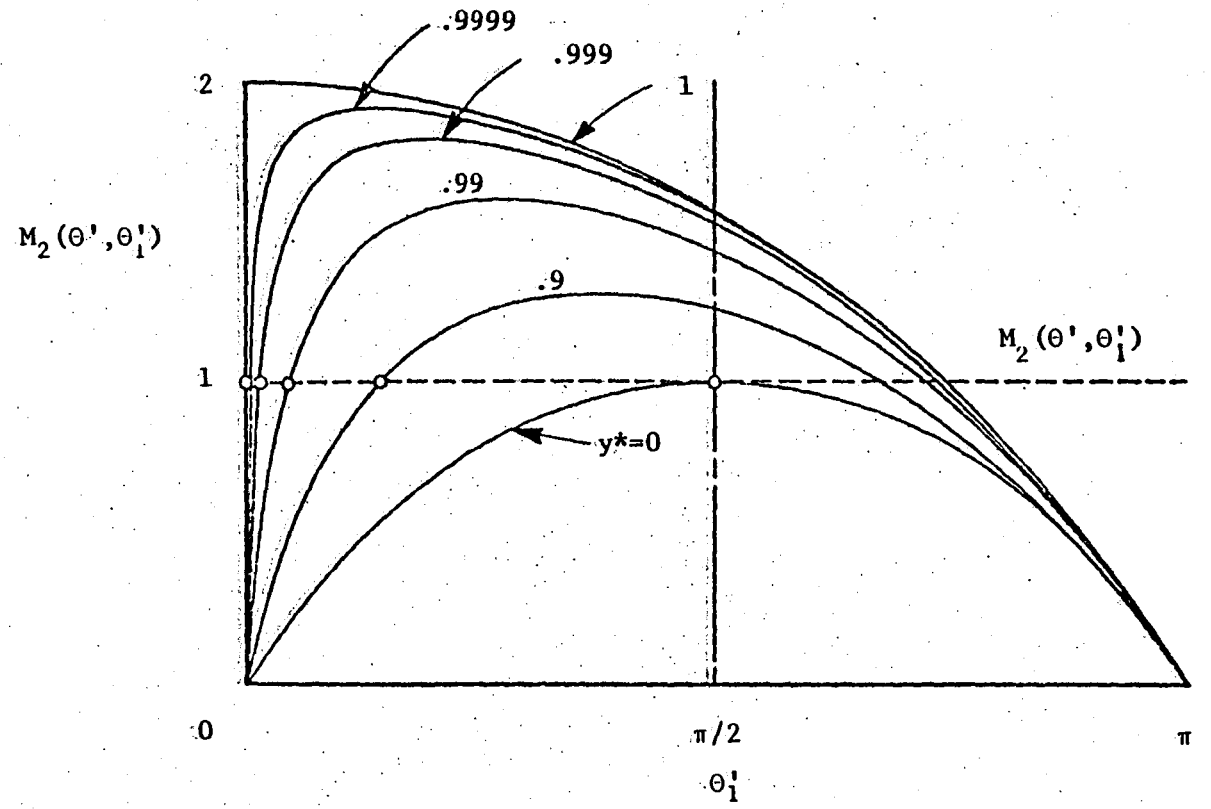

Figure B.3. The function $M_2(\theta', \theta_1') \equiv |\theta' - \theta_1'| \sin\theta_1' / |\cos\theta' - \cos\theta_1'|$ versus θ_1' for several values of $y^* = \cos\theta'$.

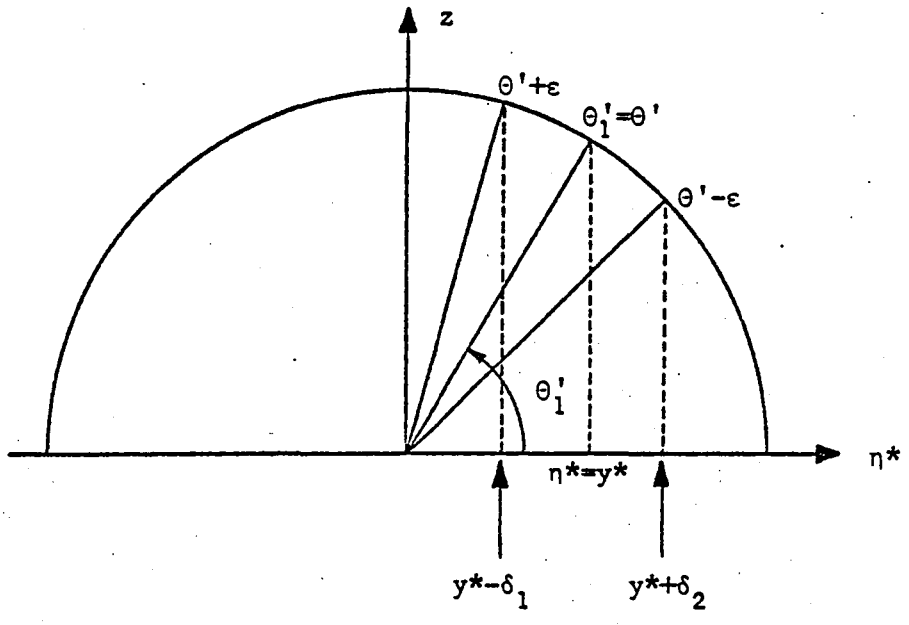

Figure B.4. Integration limits for $B_1(\theta')$, $B_2(\theta')$ and $B_\varepsilon(\theta')$ in terms of θ_1' and η^*.

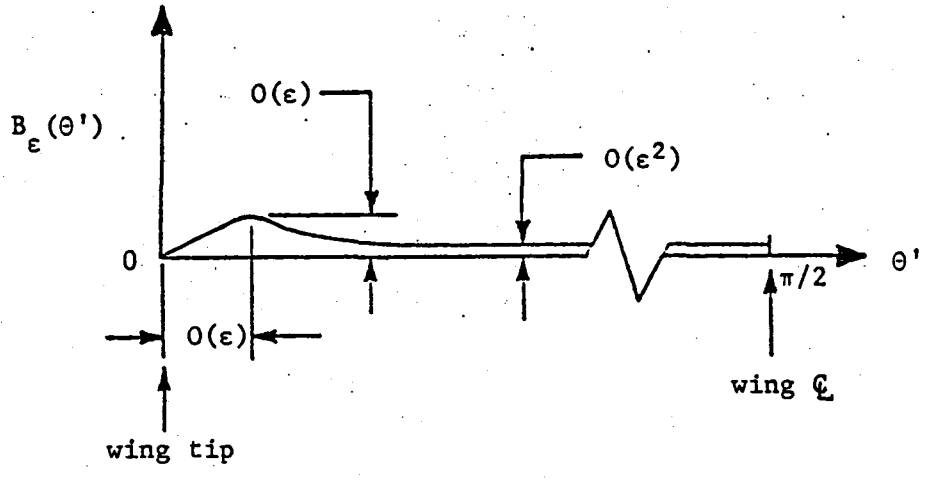

Figure B.5. Variation of $B_\varepsilon(\theta')$ across half of the span.

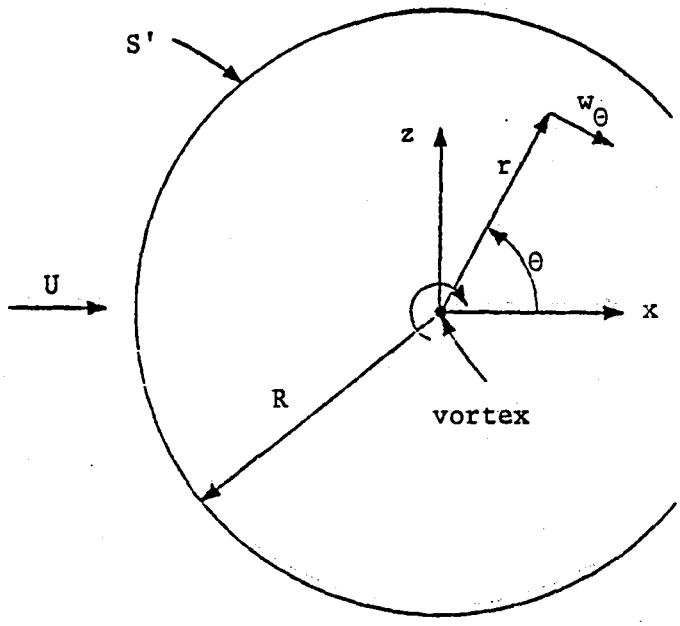

Figure D.1. Simplified far-field geometry.

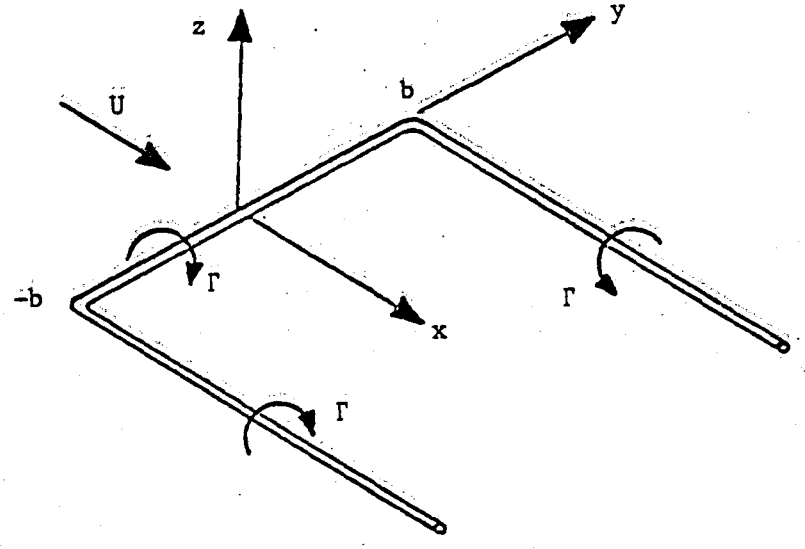

Figure F.1. The lifting line for a wing with uniform loading across the span in steady flow.

q	$\bar{K}_R$	$-\bar{K}_I$	q	$\bar{K}_R$	$-\bar{K}_I$
0.00	1.000	0.000	3.2	.024	.176
.05	.927	.138	3.4	.017	.163
.10	.863	.211	3.6	.014	.155
.20	.750	.298	3.8	.012	.148
.30	.656	.347	4.0	.008	.140
.40	.576	.374	4.2	.005	.130
.50	.507	.389	4.4	.006	.123
.60	.447	.395	4.6	.002	.120
.70	.395	.395	4.8	.002	.115
.80	.350	.391	5.0	.000	.110
.90	.309	.384	5.2	.002	.104
1.0	.274	.376	5.4	.001	.097
1.1	.242	.366	5.6	-.002	.095
1.2	.215	.356	5.8	.002	.093
1.3	.189	.345	6.0	-.002	.090
1.4	.170	.333	6.5	.000	.083
1.5	.150	.321	7.0	↓	.077
1.6	.136	.310	7.5	↓	.070
1.7	.121	.299	8.0	↓	.066
1.8	.107	.288	8.5	↓	.062
1.9	.098	.277	9.0	↓	.058
2.0	.084	.268	9.5	↓	.055
2.2	.065	.249	10.0	↓	.052
2.4	.052	.233	10.5	↓	.049
2.6	.041	.216	11.0	↓	.046
2.8	.034	.202	11.5	↓	.044
3.0	.028	.189	12.0	↓	.042
			∞	↓	$1/(2q)$

Table 3.1. Numerical values of the real and imaginary parts of the modified kernel function of Reissner $\bar{K}(q) = \bar{K}_R(q) + j\,\bar{K}_I(q)$.

REFERENCES

Abramowitz, M. and Stegun, I. A., eds. (1970), Handbook of Mathematical Functions, AMS 55, National Bureau of Standards.

Archer, R. D., Sapuppo, J. and Betteridge, D. S. (1979), "Propulsive Characteristics of Flapping Wings," Aeron. J., September, pp. 355-371.

Ashley, H. and Landahl, M. T. (1965), Aerodynamics of Wings and Bodies, Addison-Wesley.

Bennett, A. G. (1970), "A Preliminary Study of Ornithopter Aerodynamics," Ph. D. Thesis, Univ. of Illinois, Urbana.

Bisplinghoff, R. L., Ashley, H. and Halfman, R. L. (1955), Aeroelasticity, Addison-Wesley.

Bratt, J. B. (1953), "Flow Pattern in the Wake of an Oscillating Airfoil," ARC R&M 2773.

Carrier, G. F., Krook, M. and Pearson, C. E. (1966), Functions of a Complex Variable,Theory and Technique, McGraw-Hill.

Cheng, H. K. (1975), "On Lifting-Line Theory in Unsteady Aerodynamics," in Unsteady Aerodynamics, Proceedings of a Symposium Held at the University of Arizona March 18-20, R. B. Kinney, ed., pp. 719-739.

Chopra, M. G. (1974), "Hydrodynamics of lunate-tail swimming propulsion," J. Fluid Mech. 64, Part 2, pp. 375-391.

Chopra, M. G. (1976), "Large amplitude lunate-tail theory of fish locomotion," J. Fluid Mech., 74, Part 1, pp. 161-182.

Chopra, M. G. and Kambe T. (1977), "Hydrodynamics of lunate-tail swimming propulsion. Part 2," J. Fluid Mech., 79, Part 1, pp. 49-69.

Dwight, H. B. (1961), Tables of Integrals and Other Mathematical Data, Macmillan.

Erdélyi, A., ed. (1953), Higher Transcendental Functions, Bateman Manuscript Project, Vol. II, McGraw-Hill.

Filotas, L. T. (1969), "Theory of Airfoil Response in a Gusty Atmosphere. Part I - Aerodynamic Transfer Function," UTIAS Report No. 139, October.

Friedrichs, K. O. (1953), Secial Topics in Fluid Dynamics, New York Univ.

Garrick, I. E. (1936), "Propulsion of a Flapping and Oscillating Airfoil," NACA Report No. 567.

Garrick, I. E. (1957), "Nonsteady Wing Characteristics," Section F of Aerodynamic Components of Aircraft at High Speeds, Vol VII of Princeton Series in High Speed Aerodynamics and Jet Propulsion, A. F. Donovan and H. R. Lawrence, eds., Princeton Univ. Press., pp. 658-793.

Giesing, J. P. (1968), "Nonlinear Two-Dimensional Unsteady Potential Flow with Lift," J. Aircraft, 5, No. 2, March-April, pp. 135-143.

Glauert, H. (1947), The Elements of Airfoil and Airscrew Theory, Second Edition, Cambridge Univ. Press.

Gröbner, W. and Hofreiter, N. (1961), Integraltafel, Zweiter Teil, Bestimmte Integrale, Springer-Verlag.

Heaslet, M. A. and Lomax, J. (1953), "The Calculation of Pressure on Slender Airplanes in Subsonic and Supersonic Flow," NACA TN 2900.

Hildebrand, F. B. (1965), Methods of Applied Mathematics, Second Edition, Prentice-Hall.

James, E. C. (1975), "Lifting-line theory for an unsteady wing as a singular perturbation problem," J. Fluid Mech., 70, Part 4, pp. 753-771.

Jordan, P. F. (1971a), "The Parabolic Wing Tip in Subsonic Flow," AIAA Paper No. 71-10.

Jordan, P. F. (1971b), "Span Loading and Formation of Wake," in Aircraft Wake Turbulence and Its Detection, J. H. Olsen, A. Goldberg and M. Rogers, eds. Plenum Press., pp. 207-227.

von Kármán, T. and Burgers, J. M. (1935), General Aerodynamic Theory - Perfect Fluids, Division E, Vol. II, Aerodynamic Theory, W. F. Durand, ed., Julius Springer.

Kelly, H. R., Rentz, A. W. and Siekmann, J. (1964), "Experimental studies on the motion of a flexible hydrofoil," J. Fluid Mech. 19, Part 1, pp. 30-49.

Kinner, W. (1937), "Die Kreisförmige Tragfläche auf potentialtheoretischer Grundlage," Ing. Archiv., 8, pp. 47-80.

Küssner, H. G. and Schwarz, L. (1940), "The Oscillating Wing with Aerodynamically Balanced Elevator," Luftfahrt-Forsch., 17, pp. 337-354. (English translation: NACA TM 991, 1941.)

Lan, C. E. (1976), "Some Applications of the Quasi-Vortex-Lattice Method in Steady and Unsteady Aerodynamics," NASA SP-405, Vortex-Lattice Utilization, May, paper No. 21.

Lan, C. E. (1979), "The unsteady quasi-vortex-lattice method with applications to animal propulsion," J. Fluid Mech., 93, Part 4, pp. 747-765.

Landahl, M. T. (1968), "Pressure Loading Functions for Oscillating Wings with Control Surfaces," AIAA J., 6, No. 2, February, pp. 345-348.

Landahl M. T. and Stark V. J. E. (1968), "Numerical Lifting-Surface Theory - Problems and Progress," AIAA J., 6, No. 11, November, pp. 2049-2060.

Lighthill, M. J. (1970), "Aquatic animal propulsion of high hydrodynamic efficiency," J. Fluid Mech., 44, Part 2, pp. 265-301.

Mangler, K. W. (1951), "Improper Integrals in Theoretical Aerodynamics," ARC R&M 2424.

Ohashi, H. and Ishikawa, N. (1972), "Visualization Study of Flow Near the Trailing Edge of an Oscillating Airfoil," Bulletin of JSME, 15, No. 85, pp. 840-847.

Prandtl, L. (1918), "Tragflugel theorie," Nachrichten d. k. Gesellschaft d. Wiss. zu Göttingen, Math-Phys. Klasses, pp. 451-477.

Reissner, E. (1944), "On the General Theory of Thin airfoils for Nonuniform Motion," NACA TN No. 946.

Reissner, E. (1947), "Effect of Finite Span on the Airload Distributions for Oscillating Wings, I - Aerodynamic Theory of Oscillating Wings of Finite Span," NACA TN No. 1194.

Reissner, E. and Stevens, J. E. (1947), "Effect of Finite Span on the Airload Distributions for Oscillating Wings, II - Methods of Calculation and Examples of Application," NACA TN No. 1195.

Robinson, A. and Laurmann, J. A. (1956), Wing Theory, Cambridge Univ. Press.

Schwarz, L. (1940), "Berechnung der Druckverteilung einer harmonisch sich Verformenden Tragfläche in ebener Strömung," Luftfahrtforsch., 17, Nr. 11 & 12, December.

Sears, W. R. (1941), "Some Aspects of Non-Stationary Airfloi Theory and its Practical Application," J. Aeron. Sci., 8, No. 3, pp. 104-108.

Schade, T. and Krienes, K. (1947), "The Oscillating Circular Airfoil on the Basis of Potential Theory," NACA TM 1098.

Siekmann, J. (1962), "Theoretical Studies of Sea Animal Locomotion, Part I," Ing. Archiv., 31, pp. 214-228.

Siekmann, J. (1963), "Theoretical Studies of Sea Animal Locomotion, Part II," Ing. Archiv., 32, pp. 40-50.

Smith, E. H. and Stone, D. E. (1961), "Perfect fluid forces in fish profulsion: the solution of the problem in an elliptic cylinder co-ordinate system," Proc. Roy. Soc. A, 261, pp. 316-328.

Van Dyke, M. D. (1956), "Second-Order Subsonic Airfoil Theory Including Edge Effects," NACA Report 1274.

Van Dyke, M. (1963), "Lifting-Line Theory as a Singular-Perturbation Problem," SUDAER No. 165, August.

Van Dyke, M. (1975), Perturbation Methods in Fluid Mechanics, Annotated Edition, Parabolic Press, Stanford.

Van Holten, Th. (1974), "Computation of Aerodynamic Loads on Helicopter Rotorblades in Forward Flight, Using the Method of the Acceleration Potential," Proc. 9th ICAS Congress, Haifa, R. R. Dexter and J. Singer, eds., Weizmann Science Press, Jerusalem, pp. 323-334.

Van Holten, Th. (1975), "The Computation of Aerodynamic Loads on Helicopter Blades in Forward Flight, Using the Method of the Acceleration Potential," Delf Univ. Tech., Dept. Aerospace Eng. Report No. VTH-189.

Van Holten, Th. (1976), "Some notes on unsteady lifting-line theory," J. Fluid Mech., 77, Part 3, pp. 561-579.

Van Holten, Th. (1977), "On the Validity of Lifting Line Concepts in Rotor Analysis," Vertica, 1, pp. 239-254.

Wagner, S. (1969), "On the Singularity Method of Subsonic Lifting-Surface Theory," J. Aircraft, 6, No. 6, November-December, pp. 549-558.

Watkins, C. E., Runyan, H. L. and Woolston, D. S. (1955), "On the Kernel Function of the Integral Equation Relating the Lift and Downwash Distributions of Oscillating Finite Wings in Subsonic Flow," NACA Report 1234.

Watkins, C. E., Woolston, D. S. and Cunningham H. J. (1959), "A Systematic Kernel Function Procedure for Determining Aerodynamic forces on Oscillating or Steady Finite Wings at Subsonic Speeds," NASA TR R-48.

Watson, G. N. (1966), A Treatise on the Theory of Bessel Functions, Second Edition, Cambridge Univ. Press.

Weihs, D. (1972), "Seim-infinite vortex trails, and their relation to oscillating airfoils," J. Fluid Mech., 54, Part 4, pp. 679-690.

Widnall, S. E. (1964), "Unsteady Loads on Hydrofoils Including Free Surface Effects and Cavitation," Sc. D. thesis, M. I. T.

Wu, T. Y. (1961), "Swimming of a waving plate," J. Fluid Mech., 10 , Part 3, pp. 321-344.

Wu, T. Y. (1971a), "Hydrodynamics of swimming propulsion. Part 1. Swimming of a two-dimensional flexible plate at variable forward speed in an inviscid fluid," J. Fluid Mech., 46, Part 2, pp 337-355.

Wu, T. Y. (1971b), "Hydrodynamics of swimming propulsion. Part 2. Some optimum shape problems," J. Fluid Mech., 46, Part 3, pp. 521-544.

Wu, T. Y. (1972), "Extraction of Flow Energy by a Wing Oscillating in Waves," J. Ship Research, 16, March, pp. 66-78.

End of Document